Faculty of Science and Engineering
Department of Chemical Engineering

The Photocatalytic Treatment of Shower Water in a Pilot Scale Reactor: Experimentation and Modelling

Yashveersingh Boyjoo

This thesis is presented for the Degree of
Doctor of Philosophy
of
Curtin University

December 2012

Declaration

To the best of my knowledge and belief this thesis contains no material previously published by any other person except where due acknowledgment has been made.

This thesis contains no material which has been accepted for the award of any other degree or diploma in any university.

Signature: …….

Date: ……...

In memory of my brother,

Mohundass Boyjoo (27/05/1966 – 02/02/2012)

Executive Summary

The treatment of greywater deserves consideration due to its quantity produced and low pollutant loading. The main issue associated with the current methods of greywater treatment is the recalcitrant nature of xenobiotic organic compounds (XOCs) which are hazardous micropollutants present in the wastewater. Advanced oxidation processes (AOPs) are treatment methods that can be used to completely mineralise XOCs in wastewater. One such AOP is photocatalysis.

This research looks at the feasibility of photocatalysis for the treatment of greywater. The type of greywater chosen was real shower water, which was collected at the researcher's home for treatment in a pilot scale slurry photocatalytic reactor with diameter of 30 cm and maximum capacity of 31 L.

Experiments showed that up to 57% of total organic carbon (TOC) elimination was obtained after 6 hours of treatment at the following optimum conditions: pH = 3.0, catalyst concentration = 0.07 gL^{-1}, air flow rate = 1.8 $Lmin^{-1}$ and slurry recirculation rate = 4.4 $Lmin^{-1}$. The ease of operation and control of the reactor (at ambient conditions) showed that photocatalysis could be successfully transposed from bench scale to pilot scale.

Due to the unavailability of the optical parameters for the catalyst used in this research (Aeroxide® P25 TiO_2), experiments were performed at typical catalyst concentrations (0.05 and 0.10 gL^{-1}) to measure the light intensity distribution within the slurry reactor. The values obtained were then replicated by computational fluid dynamics modelling (CFD) by changing the inputs for the optical parameters (absorption and scattering coefficients) until a satisfactory fit to the experimental readings were obtained. It was found that a wavelength averaged value for the scattering coefficient could be used (analogous to that of Degussa P25 TiO_2) but the absorption coefficient was comparatively higher (in the UV-C region) and was wavelength dependent. As a result, the UV emission spectrum of the lamp used in this research was divided into 3 bands for which the absorption coefficients were determined. These optical parameters were of paramount importance in the radiation and species modelling inside the photocatalytic reactor.

A general rate equation applicable to slurry reactors with large diameter was devised and used for the rate modelling of the pollutant degradation. The rate equation took into consideration all the reaction regimes existing in the reactor (half order, transitional order and first order) with respect to the local volumetric rate of energy absorption (LVREA). In the modelling of the pollutant degradation in the reactor, the transitional regime was ignored for simplicity. By a trial and error method, it was found that using a value of 225 Wm^{-2} as the minimum incident light intensity at which half order reactions take place, a Pearson correlation coefficient of 0.88 between simulated and experimental data indicated model adequacy. Moreover, it was established that the average reaction rate was largely dependent upon first order reaction (up to 20 times higher than half order reactions) because of the square root dependency of the reaction rate with respect to the LVREA at high incident light intensities (since high electron-hole recombination lead to reduced reaction).

Finally, simulations of the photocatalytic reactor using 2 and 4 lamps at different geometrical placements instead of one powerful lamp in the middle of the reactor were implemented. It was found that within the range of catalyst concentrations investigated, multiple lamps arrangement resulted in higher average reaction rate with a maximum potential increase in reaction rate of 56% and 123% with 2 and 4 lamps respectively. The significant increase in reaction rate was attributed to a maximisation of incident radiation contours at which first order reactions took place when using multiple and less intense lamps instead of only a powerful one. The optimum lamp separation at which maximum reaction rate arose did not necessarily occur at the optimum lamp separation for which maximum LVREA occurred.

Acknowledgements

I would like to express my deepest gratitude to Dr Vishnu Pareek, my supervisor, to whom I look up to. He has always been here for me and has helped me throughout my course and through tough times. His belief in me made me believe in myself. Thanks to Professor Ming Ang, my co-supervisor, for his valuable insights and guidance. His tranquil nature always made him very approachable. Thanks to Professor Moses Tadé who always made me feel welcome in his office and always managed to find some time to fit me in his busy schedule.

My sincere thanks to the team of dedicated laboratory technicians and officers: Karen Haynes, Ann Carroll, Jason Wright, Roshanak Doroushi and Araya Abera for their help and patience. I would also like to thank Joe Justin, electrician for the engineering department and the guys from the Curtin Workshop for their invaluable help with the setting up of my rig.

Many thanks to my good friend Dr Pradeep Shukla, who helped me settle into the research environment at Curtin University and always offered his help with a smile. My appreciations go towards my friends and colleagues, Dr Amy Liu, Dr Ruh Ullah, Hussein Rasool, Dr Faye Chong, Dr Monica Gumulya, Dr Ranjeet Utikar, Joseph John, Divyamaan Wadnerkar, Dr Milin Kumar, Asim Saeed, Dr Gia Pham, Emmanuel Obanijesu, Abhishek Sharma, Dr Deeptangshu Chaudhary, Petrina Beeton and Dr Bill Atweh for their prized friendship and assistance throughout my tenure at Curtin University.

Also thanks to the staff from the Chemical Engineering department at Curtin University: Jann Bolton, Tammy Atkins, Stephenie Blakiston, Surudee Bunpitakgate and Naomi Mockford for their help and kindness.

And of course I would like to thank my mother who has been an inspirational figure to me throughout my life. For a pint sized lady, her devotion, strength and sheer grit never cease to amaze me; to my brothers and sisters for their love and endless support and to my friends in Mauritius and Australia without whom life would have been really dull.

List of Publications

1. Boyjoo Y., Ang M. and Pareek V. (2012). Photocatalytic Treatment of Shower Water Using a Pilot Scale Reactor. *International Journal of Photoenergy* 2012, 1-7.
2. Boyjoo Y., Ang M. and Pareek V. (in press). A Review of Greywater Characteristics and Treatment Options. *Water Science & Technology* 67, 1403 – 1424.
3. Boyjoo Y., Ang M. and Pareek V. (2013). Light Intensity Distribution in Multi-Lamp Photocatalytic Reactors. *Chemical Engineering Science* 93, 11 - 21.
4. Boyjoo Y., Ang M. and Pareek V. (2012). Some Aspects of Photocatalytic Reactor Modelling Using Computational Fluid Dynamics. *Chemical Engineering Science* 101, 764 - 784.
5. Boyjoo Y., Ang M. and Pareek V. (2012). CFD Simulation of a Pilot Scale Slurry Photocatalytic Reactor with Large Diameter and Using 1 or Multiple Lamps. *Chemical Engineering Science – to be submitted*.

Contents

Chapter 1 – Introduction

Fresh water supply to an ever increasing world population is getting harder. As a result, soft path or hard path solutions are being employed. Hard path solutions involve the construction of massive infrastructures such as dams, aqueducts and desalination plants to meet human demands. Such solutions have been the main means of supplying water in the twentieth century. However, with the related economic, ecological and social costs, soft path solutions are now being favoured. Soft path solutions look at more efficient and sensible ways of using our water. Some examples include dual flush toilet systems, increase in the effectiveness of irrigation, and wastewater treatment and reuse.

One type of wastewater that deserves consideration for reuse is greywater. Greywater is household wastewater excluding toilet and sometimes kitchen wastewater. The production of greywater varies widely amongst countries and depends on factors such as water availability, geographical location, infrastructure, living standards, customs and habits. If reused for other household duties that do not require potable water, such as toilet flushing, garden irrigation and floor cleaning, up to 46% of domestic water savings can be achieved. However, according to wastewater reuse standards, the greywater need proper treatment prior to reuse due to aesthetic and hygienic concerns. The current preferred treatment methods for greywater treatment use physical and biological or natural systems.

Bathroom greywater is produced in high quantities (up to 47% of total greywater) and is relatively low in pollutant loading. However, due to the presence of recalcitrant xenobiotic organic compounds (XOCs) and surfactants, current treatment methods are inefficient such that chemical treatment is required. Techniques such as advanced oxidation processes (AOPs) have been developed and have shown encouraging results for the complete oxidation of recalcitrant organic compounds in wastewater. The main features of AOPs are that the process can be carried out at or near standard conditions (atmospheric pressure and low temperatures) and organic micropollutants are not passed from one phase to another but are indeed completely destroyed to CO_2 and H_2O.

Photocatalysis is an AOP that uses a catalyst (often TiO_2), UV light and an electron acceptor (O_2, O_3, H_2O_2) to completely decompose organic pollutants found in liquids or gases. The basis of the process is the use of low energy UV-A photons (for which the energy is greater or equal to the band gap energy of the catalyst) to excite the semiconductor catalyst into charge separation and generate electron-hole pairs. The electrons and holes, on separation, assist in the production of the very reactive hydroxyl radical which can destroy many toxic organic pollutants. This technology however works best at low pollutant concentrations (mgL^{-1} or $mmolL^{-1}$) and when the catalyst is finely dispersed within the medium. The overall process can be described by the following reaction equation:

$$\text{Organic Pollutants} + O_2 \xrightarrow{\text{Semiconductor} + \text{UVA Light}} CO_2 + H_2O + \text{Mineral Acid}$$

For the past 30 years, the majority of research regarding photocatalysis has been dealing with bench scale experiments. In this research a pilot scale slurry reactor (diameter of 30 cm and maximum capacity of 31 L) is to be used to investigate the feasibility of the treatment of shower water. Real shower water, collected from the researcher's home will be treated. Furthermore, a rate equation will be devised to model the rate of pollutant degradation and validate experimental results. Once validated, the model will be used to predict the effect of using multiple lamps (2 and 4 lamps) and their geometrical placement in the reactor on the average reaction rate as opposed to using only one powerful lamp in the middle of the reactor.

1.1 Objectives

The objectives of this research are outlined below:

- To determine the treatability of real shower water by photocatalysis, in terms of total organic carbon (TOC) reduction, using a pilot scale slurry annular photocatalytic reactor (diameter of 30 cm and maximum capacity of 31 L)
- To experimentally determine the optimum variables (air flow rate, slurry recirculation rate, slurry pH and catalyst concentration) at which maximum degradation takes place
- Since no published data regarding the optical parameters (scattering and absorption coefficients) of the catalyst used (Aeroxide® P25 TiO_2, 21 nm

average particle size) were available, those values have to be determined by experimentation and radiation modelling using computational fluid dynamics

- To devise and validate (via modelling) a rate equation for slurry reactors with large annulus (as is the case in this study), in terms of the reaction regimes (half order, transitional order and first order) that exist within the reaction space due to light attenuation by the catalyst particles
- To predict the effect of using multiple lamps (2 and 4 lamps) and their geometrical placement in the reactor on the average reaction rate as opposed to using only one powerful lamp in the middle of the reactor

1.2 Organisation of the Thesis

The thesis has been organised so that each chapter follows from the previous one in a smooth manner but can be stand-alone as well. As a result, some of the materials might be repeated so as to ease the reader's understanding.

Chapter 2 - Greywater Characteristics and Treatment Processes is an extensive literature review of the characteristics of greywater and its current treatment methods.

Chapter 3 - Modelling of Photocatalytic Reactors looks at the modelling of photocatalytic reactors by computational fluid dynamics (CFD) and gathers useful information that are intended to assist the reader at the modelling of either immobilised or slurry photocatalytic reactors. From this chapter, the equations and data pertaining to multiphase flow, radiation and reaction rate modelling are used to model the slurry reactor used in this research project to treat shower water.

Chapter 4 - Photocatalytic Treatment of Shower Water Using a Pilot Scale Reactor is the main experimental section of this thesis. It presents the data and findings obtained from the photocatalytic treatment of real shower water in a pilot scale slurry type reactor.

Chapter 5 - Determination of Catalyst Optical Parameters and Multiple Lamp contains both experimental and modelling sections for the determination of the optical parameters of the photocatalyst used in this research. The photocatalyst is Aeroxide® P25 TiO_2, which is different from Degussa P25 TiO_2 in that the former has been recently developed and is known to have enhanced photocatalytic activity

as compared to the latter. Since no information is available on the optical parameters (absorption and scattering coefficients) of Aeroxide® P25 TiO_2, experiments and modelling were carried out to obtain those values as a function of the catalyst concentration within the reactor. The optical parameters once obtained were then used to assess the effect of using multiple lamps (2 and 4 lamps, having a combined power equivalent to the power of a single lamp) on the local volumetric rate of energy absorption (LVREA) within the reactor, via 2-dimensional computational fluid dynamics simulations.

Chapter 6 - Hydrodynamics and Kinetic Rate is the modelling and validation of the average rate of pollutant degradation in the reactor with respect to the catalyst loadings. Information from Chapter 3 (including a rate equation devised by the author) was used as well as the optical parameters obtained from Chapter 5 to validate results achieved in Chapter 4.

Chapter 7 – presents and compares 3-dimensional simulation results for the average reaction rates obtained when using multiple lamps (2 and 4 lamps, having a combined power equivalent to the power of a single lamp) within the reactor instead of one powerful lamp only.

The thesis ends with **Chapter 8 - Conclusions and Recommendations for Future Work** which draws conclusions and recommendations for future work.

Supplementary materials that are referred to in the thesis body are included in the **Appendices**.

Figure 1. 1 depicts the organisation of the thesis and how the chapters are linked to each other.

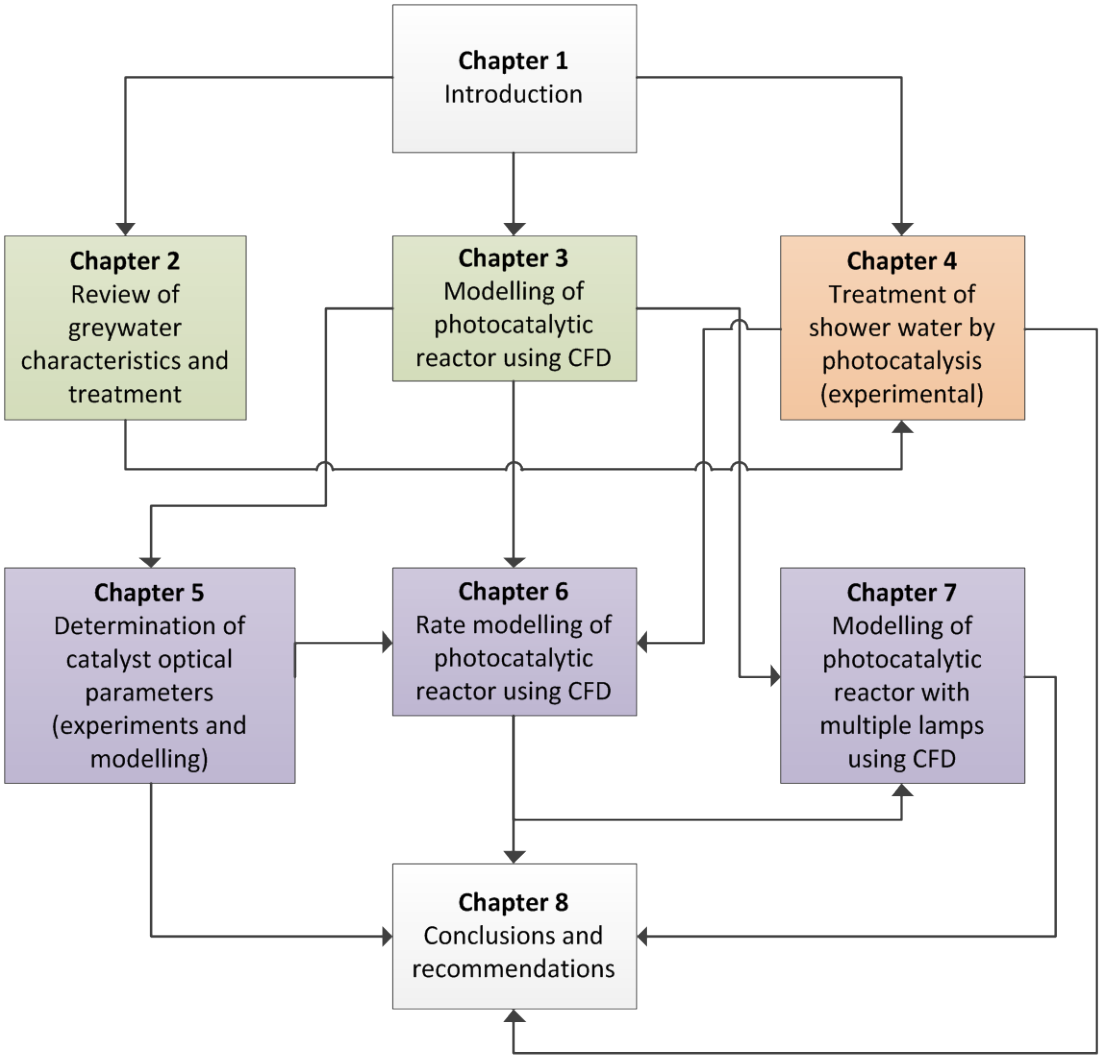

Figure 1. 1: Organisation of the thesis.

Chapter 2 - Greywater Characteristics and Treatment Processes

Water is life. It is globally supplied via rainfall at a relatively constant rate of 47,000 $km^3 year^{-1}$ from which only 6800 km^3 are withdrawn for use (Hanjra and Qureshi, 2010; Seckler, 1998). Yet, with the world population increasing by about 85 million per year, the availability of fresh water per person keeps decreasing (Stikker, 1998). At this rate, the number of people living in water stressed or water scarce countries is estimated to increase from half a billion to three billion in 2025 (Hanjra and Qureshi, 2010). To address such a gigantic issue, either soft or hard path solutions exist.

Hard path solutions involve the construction of massive infrastructures such as dams, aqueducts and desalination plants to meet human demands. Those have been the main means of supplying water in the twentieth century and will remain a necessary evil. However, with the related economic, ecological and social costs, soft path solutions are favoured. The latter looks at more efficient and sensible ways of using our water by the implementation of water reduction strategies via hardware such as dual flush/composting toilets, water free urinals, metering faucets and flow optimised showerheads which presently are being employed in “green” buildings (Hills et al., 2002; Kubba, 2009). Other soft path solutions look at increasing the effectiveness of irrigation systems (Cosgrove and Rijsberman, 2000; De Fraiture and Wichelns, 2010; Molden et al., 2010; Seckler, 1998), and wastewater treatment and reuse (Chanan et al., 2009).

Potential sources of water for recycling are sewage, greywater and rainwater. Sewage is treated and reused for irrigation purposes in countries such as the USA, Australia, Europe, the Mediterranean region, China, India and Africa (Kivaisi, 2001; Lazarova et al., 2001; Po et al., 2003) and rainwater harvesting is encouraged in Brazil, Central Africa, Australia and the USA (Mankad and Tapsuwan, 2011).

Greywater is domestic wastewater excluding toilet wastewater. The amount of greywater produced in a household varies during the day with the highest amounts being produced before and after normal working hours. Greywater also varies widely in quantity as well as composition depending on the amount and type of chemicals

used (detergents, soaps, toothpastes etc.), household occupancy, gender, age, water availability, country etc. Greywater is less polluted than domestic WW due to the absence of faeces, urine and toilet paper but its chemical nature is quite different (Eriksson et al., 2002; Jefferson et al., 2000). The COD:BOD ratio can be as high as 4:1, indicating a high chemical content and the major part of the heavy metal load is in greywater. However pathogens and nutrients P and N are generally lower than in domestic WW (Jefferson et al., 2000; World Health, 2006). The most common constituents of greywater are surfactants and detergents products, which are toxic to plants and marine animals at varying concentrations. Household washing detergents and softeners are toxic to aquatic animals at concentrations from 0.07 mgL^{-1} to 35.4 mgL^{-1} while anionic surfactants, non-ionic surfactants, phosphate and boron are toxic to marine organisms at concentrations around 0.0025-300 mgL^{-1}, 0.3-200 mgL^{-1}, 5-9 mgL^{-1} and 4.6-226 mgL^{-1} respectively (Pettersson et al., 2000). Pettersson *et al.* (2000) found that only 1 out of 26 detergents and 2 out of 5 softeners commonly used in Sweden could be considered not harmful to aquatic animals.

Greywater is commonly used intermittently within individual households without treatment for irrigation or lawn watering. At such small scale it is not expected to be detrimental to the environment or personal hygiene. However, when considering reuse at a larger scale (apartments, buildings or communities), proper treatment is required. This will necessitate a characterisation of the greywater, which will indicate the treatment technique to be adopted. The treated greywater will need to be within the required standards (depending on the country's regulations) for reuse. Some greywater reuse applications include toilet flushing, irrigation (crops, landscape), car washing and fire extinguishing.

This chapter is a result of an intensive literature review. It includes the characterisation of greywater, the pollutants of concern and their reasons for concern, standards and regulations for water reuse in various countries, public perception regarding greywater treatment, the different treatment techniques used, some successful case studies and ends with a critical discussion of the available treatment methods as well as some recommendations for future studies.

2.1 Characteristics of Greywater

This section looks at the different characteristics of greywater such as quantity produced, reuse potential, chemical and physical composition and the reasons for their concern.

2.1.1 Greywater production

Greywater is domestic wastewater excluding toilet wastewater. It is the greater part of domestic wastewater and comprises wastewater from bathtubs, showers, laundry machines, washbasins and kitchen sinks. The domestic usage of water varies among countries depending on geographical location, infrastructure, living standards, custom and habits, among others and as a result, the generation of greywater varies widely. In Africa and the middle east greywater production is between 14 and 161 $Lperson^{-1}day^{-1}$ (Al-Hamaiedeh and Bino, 2010; Halalsheh et al., 2008; Morel and Diener, 2006; Prathapar et al., 2005), with water scarce countries such as Jordan, Mali and South Africa lying on the lower production end (between 14 and 59 $Lperson^{-1}day^{-1}$) while Oman lies on the high end due to the numerous well fields and desalination plants installed across the country (Prathapar et al., 2005). The volumes of greywater produced in Asia, Europe and the USA are 72-225 $Lperson^{-1}day^{-1}$ (Mandal et al., 2011; Morel and Diener, 2006), 35-150 $Lperson^{-1}day^{-1}$ (World Health, 2006) and 200 $Lperson^{-1}day^{-1}$ (World Health, 2006) respectively. The low ranges of greywater production in some European communities arise due to the water saving mentality and existence of Eco-villages in countries such as Germany, Sweden, Norway and Holland.

2.1.2 Reuse potential

A breakdown of the domestic water usage for different countries is presented in Table 2. 1. Between 41 and 91% of domestic water is turned into greywater. Since the water requirement for duties such as toilet flushing, garden irrigation and floor cleaning do not require potable quality standards, the domestic water savings potential from reusing treated greywater for such duties lies between 9 and 46%. From Table 2. 1, this water saving can easily cover toilet flushing duties as well as most of the irrigation requirements.

Table 2. 1: Breakdown of domestic water usage for different countries.

Domestic Water Use (%)	Denmark (Revitt et al., 2011)	Australia (Christova-Boal et al., 1996)	UK (Pidou et al., 2007)	Austra lia (2008)	Oman (Prathapar et al., 2005)	India (Mandal et al., 2011)	Ireland (Li et al., 2010)	Holland (Krozer et al., 2010)
Bathroom	36	26	28	18	47	39	38	38
Laundry	14	15	12	14	7	20	10	20
Kitchen (inc drinking)	21	5	19	9	37	23	13	6
Toilet flushing	23	34	35	12	4	15	27	29
Other (garden, cleaning)	6	20	6	47	5	3	12	7

2.1.3 Greywater contents and reasons for concern

Greywater can be classified as either high load greywater (HGW) or low load greywater (LGW). HGW is more concentrated and includes greywater from the kitchen and laundry. On the other hand, LGW is considerably less polluted and excludes greywater from the laundry and/or kitchen (Al-Jayyousi, 2003; Gross et al., 2008; Gulyas, 2007; Nolde, 2000). LGW makes up for 44 – 62% of the total greywater produced (Table 2. 1). Christova Boal *et al.* (1996) do not recommend using kitchen greywater due to its high load of pollutants and oils as well as low quantity produced. Yet, some researchers do use kitchen greywater since it is high in biodegradable organics and nutrients that can boost the COD:N:P ratio of the greywater up to the suggested value of 100:20:1 for biological treatment (Li et al., 2009b) but necessitates further treatment, such as grease traps (Morel and Diener, 2006) as primary treatment as well as disinfection. Laundry greywater is high in phosphates and heavy metals (Aonghusa and Gray, 2002; Jenkins, 1998) and its biodegradability can be 5 times less than shower water due to the recalcitrant nature of its organic contents (Nolde, 2000).

It is necessary to characterize greywater with respect to its physical parameters as well as the content of both chemical compounds and micro-organisms prior to reuse (Eriksson et al., 2002). The physical parameters include temperature, colour, turbidity and suspended solids from food particles, hair and fibres and electrical conductivity (due to ionic concentration). The chemical parameters comprise of dissolved organic matter (BOD, COD and TOC), nutrients (N and P), pH, heavy metals content, residual chlorine and recalcitrant organic compounds such as xenobiotic organic compounds (XOC's) that originate from household chemical products such as detergent, soaps and dyes (Eriksson et al., 2002). Table 2. 2 lists the

physical and chemical parameters measured in greywater and their reasons for concern (1992; Fatta-Kassinos et al., 2010; Gulyas, 2007).

Table 2. 2: Physical and chemical properties of WW and their reasons for concern.

Constituent	Reasons for concern
Suspended solids	Can adsorb organic contaminants and heavy metals Shield microorganisms from disinfectants such as UV Excessive amount can cause plugging in systems
BOD, COD, TOC	Provide food to microorganisms leading to an increase in their numbers Food breakdown can lead to aesthetic problems (colour and odour)
Nutrients (N, P)	Excessive discharge can lead to eutrophication on surface waters
XOCs	Accumulate and cause harm to plants and animals
pH	Water pH affects disinfection, coagulation, metal solubility as well as soil alkalinity
Heavy metals (e.g., Cd, Zn, Ni and Hg)	Can accumulate in the environment and are toxic to flora and fauna
EC/TDS (due to specific elements such as Na, Ca, Mg, Cl, Ba)	Excessive salinity may damage some crops Specific ions such as chloride, sodium and boron are toxic to some plants When EC < 500 - no detrimental effects on plants When EC = 500- 1000 - can affect sensitive plants When EC = 1000-2000 - can affect many crops and careful management practice should be followed When EC > 2000 - can be used only for tolerant plants on permeable soils
Residual chlorine	Excessive amount of free residual chlorine (<0.05 ppm) can be damaging to some sensitive crops (leaf burn) Chlorination of high organic loads water can form carcinogenic chloroforms or other halogenated organics

Table 2. 3 and Table 2. 4 list some of the common parameters of LGW and HGW respectively, obtained from various sources while Table 2. 5 and Table 2. 6 list the elemental composition of LGW and HGW respectively.

Table 2. 3: LGW characteristics from several countries. B – Bath, F – Floor cleaning, S – Shower, W – Washbasin, * - BOD_7.

LGW Characteristics	Units	Australia (Christova-Boal et al., 1996) B	Taiwan (Lin et al., 2005) S	Korea (Kim et al., 2007) F	France (Chaillou et al., 2011) B, S	Germany (Nolde, 2000) B, S	UK (Pidou et al., 2008; Winward et al., 2008b) B, S, W	Spain (Gual et al., 2008; March et al., 2004) B, S, W	Israel (Friedler and Gilboa, 2010; Friedler et al., 2008; Friedler et al., 2005; Ramona et al., 2004) B, S, W	Morocco (Merz et al., 2007; Scheumann et al., 2007) S	Oman (Prathapar et al., 2005) S, W
pH		6.4 - 8.1	7	7.27	7.58	-	6.6 - 7.3	6.8 - 7.6	7.5	7.6	7.1 - 7.4
EC	µS/cm	82 - 250	-	194	468	-	-	921	1241	645 - 855	14 - 15
Turbidity	NTU	60 - 240	43.1	12.6	150	-	35 - 42	20 - 38.8	23 - 34	29	133 - 375
Suspended solids	ppm	48 - 120	29	-	125	-	29	32.2 - 44	29.8 - 61.3	-	353 - 505
Nitrate (NO_3^-)	ppm	<0.05 - 0.20	-	-	-	-	3.9 - 7.5	-	0.67	0	10.2 - 28.7
Ammonia (NH_3/NH_4^+)	ppm	<0.1 - 15	0.146	-	-	-	0.7 - 1	-	2.7	6.6 - 11.8	-
TKN	ppm	4.6 - 20	-	-	-	-	-	-	-	11.9 - 15.2	-
Total N	ppm	-	-	-	9.5	5 - 10	7.6 - 16.4	4.1 - 11.4	-	-	-
Phosphate (PO_4^{3-})	ppm	-	-	-	-	-	0.5 - 1.3	-	0.09	1	-
Total P	ppm	0.11 - 1.8	-	-	0.42	0.2 - 0.6	-	-	-	0.98 - 1.6	-
BOD_5	ppm	76 - 200	23	-	240	50 – 300*	20 - 166	-	59 - 104	53 - 59	42.1 - 130
COD total	ppm	-	-	-	399	-	-	-	148 - 170	-	-
COD dissolved	ppm	-	55	22.9	136	100 - 633	86 - 575	72.7 - 171	86 - 110	109 - 122	58 - 294.3
TOC	ppm	-	-	-	50.6	26 - 95	12 - 56	41 - 58	-	-	70.2 - 83.5
DO	ppm	-	-	-	-	-	-	-	-	0.4	2.6 - 3
Surfactants	ppm	-	-	-	6.8	-	-	-	-	-	14.9 - 41.9
Heterotrophic plate count	counts/100 ml	-	-	-	1.87E+09	1E+05 - 1E+06	-	-	1.3E+07 - 2E+09	-	-
Total coliforms	counts/100 ml	500 - 2.4E+07	-	0	-	10 - 1E+03	4.00E+05	-	-	-	>200.5
Faecal coliforms	counts/100 ml	170 - 3.3E+03	-	-	3.42E+05	0.1 - 10	-	-	5.60E+05	1.4E+05 - 2.48E+05	-
Faecal streptococci	counts/100 ml	79 - 2.4E+03	-	-	-	-	-	-	-	-	-
E.Coli	counts/100 ml	-	5.1E+03	-	4.76E+05	-	-	-	-	-	>200.5

Table 2. 4 (Continued on next page): HGW characteristics from several countries. K – Kitchen, L – Laundry, M – Mixed, S – Shower, * - BOD_7.

Moderate/Heavy greywater Characteristics	Units	Australia (Christova-Boal et al., 1996) L	Japan (Itayama et al., 2006) K	Korea (Kim et al., 2009) K,S	India (Mandal et al., 2011) M	Nepal (Morel and Diener, 2006) M	Costa Rica (Dallas et al., 2004) M	Brazil (Paulo et al., 2009) S,K,L	Holland (Hernández Leal et al., 2010b, 2011; Leal et al., 2007) M	Slovenia (Sostar-Turk et al., 2005) L	Italy (Ciabatti a et al., 2009) L	Germany (Elmitwalli and Otterpohl, 2007; Li et al., 2003) M	Sweden (World Health, 2006) - M	Israel (Gross et al., 2005) M	Turkey (Atasoy et al., 2007; Masi et al., 2010; Scheumann et al., 2007) M	Jordan (Halalsheh et al., 2008) M	Oman (Prathapar et al., 2005) L
pH		9.3-10	-	-	7.3-8.1	-	-	-	-	9.6	7-9	6.9-8.1	-	6.7	7.1-7.2	6.35	8.3
EC	µS/cm	190-1400	-	-	489-550	-	-	-	-	-	1300-3000	-	-	-	401-495	1830	-
Turbidity	NTU	50-210	-	19-84.8	20.6-38.7	-	96	254	-	-	40-150	-	-	-	-	-	444
SS	ppm	88-250	105	30-130	12-17.6	98	-	120	-	35	90-200	-	-	138	48-54	168	315
NO_3^- - N	ppm	0.1-0.31	-	-	0.5-0.63	-	-	0.05	0.12-0.77	-	-	-	-	-	0.13-1.3	-	25.8
Ammonia (NH_3/NH_4^+)	ppm	<0.1-1.9	-	-	-	13.3	-	2.4	0.8-11.8	2.45	-	-	-	-	1.2-1.3	75	-
TKN	ppm	1-40	-	-	-	-	-	-	-	-	-	27.2	-	-	7.6-9	128	-
Total N	ppm	-	21	-	42.8-57.7	-	-	8.8	26.3-35.2	2.75	-	9.7-16.6	13.6	14	-	-	-
PO_4^{3-} - P	ppm	-	-	-	1.52-3.36	3.1	16	5.6	2.3-2.36	-	-	9.8	-	-	-	-	-
Total P	ppm	0.062-42	4	-	-	-	-	-	6.2-7.8	9.9	-	5.2-9.6	5.2	17.7	7.2-7.3	19.5	-
BOD_5	ppm	48-290	477	-	56-100	200	167	435	-	195	-	-	260*	270	90-116	1056	179.7
COD total	ppm	-	-	-	-	-	-	-	724-1004	-	-	640	-	-	245	-	-
COD Dissolved	ppm	-	271	50-400	244-284	411	-	646	210-376	280	400-1000	125-354	520	686	177-277	2568	231.3
TOC	ppm	-	-	-	-	-	-	-	157-184.3	-	-	80.2-93.8	-	-	-	-	174.6
DO	ppm	-	-	-	2-2.7	-	-	-	-	-	-	-	-	-	-	-	2.9
Surfactants	ppm	-	-	-	-	-	-	-	43.5 -54	10.1	0.01-25	-	-	40	-	-	118.3
Total Coliforms	counts/100 ml	2.3E+03-3.3E+05	-	1.20E+03	3.74E+04-3.8E+04	-	-	5.40E+08	-	-	-	-	-	-	1.36E+04	1.0E+07	>200.5
Faecal Coliforms	counts/100 ml	110-1.09E+03	-	-	3.48E+04-3.56E+04	-	4.60E+08	-	-	-	-	-	-	1.0E+06	3.57E+03-1.1E+04	3.0E+05	-

Moderate/Heavy greywater Characteristics	Units	Australia (Christova-Boal et al., 1996) L	Japan (Itayama et al., 2006) K	Korea (Kim et al., 2009) K,S	India (Mandal et al., 2011) M	Nepal (Morel and Diener, 2006) M	Costa Rica (Dallas et al., 2004) M	Brazil (Paulo et al., 2009) S,K,L	Holland (Hernández Leal et al., 2010b, 2011; Leal et al., 2007) M	Slovenia (Sostar-Turk et al., 2005) L	Italy (Ciabatti a et al., 2009) L	Germany (Elmitwalli and Otterpohl, 2007; Li et al., 2003) M	Sweden (World Health, 2006) - M	Israel (Gross et al., 2005) M	Turkey (Atasoy et al., 2007; Masi et al., 2010; Scheuman n et al., 2007) M	Jordan (Halalsheh et al., 2008) M	Oman (Prathapar et al., 2005) L
E.Coli	counts/100 ml	-	-	4.00E+03	-	-	-	5.40E+06	-	-	-	7.5E+03-2.6E+05	-	-	-	2.0E+05	>200.5
Staphylococcus aureus	counts/100 ml	-	-	1.80E+03	-	-	-	-	-	-	-	-	-	-	-	-	-
Salmonella tyohimurium	counts/100 ml	-	-	5.40E+03	-	-	-	-	-	-	-	-	-	-	-	-	-

Table 2. 5: LGW elemental content.

B – Bathroom, S – Shower, W – Washbasin.

Element (ppm)	Australia (Christova-Boal et al., 1996) - B	Israel (Ramona et al., 2004) - S	Oman (Prathapar et al., 2005) – S, W
Ca	3.5-7.9	79.6	15.8-19.7
Mg	1.4-2.3	47.6	21-56.1
Na	7.4-18	106	149-184.5
K	1.5-5.2	10.4	5.5-43.1
B	-	0.14	-
Fe	0.34-1.1	0.19	-
Zn	0.2-6.3	0.18	0.04-2.4
Cu	0.06-0.12	-	0-0.013
Pb	-	<0.02	0.062-0.104
Ni	-	<0.02	0.035
Al	<1	0.03	0.011-0.014
Ba	-	0.13	0
S	1.2-3.3	-	-
Si	3.2-4.1	-	-
Cd	<0.01	-	-
As	0.001	-	0.015-0.03
Se	<0.001	-	-
Cl	9-88	-	-

Table 2. 6: Moderate/Heavy greywater elemental content. L – Laundry, M – Mixed.

Element (ppm)	Australia (Christova-Boal et al., 1996) - L	India (Mandal et al., 2011) - M	Holland (Hernández Leal et al., 2011; Leal et al., 2007) - M	Oman (Prathapar et al., 2005) - L	Sweden (Palmquist and Hanæus, 2005) - M
Ca	3.9-12	-	30-63.2	18.7	31.6-38
Mg	1.1-2.9	-	10-18.4	60.8	5.3-6.22
Na	49-480	43.8-48.1	123.1-144	667	61.4-92.4
K	1.1-17	8.3-15.2	12	23.4	7.69-8.85
B	-	1.3-1.5	0.53-0.65	-	-
Fe	0.29-1	-	0.7-0.74	ND	0.18-0.57
Zn	0.09-0.32	-	0.05-0.13	0.14	0.055-0.078
Cu	<0.05-0.27	-	0.07-0.1	0.0064	0.047-0.07
Pb	-	-	-	0.083	0.002-0.003
Ni	-	-	-	0.035	0.0045-0.028
Al	<1-21	-	1.22-3.9	0.081	1.48-3.39
Ba	-	-	-	ND	0.016-0.022
S	9.5-40	-	20-26.1	-	22.4-25.7
Si	3.8-49	-	16.7	-	-
Cd	<0.01	-	-	ND	0.00006-0.00016
As	0.001-0.007	-	-	0	ND
Se	<0.001	-	-	-	-
Cl	9-88	7.4-12.9	65.4	-	-

Table 2. 7 (Continued next page): Water reuse guidelines and standards for different countries. TC – Total Coliforms (counts/100 ml), FC – Faecal Coliforms (counts/100 ml), E.C – E. Coli (counts/100 ml), ThC – Thermotolerant Coliforms (counts/100 ml), PA – Pseudomonas Aeruginosa (counts/100 ml), NE – Nematode Eggs (counts/l), ND – Non Detectable, * - BOD_7 value reported.

Standards	Application	Turbidity (NTU)	BOD_5 (ppm)	COD (ppm)	SS (ppm)	Residual Cl (ppm)	N (ppm)	P (ppm)	pH	TC	FC	EC	ThC	PA	NE
Australia - Victoria (Victoria. Environment Protection, 2003)	Urban, agricultural and environmental with human exposure	<2	<10	-	<5	1	-	-	6-9	-	-	<10	-	-	-
	Urban, agricultural and environmental with controlled human exposure	-	<20	-	<30	-	-	-	6-9	-	-	<1000	-	-	-
Australia - ACT (2004)	Subsurface Irrigation	-	≤20	-	≤30	-	-	-	-	-	-	-	-	-	-
	Surface irrigation, toilet flushing	-	≤20	-	≤30	-	-	-	-	-	-	-	<10	-	-
Canada (Chaillou et al., 2011)	Household reclaimed water (e.g., toilet flushing)	<2	<10	-	<10	>0.5	-	-	-	-	-	ND	ND	-	-
China (Lin et al., 2005)	Non potable use (e.g. toilet flushing)	≤10	≤10	≤50	≤10	≥0.2	-	-	6.5-9	-	-	≤0.3	-	-	-
EU (Nolde, 2005)	Bathing water	-	<5*	-	-	-	-	-	-	<1E+04	-	<1000	-	<100	-
Germany (Nolde, 2000)	Service water reuse	-	<5*	-	-	-	-	-	-	<1E+04	<1000	-	-	<100	-
Greece (Andreadakis et al., 2001)	Restricted irrigation	-	<25	-	<35	-	-	-	-	-	<200	-	-	-	-
	Unrestricted irrigation/Urban non potable reuse	<2	<10	-	<10	-	-	-	-	-	<5	-	-	-	-
Italy (Ciabattia et al., 2009)	Release into surface water	-	-	<160	<80	-	-	<10	5.5-9.5	-	-	-	-	-	-
Japan (Asano et al., 1996)	Toilet flushing	-	-	-	-	Trace	-	-	5.8-8.6	≤10	-	-	-	-	-
	Landscape irrigation	-	-	-	-	≤0.4	-	-	5.8-8.6	ND	-	-	-	-	-
	Environmental water	≤10	≤10	-	-	-	-	-	5.8-8.6	ND	-	-	-	-	-
Jordan (Halalsheh et al., 2008)	Category A irrigation (cooked vegetables)	-	<30	<100	<50	-	<45	-	6-9	-	-	<100	-	-	≤1
	Category B irrigation (tree crops)	-	<200	<500	<150	-	<70	-	6-9	-	-	<1000	-	-	≤1
	Category C irrigation (fodder crops)	-	<300	<500	<150	-	<70	-	6-9	-	-	-	-	-	≤1
Korea (Kim et al., 2009)	Unrestricted non potable reuse	<2	-	<20	<5	-	-	-	-	-	-	0	-	-	-
Slovenia (Sostar-Turk et al., 2005)	Release into surface water	-	<30	<200	<80	0.2	<10	<1	6.5-9	-	-	-	-	-	-
Spain (Chaillou et al., 2011)	Residential urban reuse	<2	-	-	<10	-	-	-		-	-	0	-	-	≤0.1

Standards	Application	Turbidity (NTU)	BOD^5 (ppm)	COD (ppm)	SS (ppm)	Residual Cl (ppm)	N (ppm)	P (ppm)	pH	TC	FC	EC	ThC	PA	NE
Taiwan (Lin et al., 2005)	Non potable use (e.g. toilet flushing)	-	≤10	-	-	Trace	-	-	6.8-8.5	-	-	≤10	-	-	-
Turkey (Ref 42)	Irrigation	-	≤100	-	≤45	-	-	-	6.5-8.5	-	≤100	-	-	-	-
USA - EPA (1992)	Urban reuse (landscape irrigation, toilet flushing)	≤2	≤10*	-	-	≥1	-	-	6-9	-	ND	-	-	-	-
WHO guidelines for greywater reuse (World Health, 2006)	Restricted irrigation	-	-	-	-	-	-	-	-	-	-	<1E+04	-	-	<1
	Unrestricted irrigation	-	-	-	-	-	-	-	-	-	-	<1,000	-	-	<1

2.1.3.1 Physical parameters

The ranges of electrical conductivity, turbidity and suspended solids for HGW are 190 - 3000 μScm^{-1}, 19 - 444 NTU and 12 - 315 ppm respectively while for LGW these ranges are 14 - 1241 μScm^{-1}, 12.6 - 375 NTU and 29 - 505 ppm respectively. Except for the high turbidity and suspended solids found in Omani LGW (probably due to the presence of sand), the physical characteristics of HGW are higher than those of LGW due to the input from laundry and kitchen greywater. Moreover, the high end range of electrical conductivity (645 – 1241 μScm^{-1}) for LGW arises in water scarce countries Morocco, Spain and Israel.

Laundry greywater has high metal and soiling content, hence increases the EC and turbidity while kitchen greywater adds food particles to the HGW. It needs to be pointed out however that poor or old plumbing and piping systems may suffer from corrosion and leaching of dissolved elements in greywater, increasing the EC concentration.

2.1.3.2 Chemical parameters

The pH range for HGW (6.35 - 10) is generally higher than that of LGW (6.4 - 8.1), probably due to a higher detergent concentration. The BOD and $COD_{dissolved}$ are within the ranges 44 - 1056 ppm and 50 - 2568 ppm for HGW and 23 - 300 ppm and 23 - 633 ppm for LGW. Kitchen greywater contains biodegradable dissolved food particles which contribute to the BOD while the high $COD_{dissolved}$ for HGW is probably due to the presence of detergents from laundry powders and dishwashing liquids. The nutrients N and P are also higher in HGW (2.75 - 57.7 ppm and 0.062 - 42 ppm respectively) compared to LGW (4.1 - 16.4 ppm and 0.11 - 1.8 ppm respectively) due to kitchen greywater and phosphates from laundry detergents. The high BOD and $COD_{dissolved}$ values in the regions of 300 and 633 ppm for LGW in Germany arose due to the water saving fittings used in the study as well as BOD_7 being used as testing means instead of BOD_5 (which entailed a multiplication factor of 1.17 compared to BOD_5) (Nolde, 2000). Also, the unusually high $COD_{dissolved}$ value for UK LGW (maximum of 575 ppm) that was collected from a university campus, was attributed to the choice of cleaning products as well as the LGW residence time in the collection system (Pidou et al., 2008).

Elemental concentrations will vary according to the water quality and plumbing conditions that prevail in each country. However it is well known that laundry

detergents are a source of heavy metals such as Cd, Cu, Pb, Cr and Zn (Aonghusa and Gray, 2002; Jenkins, 1998). Table 2. 8 lists the recommended elemental concentration for both long and short term irrigation use. From Table 2. 8, both LGW and HGW can be used for long term irrigation except in a few cases where the amounts of B (Mandal et al., 2011), Zn and Cu (Christova-Boal et al., 1996) are too high (1.5, 6.3, 0.27 ppm respectively) such that short term irrigation only is feasible and one case where the concentration of Al reported (Christova-Boal et al., 1996) is too high (21 ppm) for any irrigation type.

Table 2. 8: Recommended elemental composition of WW for long and short term irrigation (1992).

NA – Not Applicable, TDS Component – Element is a TDS component for which the sum should lie between 500 and 2000 ppm.

Element	Long term (ppm)	Short term (ppm)
Ca	TDS Component	TDS Component
Mg	TDS Component	TDS Component
Na	TDS Component	TDS Component
K	TDS Component	TDS Component
B	0.75	2
Fe	5	20
Zn	2	10
Cu	0.2	5
Pb	5	10
Ni	0.2	2
Al	5	20
Ba	TDS Component	TDS Component
S	NA	NA
Si	NA	NA
Cd	0.01	0.05
As	0.1	2
Se	0.02	0.02
Cl	TDS Component	TDS Component

2.1.3.3 Xenobiotic organic compounds (XOC's)

XOC's are synthetic organic compounds that are present in household chemicals and pharmaceuticals. XOC's can also be formed when chemicals are partially modified via chemical/biological treatment (Fatta-Kassinos et al., 2010). XOC's are hazardous in that they are recalcitrant to treatment processes and can accumulate in plants and animals, inducing biological effects (Fatta-Kassinos et al., 2010). On the other hand, some pharmaceuticals such as antibiotics, when discharged in the environment may lead to the creation or proliferation of resistant strains bacteria (Le-Minh et al.,

2010). Due to the vast number of those chemicals, it is impossible to measure all hazardous substances possibly contributing to the chemical risks associated with wastewater (Palmquist and Hanæus, 2005). Revitt *et al.* (2011) measured the presence of benzene and 4-Nitrophenol in greywater. Palmquist and Hanaeus (2005) discovered 46 hazardous organic substances (nonylphenol- and octylphenol ethoxylates, brominated flame retardants, organotin compounds, PAH, phthalates, monocyclic aromatics and triclosan) in greywater out of a selection of 81 measured substances. Eriksson et al (2002) identified 900 potential XOC's in greywater solely based on the ingredients of different types of common cosmetics and detergents used in Denmark.

Other priority pollutants in greywater are heavy metals such as As, Cu, Cr, Cd, Pg, Hg and Ni. Heavy metals can originate from various sources such as laundry detergents (Aonghusa and Gray, 2002; Jenkins, 1998), plumbing materials and dental amalgams (Hg) (Donner et al., 2008).

XOCs are usually not an issue when the duties include toilet flushing or floor cleaning but should be considered if the water is reused for irrigation or groundwater recharge (Gulyas et al., 2007b).

2.1.3.4 Microorganisms

Microorganisms such as bacteria, protozoa and helminths can be introduced in greywater via bodily contact. Occasionally, enteric pathogenic bacteria such as Salmonella and Campylobacter can be introduced by inadequate food handling in the kitchen although the individual risk is higher from direct handling of the contaminated food (Ottosson, 2003; World Health, 2006). The most common indicators to assess faecal contamination are Coliform bacteria (e.g., Faecal Coliforms, Thermotolerant Coliforms), Faecal Streptococci (Enterococci) and E. Coli. Skin associated bacteria Staphylococcus Aureus and Pseudomonas Aerugina can also be expected in greywater and were detected by Winward *et al.* (2008a) and Gilboa and Friedler (2008), who also found Clostridium Perfringes spores, which are present in human and animal faecal matter (Ottosson, 2003). A list of water and excreta related pathogens has been reported in the literature (Eriksson et al., 2002; Ottosson, 2003).

2.2 Greywater Reuse and Guidelines

Many countries have individually produced their own water reuse guidelines depending on their needs (Pidou et al., 2007). Some standards for greywater reuse/release have been adapted from those of reclaimed domestic wastewater. However, countries such as Australia, Japan and USA, where greywater recycling is an established operation, greywater reuse guidelines are available (Jefferson et al., 2000). In some European countries such as the UK and Germany, bathing water standards are used. Some wastewater reuse/release standards for several countries are presented in Table 2. 7. Each country has its level of stringency; for instance, the water quality requirement for irrigation according to the USA EPA is much higher than the Jordanian standards (aesthetically and hygienically) or the European bathing water quality standards (hygienically).

The standards in general cover the aesthetic (BOD, COD, turbidity), hygienic (total coliforms, faecal coliforms) and technical (suspended solids) issues associated with greywater.

2.3 Public Acceptance

The successful implementation of any reuse projects hinges on public acceptance (Farrelly, 2009; Po et al., 2003). The factors that can influence public acceptance towards greywater treatment are socio demographic, age, level of education, religion, water availability, cost, source of the influent, use of the effluent, environmental awareness, health risks and income (Domenech and Saurí, 2010; Friedler et al., 2006; Madany et al., 1992; Pham et al., 2011; Po et al., 2003; Ryan et al., 2009). The common trend for recycled water reuse is that the closer the water is to human contact (e.g., laundry, shower) or ingestion, the more opposition towards public acceptance will be faced.

The implementation of greywater treatment should not be a difficult feat since the degree of acceptance from the public is higher for recycled greywater reuse than for domestic WW reuse (Po et al., 2003). Moreover, people are willing to trade-off some comfort level such as smells from greywater treatment system (Domenech and Saurí, 2010) as long as it had a positive impact on the environment.

The government and public sectors need to do their part too such as subsidies or rebates for the installation of a dual piping and storage system for separately

collected greywater (Pinto and Maheshwari, 2010). Before implementation of any reuse project, the media should be used to increase the public awareness regarding the science and benefits involved with recycling as well as successful past projects. User friendly information packages should be easily accessible to create a "greywater reuse literacy" within the community (Pinto and Maheshwari, 2010). Public trust could be earned by building demonstration sites that are open to the public prior to the full scale implementation of a greywater recycling project (Po et al., 2003).

2.4 Treatment of Greywater

This section looks at the different methods of greywater treatment, including the effect of reuse without treatment.

2.4.1 Greywater reuse without treatment

Greywater reuse without treatment is common. Bath water reuse for garden watering has been practiced for centuries (Jefferson et al., 2000). Greywater is now commonly used in countries such as Australia, Syria and South Africa for garden and lawn watering (Dalahmeh et al., 2009; Jacobs and Van Staden, 2008; Ryan et al., 2009), Israel for landscape irrigation (Ronen et al., 2010) and Jordan to irrigate fruit trees (Halalsheh et al., 2008).

The variety and amount of nutrients found in greywater can be either good or bad for plants, depending on the plant used (Jacobs and Van Staden, 2008). Use of greywater was found to have no adverse effects on tomato (Misra et al., 2010), silverbeet (Pinto et al., 2010) and residential lawns (Jacobs and Van Staden, 2008) and even increased the growth and yield of Swiss chard and carrots due to the presence of micronutrients (Zn, Mn and Cu) and macronutrients (N, S, P, Ca, K and Mg) (Rodda et al., 2011), while another research (Garland et al., 2004) found that relatively small areas (3-5 m^2) of dwarf wheat can process per capita production of mixed surfactants with minimal effects on plant growth. However, long term studies (Garland et al., 2004; Misra et al., 2010) and health and safety effects on humans had not been addressed (Jacobs and Van Staden, 2008; Misra et al., 2010).

Nevertheless, greywater treatment before reuse is strongly recommended. Pathogens present in greywater can be transmitted as volatiles during toilet flushing or irrigation. Long term irrigation with untreated greywater can lead to build up of salts, surfactants, alkalinity, oil, grease and boron which can affect plants' health, soil

properties (such as water retention capacity) and eventually contaminate groundwater (Christova-Boal et al., 1996; Gross et al., 2005; Gross et al., 2007b; Gross et al., 2008; Misra et al., 2010; Misra and Sivongxay, 2009; Pinto and Maheshwari, 2010; Travis et al., 2008; Wiel-Shafran et al., 2006). Untreated greywater used for toilet flushing may leave stains on the toilet bowl, encouraging the user to use increased amounts of toilet cleaner hence reducing the viability of greywater reuse (Christova-Boal et al., 1996).

The minimum treatment required for irrigation is filtration so as to prevent clogging in piping systems. Subsurface irrigation is preferred for filtered greywater so as to prevent transmission of harmful volatile organics and pathogens as well as pooling (breeding space for mosquitoes) (Christova-Boal et al., 1996; Gulyas, 2007).

2.4.2 Greywater storage

Storing greywater can be aesthetically and hygienically detrimental. The organic matter within the greywater can undergo anaerobic degradation and release unpleasant odours while the settled solids release soluble COD fractions in the greywater (Dixon et al., 2000). Moreover, tanks storing greywater provide an ideal breeding ground for mosquitoes and pathogenic organisms (Christova-Boal et al., 1996). Within 48 hours, the number of counts of total coliforms and faecal coliforms in stored greywater can increase from 10^0-10^5/100 ml to above 10^5/100 ml (Al-Jayyousi, 2003).

Dixon *et al.* (2000) studied the change in quality of stored untreated greywater. They concluded that storing greywater for 24 hours can significantly improve water quality due to the rapid settlement of organic particles while not greatly affecting the coliform counts, except for families with young children (Rose et al., 1991), whereby the coliform levels are higher. This, in turn, reduces the load on subsequent treatment systems. However, beyond 48 hours DO levels drop substantially and lead to aesthetic problems.

2.4.3 Biological systems

The suggested COD:N:P ratio for biological treatment as per the treatment of domestic WW is 100:20:1 (Li et al., 2009b) while the dosing of micronutrients Zn and Cu was also suggested for greywater (Jefferson et al., 2001). Furthermore, a ratio of BOD:COD $\geq$ 0.5 indicates good potential for biological treatment (Palmquist and

Hanæus, 2005). Biological systems that have been used to treat greywater include, among others, the BAF (Biological Aerated Filter) (Lodge et al., 2004), MBR (Membrane Bio-Reactor) (Atasoy et al., 2007; Hernández Leal et al., 2010a; Huelgas and Funamizu, 2010; Merz et al., 2007; Paris and Schlapp, 2010), SBR (Sequencing Batch Reactor) (Kraume et al., 2010; McAdam et al., 2005; Shin and Lee, 1998), UASB (Upflow Anaerobic Sludge Blanket) (Elmitwalli and Otterpohl, 2007; Leal et al., 2007), RBC (Rotating Biological Contactor) (Friedler et al., 2005; Nolde, 2000) and the FBR (Fluidised Bed Reactor) (Nolde, 2000). Biological systems are usually preceded by a coarse filtration stage and followed by sedimentation/filtration to remove biosolids or sludge and a disinfection stage (chlorination, UV) to remove micro-organisms. Some systems have in-built filters such as the MBR which has a membrane filter within the reactor. Examples of biological systems are included in Table 2. 9. Such systems can efficiently reduce organics and nutrients with both LGW and HGW but disinfection as a final step is required to remove pathogens.

The MBR has been used successfully with either LGW or HGW (Atasoy et al., 2007; Huelgas and Funamizu, 2010; Merz et al., 2007; Winward et al., 2008a), even when urine was present (Paris and Schlapp, 2010). Atasoy *et al.* (2007) used a pilot scale MBR (600 L) to treat mixed greywater of initial average COD_{Total} = 245 ppm. The removal of BOD, COD, TSS and TN were >95%, 95%, 94% and 92% respectively while total and faecal coliforms were not detected in the effluent. This resulted in a high quality effluent standard that complied with reuse standards for different purposes. MBR technology was also successful treating lower strength shower water (initial COD = 109 ppm) from a sports and leisure club (Merz et al., 2007). The permeate was of excellent aesthetic and hygienic quality and met the commonly adopted standards for toilet flushing or other household uses. The microfiltration membranes within the MBR act as a barrier against microorganisms such that additional disinfection stage is not required. Whenever bacterial contamination did occur, this was attributed to the design of the treatment rig (permeate reservoir was too close to the reactor) rather than membrane performance. MBRs can deal with varying influent quality and quantity and are an attractive option whenever space is limited as they occupy a small footprint (Merz et al., 2007). Still, MBRs have a high investment and maintenance cost mainly due to membrane fouling and a low hydraulic residence time (HRT) meaning high energy demand to maintain permeate

flux and aerate the slurry. Additionally, appropriate control strategies should be implemented so as to prevent biomass washout (Winward et al., 2008a) and allow daily aeration in the sludge even during vacation periods so as to maintain biological activity (Abegglen et al., 2008).

The RBC and FBR were efficient at treating LGW (Nolde, 2000). Nolde (2000) found that the effluent BOD concentration was always less than 5 ppm when treating greywater from the shower, bath and/or washbasins with initial BOD concentration in the range 50-250 ppm and 70-300 ppm for the RBC and FBR respectively. Good effluent microbial quality was obtained even when the influent was spiked with faecal bacteria from the washing of baby diapers. Both systems had small footprints but the RBC was fed at a much higher rate (2100-2450 $Lday^{-1}$ versus 30-40 $Lday^{-1}$ for the FBR). Friedler *et al.* (2005) obtained very high quality effluent that met the highest Israeli regulations for urban reuse by treating LGW with initial BOD and COD_{Total} of 59 ppm and 158 ppm respectively. The RBC necessitates lower maintenance if the number of stages are increased (while keeping the same volume) (Nolde, 2000) but are more efficient at removing BOD instead of COD (Friedler et al., 2005). The RBC was also found to remove micropollutants such as parabens in greywater (Eriksson et al., 2009).

Anaerobic treatment of greywater has been investigated using the UASB (Elmitwalli and Otterpohl, 2007; Leal et al., 2007) and anaerobic reactor (Leal et al., 2007). While the methanogenic activity was deemed sufficient to perform biodegradation process (Abu Ghunmi et al., 2010; Elmitwalli and Otterpohl, 2007), anaerobic treatment can be slow (Hernández Leal et al., 2011) and not very efficient at removing pollutants. Only 40% COD removal were achieved at an HRT of 12-24 h with a UASB compared to 90% COD removal using an aerobic fed batch reactor of similar volumetric size (3.6 L) (Leal et al., 2007). Nutrients removal, TN and TP, were 21.7-29.8% and 15.2-20.6% respectively for the UASB (Elmitwalli and Otterpohl, 2007) and 17% and 10% respectively for the anaerobic reactor. Nevertheless, good treatment can be achieved if anaerobic treatment is used as pre-treatment and combined with aerobic treatment (Abu Ghunmi et al., 2010); however, proper insulation and effluent disinfection are required. On the other hand, it has been argued that the limited energy gain from such combined system renders the option unfeasible (Hernández Leal et al., 2010b). The presence of a high

concentration of surfactants can heavily impair the production of methane during anaerobic treatment (Abu Ghunmi et al., 2010; Hernández Leal et al., 2010b, 2011). Hernandez *et al.* (2007) showed that dilution of greywater had a positive effect on the UASB reactor as no methane was generated with concentrated greywater probably due to the toxic effect of surfactants on bacteria. The UASB is much more efficient at removing suspended COD rather than colloidal or dissolved COD (Hernández Leal et al., 2010b) which, along with its low cost and simplicity, makes it an attractive prospect for the treatment of Jordanian greywater, which is high in suspended COD fraction (Halalsheh et al., 2008). Furthermore, a recent study (Hernández Leal et al., 2012) has shown that aerobic treatment was better than anaerobic treatment at the removal of toxic effects in greywater.

Greywater methane production can be boosted via bioflocculation. Hernandez *et al.* (2010a) used a high loaded MBR operating at short HRT and SRT to achieve high COD concentration and minimize mineralisation. The concentrate obtained, if added to the anaerobic treatment of BW, had the potential of increasing methane production by 73%. The permeate produced had a COD in the range of 200 ppm meaning that further treatment would be necessary before reuse or discharge.

2.4.4 Physical systems

Physical systems include filtration and sedimentation. Filtration is usually used as a pre-treatment stage before biological or chemical treatment or as a post treatment prior to disinfection. Filtration as a pre-treatment include screen meshes (Mandal et al., 2011), sand bed filtration (Chaillou et al., 2011), nylon sock type filtration (March et al., 2004), metal strainers (Al-Jayyousi, 2003), gravel filtration (Al-Hamaiedeh and Bino, 2010; Mandal et al., 2011) and mulch tower system (Tandlich et al., 2009; Zuma et al., 2009). As can be seen from Table 2. 10, physical systems on their own are not very efficient at removing organics, nutrients and pathogens. They are mainly used in cases where the water quality required is not high or alternatively as a pre-treatment step.

Filtration as a pre-treatment is required to remove as much TSS and COD_{ss} as possible before further treatment. Solid particles can shed pathogens from disinfectants (UV, chlorine) and organic matter can form disinfectant by-products (chloramines, trihalomethanes) which have lower disinfectant capabilities.

Furthermore a short residence time is required so as to maintain the chemical nature of the greywater. While solid particles get trapped within the filtration matrix, COD and BOD removal is assisted by a biofilm layer that eventually forms on the surface of the filtration medium (gravel, sand, mulch) (Chaillou et al., 2011; Zuma et al., 2009). However, occasional detachment of the biofilm layer that gets entrained in the effluent, leading to increases in COD and TSS have been observed (Chaillou et al., 2011; Zuma et al., 2009). Chaillou *et al.* (2011) investigated the potential of a sand bed filter to treat bathroom greywater. A mean removal of 30% COD and a maximum E.Coli removal of two log CFU/100 mL was observed. In some cases, there were increases in TSS, COD and total coliforms which were attributed to biofilm detachment. The poor overall treatment showed that secondary treatment followed by disinfection was required. Similarly, Zuma *et al.* (2009) observed that a mulch tower system consisting of mulch, coarse sand, fine gravel and coarse gravel removed 26% of COD and 52% of TSS while the level of faecal coliforms and total coliforms remained unchanged.

Filtration has also been used as a main treatment for greywater. March *et al.* (2004) reported the use of a filtration system (nylon sock type) followed by sedimentation and disinfection by hypochlorite addition in a hotel in Spain. The system treats greywater from the shower and washbasins which is then used for toilet flushing. Despite having a low aesthetic level due to turbidity and suspended solids, the use of treated greywater was publicly accepted for its contribution to water savings.

Gravel used as a filtration medium produced an effluent of quality enough for crop irrigation (Al-Hamaiedeh and Bino, 2010) although occasional soil leaching with fresh water was recommended to remove accumulated salts and organic matter. In another case (Mandal et al., 2011) the effluent was used for toilet flushing and irrigation even though pathogens such as E.Coli and salmonella sp. were still present.

Membrane filtration (metal membranes (Kim et al., 2007), MF, UF and NF (Ramona et al., 2004; Shin and Lee, 1998)) produce an effluent of high quality that is proportional to the molecular weight cut-off (MWCO) of the membrane. UF membranes with pores in the range 30-200 kDa have been reported to reject turbidity and organic matter between 92-97% and 45-70% respectively (Ramona et al., 2004). The permeate obtained with NF membranes is of even better quality as they remove

soluble organic matter and ionic species, pathogens and even viruses. Ramona *et al.* (2004) obtained a very high permeate quality when treating shower water via NF. The removal of COD, TOC and soluble ionic species were 93%, 84% and 50% respectively resulting in a permeate quality well suited for all purpose unrestricted reuse. However, trace contaminants responsible for fouling such as SDS, humic acid and calcium need to be monitored (Oschmann et al., 2005; Schafer et al., 2006) and a proper cleaning strategy needs to be devised.

2.4.5 Chemical systems

The chemical treatment of greywater is getting more attention, the main processes being coagulation (Ciabattia et al., 2009; Friedler et al., 2008; Pidou et al., 2008; Sostar-Turk et al., 2005), electrocoagulation (Lin et al., 2005), adsorption using granular activated carbon (GAC) (Ciabattia et al., 2009; Sostar-Turk et al., 2005) and natural zeolites (Widiastuti et al., 2011; Widiastuti et al., 2008), magnetic ion exchange resin (MIEX®) (Pidou et al., 2008), powdered activated carbon (PAC) (Gulyas et al., 2007a)) and advanced oxidation processes (AOPs) such as ozonation (Ciabattia et al., 2009; Leal et al., 2011), photocatalysis (Gulyas et al., 2007a; Li et al., 2003; Rivero et al., 2006; Sanchez et al., 2010b; Zhu et al., 2008) and UVC/H_2O_2 (Chin et al., 2009). Examples of chemical systems are shown in Table 2. 11. They are efficient with LGW and in some cases, laundry greywater. They can also be used with HGW (Mixed) as a final treatment step, following biological treatment (Li et al., 2003). Moreover, when photocatalysis is used, disinfection is generally not required since UV light assists at eliminating pathogens (Li et al., 2003).

Sostar-Turk *et al.* (2005) used coagulation followed by adsorption on granular activated carbon (GAC) to treat laundry effluent. Coagulation is the agglomeration of dispersed particles via a flocculant. The greywater was flocculated with Al^{3+} and filtered through a sand bed. Since the resulting filtrate was still high in organic content, it was subjected to adsorption by GAC. A more complicated system (coagulation-flocculation-dissolved air flotation-sand filtration-ozonation-GAC adsorption) was used at pilot scale to treat 15 m^3day^{-1} laundry effluents (Ciabattia et al., 2009). In both cases, the effluent was within the local regulatory limits for discharge to surface water. Standalone coagulation (alum or ferric) or adsorption treatment using MIEX® can be suitable for low strength bathroom greywater but not medium to high strength bathroom greywater (even when combined and at higher

doses), due to a recalcitrant proportion of the greywater towards chemical treatment (Pidou et al., 2008).

Electrocoagulation was effective at treating shower water from a building (Lin et al., 2005). The coagulant was produced from the evolution of Al^{3+} at the aluminium anodes. Hydrogen was produced at the cathodes and the bubbles assisted at floating the particles which were skimmed out in a separate vessel. Disinfection with sodium hypochlorate was required to eliminate all E.Coli in the greywater. The water quality obtained satisfied the general guidelines for non potable reuse. The system capacity was 28 m^3day^{-1}, had footprint of only 8 m^2 and total cost of US\$0.27m^{-3}, which was below the local potable water rate.

Coagulation or chlorination was found to be a useful pre-treatment step for greywater treatment with membranes (Friedler et al., 2008). Addition of chlorine at a dose of 10-20 ppm reduced biofouling in an UF membrane by 33% by inhibiting microbial activity while dosing 50 ppm ferric chloride reduced the UF flux decline by 43% due to the formation of larger, more porous particles. However combined coagulation and chlorination increased the fouling rate in a RO membrane due to an increase in the concentration polarization phenomenon.

Natural zeolites can remove inorganic anions and cations as well as microorganisms from wastewater (Widiastuti et al., 2008). Zeolites are porous structures that have a large surface area for absorption. Widiastuti *et al.* (2011) reported up to 97% removal of ammonium from greywater with Australian natural zeolite.

Photocatalysis with titanium dioxide (TiO_2) catalysts was an efficient post-treatment to biological systems (Gulyas et al., 2007a; Li et al., 2003) giving very high quality water that could be used for groundwater recharge. Photocatalysis is the use of a catalyst, UV light and an oxidant to oxidise organic pollutants in air or water. The photocatalytic stage assisted at mineralising recalcitrant dissolved organics as well as partially degrading organic compounds resulting from the biological stage. Moreover a disinfection step is not required as photocatalysis can greatly reduce pathogens in water (Li et al., 2003; Van Grieken et al., 2009). Sanchez *et al.* (2010b) successfully obtained 65% dissolved organic carbon (DOC) removal from hotel grey water using photocatalysis. Biotreated water was found to have a tendency to agglomerate TiO_2 particles such that mixing powdered activated carbon (PAC) with TiO_2 showed better

results than using TiO_2 alone, due to adsorption of pollutants onto PAC (Gulyas et al., 2007a). However, a long irradiation time (49 hours) was required to reduce the TOC levels of the greywater from 10 ppm to ≤2 ppm. Combined photocatalysis and membrane filtration of shower greywater was studied by Rivero *et al.* (2006). This system was advantageous in that greywater could be treated in a continuous mode and the membrane could fully recover the catalyst as well as reject partially organic species. However, products such as shower gels and conditioners can rapidly foul membranes in membrane coupled photoreactors (Pidou et al., 2009). This fouling is caused by the formation of large organo-TiO_2 aggregates caused from polymers in the products, which upon breaking release a large proportion of fines that clog the membranes. Membrane fouling can be reduced by increasing the irradiation time (Pidou et al., 2009).

Both ozonation and adsorption onto GAC were found to be effective post treatments at removing recalcitrant micropollutants from greywater following biological treatment (Leal et al., 2011). Conversely, AOPs could also be an effective pre-treatment for greywater. Chin *et al.* (2009) obtained good COD removal (87%) from HGW after 3 h treatment with a combination of UVC and 10 mM H_2O_2. The resulting effluent had a BOD_5:COD ratio of 0.41, which had the potential to be bio-treated.

2.4.6 Natural systems

Natural systems that use natural media for filtration and biological degradation are very common, mainly in low to middle income countries due to their low cost. They can be used as primary or secondary treatment but a disinfection stage is required if a low pathogen effluent is wanted. Some examples are sand filter, horizontal flow constructed wetland (HFCW), vertical flow constructed wetland (VFCW), anaerobic filter and vertical flow filter (VFF). These systems undergo combined physical processes such as filtration through a filter media (sand, gravel, rocks, cinder) with biological processes such as aerobic or anaerobic degradation via microorganisms found within the system (biofilm, plant roots, slugs, earthworms). Chemical precipitation and adsorption processes are also believed to take place (Kivaisi, 2001). Nutrient uptake in planted systems (VFCW, HFCW) assists at the removal of nutrients such as phosphorus and nitrogen. Natural systems (Table 2. 12) are generally used with HGW and sometimes give very good quality effluents (Gross et

al., 2007b; Masi et al., 2010). Depending on the reuse objective, disinfection is required as final step.

Itayama *et al.* (2006) used a slanted soil system to treat kitchen greywater. The system used a special soil (Kanuma soil) and was slanted to allow gravity flow. Organic pollutants and suspended solids were efficiently removed. The presence of slugs and earthworms in the soils assisted at removing solid food particles such that no clogging occurred in the system. Phosphorus was removed by adsorption onto soil while the presence of aerobic and anaerobic zones helped at nitrogen depletion.

Constructed wetlands/reedbeds have been used as primary (Dallas et al., 2004; Masi et al., 2010; Morel and Diener, 2006; Paulo et al., 2009) or secondary treatment (Masi et al., 2010; Winward et al., 2008a) successfully but a disinfection step is required if high quality effluent is desired. Winward *et al.* (2008a) established that the VFRB was better at removing pathogens compared to HFRB and green roof water recycling technology (GROW). The quality of the effluent can be improved if the system is operated with recirculation (Gross et al., 2007a; Gross et al., 2007b).

Despite their low cost and satisfactory water treatment, natural systems require a large surface area (0.5-3 $m^2 person^{-1}$), experience clogging (Paulo et al., 2009), have long HRT (2-14 days) (Abu Ghunmi et al., 2010), are potential breeding habitats for disease vectors, produce bad odours, are not suited for hot climates where evapotranspiration from plant leaves could exceed inflow (Kivaisi, 2001) and do not remove XOCs efficiently (Gulyas et al., 2007b).

Table 2. 9: Biological treatment systems for greywater.

A – E. Coli, B – TOC, C – PO_4^{3-}, D – HPC, NR – Not Reported.

Treatment train	Greywater source	BOD (ppm)		COD (ppm)		TN (ppm)		TP (ppm)		Total Coliforms (counts/100mL)		Faecal Coliforms (counts/100mL)		Ref
		In	Out	In	Out	In	Out	In	Out	In	Out	In	Out	
Screening (coarse+fine)-Submerged MBR	M	90	<5	245	13	9	0.55	7.3	NR	1.40E+04	0	3.60E+03	NR	(Atasoy et al., 2007)
Anaerobic unit-Aerobic unit	S, L, W	150	60	366	95	12	8	11	7	7.10E+07	1.60E+05	1.4E+06[A]	5.9E+04[A]	(Abu Ghunmi et al., 2010)
MBR	S	59	4	109	15	15.2	5.7	1.6	1.3	-	-	1.40E+05	68	(Merz et al., 2007)
Sedimentation-RBC-UV disinfection	S	50-100	<5	10-200	NR	5-10	NR	0.2-0.6	NR	10E+02-10E+03	<100	0.1-10	<10	(Nolde, 2000)
Sedimentation-FBR-UV disinfection	S	70-300	<5	113-633	4-8[B]	-		-	-	10E+01-10E+03	<100	0.1-10	<10	(Nolde, 2000)
Storage tank-UASB reactor (16 h HRT)	M	-	-	618	222	27.1	19	9.9[C]	8.4[C]	-	-	-	-	(Elmitwalli and Otterpohl, 2007)
Storage tank-RBC-Sedimentation tank-Sand filtration-Chlorination	B, S, W	59	2.3	110	40	-	-	-	-	6.5E+06[D]	3.7E+02[D]	2.90E+05	0	(Friedler et al., 2005)

Table 2. 10: Physical treatment systems for greywater.

Treatment train	Greywater source	BOD (ppm)		COD (ppm)		TN (ppm)		TP (ppm)		Total Coliforms (counts/100mL)		Faecal Coliforms (counts/100mL)		Ref
		In	Out	In	Out	In	Out	In	Out	In	Out	In	Out	
Filtration (nylon sock)-Sedimentation-Chlorination	B, W	-	-	171	78	11.4	7.1	-	-	-	-	-	-	(March et al., 2004)
UF Membrane (200-400 kDa membranes)	S	-	-	74.3-80	37.8-43.8	-	-	-	-	-	-	-	-	(Ramona et al., 2004)
NF Membrane (0.2 kDa membranes)	S	-	-	226	15	-	-	-	-	-	-	-	-	(Ramona et al., 2004)
Sponge/Foam-Coarse filter-Equalisation tanks-Gravel filtration-Aeration and Storage tank	M	56-100	40	244-284	56-140	42.8-57.7	28-52.4	1.5-3.4	1.5-2.1	3.74E+04-3.8E+04	9E+02-1.6E+03	3.48E+04-3.56E+04	2E+02-1.2E+03	(Mandal et al., 2011)
Storage tank-Gravel filtration	M	942	108	1712	489	52	11	-	-	-	-	-	-	(Al-Hamaiedeh and Bino, 2010)
Mulch tower system	M	-	-	965-7900	680-5390	-	-	-	-	-	-	-	-	(Zuma et al., 2009)

Table 2. 11: Chemical treatment systems for greywater.

A – NH_3; B – E.Coli; C – TOC; D – Results before and after photocatalytic stage; NR – Not Reported.

Treatment train	Greywater source	BOD (ppm)		COD (ppm)		TN (ppm)		TP (ppm)		Total Coliforms (counts/100mL)		Faecal Coliforms (counts/100mL)		Ref
		In	Out	In	Out	In	Out	In	Out	In	Out	In	Out	
Storage tank-Electrocoagulation-Flotation-Chlorination	S, W	10-41	5-16	27-102	14-44	0.145-0.148[A]	0.006-0.007[A]	-	-	-	-	3.8E+02-5.6E+02[B]	ND	(Lin et al., 2005)
Coagulation-Sand filtration-GAC adsorption	L	195	10	280	20	2.75	2.6	9.9	1	-	-	-	-	(Sostar-Turk et al., 2005)
Coagulation-DAF-Sand filtration-Ozonation-GAC adsorption	L	-	-	602	140	-	-	-	-	-	-	-	-	(Ciabattia et al., 2009)
VFCW-TiO_2 photocatalysis	M	80.2-93.8[C]	<10[C]	258-354	NR	9.7-16.6	NR	5.2-9.6	NR	3.6E+04[D]	14[D]	7.5E+03-2.6E+05[B]	1[B]	(Li et al., 2003)
TiO_2 photocatalysis combined with MF membrane	S	114-135	2-17	252-324	56-72	-	-	-	-	-	-	-	-	(Rivero et al., 2006)

Table 2. 12: Natural treatment systems for greywater.

A – NH_4^+; B – E. Coli; C – PO_4^{3-}; NR – Not Reported; TS – To Standards.

Treatment train	Greywater source	BOD (ppm)		COD (ppm)		TN (ppm)		TP (ppm)		Total Coliforms (counts/100mL)		Faecal Coliforms (counts/100mL)		Ref
		In	Out	In	Out	In	Out	In	Out	In	Out	In	Out	
HFCW-Pond	M	91	<10	190	<50	1.2[A]	0.5[A]	7.2	NR	-	-	1.10E+04	NR	(Masi et al., 2010)
HFCW-Sand filtration-UV disinfection	M	44	8.8	120	30	9.14[A]	4.5[A]	1.46	0.73	-	-	1.30E+05	TS	(Masi et al., 2010)
UASB-HFCW	M	276	NR	470	63.5	7[A]	4[A]	3.1	NR	-	-	-	-	(Masi et al., 2010)
HFCW-VFCW	M	435.0	21.8	646.0	77.5	8.8	1.6	5.6	2.4	5.4E+08	1.1E+07	5.4E+06[B]	3.8E+05[B]	(Paulo et al., 2009)
Slanted soil system	K	476.7	81.0	270.9	40.6	20.7	4.6	3.8	0.5	-	-	-	-	(Itayama et al., 2006)
RVFCW	M	466	0.7	839	157	34.3	10.8	22.8	6.6	-	-	5.0E+07	2.0E+05	(Gross et al., 2007a)
Settling tank-2 stage reedbeds-Pond	M	167	2.5	-	-	-	-	16[C]	4[C]	-	-	1.5E+08	132	(Dallas et al., 2004)

Table 2. 13: Examples of greywater treatment systems being used around the world.

Project location	Project Description	Treatment Method	Effluent Use	Ref
Vibyasen housing, Sweden	Treatment of greywater (M) for a block of 47 houses consisting of 169 persons	Sedimentation tank-Biofilm (Puracomb©) treatment-Filter beds-Pond system	Environmental discharge/Ornamental	(Palmquist and Hanæus, 2005)
Mallorca Island, Spain	Treatment of mixture of RO rejection flow and greywater (B) for a hotel with maximum occupancy of 1000 clients	Chlorination-2 step filtration (nylon sock followed by sand filtration)	Toilet flushing	(Gual et al., 2008)
Inkeman oasis, Melbourne, Australia	Treatment of greywater (S, B, W) from 100 apartments	MBR-UV disinfection-Storage tank	Toilet flushing, garden irrigation	(Farrelly, 2009; Goddard, 2006)
Palmyra project, Western Australia	Treatment of greywater (M) for a block of 6 units consisting of a maximum of 10 persons	Aerobic treatment-Chlorination	Toiler flushing, garden irrigation	(Bingley, 1996)
	Treatment of greywater (S, B, W) for a housing block consisting of 70 persons	Sedimentation tank-4 stage RBC-UV treatment	Toilet flushing	(Nolde, 2000)
Berlin, Germany	Treatment of greywater for a house consisting of 2 persons	Sedimentation tank-2 stage FBR-UV treatment	Toilet flushing	(Nolde, 2000)
Santa Elena-Monteverde, Costa Rica	Treatment of greywater (M) for 3 houses with 7 persons	Settling tank-2 stage reedbeds-Pond system	Environmental discharge/Ornamental	(Dallas et al., 2004)
Kathmandu, Nepal	Treatment of greywater (M) for a 7 persons household	Settling tank-Dosing chamber-VFCW-Storage tank	Irrigation, vehicle washing, toilet flushing	(Morel and Diener, 2006)
Millenium dome, UK	Treatment of a mixture of rainwater, groundwater and greywater (W) for a stadium (500 m^3day^{-1})	BAF-UF-RO	Toilet/urinal flushing	(Smith et al., 2000)
Tokyo dome, Japan	Treatment of a mixture of rainwater and greywater (B, K) for a stadium (622 m^3day^{-1})	Aerobic treatment (Deep shaft process)-Sand filtration-Storage tank	Toilet flushing	(Lazarova et al., 2003; Zaizen et al., 2000)
Technion campus, Israel	Treatment of greywater (B, S, W) from 7 flats in a campus	Equalisation tank-RBC-Sedimentation tank-Sand filtration-Chlorination	Toilet flushing	(Friedler et al., 2005)

2.4.7 Disinfection

Following treatment, the treated greywater has to undergo disinfection. The most common disinfection procedure for greywater is chlorination using sodium hypochlorite (Chaillou et al., 2011; Friedler et al., 2005; Gual et al., 2008; Lin et al., 2005; March et al., 2004). However chlorination presents a few drawbacks. Organics present in greywater can react with the chlorine to form carcinogenic chloroforms or other halogenated organics (Gual et al., 2008; Gulyas, 2007) that can be harmful to plants and animals. As a result, the amount of chlorine required will depend on the treatment applied such that studies on the minimization of the disinfectant dosage will need to be carried out (Gual et al., 2008). Gulyas *et al.* (2007) warned against the use of chlorinated greywater for irrigation reuse as residual chlorine is toxic to plants.

Alternatives to chlorination are UV (Friedler and Gilboa, 2010; Gilboa and Friedler, 2008; Goddard, 2006; Nolde, 2000, 2005), hydrogen peroxide plus (HPP) (Ronen et al., 2010), ozonation (Kim et al., 2009) and essential oils (Winward et al., 2008c). Ronen *et al.* (2010) showed that HPP could be an attractive alternative to chlorination for greywater disinfection in small communities and households with the added benefit that it does not produce toxic by-products. Essential oils such as Origanum EO was found to almost completely remove total coliforms in treated greywater and prevent their regrowth for up to 14 days (Winward et al., 2008c). Ozonation for up to 15 minutes could remove 100% of pathogens from greywater following biological-membrane filtration treatment (Kim et al., 2009).

UV irradiation was applied in Germany (Nolde, 2000, 2005) and offers a number of advantages over chlorination such as: no need for dosage and storage units for disinfectant, removal of a wide range of pathogens including many chlorine resistant ones (Friedler and Gilboa, 2010; Gilboa and Friedler, 2008), safety and no toxic by-products formed (Friedler and Gilboa, 2010). Nolde (2000) recommended a UV dose between 250 and 400 Jm^{-2} for biologically treated greywater. Gilboa and Friedler (2008) performed a more detailed work on the effect of UV treatment on RBC treated greywater by monitoring its effect on heterotrophic plate counts HPC), faecal coliforms (FC), P. aeruginosa sp. and S. aureus sp. At doses of up to 690 Jm^{-2}, FC were the most resistant bacteria, followed by HPC, P. aeruginosa sp. and S. aureus sp. At higher doses (690-4390 Jm^{-2}), all but HPC were completely eliminated. FC, P.

aeruginosa sp. and S. aureus sp did not show regrowth up to 6 h after exposure to increasing UV doses (190-4390 Jm^{-2}) but HPC regrowth was significant with high UV doses (1470-4390 Jm^{-2}) due to UV resistant bacteria.

Irrespective of the disinfectant used, maximum removal of suspended solids from greywater is required to optimise disinfection, since the presence of particles provides a shielding effect to bacteria. Winward *et al.* (2008b) found that up to 91% of total coliforms in greywater were particle associated, hence affecting the chlorine demand for disinfection.

For natural systems, a pond is sometimes used as the disinfecting stage (Dallas et al., 2004; Masi et al., 2010).

2.5 Examples of Case Studies

Simple treatments exist for individual houses such as filtration in Australia (2008), soil infiltration in Sweden (Ottosson, 2003) or the 2 stage system (filtration and disinfection) in the UK and Ireland (Al-Jayyousi, 2003; Li et al., 2010). However, on larger scales such as blocks of apartments or small communities, various greywater treatment schemes have been implemented in different countries. Some successful case studies are included in Table 2. 13.

2.6 Discussion

It has been established that a high proportion of people would be willing to reuse greywater to cope with water scarcity. As a result, greywater treatment systems of varying complexities are being used around the world. It is very difficult at the moment to suggest the best alternative to greywater treatment since each system has its advantages and disadvantages and each country has its own preference and specialisation. The case studies presented in Table 2. 13 show that natural and biological systems are currently being preferred as the main treatment step for greywater reuse.

Table 2. 14 presents the costs (capital, operational and maintenance) for major greywater systems while Table 2. 15 presents the environmental impact, land usage and removal efficiency of some systems.

Table 2. 14: Treatment costs of typical greywater systems.

* - Treatment of herbicides, # - Treatment of Industrial Bayer liquor, ** - Converted from Jordanian Dinar (1 JD = 1.42 US$ in 2009), *a* – Required for air blowers, diffusers and pneumatic valves, *b* – Harvesting cost, *c* – Zeolites replacement cost, *d* – Suspended TiO_2 system at laboratory scale, *e* – Suspended TiO_2 system at pilot scale, *f* – Includes maintenance cost, *g* – With aluminium sulphate as coagulant, *h* – with iron sulphate as coagulant, *Q* – Greywater flowrate (m^3h^{-1}).

			Costs			
Treatment type	System	Capacity	Capital	Operating	Maintenance	Ref
Natural	RVFCW	210 m^3/year	600 US$	-	100 US$$year^{-1}$	(Gross et al., 2007a)
Biological	Reedbeds-Pond	2500 L/day	1000 US$	-	-	(Dallas et al., 2004)
	Constructed Wetland	25 m^2/2 m^3, 1-2 m^2/200 L	170 US$/$m^2$**	340 US$$year^{-1}$**^{b} + 280 US$**^{c}	-	(Dalah meh et al., 2009)
	UASB	350 L	430 US$**	Zero	-	
	Septic tank	2.4 m^3	570 US$**	28 US$$year^{-1}$ (Desludging)**	-	
	Aerobic		-	8 kWh$person^{-1}year^{-1}$ required	-	(Hernández Leal et al., 2010b)
	Anaerobic		-	18 kWhperson-1year-1 gained	-	
	Anaerobic-Aerobic	70 L$person^{-1}day^{-1}$	-	14 kWh$person^{-1}year^{-1}$ gained	-	
	Septic tank-Anaerobic-Aerobic	240-400 Lday^{-1}	2000 US$	-	36 US$$year^{-1}$	(Morel and Diener, 2006)
	SBR	-	>1420 US$**^{a}	Air blower power, sludge disposal	-	(Dalah meh et al., 2009)
	RBC	-	RBC (US$) = $3590Q^{0.6776}$, Chlorination unit	Power (W) = $42.2e^{(2.5104Q)}$, Chlorine (US$$year^{-1}$)	Labour = 1040 US$$year^{-}$	(Friedle

			(US$) = 1670	= 62.11Q, *Or* Operating cost for large systems = 1.5 kWhm^{-3}	[1]	r and Hadari, 2006; Nolde, 2000)
	MBR	-	Pump cost (US$) = 594$Q^{0.0286}$, MBR (US$) = 18853 + 17945ln$Q$	1-1.5 kWhm^{-3} (small units), 0.5-0.75 kWhm^{-3} (big units 650 - 10000 m^{3}day^{-1})	Labour = 1040 US$year-1, Membrane treatment = 0.02-0.03 US$m^{-3}year^{-1}	(Friedler and Hadari, 2006)
Physical						
	Grease trap-Infiltration trench	30 Lperson^{-1}day^{-1}	121 US$	-	5.5 US$	(Morel and Diener, 2006)
	Intermittent Sand Filter	-	570 US$**	-	-	(Dalahmeh et al., 2009)
	Sponge filt.-Sedimentation-Gravel filt.-Aeration-Chlorination	1 m^3	-	124 US$year^{-1}	11.2 US$year^{-1}	(Godfrey et al., 2009)
	Ultrafiltration	0.7 m^{3}h^{-1}	-	0.16 Eurosm^{-3}	-	(Ciabattia et al., 2009)
	Nylon sock type filt.-Sedimentation-Disinfection	5.2 m^{3}day^{-1}	17000 Euros	0.75 Eurosm^{-3}[f]	-	(March et al., 2004)
	Ultrafiltration-Reverse osmosis	200 m^{3}day^{-1}	0.63 Eurosm^{-3}	0.56 Eurosm^{-3}	0.16 Eurosm^{-3}	(Sostar-Turk et al., 2005)
Chemical-Physical						
	Flocculation-Sand filtration-GAC adsorption	200 m^{3}day^{-1}	0.11 Eurosm^{-3}	0.07 Eurosm^{-3}	0.33 Eurosm^{-3}	(Sostar-Turk et al., 2005)
	Coagulation-DAF-Sand filt.-Ozonation-GAC adsorption	15m^{3}h^{-1}	-	0.65 Euros/m^3	-	(Ciabattia et al., 2009)

Chemical	Coagulation	-	-	0.0012-0.0048 £m^{-3} [g]	-	(Pidou et al., 2008)
		-	-	0.0040-0.0185 £m^{-3} [h]	-	
	Electrocoagulation-Flotation-Disinfection	28 m^3day^{-1}	0.08 US$$m^{-3}$	0.19 US$$m^{-3}$	-	(Lin et al., 2005)
	Photocatalytic Oxidation *	0.134 L [d]	-	3.75 Eurosm^{-3}	-	(Li Puma et al., 2007)
	Photocatalytic Oxidation #	18 L [e]	-	60-270 US$$m^{-3}$	-	(Pareek et al., 2001)

Table 2. 15: Environmental impact, land requirement and removal efficiency of some greywater technologies.

+ - <50%, ++ - 50-80%, +++ - >80%, NDL – Non-Detectable Limits reached in effluent.

			Removal Efficiency	
Technology	Environmental Impact	Land Requirement	BOD/COD	Pathogens
Reedbed/CW	Medium	High	+++	Low
MBR	High	Low	+++	High
Aerobic	Low	Low	++	Low
Anaerobic	None	Low	+	Low
RBC	Low	Low	+++	Low
Coagulation	Medium	Low	++	NDL
GAC	Medium	Low	+	Low
Photocatalysis	High	Low	++	NDL
UF	High	Low	++	Low
RO	High	Low	+++	NDL

Natural systems such as CW are a cheap alternative and can be used to treat greywater from all sources of the house. They can cope well with influent fluctuations when used in combination (HFCW-VFCW) (Paulo et al., 2009), are well suited for middle income countries since the raw materials are readily available and have ornamental properties. They are the cheapest to construct, maintain and operate (Dalahmeh et al., 2009; Memon et al., 2007), consume little energy (intermittent pumping) and are environmentally friendly in terms of energy requirement. However CWs require large areas (25 m^2/2 m^3, 1-2 m^2/200 L) (Dalahmeh et al., 2009) which impacts on the environment, have long HRTs and cannot be used in hot climates due to excessive evaporation. The poor removal of pathogens from natural systems also means that a disinfection stage is needed. CWs are not suitable for cities and other densely populated areas and do not guarantee a very good quality effluent.

Biological systems such as MBR or RBC have small footprints and give good quality effluents. MBRs consistently give excellent permeate quality, are stable and robust whilst RBCs are similarly efficient, albeit with LGW (Friedler et al., 2005; Nolde, 2000). The biggest disadvantage of the MBR and RBC lies in their capital costs which make them economically feasible either for tall buildings (for RBC) or clusters of buildings (for MBR) only. Also the requirement of well trained professional staff does not make these options favourable in developing countries. MBRs are very efficient at

removing pathogens (non detectable limits in effluent) contrary to the RBC but require frequent membrane cleaning using toxic chemicals (NaOH/HCl), which is detrimental to the environment. The RBC on the other hand may not require as much maintenance (0.2 $hweek^{-1}$) (Nolde, 2000).

Aerobic treatment such as the BAF (Lodge et al., 2004) or SBR (Shin and Lee, 1998) gives good quality effluents while standalone anaerobic treatment have limited energy gain and is not advised unless being used in conjunction with aerobic treatment. Despite its low pollutant and nutrient removal, anaerobic treatment using UASB is cheap, simple and proficient at removing suspended COD and is recommended for countries that produce low quantity, concentrated greywater (e.g., Jordan, Israel), however, since high sludge age is undesirable, the sludge will have to be discharged regularly (Halalsheh et al., 2008). Conversely, disposal of sludge is of concern following biological treatment since XOCs do not readily degrade (Fatta-Kassinos et al., 2010; Le-Minh et al., 2010) but instead remain adsorbed, together with some heavy metals, onto the sludge (Revitt et al., 2011). This can be of concern if the sludge is disposed of in landfills. Conventional biological systems are much cheaper to construct and maintain compared to the MBR or RBC, however their best operating practice has not been fully established yet.

Physical treatment, while a common pretreatment step, is barely used as a main treatment for greywater. Nevertheless, filtration as main treatment has been used in India (Godfrey et al., 2009; Mandal et al., 2011), whereby despite its low quality, the effluent was deemed satisfactory for toilet flushing or irrigation. As a matter of fact, the monetary and health benefits of a greywater treatment system in a school (sponge filtration-sedimentation-gravel and sand filtration-aeration and chlorination) has encouraged the government of the state of Madhya Pradesh to build 412 more similar greywater reuse systems, out of which 200 have already been built in schools (Godfrey et al., 2009). Membranes (MF, UF and NF membranes) give very good effluent quality while also providing a complete barrier to bacteria and viruses (Lodge et al., 2004). Membranes (MF, UF and RO) are very high energy demanding and require large service area and professional staff for operation and maintenance (Lin et al., 2005). RO membranes use chemicals for water softening and pH adjustments, adding to their

environmental detrimental factor. Membranes with bigger pore size (0.2 μm) can be less energy demanding but hardly reduce BOD, which can lead to slime formation in the distribution network (Nolde, 2000). Nevertheless, physical systems do not eliminate pollutants but merely transfer them from one medium to another leading to potential disposal problems.

Chemical treatment such as electrocoagulation, coagulation, adsorption and AOPs seem as attractive prospects for the future of greywater treatment. Chemical treatments such as coagulation and adsorption are cheap, have short HRT and are simple to maintain (Lin et al., 2005; Sostar-Turk et al., 2005) but are mostly successful with greywater with low pollutant loadings. Adsorbents such as GAC and natural zeolites are abundant, cheap, require low technology, and are easily regenerated. Additionally, GAC is a cheap alternative to ozone for the removal of micropollutants (Leal et al., 2011). However, these systems require the use of chemicals (coagulants) and similarly to physical treatment, pollutants are transferred instead of being eliminated. AOPs can be used as a pre-treatment or polishing stage since they can get rid of otherwise recalcitrant organic compounds. Several AOPs such as photocatalysis, Fenton's reagent, photo-Fenton and ozonation have been used successfully on industrial WW. All of the abovementioned AOPs, except for Fenton's reagents, have been used to treat greywater but only a few researches have been carried out, possibly due to the high costs involved (e.g., UV light, ozone generation). In terms of cost, electrocoagulation of LGW could be as low as US$0.27 m^{-3} (Lin et al., 2005); the treatment of laundry greywater was evaluated at 0.51 €m^{-3} using a coagulation/GAC plant compared to 1.35 €m^{-3} using a UF/RO membrane treatment (Sostar-Turk et al., 2005) and ozonation as a post- treatment was between 0.05-0.20 €m^{-3} (Leal et al., 2011).

TiO_2 mediated photocatalysis is a relatively new and attractive AOP that has been found to completely oxidize various kinds of recalcitrant dissolved organics (Belgiorno et al., 2007; Gaya and Abdullah, 2008; Pera-Titus et al., 2004) and nitrogenous BOD (Zhu et al., 2008) from wastewater as well as the toxic metal ions Fe^{3+}, Hg^{2+}, Ag^{+} and Cr^{4+} (Chen, 2001) via redox reactions. Moreover, its disinfection properties has been reported (Van Grieken et al., 2009; Winward et al., 2008a) meaning that an extra disinfection

stage is redundant. Photocatalysis has a high environmental impact (Memon et al., 2007) since it requires a high treatment time, UV source, cooling equipment, a catalyst separation step and costly consumables such as quartz tubes and TiO_2. Currently, the operational costs are too expensive for this process to be a viable option for greywater treatment. However, solar photocatalysis with immobilised catalyst can significantly reduce the cost of the process and is a field that calls for more research.

To obtain greywater that is relatively low in pollutants, it is recommended to ignore the kitchen fraction of greywater (unless biological treatment is being used); however, laundry greywater as from the second rinsing cycle could be included. The intermittent nature of greywater flow means that a storage tank is required. Storing greywater for no more than 24 hours will assist with the settling of some suspended solids such as hair, lint and other soils. Biological treatment such as aerobic treatment and RBC are currently the most environmentally friendly (in terms of chemicals required and energy demand). Aerobic treatment is more suitable for low income countries where the water reuse guidelines are not too stringent, due to the low construction, operating and maintenance costs involved. RBCs have a high capital cost and require skilled personnel for repair and maintenance and as such, are suitable for buildings in developed countries. Since the above mentioned methods do not remove recalcitrant organic compounds (XOCs), AOPs such as photocatalysis could be viable option and has the added advantage of disinfecting the effluent. However, due to the high operating costs involved with this process, more research in the field of solar photocatalysis using immobilised catalyst is required.

2.7 Conclusions

A qualitative and quantitative review on the characteristics of greywater has been presented. The treatment methods from storage to disinfection have been thoroughly reviewed. Each of the treatment systems (biological, physical, chemical or natural) have their respective advantages and drawbacks and examples have been given whereby each system has been used successfully. The presence of hazardous XOCs is receiving more attention due to their recalcitrant behaviour and hazardous nature. Since the conventional treatment methods are not successful at removing those micropollutants,

new treatment methods such as AOPs (e.g., photocatalysis) could be considered. However, AOPs such as photocatalysis are costly and more research need to be carried out in that area in the aim to reduce its costs, e.g., catalyst recovery and reuse and the use of solar radiation instead of UV light.

Abbreviations List

AOP	Advanced Oxidation Process
B	Bathroom greywater
BAF	Biological Aerated Filter
BOD	Biological Oxygen Demand
BOD5	BOD over 5 days period
BOD7	BOD over 7 days period
CFU	Colony Forming Units
COD	Chemical Oxygen Demand
CW	Constructed Wetland
DO	Dissolved Oxygen
DOC	Dissolved Organic Carbon
EC	Electrical Conductivity
E.C	E. Coli
EPA	Environmental Protection Agency
F	Floor cleaning greywater
FBR	Fluidised Bed Reactor
FC	Faecal Coliforms
GAC	Granular Activated Carbon
GROW	Green ROof Water recycling system
GW	GreyWater
HFCW/RB	Horizontal Flow Constructed Wetland/ReedBed
HGW	High load GreyWater
HPC	Heterotrophic Plate Count
HRT	Hydraulic Residence Time
K	Kitchen greywater
L	Laundry greywater
LGW	Low load GreyWater
M	Mixed greywater
MBR	Membrane BioReactor
MF	MicroFiltration
MIEX®	Magnetic Ion Exchange Resin
MWCO	Molecular Weight Cut Off
NE	Nematode Eggs
NF	NanoFiltration
PA	Pseudomonas Aeruginosa
PAC	Powdered Activated Carbon
PAH	Polycyclic Aromatic Hydrocarbon
RBC	Rotating Biological Contactor
RO	Reverse Osmosis
S	Shower greywater
SBR	Sequencing Batch Reactor
SDS	Sodium Dodecyl Sulphate
SRT	Sludge Residence Time
SS	Suspended Solids
TC	Total Coliforms
TDS	Total Dissolved Solids
ThC	Thermotolerant Coliforms
TiO_2	Titanium Dioxide
TKN	Total Kjeldahl Nitrogen
TN	Total Nitrogen
TOC	Total Organic Carbon
TP	Total Phosphorus
TSS	Total Suspended Solids
UASB	Upflow Anaerobic Sludge Blanket
UF	UltraFiltration
UVC	UltraViolet C
VFCW/RB	Vertical Flow Constructed Wetland/ReedBed
VFF	Vertical Flow Filter
W	Washbasin greywater
WW	WasteWater
XOC	Xenobiotic Organic Compound

Chapter 3 - Modelling of Photocatalytic Reactors

Photocatalysis is an advanced oxidation process (AOP) that uses a catalyst (often TiO_2), UV light and an oxidant (O_2, O_3, H_2O_2) to completely decompose organic pollutants found in liquids or gases. This technology however works best at low pollutant concentrations (ppm or $mmolL^{-1}$). Photocatalytic reactors can be either in immobilized form (with the catalyst attached to a surface) or in suspended form (where the catalyst is dispersed in the wastewater). As a result, several designs of photocatalytic reactors have been investigated. Some of the types of immobilized reactors are: corrugated plate (Passalia et al., 2011a), optical fiber (Denny et al., 2009), falling film closed loop step (Stephan et al., 2011), tubular (Dijkstra et al., 2003), flat plate (Salvado-Estivill et al., 2007b), monolith (Chong et al., 2011), annular venturi (Romero-Vargas Castrillon et al., 2006), packed bed (Vella et al., 2010), fixed bed (Alexiadis et al., 2001), parallel plate mesh (Esterkin et al., 2005), multi annular (Imoberdorf et al., 2007), parallel flat plates (Esterkin et al., 2002) and taylor vortex (Dutta and Ray, 2004). Slurry reactors however do not have a wide variety of designs. They are usually: thin film slurry (TFS) (Li Puma and Yue, 2003), annular (Pareek et al., 2003b) and externally illuminated aerated rectangular tank (Trujillo et al., 2010) reactors.

Figure 3. 1 and

Figure 3. 2 show some examples of immobilized and slurry reactors respectively.

Immobilized reactors are more appropriate pertaining to solar light utilization and do not require post treatment for nano to micro sized catalyst recovery, which can end up being costly. On the other hand, slurry reactors ensure better catalyst particle light exposure and high mass transfer coefficients and generally perform better than immobilized systems (Mehrotra et al., 2005; Pozzo et al., 1999). As a result, researchers have been working towards the new design of immobilized systems to account for their limitations, leading to the development of above-mentioned reactors.

3.1 Modelling Methods

The modelling of photocatalytic reactors requires solving the solution of the radiation transport equation (RTE). Mathematical models such as emission models have been developed for simple systems without absorption and scattering. Other mathematical models have been developed for idealized flows (TFS reactors) or for specific designs, with varying levels of complexity that require numerical methods to be solved. Methods that involve statistical treatment (Monte Carlo) and approximations to the solution of the RTE (P1 model, DOM) have also been devised and tested. A review of all those techniques will be presented in this chapter.

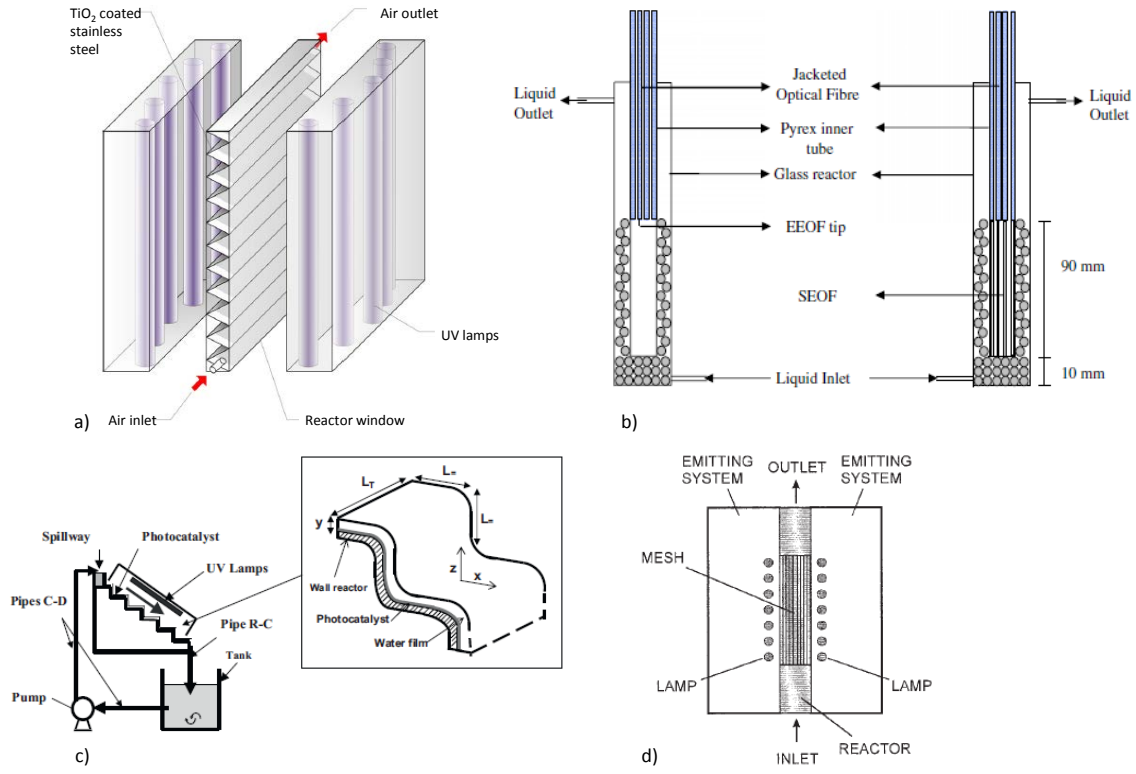

Figure 3. 1: Examples of immobilized photocatalytic reactors; a) corrugated plate (Passalia et al., 2011a), b) end-emitting (EEOF) and side-emitting (SEOF) optical fibre (Denny et al., 2009), c) falling film closed loop (Stephan et al., 2011), d) parallel plate mesh (Esterkin et al., 2005).

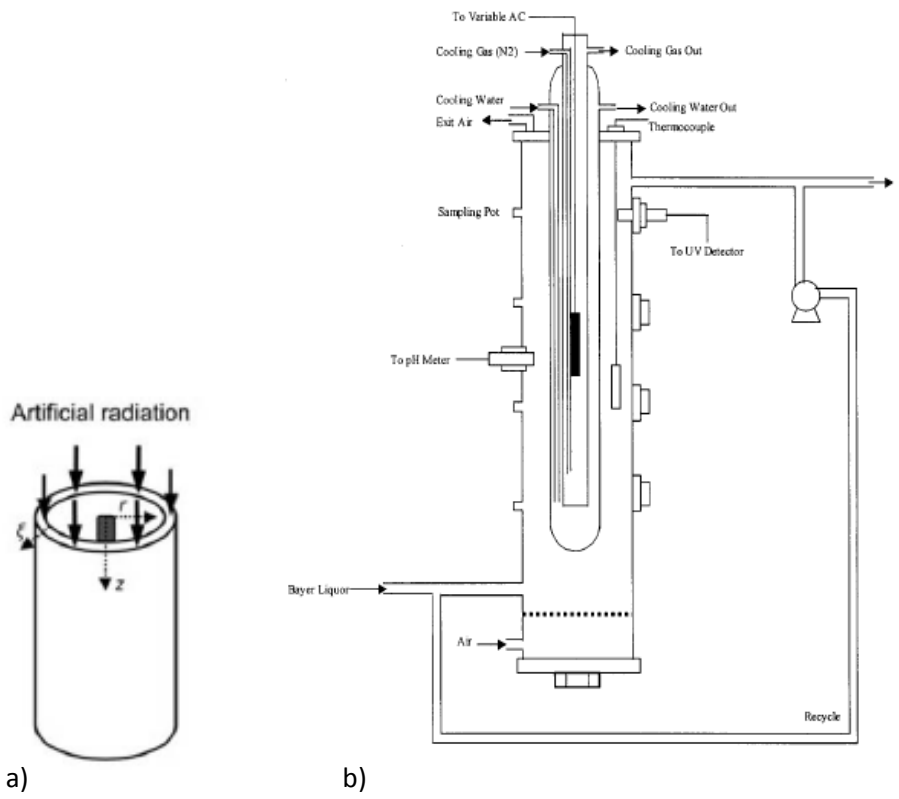

Figure 3. 2: Examples of slurry reactors; a) thin film (Li Puma, 2005), b) annular recirculating (Pareek et al., 2001).

In simple systems with neither absorption nor scattering, the radiation field can be estimated from an emission model. Consequently the line source specular emission (LSSE) has been employed for flat plate photocatalytic systems using either single or multiple lamps (Salvado-Estivill et al., 2007a; Salvado-Estivill et al., 2007b). When scattering effects are non-existent or negligible and absorption is present, the solution of the RTE can be reduced to the Beer-Lambert law, which is easily solvable for all rays from any complex UV source using numerical methods. However in such cases, an emission model is required so as to represent the UV source. Alexiadis *et al.* (2001) found that the Beer-Lambert law using LSPP (line source model with emission in parallel planes) and LSSE could be used for small and high bed thickness respectively in fixed bed reactors. However for intermediate thickness (between 4 – 8 cm), the complete solution of the RTE had to be solved. Elyasi and Taghipour (2010a) have reported a general methodology integrating the Fresnell, Snell and Beer-Lambert laws for modelling the radiant distribution in a medium. The model considers refraction/reflection through/from the body of the UV lamp and sleeve, as well as the

reflections from other sources, such as the reactor body. This model has produced reliable results when using the LSSE model as UV emission source (Elyasi and Taghipour, 2010a; Elyasi and Taghipour, 2010b). However to obtain reliable results, it was recommended that the radiation intensity be measured experimentally close to the lamp surface for a specific lamp at specific operating conditions so as to be integrated into the model as a boundary condition (Elyasi and Taghipour, 2010a; Elyasi and Taghipour, 2010b).

Puma and Yue (2003) developed a simple and generic mathematical model for thin film slurry (TFS) reactors whereby scattering could be neglected. When scattering is important, approximations to the solution of the RTE in slurry annular photoreactors have been developed, such as the two-flux model (TFM) which represent back-scattering of photons and the six flux model (SFM) which represent out-scattering in the six directions of the cartesian coordinates. Puma (2005) has presented a dimensionless analysis of TFS and geometrically thick reactors using the TFM and SFM respectively at idealized flow conditions. The SFM was used successfully by Toepfler *et al.* (2006) and Puma *et al.* (2004) to model TFS reactors. Pareek *et al.* (2003a) on the other hand represented in-scattering of photons in a reactor with large annulus by partitioning the reaction space into finite hexagonal elements to permit reception of incident radiation in six directions (from six neighbouring hexagons). An approximation of the RTE was obtained by combining the in-scattering component with the solution of the Lambert form. The model predictions compared well with experimental data with less than 8% error. Mathematical models describing the radiation field in immobilized systems of different configurations such as the multi annular reactor (Imoberdorf et al., 2007), honeycomb monolith reactor (Hossain et al., 1999; Zhong and Haghighat, 2011) and corrugated plate reactor (Passalia et al., 2011b) are also available.

The Monte Carlo method is a class of numerical techniques based on the statistical characteristics of physical processes, or of analogous models that mimic physical processes (Howell, 1998). In photocatalytic processes, it can be used to solve the solution of the RTE by simulating the trajectory of photons in a medium including absorption, scattering and reflection. This technique has been used mainly to model the

radiation field in immobilized systems such as monolith (Alexiadis, 2006; Singh et al., 2007), packed bed (Imoberdorf et al., 2010; Vella et al., 2010) and fluidized bed (Imoberdorf et al., 2008) reactors giving good agreement with experimental data.

The P1 approximation of solving the RTE is the simplest case of the more general P-N model to solve the radiative problem (Cuevas et al., 2007; Fluent, 2005). Cuevas et al (2007) obtained good agreement in the modelling of an annular slurry reactor at high scattering (0.03 gL^{-1} and 0.05 gL^{-1} catalyst concentration) but at low scattering, only the central portion of the reactor length could be replicated. This was attributed to the non-isotropic nature of scattering at low loads, which is an assumption of the P1 approximation. Conversely, a medium at low absorption coefficient and zero scattering could be modelled satisfactorily with the P1 model (Chen et al., 2011; Yu et al., 2008) but a relatively large discrepancy was obtained at higher concentrations (i.e. high absorption coefficients) (Yu et al., 2008).

The discrete ordinate model (DOM) transforms the integro-differential form of the RTE into a system of algebraic equations that can be solved by machine computation (Romero et al., 2003). In the DOM, the radiation field is divided into a number of discrete directions and the RTE is written and solved separately for each of the directions (Pareek et al., 2008). The DOM is known to give the most accurate results in radiation problems (Alfano et al., 1997; Romero et al., 1997, 2003) and has been the reference tool for many authors to model either suspended or immobilized systems (Alfano et al., 1995; Chong et al., 2011; Denny et al., 2009; Denny et al., 2010a; Duran et al., 2011; Huang et al., 2011; Pareek, 2005; Pareek and Adesina, 2004; Pareek et al., 2003b; Qi et al., 2011; Romero et al., 2003, 2009; Trujillo et al., 2007, 2010). Nowadays, computer simulation softwares use a variant of the DOM called the finite volume (FV) method. In the FV method the RTE is integrated over both the control angle and the control volume unlike the DOM, in which the RTE is integrated over the control volume only (Pareek et al., 2008). Moreover, the DOM offers the advantages of spanning over the entire range of optical thickness and allows computation of non-grey radiation using a non-grey model (Fluent, 2005). The DOM has been used by computational fluid dynamics (CFD) software to model radiation in a variety of reactor

designs such as slurry (Pareek, 2005; Pareek and Adesina, 2004; Pareek et al., 2003b; Qi et al., 2011; Trujillo et al., 2010), flat plate (Trujillo et al., 2007), packed bed (Denny et al., 2009), optical fibers (Denny et al., 2010a), monoliths (Chong et al., 2011) and immobilized annular (Duran et al., 2011) reactors.

The DOM has been used successfully to validate experimental data obtained by researchers. Denny *et al.* (2010a) obtained very good agreement between experimental and simulated results for ethylene conversion in a channelled optical fiber reactor with variation of 3 experimental parameters: incident radiant power, inlet gas flow rate and initial ethylene concentration with a correlation coefficient of 0.995, 0.997 and 0.997 respectively. Pareek *et al.* (2003b) and Qi *et al.* (2011) have performed simulations to determine the optimum catalyst loading within a slurry reactor, getting good agreement with experimental results. Denny *et al.* (2009) modelled the axial radiation distribution of an end emitting optical fiber. The best match was obtained when the outer reflective wall was taken as specularly reflective. Chong *et al.* (2011) modelled the individual monoliths in a honeycomb monolith reactor by using porous media formulations (i.e. where each "pore" was assumed to function as a plug flow reactor) instead of introducing computational grids, which would have been much more computationally intensive. They obtained good prediction for toluene conversion in a monolith reactor; however the prediction was not as good for formaldehyde. The mismatch was attributed to the failure of the adopted Langmuir-Hinshelwood (L-H) model in predicting the oxidation rates due to a different humidity (as that specified for that specific L-H model) in the system. They also found via their simulations that the major drawback of such types of reactors is the insufficient penetration of light through the monoliths. Trujillo *et al.* (2010) investigated the effect of catalyst loading, air superficial velocity, pollutant concentration and radiation intensity on the rate of degradation of dichloroacetic acid in an externally irradiated slurry rectangular reactor and obtained good agreement between numerical results and experimental data. However, since their attempt to use a small particle diameter ($D_p \leq 1\mu m$) failed to converge, an alternative particle size of 10 μm had to be utilized. Finally, Duran *et al.* (2011) used the DOM to successfully predict the degradation rate of benzoic acid in a U and L-shaped annular reactor.

The DOM is useful for predictive simulations as well. Pareek *et al.* (2004) performed 2D simulations of a large annular reactor and found that utilizing the TiO_2 catalyst anatase at concentrations higher than 0.5 gL^{-1} was redundant since the local volumetric rate of energy absorption (LVREA) increased marginally beyond that point. Pareek (2005) investigated the light intensity distribution in a dual lamp annular reactor and determined that an optimum lamp separation with maximum LVREA existed when scattering was present. Furthermore the optimum lamp separation was independent of the catalyst loading while in the absence of scattering (homogeneous system), the LVREA was independent of lamp separation. Trujillo *et al.* (2007) investigated the light distribution in an externally illuminated rectangular reactor with coated plates whereby light scattering was initiated by air bubbles. Simulation allowed the determination of the optimum plate inclination (45 degrees to horizontal), plate interspacing and air bubbles superficial velocity to give the best illumination onto the plates. In their simulations of a glass bead reactor illuminated by optical fibers, Denny *et al.* (2009) found that at low radiant power ($P/P_0 \leq 8$), side emitting optical fiber (SEOF) and end emitting optical fiber (EEOF) performed similarly but at higher radiant power ($P/P_0 > 10$), the SEOF performed better. This was because the EEOF had high transmitted radiation at the top end of the reactor (hence producing half order reaction) which decreased radically along the reactor length, hence giving overall less degradation than the otherwise more constant illumination offered by the SEOF. Denny *et al.* (2010a) used the DOM to design an optimum arrangement of hexagonal channels in a channelled optical fiber reactor that could improve conversion by up to 33% compared to the original design.

Solving the hydrodynamics of the photocatalytic reactor is essential when computing the radiation field in the reactor. Although both flow and radiation fields need to be solved simultaneously, this is not possible with current CFD softwares. So far, researchers have used CFD to solve the flow first and then used the time-averaged or steady state results to calculate the radiation field. Flow simulations can show catalyst distribution in slurry reactors (Pareek et al., 2003b; Qi et al., 2011; Trujillo et al., 2010) while zones of recirculation (Pareek et al., 2003b; Qi et al., 2011; Romero-Vargas Castrillon et al., 2006) or non-uniformity (Mohseni and Taghipour, 2004) are of concern. However, great care needs to be taken to model objects in the reactor stream as they may have an impact

on the flow field (Sozzi and Taghipour, 2006). Castrillon *et al.* (2006) performed flow simulations of a square venturi type photocatalytic reactor for air treatment. Recirculation zones were found and a resulting cylindrical design was proposed following further simulations (Castrillon and de Lasa, 2007). Researchers in general have preferred Euler-Euler formulations in solving multiphase flows compared to the inherently more computationally rigorous Euler-Lagrange approach. Figure 3. 3 shows the results obtained by Pareek *et al.* (2003b) in their hydrodynamics modelling of an annular slurry reactor. The Euler-Euler formulations were used to simulate the three phase gas-liquid-solid flow. From the results obtained, the TiO_2 concentration could be used to solve for the LVREA. Ultimately, the LVREA and velocity vectors were used to model species transport and reaction in the reactor.

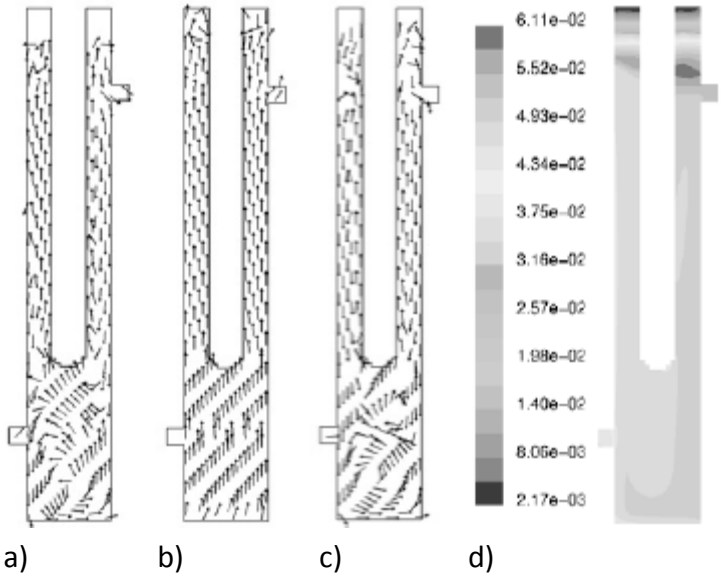

Figure 3. 3: Multiphase modelling of an annular slurry reactor obtained by Pareek *et al.* (2003b) using the Euler-Euler formulations. The results show: a) liquid velocity vectors, b) gas velocity vectors, c) TiO_2 velocity vectors and d) TiO_2 catalyst concentration (gL^{-1}) within the reactor. A recirculation zone can be seen near the slurry inlet for the liquid and solid velocity vectors.

The air in buildings is usually polluted with low concentration of volatile organic carbons (VOC), in the order of ppm or ppb and is a good candidate for photocatalytic treatment. It is therefore not surprising that the majority of CFD models for photocatalytic reactors reported in literature deal with the simulation of immobilized

photocatalytic reactors designed for air treatment compared to slurry reactors for wastewater treatment.

This chapter results from an extensive literature review and presents the pertinent information required in the modelling of photocatalytic reactors using CFD. The hydrodynamics modelling is considered first followed by the radiation modelling using the DOM. Useful equations, findings and data related to suspended (with reference to bubble columns) and immobilized reactors are included in the aim of assisting the reader at the CFD modelling of photocatalytic reactors.

3.2 Hydrodynamics Modelling

Multiphase hydrodynamics modelling can be performed by either the Eulerian-Eulerian (E-E) or Eulerian-Lagrangian (E-L) model. Both models are described here with higher emphasis on the E-E model.

3.2.1 The Eulerian-Eulerian approach

The Eulerian-Eulerian model allows for the modelling of multiple separate, yet interacting phases (Fluent, 2005). The phases are considered as interpenetrating continua for which equations representing the conservation of mass and momentum are solved. These are presented below (Fluent, 2005; Ranade, 2002).

The concept of volume fraction for n phases in total is introduced,

$$\sum_{k=1}^{n} \alpha_k = 1 \tag{3.1}$$

where α_k is the volume fraction of phase k

The continuity equation for each phase can therefore be written as:

$$\frac{\partial(\alpha_k \rho_k)}{\partial t} + \nabla \cdot (\alpha_k \rho_k U_k) = \sum_{p=1, p\neq k}^{n} S_{pk} \tag{3.2}$$

where the subscript k denotes phase k and S_{pk} is the rate of mass transfer from phase p to phase k.

The momentum balance for phase k can be written:

$$\frac{\partial(\alpha_k \rho_k U_k)}{\partial t} + \nabla \cdot (\alpha_k \rho_k U_k U_k) = -\alpha_k \nabla p - \nabla \cdot (\alpha_k \tau_k) + \alpha_k \rho_k g + F_k + F_g \quad (3.3)$$

where F_k denotes the interphase momentum exchange terms between phase k and all other phases present in the system. Additional terms relevant to granular multiphase flows (between solid phases) are grouped together in F_g.

The interphase coupling term in equation 3.3 for phase k can be written as:

$$F_k = \sum_{q=1}^{n} K_{kq}(U_q - U_k) \quad (3.4)$$

where K_{kq} is the interphase momentum exchange coefficient. The interphase coupling terms must satisfy the following relation:

$$F_{kq} = -F_{qk} \quad (3.5)$$

3.2.1.1 Solid phase – kinetic theory of granular flow

The kinetic theory of granular flows is based on similarities between the flow of a granular material and the molecules of a gas. This treatment uses classical results from the kinetic theory of gases to predict the form of transport equations for a granular material. Kinetic theory based models introduce several additional terms in the solids stresses and, therefore, modify momentum conservation equations for solid phases. The solids stress can be written as:

$$\alpha_s \bar{\tau}_s = -P_s \bar{I} + 2\alpha_s \mu_s \bar{S} + \alpha_s \left(\lambda_s - \frac{2}{3}\mu_s\right) \nabla \cdot U_s \bar{I} \quad (3.6)$$

where P_s is solids pressure, μ_s is solids shear viscosity and λ_s is solids bulk viscosity. $\bar{S}$ is given by:

$$\bar{S} = \frac{1}{2}(\nabla U_s + (\nabla U_s)^T) \quad (3.7)$$

The solids pressure, P_s consists of a kinetic and a collisional part:

$$P_s = \propto_s \rho_s \theta_s (1 + 2(1 + e_s) \propto_s g_{0s}) \quad (3.8)$$

where e_s is the coefficient of restitution for particle collisions, g_{0s} is the radial distribution function and θ_s is the granular temperature. Granular temperature is a

measure of the kinetic energy contained in the fluctuating velocity of particles, and is defined as:

$$\theta_s = \frac{1}{3}\bar{u}_s^2 \tag{3.9}$$

The radial distribution function accounts for the increase in probability of collisions when the solid particles become denser. Lun and Savage (1986) proposed:

$$g_{0s} = \left(1 - \frac{\propto_s}{\propto_{s,max}}\right)^{-2.5\propto_{s,max}} \tag{3.10}$$

while Ogawa *et al.* (1980) proposed:

$$g_{0s} = \left[1 - \left(\frac{\propto_s}{\propto_{s,max}}\right)^{1/3}\right]^{-1} \tag{3.11}$$

The solids shear viscosity comprises collisional, kinetic and frictional contributions:

$$\mu_s = \mu_{s,coll} + \mu_{s,kin} + \mu_{s,fr} \tag{3.12}$$

The collisional part of the shear viscosity is modelled as:

$$\mu_{s,coll} = \frac{4}{5} \propto_s \rho_s d_s g_{0s}(1 + e_s)\left(\frac{\theta_s}{\pi}\right)^{0.5} \tag{3.13}$$

The kinetic viscosity is given by Syamlal *et al.* (1993):

$$\mu_{s,kin} = \frac{\propto_s \rho_s d_s (\theta_s \pi)^{0.5}}{6(3-e_s)}\left[1 + \frac{2}{5}(1 + e_s)(3e_s - 1) \propto_s g_{0s}\right] \tag{3.14}$$

Or Gidaspow *et al.* (1991):

$$\mu_{s,kin} = \frac{10\rho_s d_s (\theta_s \pi)^{0.5}}{96(1+e_s) g_{0s}}\left[1 + \frac{4}{5}(1 + e_s) \propto_s g_{0s}\right]^2 \tag{3.15}$$

Frictional contribution applies at the limit of maximum packing, where flow becomes incompressible and friction between particles dominates. In the case of dilute granular flow such as in slurry photocatalytic reactors, this term can be ignored, hence:

$$\mu_{s,fr} = 0 \tag{3.16}$$

The solids bulk viscosity accounts for the resistance of the granular particles to compression or expansion. Lun *et al.* (1984) suggest:

$$\lambda_s = \frac{4}{3} \propto_s \rho_s d_s g_{0s} (1 + e_s) \left(\frac{\theta_s}{\pi}\right)^{0.5} \tag{3.17}$$

The granular temperature θ_s is proportional to the kinetic energy of the random motion of the particles. It is obtained by solving its transport equation, which has the form:

$$\frac{3}{2}\left(\frac{\partial(\alpha_s \rho_s \theta_s)}{\partial t}\right) + \nabla \cdot (\alpha_s \rho_s \theta_s U_s) = (-P_s \bar{I} + \bar{\tau}_s) : \nabla U_s + \nabla \cdot (\kappa_\theta \theta_s) - \gamma_\theta + \phi_{ls} \tag{3.18}$$

where the first term on the right hand side represents the generation of energy by solid stress tensor, the second term represents the diffusion of energy (κ_θ is the granular temperature conductivity, the third term represents the collisional dissipation of energy and the final term is the energy exchange between the l^{th} fluid and solid phase. The granular temperature conductivity can be expressed by the following equation from Syamlal *et al.* (1993):

$$\kappa_\theta = \frac{15 \propto_s \rho_s d_s (\theta_s \pi)^{0.5}}{4(41 - 33\eta)} \left[1 + \frac{12}{5}\eta^2 (4\eta - 3) \propto_s g_{0s} + \frac{16}{15\pi}\eta^2 (41 - 33\eta)\eta \propto_s g_{0s}\right] \tag{3.19}$$

where

$$\eta = \frac{1}{2}(1 + e_s) \tag{3.20}$$

Alternatively, Gidaspow *et al.* (1991) propose:

$$\kappa_\theta = \frac{75 \rho_s d_s (\theta_s \pi)^{0.5}}{192(1 + e_s) g_{0s}} \left[1 + \frac{6}{5} \propto_s g_{0s} (1 + e_s)\right]^2 + 2\alpha_s^2 \rho_s d_s (1 + e_s) g_{0s} \left(\frac{\theta_s}{\pi}\right)^{0.5} \tag{3.21}$$

The collisional dissipation of energy was derived by Lun *et al.* (1984):

$$\gamma_\theta = \frac{12(1 - e_s^2) g_{0s}}{d_s \pi^{0.5}} \alpha_s^2 \rho_s {\theta_s}^{3/2} \tag{3.22}$$

Finally, the energy exchange between the fluid and the solid phase is modelled as:

$$\phi_{ls} = -3 K_{fs} \theta_s \tag{3.23}$$

3.2.2 The Eulerian-Lagrangian approach

In this approach, the trajectories of the dispersed phase particles are simulated by solving an equation of motion for each dispersed phase particle while the motion of the continuous phase is modelled using a conventional Eulerian framework. For the equation of motion of the dispersed particles, a general force balance over each dispersed phase particle is used:

$$m_P \frac{dU_P}{dt} = F_p + F_G + F_D + F_{VM} + F_L + F_H \tag{3.24}$$

where m_P and U_P represent the mass and velocity vector of the particle respectively. The right hand side represents the sum of forces due to continuous phase pressure gradient, gravity, drag, virtual mass, lift and Basset history respectively.

The sum of forces due to continuous phase pressure gradient and gravity is:

$$F_p + F_G = V_P \nabla p - \rho_P V_P \mathrm{g} \tag{3.25}$$

where p is the pressure in the continuous phase and V_P is the volume of the particle. The drag force, F_D can be written as:

$$F_D = -\frac{\pi}{8} C_D \rho_C d_P^2 |U_P - U_C|(U_P - U_C) \tag{3.26}$$

where subscript P and C represent particulate and continuous phase respectively, d_P is the particle diameter, C_D is the drag coefficient and the term $|U_P - U_C|$ represents the resultant slip velocity between particulate and continuous phase.

3.2.3 Species balance

The concentration of reactants or final products in each control volume of the computational grid can be expressed in terms of mass fraction, Y_i. The species balance can be represented as:

$$\frac{\partial}{\partial t}(\rho_i Y_i) + \nabla \cdot (\rho_i U Y_i) = -\nabla \cdot J_i + r_i \tag{3.27}$$

where J_i and r_i are the diffusion flux and net rate of production/destruction of species *i* respectively.

3.2.4 Empirical data

Two empirical values, the packing limit and the coefficient of restitution, are required in the solution of the Eulerian-Eulerian approach. These are discussed in this section.

3.2.4.1 Packing limit

The packing limit of a material is the maximum volume fraction of solid objects when they are packed randomly. Packing limits vary depending on material types and sizes. Some values of packing limits for different materials are presented in Table 3. 1 while Table 3. 2 lists the dense and loose random packing limits for a mixture of particles of different sizes.

Table 3. 1: Packing limit values for some materials.

Material	Diameter (m)	Packing limit	Ref
TiO_2	0.70×10^{-6}	0.55	(Turian et al., 1997)
Laterite	4.40×10^{-6}	0.35	(Turian et al., 1997)
Gypsum	18.6×10^{-6}	0.69	(Turian et al., 1997)
Glass beads	200×10^{-6}-3.00×10^{-3}	0.59 - 0.63	(Cornelissen et al., 2007; Du et al., 2006; Hulme et al., 2005; Xiaoyan, 2011)

Table 3. 2: Dense and loose random packing for mixture of particles with different sizes (Sudduth, 1993).

Number of particle sizes in mixture	Dense Random Packing	Loose Random Packing
1	0.639	0.589
2	0.87	0.831
3	0.953	0.931
4	0.983	0.972

3.2.4.2 Coefficient of restitution

The coefficient of restitution (COR), e, of two colliding objects is a fractional value that describes the amount of kinetic energy that is conserved after impact. For instance, a value of 1 means completely elastic collision, hence, no loss in kinetic energy. The measured CORs of various materials have been found to vary between 0.8 and 0.97 (Foerster et al., 1994; Hussainova et al., 1999; Imre et al., 2008; Lorenz et al., 1997). In CFD simulations, values of COR used usually vary between 0.9 and 1 (Cornelissen et al., 2007; Coroneo et al., 2011; Du et al., 2006; Esmaili and Mahinpey, 2011; Gamwo et

al., 2003; Hulme et al., 2005; Xiaoyan, 2011). Cornelissen *et al.* (2007) found negligible difference in voidage when four different values (0.5, 0.9, 0.95 and 1.0) of COR were used in the CFD modelling of a liquid-solid fluidized bed. On the other hand, Goldschmidt *et al.* (2001) found that the hydrodynamics of a dense gas-fluidized bed strongly depended on the COR value used.

Nonetheless the studies described above deal with either dry collisions (i.e. collisions in air) (Coroneo et al., 2011; Du et al., 2006; Esmaili and Mahinpey, 2011; Hulme et al., 2005) or collisions of relatively big particles (in mm) (Cornelissen et al., 2007; Gamwo et al., 2003; Xiaoyan, 2011). In photocatalytic slurry systems, the catalyst particles are usually in microns or nanometer sizes and are dispersed in a viscous liquid (wastewater). When two solid spheres collide in a liquid, the dynamic collision process is slowed by viscous dissipation and the increased pressure in the interparticle gap as compared with dry collisions (Yang and Hunt, 2006). The COR for various materials in a viscous liquid has been measured by several authors (Gondret et al., 2002; Joseph et al., 2001; Marshall, 2011; Yang and Hunt, 2006) and was found to be a function of the Stokes number (St), which is a ratio of the particle inertia to the viscous force. It has been determined that below St ≈ 10, no rebound of the particle occurred, i.e. $e = 0$. Beyond St ≈ 10, the COR increases exponentially and eventually asymptotes to the COR values for dry collisions. Figure 3. 4 shows the COR of some materials as a function of the Stokes number in a viscous fluid.

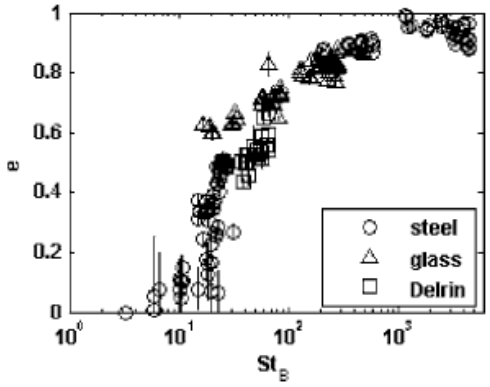

Figure 3. 4: COR as a function of St for some materials in a viscous fluid (Yang and Hunt, 2006).

The St number is represented by equation 3.28.

$$St = \frac{mv_0}{6\pi\mu r^2} \tag{3.28}$$

where m is the particle mass, v_0 is the approach velocity, μ is the fluid dynamic viscosity and r is the particle radius. For photocatalytic slurry systems using TiO_2 at a maximum agglomerated size of 900 nm (Cabrera et al., 1996) and maximum density of 4260 kgm^{-3} (Degussa P25 TiO_2), using the dynamic viscosity of water (8×10^{-4} Nsm^{-2} at 27ºC) and assuming an approach velocity of 2 ms^{-1} (since slurry systems are usually operated at low slurry recirculation and gas flow rates), the maximum St obtained using equation 3.28 is 1.1. Hence in TiO_2 slurry photocatalytic systems, it is advised to use a COR value of $e = 0$.

3.2.5 Factors affecting hydrodynamic modelling

The hydrodynamic behaviour of liquid and gas bubbles in the modelling of bubble columns are affected by the choice of interfacial forces, turbulence model, degree of bubble coalescence and break-up and air distributor model used. Table 3. 3 lists the conditions used by some researchers for the modelling of bubble columns. 2-Dimensional simulations have provided reasonable results in the past (Olmos et al., 2001; Sanyal et al., 1999); however, 3-Dimensional simulations are always closest to reproducing experimental data (Chen et al., 2004, 2005; Ekambara et al., 2005; Jakobsen et al., 2005; Krishna et al., 2000; Panneerselvam et al., 2009) and should be used from now on, since with current technology, computers are much more powerful.

3.2.5.1 Drag force

The main interfacial force affecting the motion of particles in a liquid is the drag force. The fluid-fluid exchange coefficient (also applicable for granular flows), K_{kq}, in equation 3.4 is written as:

$$K_{kq} = \frac{\propto_q \propto_k \rho_k f}{\tau_k} \tag{3.29}$$

where f is the drag function and τ_k is the particulate relaxation time, defined as:

$$f = \frac{C_D\, Re}{24} \tag{3.30}$$

$$\tau_k = \frac{\rho_k d_k^2}{18\mu_q} \tag{3.31}$$

where C_D is the drag coefficient and Re is the relative Reynolds number. The drag coefficient can be calculated from the Morsi and Alexander (MA) model (1972) or the more generic Schiller and Naumann (SN) (1935) model. The MA model is the most complete model and can adjust the function definition frequently over a large range of Reynolds number (Fluent, 2005).

For the SN model;

$$C_D = \begin{cases} \frac{24}{Re}(1 + 0.15Re^{0.687}) & Re \leq 1000 \\ 0.44 & Re \geq 1000 \end{cases} \tag{3.32}$$

For the MA model;

$$C_D = a_1 + \frac{a_2}{Re} + \frac{a_3}{Re^2} \tag{3.33}$$

where

$$a_1, a_2, a_3 = \begin{cases} 0, 18, 0 & 0 < Re < 0.1 \\ 3.69, 22.73, 0.0903 & 0.1 < Re < 1 \\ 1.222, 29.1667, -3.889 & 1 < Re < 10 \\ 0.6167, 46.5, -116.67 & 10 < Re < 100 \\ 0.3644, 98.33, -2778 & 100 < Re < 1000 \\ 0.357, 148.62, -47500 & 1000 < Re < 5000 \\ 0.46, -490.546, 578700 & 5000 < Re < 10000 \\ 0.5191, -1662.5, 5416700 & Re \geq 10000 \end{cases}$$

3.2.5.2 Other forces

This section assesses the importance of the other types of interfacial forces that can occur in photocatalytic reactors.

3.2.5.2.1 Multiphase systems

The other contributing forces are the virtual mass, lift and turbulent dispersion. It is generally accepted that the inclusion of virtual mass force does not affect the final results of the CFD modelling of bubble columns (Buwa et al., 2006; Chen et al., 2004; Deen et al., 2001; Selma et al., 2010; Tabib et al., 2008), unless high particle acceleration need to be modelled such as impeller mixing (Srinivasa and Jayanti, 2007)

and near sparger region (Simonnet et al., 2008). Moreover the effect of virtual mass was deemed negligible for column diameters greater than 0.15 m (Tabib et al., 2008). Lift force is required at high liquid level ($H/W \geq 4.5$) (Buwa et al., 2006; Selma et al., 2010), high V_g (to capture the parabolic profile of gas hold-up and liquid velocity) (Olmos et al., 2001; Tabib et al., 2008) and to reproduce the transient behaviour of bubble plumes (Deen et al., 2001; Simonnet et al., 2008). Elena Diaz *et al.* (2009) studied the effect of lift force in a bubble column operating in homogeneous, heterogeneous and churn turbulent regime. They found that the lift force did not improve the prediction of experimental values and hence do not recommend its use in the modelling of bubble columns. Tabib *et al.* (2008) found that the effect of turbulent dispersion was significant at only high superficial gas velocity ($V_g = 9.6$ cms^{-1}).

3.2.5.2.2 Gas phase systems

In the case of gas phase hydrodynamics modelling, the loss of momentum occurs due to an obstacle such as a wire mesh or a photocatalytic support and needs to be accounted for. Some correlations are available in (Chong et al., 2011; Romero-Vargas Castrillon et al., 2006).

3.2.5.3 Turbulence models

As can be seen from Table 3. 3, for bubble columns and photocatalytic reactors (last two rows), the standard κ-ε model, at times modified to account for bubble induced turbulence (BIT), is the most adopted turbulence model due to its simplicity and lesser computational requirement. The standard κ-ε model also performed well in the case of impinging jet flows (Esteban Duran et al., 2009) but not for expanding jet flows in annular reactors (Sozzi and Taghipour, 2006). The other models such as the Reynolds Stress Modelling (RSM) and Large Eddy Simulation (LES) are efficient at capturing transient behaviours and high turbulence regions in a bubble column but at the expense of higher computational requirement (Dhotre et al., 2008; Sozzi and Taghipour, 2006; Tabib et al., 2008). For low Reynolds number (350-11,000), the Abe-Kondoh-Nagano (AKN) model performed better than RSM and was less computationally intensive (Duran et al., 2010a; Duran et al., 2011). In gas phase photocatalytic reactors, the laminar model is used due to the low flow rates usually employed (Chong et al., 2011;

Denny et al., 2010a; Jarandehei and De Visscher, 2009; Passalia et al., 2011b; Salvado-Estivill et al., 2007a; Salvado-Estivill et al., 2007b).

3.2.5.4 Effect of bubble diameter

The use of a constant bubble diameter can give reasonable predictions for the homogeneous regime because the bubble size distribution in such a condition is narrow and bubble interaction is relatively weak (Wang et al., 2007). Bubble coalescence and break up models have been used successfully in the cases of transitional and churn turbulent regimes (Chen et al., 2004; Farzpourmachiani et al., 2011; Olmos et al., 2001), however such regimes are not usually used in slurry photocatalytic reactors.

The average bubble diameter for the homogeneous regime can be predicted from the Akita and Yoshida correlation (Deckwer and Field, 1992), equation 3.34. This correlation applies for air-water systems and covers bubble columns up to 30cm in diameter with air supplied via perforated or sintered plates. Equation 3.34 is applicable to gas rates up to about 7 cms^{-1}.

$$\frac{d_B}{d_R} = 26\left(\frac{gd_R^2\rho_L}{\sigma}\right)^{-0.5}\left(\frac{gd_R^3}{\nu_L^2}\right)^{-0.12}\left(\frac{u_G}{\sqrt{(gd_R)}}\right)^{-0.12} \quad (3.34)$$

3.2.5.5 Effect of gas distributor

The modelling of the gas distributor can affect the overall hydrodynamics in a bubble column (Ciabattia et al., 2009). Despite this, the approximation of perforated plate distributors as open areas has been used successfully as seen from Table 3. 3. Such approximation has the benefit of making the modelling of individual holes in the distributor redundant.

Table 3. 3: Conditions used in the modelling of bubble column reactors.

V_g – Gas Superficial Velocity, W – Width, D – Diameter, H – Height, Di – Diameter, NS – Not Specified, TD – Turbulent Dispersion, G – Gravity, B – Buoyancy, P – Pressure, RANS – Reynolds Average Navier Stokes, BIT – Bubble Induced Turbulence, LES – Large Eddy Simulations, RSM – Reynolds Stress Modelling, E-E – Euler-Euler, ASMM – Algebraic Slip Mixture Model, E-L – Euler-Lagrange, * - For Gas-Liquid and Solid-Liquid interaction.

N.B: The two last rows represent data for photocatalytic reactors.

Ref #	Dimensions (m)	Distributor Model	Interfacial Forces				Turbulence Model(s)	V_g (cms^{-1})	Model Used
			Drag	Virtual Mass	Lift	Other			
(Dhotre et al., 2008)	0.15W×0.15D×0.45H	Open area	Yes	Yes	Yes	TD (for RANS only)	Std κ-ε with BIT, LES	0.49	3D E-E
(Sanyal et al., 1999)	0.19Di×1.00H	Open area	Yes	No	No	No	Std κ-ε	2, 12	2D E-E
(Olmos et al., 2001)	0.10Di×1.35H	Discrete orifices	Yes	No	No	TD	Std κ-ε with BIT	0.5-9.6	2D E-E
(Chen et al., 2004)	0.19Di	NS	Yes	No	No	No	Std κ-ε with BIT	12	2D E-E, ASMM
(Farzpourmachiani et al., 2011)	0.2W×0.05D, H/W = 1, 2.25, 4.5, 7.7	Open area	Yes	Yes	Yes	G, B, P	Std κ-ε	14, 73	3D E-L
(Selma et al., 2010)	0.2W×0.05D×1.2H	Open area	Yes	No	Yes (When H/W≥4.5)	No	Std κ-ε with BIT	0.14, 0.73	3D E-E
(Tabib et al., 2008)	0.6Di×5.44H	Discrete orifices	Yes	No	Yes at high Vg (9.6 cms^{-1})	TD at high Vg (9.6 cms^{-1})	Std κ-ε, RSM, LES	1.2 - 9.6	3D E-E
(Buwa et al., 2006)	0.2W×0.05D×1.2H	Open area	Yes	No	Yes (When H/W≥4.5)	G, B, P	Std κ-ε	0.14 - 0.73	3D E-L
(Elena Diaz et al., 2009)	0.2W×0.04D×1.8H	Open area	Yes	No	No	No	Std κ-ε	0.24 - 2.13	3D E-E
(Qi et al., 2011)	0.149Dx0.05H	Open area	Yes*	No	Yes*	TD*	Std κ-ε with BIT	1.8 - 5.4	3D E-E
(Trujillo et al., 2010)	0.24Wx0.14Dx0.13H	Open area	Yes*	No	No	No	Std κ-ε	25	3D E-E

3.3 Radiation Modelling

This part of the review looks at the radiation modelling of photocatalytic reactors and the relevant equations involved.

3.3.1 Solutions of the radiative transport equation (RTE)

The radiative transport equation (RTE) describes the traveling of photonic rays with their corresponding energy loss due to absorption and out-scattering and gain due to in-scattering of photonic energy. The following section describes the solution of the RTE for slurry and immobilized systems.

3.3.1.1 Slurry systems

For a monochromatic ray of light or wavelength band (interval) of intensity I and wavelength υ (or interval $\Delta\upsilon$) travelling in the direction s and solid angle Ω through an absorbing and scattering medium the solution of the RTE for an elemental distance ds is as follows (Cassano and Alfano, 2000; Pareek et al., 2008; Romero et al., 1997):

$$\frac{dI_\upsilon(s,\Omega)}{ds} = -\kappa_\upsilon I_\upsilon(s,\Omega) - \sigma_\upsilon I_\upsilon(s,\Omega) + \frac{1}{4\pi}\sigma_\upsilon \int_0^{4\pi} p(\Omega' \longrightarrow \Omega) I_\upsilon(s,\Omega') d\Omega' \qquad (3.35)$$

where the first term on the right hand side is the absorbed radiation, the second term is the out scattering of radiation and the third term is the gain of energy due to in-scattering of radiation. The parameters κ_υ and σ_υ are the wavelength dependent absorption and scattering coefficients of the medium and $p(\Omega' \longrightarrow \Omega)$ is a phase function describing the incident radiation from all other directions surrounding ds.

The incident intensity at any point from all the directions is given by

$$G_\upsilon(s) = \int_{\Omega=0}^{\Omega=4\pi} I_\upsilon(s,\Omega) d\Omega \qquad (3.36)$$

And the local volumetric rate of energy absorption (LVREA) at any point is given by:

$$E_\upsilon(s) = \kappa_\upsilon(s) G_\upsilon(s) \qquad (3.37)$$

For polychromatic light, radiation is emitted in a range of wavelengths. As a result the LVREA will have to be summed over the whole absorbable wavelength range. Hence,

$$E(s) = \int_{\upsilon_{min}}^{\upsilon_{max}} \kappa_\upsilon(s) G_\upsilon(s) \qquad (3.38)$$

3.3.1.2 Immobilized systems

For some immobilized systems such as optical fibers, coated plates and monoliths, there is no scattering of light and radiation absorption occurs in the TiO_2 coating. The resulting RTE (equation 3.35) reduces to the Beer-Lambert law:

$$I_0 = I_{in} - I_{ref} \tag{3.39}$$

$$\frac{dI_{0,z}}{dz} = -\alpha_v I_0 \tag{3.40}$$

where I_0 is intensity of light that penetrates the TiO_2 coating and is obtained by subtracting the reflected portion from the incident radiation (equation 3.39). $I_{0,z}$ is the transmitted irradiance at a distance z inside the TiO_2 coating and α_v is the attenuation coefficient, analogous to the absorption coefficient. Attenuation coefficient values of 1 micron^{-1} have been used in modelling (Chong et al., 2011; Denny et al., 2010a; Trujillo et al., 2007) although values up to 5 micron^{-1} and 8 micron^{-1} have been measured in optical fibers (Danion et al., 2004).

Trujillo *et al.* (2007, 2010) enhanced the illumination of coated plates by bubbling air into an externally irradiated reactor. The air bubbles were responsible for light scattering onto the plates due to reflection from the bubble surface. As a result, the RTE from equation 3.35 can be reduced to:

$$\frac{dI_v(s,\Omega)}{ds} = -\sigma_v I_v(s,\Omega) + \frac{1}{4\pi}\sigma_v \int_0^{4\pi} p(\Omega' \longrightarrow \Omega) I_v(s,\Omega') d\Omega' \tag{3.41}$$

3.3.2 Optical parameters

The scattering and absorption coefficients along with the phase function parameter are optical parameters that are all dependent of the type of catalyst used. This section describes the optical parameters formulated for TiO_2 particles.

3.3.2.1 Absorption and scattering coefficients

Cabrera *et al.* (1996) have evaluated the specific absorption, κ_v^* , and scattering, σ_v^* , coefficients at different wavelengths, in m^2g^{-1} for the six main types of TiO_2 powders, namely: Aldrich, Merck, Fisher, Fluka, Degussa and Hombikat.

The wavelength dependent absorption and scattering coefficients for any TiO_2 catalyst type in a suspension are:

$$\kappa_\upsilon = \kappa_\upsilon^* W_{cat} \tag{3.42}$$

$$\sigma_\upsilon = \sigma_\upsilon^* W_{cat} \tag{3.43}$$

where W_{cat} is the catalyst loading, gm^{-3}.

Since solving the RTE at each individual wavelengths can be computationally intensive, Romero *et al.* (1997) recommend using wavelength averaged properties as an approximation for polychromatic light. These values are given in Table 3. 4 for Aldrich and Degussa TiO_2 and are specifically for lamp type Hanovia LL-189a-10/1200 having a nominal input power of 1200 W and a photochemical power (between 295 and 405 nm) of 6.4×10^{-4} einstein s^{-1}.

Table 3. 4: Wavelength average absorption and scattering coefficients for Aldrich and Degussa TiO_2 (Romero et al., 1997) for lamp type Hanovia LL-189a-10/1200.

TiO_2 Type	Nominal Diameter (nm)	Wavelength Range (nm)	$\langle\kappa_\upsilon^*\rangle$ (m^2g^{-1})	$\langle\sigma_\upsilon^*\rangle$ (m^2g^{-1})
Aldrich	150 - 200	295 - 405	0.2758	3.598
Degussa	30 - 90	295 - 405	0.5316	5.3502

Hence the wavelength averaged absorption and scattering coefficients for a particular catalyst type are represented by:

$$\kappa_\upsilon = \langle\kappa_\upsilon^*\rangle W_{cat} \tag{3.44}$$

$$\sigma_\upsilon = \langle\sigma_\upsilon^*\rangle W_{cat} \tag{3.45}$$

Wavelength averaged values have been used reliably for Aldrich TiO_2 (Pareek, 2005; Pareek and Adesina, 2004; Pareek et al., 2003b; Qi et al., 2011) and Degussa P25 TiO_2 (Toepfer et al., 2006) in the modelling of slurry reactors. Pareek (2005) calculated the LVREA for both wavelength averaged and discrete values of absorption and scattering coefficients for a range of catalyst loading and found that wavelength averaged values of optical parameters lead to a maximum overprediction of 10%. It has to be noted that the

absorption by water can be safely neglected in slurry systems since its optical thickness is much less than 1 (Trujillo et al., 2007). The optical thickness ω, of a non-scattering medium is calculated by equation 3.46, where for water, $\kappa_\upsilon \approx 0.01 m^{-1}$.

$$\omega = \kappa_\upsilon L \tag{3.46}$$

where L is the longest characterictic length (annulus thickness).

In the case of fixed bed reactors where the light source is in the middle of the reactor, taking the example of coated glass beads from Denny *et al.* (2009), both absorption and scattering will occur. Hence equation 3.35 can be used to solve the RTE. However, in such a case the specific absorption and scattering coefficients were multiplied by the TiO_2 density to account for the continuous film of the TiO_2 coating on the glass beads, equations 3.47 and 3.48.

$$\kappa_\upsilon = \kappa_\upsilon^* \rho_{cat} \tag{3.47}$$

$$\sigma_\upsilon = \sigma_\upsilon^* \rho_{cat} \tag{3.48}$$

For the scattering by gas bubbles, Trujillo *et al.* (2007, 2010) used an expression for large spherical particles with a specularly reflecting surface:

$$\sigma_{\upsilon,B} = \rho_\upsilon \pi R^2 N_s \tag{3.49}$$

where ρ_υ is the hemispherical spectral reflectivity, R is the bubble radius and N_s is the number of bubbles per unit volume which can be calculated by:

$$N_s = \frac{\alpha_G}{V_B} \tag{3.50}$$

where α_G is the gas hold up and V_B is the volume of a single bubble.

3.3.2.2 Phase function

The phase function describes the directional distribution of scattered radiation (Siegel and Howell, 2002). There are various expressions that can be used to calculate the phase function. To choose the most appropriate one, a size parameter is used. The size

parameter is the particle size relative to the wavelength υ of the radiation inside the particle and is given by equation 3.51 (Alfano et al., 1995; Siegel and Howell, 2002).

$$\xi = \left[\frac{\pi d_p}{\upsilon}\right]_{min} \tag{3.51}$$

where d_p is the spherical particle diameter.

For a large sphere ($\xi > \sim 5$), with diffusely reflecting surface the phase function can be described by:

$$p(\theta) = \frac{8}{3\pi}(\sin\theta - \theta\cos\theta) \tag{3.52}$$

where θ is the angle between 2 directions of propagation.

For the range $0.3 < \xi < 5$, an approximation to the Mie scattering theory can be used. One approximation is the linear anisotropic scattering form (Fiveland, 1984):

$$p(\theta) = 1 + A\cos\theta \tag{3.53}$$

with $A = -1, 0, 1$ for backward, isotropic and forward scattering respectively.

For small spheres ($\xi < \sim 0.3$), the Rayleigh scattering phase function is proposed:

$$p(\theta) = \frac{3}{4}(1 + \cos^2\theta) \tag{3.54}$$

Since TiO_2 particles tend to agglomerate in water (Alfano et al., 1997; Cabrera et al., 1996; Toepfer et al., 2006), equation 3.52 is appropriate and has been used successfully by Toepfler *et al.* (2006). However, due to its mathematical simplicity, the linear anisotropic phase function with A = 0 has been preferred and used successfully by several researchers in the modelling of slurry reactors (Cassano and Alfano, 2000; Pareek et al., 2003a; Pareek et al., 2008; Pareek and Adesina, 2004; Romero et al., 2003) as well as to model scattering by large particles such as TiO_2 coated glass beads (Denny et al., 2009) and air bubbles (Trujillo et al., 2010). There was only one occurrence where backward scattering (A = -1) was used for Aldrich TiO_2 in a slurry reactor (Pareek et al., 2003b).

The phase function parameter (constant A in equation 3.53) has a relatively low sensitivity on the light intensity distribution within a slurry photocatalytic reactor (Pareek et al., 2003a; Pareek et al., 2008; Yu et al., 2008). Pareek (2003a) investigated the effect of the phase function parameter on Aldrich TiO_2 in a slurry reactor. It was found that at low catalyst loading (0.03 gL^{-1}), backward scattering was favoured while at higher catalyst loading, isotropic scattering became dominant. Nonetheless, in most cases, isotropic scattering gave a mean absolute percentage error of less than 10% when compared to experimental values of radial incident intensity. Furthermore, when comparing the two extremes of scattering ($A = -1$ and 1), the maximum difference in volume averaged intensity for four different catalyst loadings was less than 2.5% for non-reflecting and 10% for reflecting walls (Pareek et al., 2008).

3.3.3 Lamp emission models

Several mathematical models have been derived for the radiation emission of UV lamps. The basic models regard the lamp as an emitting line, a surface or a volume source, a detailed explanation of which can be found elsewhere (Pareek et al., 2008). Since all three models produce accurate results with marginal differences (Elyasi and Taghipour, 2010a; Pareek et al., 2008; Quan et al., 2004), the line source model is preferred due to its lesser computational time requirement, simplicity and accuracy. Diffuse rather than specular emission is more appropriate for mercury lamps (Duran et al., 2010b; Quan et al., 2004; Yang et al., 2005b; Zhang and Anderson, 2010), however due to its simplicity and high degree of accuracy, the specular model has been deemed satisfactory for UV lamps in general (Quan et al., 2004; Salvado-Estivill et al., 2007a; Salvado-Estivill et al., 2007b; Toepfer et al., 2006). In the modelling of photocatalytic reactors, the line source model has been used preferentially (Elyasi and Taghipour, 2010b; Pareek and Adesina, 2004; Qi et al., 2011; Salvado-Estivill et al., 2007b; Toepfer et al., 2006; Yang et al., 2005b) to describe the emitting lamp surface (equation 3.55) while only one occurrence has been found where a surface source model was used (Pareek et al., 2003b).

Some adjustment may be necessary on the emission model for the gas phase treatment of pollutants. Zhang and Anderson (2010) proposed a modification of the line source model to account for reflection and refraction by the quartz sleeve, Duran *et al.* (2010b)

modified the volumetric emission model to incorporate photon absorbance/re-emission effect produced by the mercury vapour in the lamp and found excellent agreement with near and far field data. Yang *et al.* (2005b) accounted for the effect of a cylindrical reflector wall in a gas-phase annular photoreactor by adjusting the line source model. However, if the radiant intensity is measured close to the lamp/quartz sleeve using a radiometer, no adjustments will be necessary in the model used. In the modelling of multi-lamps reactors, reflection from the bodies of other lamps can have an impact on radiation distribution and should be taken into consideration (Elyasi and Taghipour, 2010a). Jin *et al.* (2005) determined that reflection from another lamp surface added 3 - 9% to the fluence rate, depending on its position in the reactor.

In the modelling of slurry reactors, UV absorption within the quartz sleeve is negligible compared to that in the annular reaction space, hence the central lamp assembly can be discarded from mathematical consideration (Pareek and Adesina, 2004). Assuming a uniform distribution of radiant energy over the entire length of the lamp may not represent its true characteristics, especially in the region close to the surface of the lamp (Elyasi and Taghipour, 2010a), hence the boundary of the lamp with the quartz sleeve can be simplified by a model with suitable emission (equation 3.55) and reflection conditions (Huang et al., 2011). Huang *et al.* (2011) found that a reflection coefficient of 0.2 for the quartz sleeve was suitable to predict light intensity profiles in an ozone filled reactor, although not much difference was observed with a coefficient between 0 and 0.2. Qi *et al.* (2011) and Pareek *et al.* (2003b) used a reflection coefficient of zero in their modelling of a slurry reactor. Usually, the radiation emission from the source is considered constant with respect to time.

$$G_v = \frac{K_l}{4\pi r}\left(tan^{-1}\left(\frac{z+L}{r}\right) - tan^{-1}\left(\frac{z-L}{r}\right)\right) \tag{3.55}$$

$$K_l = \frac{P}{2L} \tag{3.56}$$

where L is the semilength of the lamp and P is the useful power of the lamp. From Table 3. 5, the useful power for some types of UV lamps lies between 7 and 46% of the total power.

Table 3. 5: Nominal and useful power for various types of UV lamps.

Lamp Type	Nominal Power (W)	Useful Power (W)	Ref
Medium pressure Hg lamp - Primarc AVP06C	300	22	(Pareek et al., 2003b)
Philips TLK 40/09N	40	4.2	(Brandi et al., 2000)
Philips TL/09	80	37	(Romero et al., 2009)
Philips TL 8W/08 F8 T5/BLB	8	1.2	(Salvado-Estivill et al., 2007b)

3.3.4 Wall treatment

Reactor wall surfaces are non-emitting but may be reflecting diffusely or specularly (Pareek and Adesina, 2004). Smooth walls are specularly reflecting and are preferred in immobilized TiO_2 systems such as packed beds (Denny et al., 2009), channelled optical fiber reactor (Denny et al., 2010a) and monolith type reactors (Chong et al., 2011) for maximum use of radiation, since low opacities are involved. As an example, Chong *et al.* (2011) found 67% of toluene degradation with completely reflective walls while 61% and 54% degradation could be achieved with partially reflective and non-reflective walls respectively. However, the advantages of using completely reflective walls will have to be weighed against the extra costs for their manufacture and periodic cleaning due to fouling. On the other hand, wall reflectivity is not an issue in annular slurry reactors. In such reactors with highly absorbing and scattering media, the effect of reactor walls can be neglected from reactor design and modelling (Pareek and Adesina, 2004), although this might not apply to optically thin media. Pareek *et al.* (2004) found that at a $W_{cat} \geq 0.05 gL^{-1}$, wall reflectivity had no effect on LVREA or incident radiation for the 3 types of wall investigated (non-reflecting, partially reflecting and completely reflecting). Yang *et al.* (2005b) mentioned that high wall reflection is not beneficial when the extinction coefficient is moderately high ($0.5\ cm^{-1}$) or the radius of the photoreactor is too large since in both cases, the amount of radiation reaching the wall is very small. In general, the reactor wall has been taken as diffusely reflecting due to the nature of its rough surface (Pareek, 2005; Pareek et al., 2003b). In any case, in the CFD modelling of optically thick slurry photoreactors, the reactor wall can be assumed to behave as a blackbody, i.e., wall reflectivity of zero and an emissivity of 1 (absorbs all radiation and re-emits as thermal energy). This is advised so as to reduce the computational time requirement in solving of the RTE. Figure 3. 6 shows the incident radiation contours

within a 30 cm diameter slurry reactor containing a TiO_2 loaded medium (Degussa P25, 0.05 gL^{-1}) and having a central lamp with emissive power of 200 Wm^{-2}. It can be seen that negligible radiation reaches the reactor wall.

3.3.5 Effect of catalyst loading

In annular slurry reactors, an increase in the catalyst loading results in a decrease in the overall incident intensity within the reactor. Pareek *et al.* (2004) determined that for a catalyst loading as low as 0.1 gL^{-1}, the illuminated zone was essentially confined to a narrow strip close to the quartz assembly and as such, most of the reactor space was rendered as dark, Figure 3. 5a. That strip would become narrower as the catalyst loading increased, Figure 3. 5b and c. Since the radiation intensities were negligibly small just after 2 cm from the lamp assembly, an annular thickness of more than 2 cm may not be useful in annular slurry reactors employing typical catalyst loadings (1 gL^{-1}) (Pareek and Adesina, 2004). As a matter of fact, Puma (2003) worked out that the optimal operation of TFS reactors require the optical thickness of the reactors to be in the range from 1.8 to 3.4. The optical thickness of an absorbing and scattering medium can be calculated from:

$$\tau = (\sigma + \kappa) W_{cat} \delta \tag{3.57}$$

where δ is the annulus thickness.

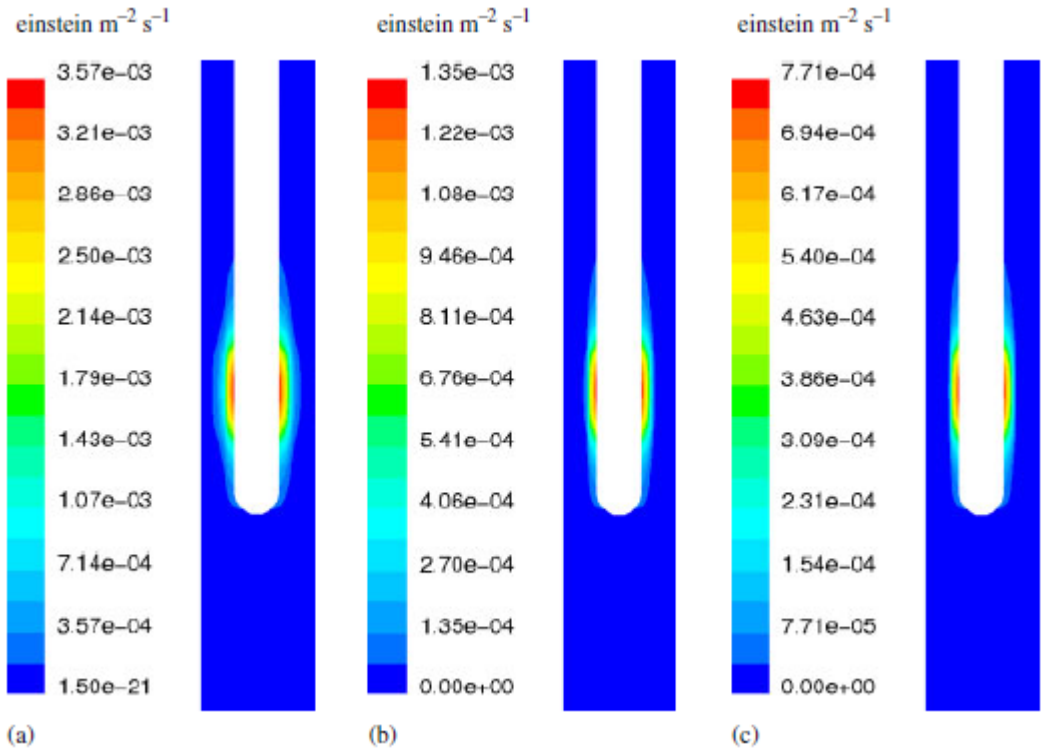

Figure 3. 5: Contours of incident radiation within an annular slurry reactor at TiO_2 (anatase) concentration of: a) 0.1 gL^{-1}, b) 0.50 gL^{-1} and c) 1.0 gL^{-1} (Pareek and Adesina, 2004).

Pareek *et al.* (2003b) found an optimum catalyst loading of 1 gL^{-1} for an annular reactor with an annulus thickness of 6 cm, which could be predicted by CFD simulations. From those works, it can be deduced that in the case of slurry reactors with a large annulus (δ > 6 cm) operation will be optimal at a much lower catalyst loading than with TFS reactors since a compromise will have to be reached between the amount of catalyst for photo-reaction and the illuminated space within the reactor.

There are situations whereby much higher optimum catalyst loadings have been reported (2 – 2.5 gL^{-1}) (Al-Sayyed et al., 1991; Chen and Ray, 1998; D'Oliveira et al., 1990; Okamoto et al., 1985; Qi et al., 2011). This is because optimum catalyst loading is not determined solely by the optical properties of the reacting medium (Pareek and Adesina, 2004). Particle agglomeration, even at low to medium catalyst concentrations (Cabrera et al., 1996; Yang et al., 2005a) and electrochemical factors such as pH and ionic strength may possibly cause a change in the optical properties of the medium itself. Furthermore properties inherent to catalytic activity other than the photoabsorption rates have strong influence on the reaction rates. Therefore it may not be possible to predict

an optimum catalyst loading from radiation absorption rate calculations alone. Nonetheless, CFD approach to modelling of light intensity distributions is useful in parametric investigation for the specific photocatalytic processes (Pareek and Adesina, 2004).

Coating thickness is analogous to catalyst loading in immobilized systems. Typical coating thicknesses are in the order of a few hundredths nanometers (Denny et al., 2009) on glass beads or micrometers (Denny et al., 2010b) for optical fibers. Danion *et al.* (2004) reported optimum coating thicknesses of 600 nm and 400 nm for 1 mm and 0.6 mm diameter optical fibers respectively. Moreover, beyond a certain thickness, a decrease in degradation will occur due to the reduced rate of diffusion of reactants.

3.3.6 Rate equations

This section presents the typical types of rate equations (related to the incident radiation or LVREA), that are used for slurry and immobilised photocatalytic reactors.

3.3.6.1 Slurry systems

The rate of photocatalytic degradation of a compound in aqueous TiO_2 suspensions will depend on the operating conditions such as pH, temperature, radiant intensity, oxygen concentration, pollutant concentration and TiO_2 loading such that:

$$-r = k(f[P]) \tag{3.58}$$

$$k = f(pH, T, I, [O_2], W_{cat}) \tag{3.59}$$

where $f[P]$ is a function of the pollutant concentration and is usually of the first order or L-H form. Here we will consider the effect of the light intensity on the reaction rate. The dependence of the photocatalytic degradation rate on illumination intensity undergoes a transition from first order to half order as intensity increases (Turchi and Ollis, 1990). As a result, some researchers have related the rate to the radiant flux of externally irradiated reactors (Al-Sayyed et al., 1991; Chen and Ray, 1998; D'Oliveira et al., 1990; Eng et al., 2010; Okamoto et al., 1985). The intensity of the radiant flux was altered via the placement of metal screens between the lamp and the reactor (Al-Sayyed et al., 1991; Chen and Ray, 1998; Okamoto et al., 1985).

$$-r_P = kI^m(f[P]) \quad (3.60)$$

However, the incident light intensity will attenuate with distance within a slurry reactor. A more sensible way of gauging the effect of intensity is by relating the rate to the LVREA:

$$-r_P = k(LVREA)^m(f[P]) \quad (3.61)$$

At the lamp wall vicinity, incident radiation is high so that the rate is half order with respect to LVREA. This shifts to first order near the back wall. An indication of both regimes being present is when the value of the exponent m is between 0.5 and 1. These conditions occur within thin film slurry reactors (Puma et al., 2004; Romero et al., 2009; Toepfer et al., 2006) as shown in Table 3. 6.

For slurry reactors with a large annulus, all regimes are expected to occur, i.e., half order, transitional and linear with respect to LVREA. As a result, there should be an optimum radiant flux or catalyst loading at which maximum reaction rate will happen. Pareek *et al.* (2003b) studied the rate of degradation of spent Bayer liquor in a large annulus slurry reactor by varying the catalyst loading and found an optimum at $W_{cat} =$ 1 gL^{-1}. The rate was modelled according to the following relationship:

$$-r_P = k_1(f[P])[LVREA - k_2 W_{cat}] \quad (3.62)$$

where the second term in between the square brackets on the right hand side represents the increasing rate of electron-hole recombination at increasing catalyst loading.

3.3.6.2 Immobilized systems

Immobilized systems are normally coated with a thin layer of TiO_2 (Danion et al., 2004). Since it is difficult to determine accurately the amount of irradiance absorbed in such systems, the incident irradiance is appropriate in such cases to define the rate equation. One can reasonably assume that for a given catalyst, the ratio between incident and absorbed irradiance is the same, whatever the photoreactor (Queffeulou et al., 2010). For immobilized systems, the rate equation is similar to equation 3.60.

3.3.6.3 Effect of light intensity on rate order

Herrmann (1999) mentioned that the rate of reaction is proportional to the radiant flux below a value of 250 Wm^{-2} and that above this value, the rate becomes proportional to the square root of the radiant flux. This value was obtained from an externally irradiated slurry batch reactor using 2.5 gL^{-1} Degussa P-25 TiO_2. However, looking at Table 3. 6 for other cases of externally irradiated slurry reactors it is obvious that this limit cannot be generalized. D'Oliveira *et al.* (1990) found that limit to occur at 200 Wm^{-2} at similar conditions while at a lower concentration of 2 gL^{-1} Degussa P-25 TiO_2, the linear regime seemed to be at approximately $\leq$ 50 Wm^{-2} (Al-Sayyed et al., 1991) with a transitional regime between 15 and 170 Wm^{-2} (Chen and Ray, 1998). It can be argued that in slurry photocatalytic reactors, all regimes exist due to the change in light intensity with penetration. As a result, with optically thick annular reactors, the half order regime will occur within a thin strip close to the lamp surface meaning that the majority of the reactor volume will operate in the first order regime (low light intensity). However this will depend upon the catalyst load being used, the annular thickness, type of catalyst as well as the lamp emission power. From Table 3. 6, it can be seen that TFS reactors (Puma et al., 2004; Romero et al., 2009; Toepfer et al., 2006) and/or high lamp emissive power give rise to operation in the half order or transitional regime due to the high light intensity occurring within the reactor volume. On the other hand, reactors with relatively larger diameters (Chen and Ray, 1998; D'Oliveira et al., 1990; Okamoto et al., 1985) generally operate in first order regime due to light shielding by the catalyst particles which reduces the half order reaction volume to a thin narrow strip close to the lamp surface.

Immobilized systems can give a better indication of the influence of radiant flux on reaction rate since the radiant fluxes are measured at the catalyst surface. From

Table 3. 7, for aqueous systems, linear regimes were reported at ≤ 28.1 Wm^{-2} (Charles et al., 2011) and ≤ 110 Wm^{-2} (Romero et al., 2003) and a transitional regime was found in the range between 55 and 210 Wm^{-2} (Mehrotra et al., 2005). For gaseous phase photocatalysis, a linear regime was reported at ≤ 28.1 Wm^{-2} (Salvado-Estivill et al., 2007b), a transitional regime in the range 13 to 144 Wm^{-2} (Peral and Ollis, 1992) and a near half order regime (exponent was 0.55) in the range 100 to 400 Wm^{-2} (Obee and Brown, 1995).

In slurry reactors with large annulus or small catalyst loading, all reaction rate regimes are expected to occur as depicted in Figure 3. 6. Moreover, as seen in

Table 3. 7, the range of incident radiation intensities at which those regimes occur will depend on the pollutant species, reactor design, type of catalyst and type of UV source.

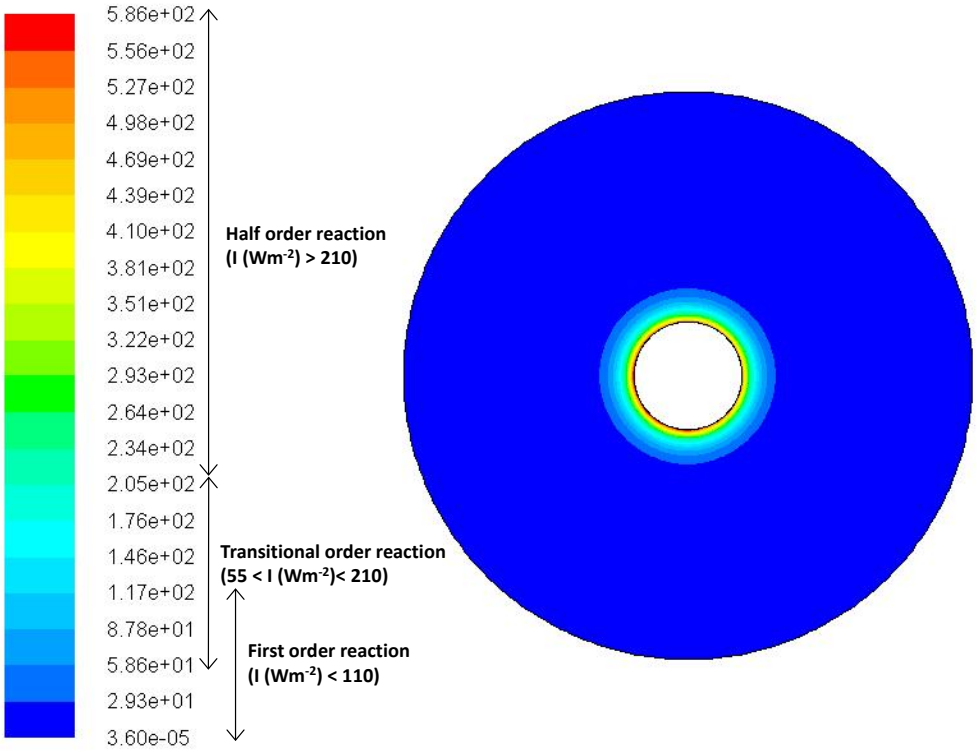

Figure 3. 6: Regimes of different reaction orders existing in a slurry photocatalytic reactor with lamp in the middle (cross sectional view at lamp middle, in the axial direction). Lamp emissive power = 200 Wm^{-2}, catalyst (Degussa P25 TiO_2) concentration = 0.05 gL^{-1}.

The reaction rate order will be dependent on the radial incident radiation intensity such that:

When $I \geq I_h$

$$-r_p = k_h(f[P])(LVREA)^{0.5} \tag{3.63}$$

where I_h is the minimum incident intensity at which half order reaction takes place and k_h is the half order reaction rate constant.

When $I_t < I < I_h$

$$-r_p = k_t(f[P])(LVREA)^m \tag{3.64}$$

where $0.5 < m < 1$, I_t is the minimum incident intensity at which transitional order reaction takes place and k_t is the transitional order reaction rate constant.

When $I < I_t$

$$-r_p = k_f(f[P])(LVREA) \tag{3.65}$$

where k_f is the first order reaction rate constant.

For a reaction volume that has been discretised into elemental volumes dV_W the total average reaction rate can be expressed as:

$$-r_p = \frac{f[P]}{V_W}\left[k_h \int LVREA\,(V_W)^{0.5}\, dV_{W,I \geq I_h} + k_t \int LVREA\,(V_W)^{m}\, dV_{W,I_t < I < I_h} + k_f \int LVREA\,(V_W)\, dV_{W,I < I_t}\right] \tag{3.66}$$

where V_W is the volume occupied by the wastewater and I_{max} is the maximum incident light intensity which occurs at the lamp surface.

Table 3. 6: Operating conditions in slurry photocatalytic reactors.

Pollutant	$[P_0]$	Reactor Dimensions	Lamp Location	υ (nm)	Catalyst	W_{cat} (gL^{-1})	Rate Equation	I_W (Wm^{-2})	Exponent m	Ref
4-chlorophenol	0.155mM, 0.62mM	90 mL flask	External	≥340	P25	2	3.60	≤50	1	(Al-Sayyed et al., 1991)
								50 - 500	0.5	
Phenol	0.5mM	200 mL beaker	External	313, 334, 366	Anatase	2	3.60	≤3.4	1	(Okamoto et al., 1985)
								3.4 - 6.8	0.5<m<1	
								≥6.8	0.5	
3-chlorophenol	0.155mM	90 mL flask	External	≥340	P25	2.5	3.60	≤200	1	(D'Oliveira et al., 1990)
								>200	0.5	
Brij 35	0.083mM	Monolith, dimensions NS	External	NS	P25	0.1	3.60	40 - 200	0.46	(Eng et al., 2010)
4-nitrophenol	20ppm	Circular glass plates, dimensions NS	External	365	P25	2	3.60	15 - 170	0.84	(Chen and Ray, 1998)
Congo red	40ppm	0.149m Diameter, 0.05m Height	Internal	NS	Anatase	2	3.61	NS	1	(Qi et al., 2011)
Herbicides	≤1ppm	0.026m Diameter, 0.255m Height	Internal	320 - 380	P25	0.4	3.61	36.5 - 67.1	0.5	(Toepfer et al., 2006)
Trichloroethylene	≤70ppm	0.06m Diameter, 0.7m Height	Internal	310 - 385	Anatase	0.25 - 1	3.61	280	0.5	(Romero et al., 2009)
Isoproturon	1.1ppm	0.038m Diameter, 0.255m Height	Internal	>300	P25	0.4	3.61	148 - 293	0.82	(Puma et al., 2004)
Spent Bayer liquor	63 - 125ppm	0.2m Diameter, 1m Height	Internal	250 - 400	Anatase	0.05 - 5	3.62	577	1	(Pareek et al., 2003b)

Table 3. 7: Operating conditions in immobilized photocatalytic reactors.

NS – Not Specified, L – Liquid Phase, G – Gas Phase.

Pollutant	$[P_0]$	Reactor Type	υ (nm)	Catalyst	I_W (Wm^{-2})	Exponent m	Ref
Trichloroethylene - G	25.1µM	Flat plate	324 - 400	P25	≤28.1	1	(Salvado-Estivill et al., 2007b)
Benzoic acid - L	<5ppm	Annular	NS	P25	≤110	1	(Duran et al., 2011)
Salicylic acid - L	10ppm	Micro channel	300 peak	P25	≤28	1	(Charles et al., 2011)
Benzoic acid - L	0.16mM	Swirl flow monolithic	365.5 peak	P25	55 - 210	0.89	(Mehrotra et al., 2005)
Toluene, formaldehyde, 1, 3 butadiene - G	0.29ppmv	Wash coated alumina reticulate	250 - 350	P25	100 - 400	0.55	(Obee and Brown, 1995)
Acetone - G	0.16ppm	Fixed bed	>300	P25	13 - 144	0.7	(Peral and Ollis, 1992)

3.3.7 Boundary conditions

Boundary conditions are the initial conditions required in the setting up of the DOM for the simulation of the solutions of the RTE. This section describes some boundary conditions that are required for the simulation of radiation in photocatalytic reactors.

3.3.7.1 Reactor wall

For an amount of radiation incident on a wall, some of it may be absorbed, some transmitted and the rest may be reflected. Hence (Pareek and Adesina, 2004):

$$a + t + r_{ref} = 1 \tag{3.67}$$

where a, t and r_{ref} are the absorptivity, transmittivity and reflectivity of the reactor wall

For a blackbody wall, Kirchoff's principle is applicable:

$$a = e \tag{3.68}$$

and for a non-transparent wall,

$$t = 0 \tag{3.69}$$

such that equation 3.67 reduces to:

$$e + r_{ref} = 1 \tag{3.70}$$

Values of the reflectivity for several materials are readily available in the literature.

3.3.7.2 Lamp surface

Due to back scattering in slurry systems or due to reflection from other surfaces in immobilized systems, the incident radiation flux at the lamp surface is given by (Pareek and Adesina, 2004):

$$G_{in}^{Lamp} = \int I_{in} s \cdot \hat{n} d\Omega \tag{3.71}$$

where s is the direction of the incident radiation and $\hat{n}$ is a unit vector normal to the plane of incidence.

The net radiative flux leaving the surface of the lamp is therefore given by:

$$G_{out}^{Lamp} = r_{Lamp} G_{in}^{Lamp} + G_{emission}^{Lamp} \tag{3.72}$$

where r_{Lamp} is the lamp reflectivity and $G_{emission}^{Lamp}$ is the emission from the lamp which can be represented by an emission model such as equation 3.55.

3.3.7.3 Gas distributor modelling

In the modelling of gas inlet for a slurry photocatalytic reactor, a uniform surface is usually used (Pareek et al., 2003b; Qi et al., 2011; Trujillo et al., 2010).

3.3.7.4 Reactor outlet (gas) – slurry systems

The outlet section (above the liquid surface) for the gas should be long enough (refer to Figure 3. 3) so as to ensure gas-liquid disengagement (Hulme et al., 2005; Pareek et al., 2003b). Alternatively, to avoid the modelling of a gas disengagement region, the top surface of the liquid was modelled as a non-shear wall which set the normal gas and liquid velocity to zero and the computational cells attached to the top surface were defined as a sink to represent escaping bubbles (Trujillo et al., 2007, 2010). The sink can be represented as (Ranade, 2002):

$$S_G = -A_B \alpha_{GB} W_{GB} \rho_G \tag{3.73}$$

where A_B is the area of the bottom surface of the computational cell attached to the top surface, W_{GB}, α_{GB} and ρ_G are the normal velocity of gas bubbles, the gas volume fraction of the computational cell lying below the computational cell attached to the top surface and the gas density respectively.

3.3.8 Angular discretization and pixelation

The spatial discretization of the computational region for the solution of the RTE is taken directly from the grid topology. However, the directional discretization for the RTE is required as a user input to the solver. The angular discretization is further divided into pixels so as to avoid the influence of overhang. In general the ranges of control angles and pixelation that have been used in modelling were 32 - 288 (Denny et al., 2009; Duran et al., 2011; Huang et al., 2011; Pareek, 2005; Pareek and Adesina, 2004; Pareek et al., 2003b; Trujillo et al., 2010) and 1×1 - 4×4 respectively (Denny et al., 2009; Duran et al., 2011; Pareek and Adesina, 2004; Pareek et al., 2003b; Trujillo et al., 2010).

3.4 Conclusions

The DOM to solve solutions of the RTE has been reviewed in this chapter. Relevant equations pertaining to the design of photocatalytic reactors using TiO_2 as catalyst

have been presented. This chapter is intended to provide useful information for the simulation of any type of photocatalytic reactor using CFD.

Notation

a – wall absorptivity

A – area (m^2)

C_D – drag coefficient (dimensionless)

d – diameter (m)

e – coefficient of restitution (granular theory) / wall emissivity (radiation modelling)

F – interphase momentum exchange force ($kgm^{-2}s^{-2}$)

g – gravitational acceleration (ms^{-2})

g_0 – radial distribution function

G – incident intensity at any point from all the directions (Wm^{-2})

I - intensity (Wm^{-2})

J – diffusion flux ($kgm^{-2}s^{-1}$)

K – interphase momentum exchange coefficient (E-E modelling, $kgm^{-3}s^{-1}$) / line emission model radiation power per unit length constant (lamp emission model, Wm^{-1})

L – length (m)

LVREA – local volumetric rate of energy absorption (Wm^{-3})

m – mass (kg)

p – pressure shared by all phases (Nm^{-2})

$p(\Omega' \longrightarrow \Omega)$ – phase function for in scattering of radiation

P – power (W)

r – rate of production/destruction (species balance, $kgm^{-3}s^{-1}$) / radius (Stokes number calculation, m) / radial direction (emission model, m)

r_{ref} – wall reflectivity

R – bubble radius (m)

Re – Reynolds number (dimensionless)

s, z– distance (m)

S – rate of mass transfer ($kgm^{-3}s^{-1}$)

St – Stokes number (dimensionless)

t – time (s) / wall transmittivity (radiation modeling)

U – velocity (ms^{-1})

v_0 – approach velocity (Stokes number calculation, ms^{-1})

V – volume (m^3)

V_g – superficial gas velocity (ms^{-1})

W – normal velocity (ms^{-1})

W_{cat} – catalyst loading (gm^{-3})

Y – mass fraction

Greek letters

α – volume fraction

γ – collisional dissipation of energy ($kgm^{-1}s^{-3}$)

δ – annulus thickness (m)

θ – granular temperature (granular theory, m^2s^{-2}) / angle between 2 directions of propagation (radiation modelling)

κ – granular temperature conductivity (granular theory, $kgm^{-2}s^{-1}$) / absorption coefficient (radiation modelling, m^{-1})

κ^* - specific absorption coefficient (m^2g^{-1})

λ – bulk viscosity (granular theory, $kgm^{-1}s^{-1}$) / of wavelength (radiation modelling, nm)

μ – shear viscosity ($kgm^{-1}s^{-1}$)

ξ – size parameter (dimensionless)

ρ – density (kgm^{-3})

σ – scattering coefficient (m^{-1})

σ^* - specific scattering coefficient (m^2g^{-1})

τ – viscous stress tensor (Nm^{-2})

ϕ – energy exchange terms (granular flow)

ω – optical thickness (dimensionless)

Ω – solid angle (steradian)

Subscripts

B– bubble

cat – catalyst

f – first order

g – terms relevant to granular multiphase flows

GB – gas bubble

h – half order

i – specie

k, l, p, q – fluid phases

P– particle

s – solid phase

t – transitional order

W – wastewater

θ – of granular temperature

υ – wavelength

Other symbols

⟨ ⟩- denotes wavelength averaged values

⌊ ⌋ - denotes concentration ($molL^{-1}$)

Chapter 4 - Photocatalytic Treatment of Shower Water Using a Pilot Scale Reactor

Fresh water is getting scarcer. The number of people living in water stressed or water scarce countries is estimated to increase from half a billion now to three billion in 2025 (Stikker, 1998). Water reuse has been dubbed as the greatest challenge of the 21st century (Asano, 2002) and as such, great emphasis is being put into the development of new technologies for the treatment of wastewater for reuse.

Since the discovery, in 1977, that titanium dioxide (TiO_2) could decompose cyanide in water (Fujishima and Zhang, 2006), the field of photocatalysis has been receiving increasing interest. Photocatalysis is an advanced oxidation process (AOP) that uses a catalyst (often TiO_2), UV light and an electron acceptor (O_2, O_3, H_2O_2) to completely decompose organic pollutants found in liquids or gases. The basis of the process is the use of low energy UV-A photons (for which the energy is greater or equal to the band gap energy of the catalyst) to excite the semiconductor catalyst into charge separation and generate electron-hole pairs. The electrons and holes, on separation, assist in the production of the very reactive hydroxyl radical in the aqueous phase which can destroy many toxic organic pollutants. This technology however works best at low pollutant concentrations (mgL^{-1} or $mmolL^{-1}$) and when the catalyst is finely dispersed within the medium. The overall process can be described by the following reaction equation:

$$\text{Organic Pollutants} + O_2 \xrightarrow{\text{Semiconductor+UVA Light}} CO_2 + H_2O + \text{Mineral Acid}$$

Shower water is part of grey water and is produced by every household at a substantial amount (15 – 55 $Lday^{-1}$) with a pollutant loading up to 100 mgL^{-1} (Eriksson et al., 2002). Existing technologies for the treatment of grey water include membrane filtration, coagulation, ion exchange and membrane bioreactors (Jefferson et al., 2000; Li et al., 2009a). However these techniques are either costly or merely transfer the pollutants from one medium to another. As a result, shower water is a good candidate for photocatalytic treatment. The treated water could be reused where potable water is not required. Such applications include toilet flushing, landscape irrigation and car washing.

Countless researches have been made on the photocatalytic treatment of single or a few organic components in water (Belgiorno et al., 2007; Gaya and Abdullah, 2008; Pera-Titus et al., 2004). Domestic and industrial wastewaters on the other hand have a multitude of pollutants and take longer to treat (typically a few hours) (Balcioglu and Arslan, 1998; El Hajjouji et al., 2008; Fotiadis et al., 2007; Pekakis et al., 2006; Rodrigues et al., 2008).

The photo-oxidation of surfactants, the main components of shower water, was extensively studied by Hidaka and co-workers (Hidaka et al., 1986; Hidaka et al., 1988; Hidaka et al.; Hidaka and Zhao, 1992; Zhao et al., 1992). They found that photodegradation decreases in the following order: anionic > non-ionic > cationic surfactants and postulated that photocatalysis was mainly a surface reaction due to the short lifetime of hydroxyl radicals. Sanchez *et al.* (2010b) successfully obtained 65% dissolved organic carbon (DOC) removal with hotel grey water at 29 mgL^{-1} initial DOC concentration while Zhu *et al.* found (2008) that photocatalysis can effectively remove carbonaceous and nitrogenous biochemical oxygen demand from synthetic grey waters. Photocatalysis has also been reported to be efficient in the disinfection of E-coli (Van Grieken et al., 2009), a microorganism bound to be present in wastewater that had had contact with humans. The vast majority of photocatalytic research has been performed at bench scale. If it is desired to commercialise this technique, pilot scale experiments are required so as to obtain a better understanding of the operational and hydrodynamic factors involved with higher throughputs.

The objective of this research was to study pollutant degradation in shower water in a pilot scale photocatalytic reactor (31 L in volume) operating in a recirculation mode. The effect of several parameters such as the initial slurry pH, air flow rate, slurry recirculation rate, and catalyst dosage was studied. All experiments were carried out for a period of 6 hours, which was deemed a reasonable treatment time.

4.1 Experimental

The following section describes the shower water characterisation, chemicals used, reactor set-up and the experimental procedure carried out for each experiment.

4.1.1 Shower water characterisation

Shower water was collected daily from the researcher's home and stocked in the laboratory prior to the experiments. The same cleaning products were used each time (shampoo, face wash and body soap) to maintain consistency. The characteristics of the collected shower water are presented in Table 4. 1. A detailed list of all the constituents present in each of the cleaning product is presented in *Appendix A1 – Shower water detailed composition.*

Table 4. 1: Shower water characterisation.

TOC (mgL^{-1})	24.62 ± 0.44
pH	7.37 ± 0.14
Main constituents (as per the products' ingredients list). *See Appendix A1 – Shower water detailed composition.*	Anionic surfactants (Sodium laureth sulphate, sodium cocoamphoacetate, sodium lauryl sulphate, ammonium laureth sulphate), Cationic surfactants (Cocamide MEA), Nonionic surfactants (Lauryl glucoside, cetyl alcohol), Fragrance, Antimicrobial agents.

The TOC level of the shower water suggests that it is a low strength grey water. The main constituents of liquid soaps and shampoos are surfactants which can add up to 80% by weight of chemicals content (Lai, 2005). Some other constituents that may be present in trace amounts in the shower water include sebum, micro-organisms and dyes.

4.1.2 Reagents and analytical methods

Aeroxide® P25 titanium dioxide was purchased from Sigma Aldrich and was used as received. The catalyst had the following properties: 21 nm particle size, 50±15 m^2g^{-1} BET specific surface area, > 99.5% TiO_2 content (2011) and a band gap energy of 3.2 eV, corresponding to photons with wavelengths less or equal to 385 nm (Cabrera et al., 1996). A 6 M hydrochloric acid was used to modify the slurry pH prior to reaction. Compressed air was used as feed gas to the reactor and for UV lamp

cooling. Tap water was used to dilute the shower water (if required). Slurry pH was measured with a TPS digital pH meter, which was calibrated periodically. Samples collected were filtered with 0.45 microns syringe filters and analysed for Total Organic Carbon (TOC) on a Shimadzu TOC-$V_{CPH/CPN}$ analyser (Shimadzu Corporation, Japan).

4.1.3 Reactor set up

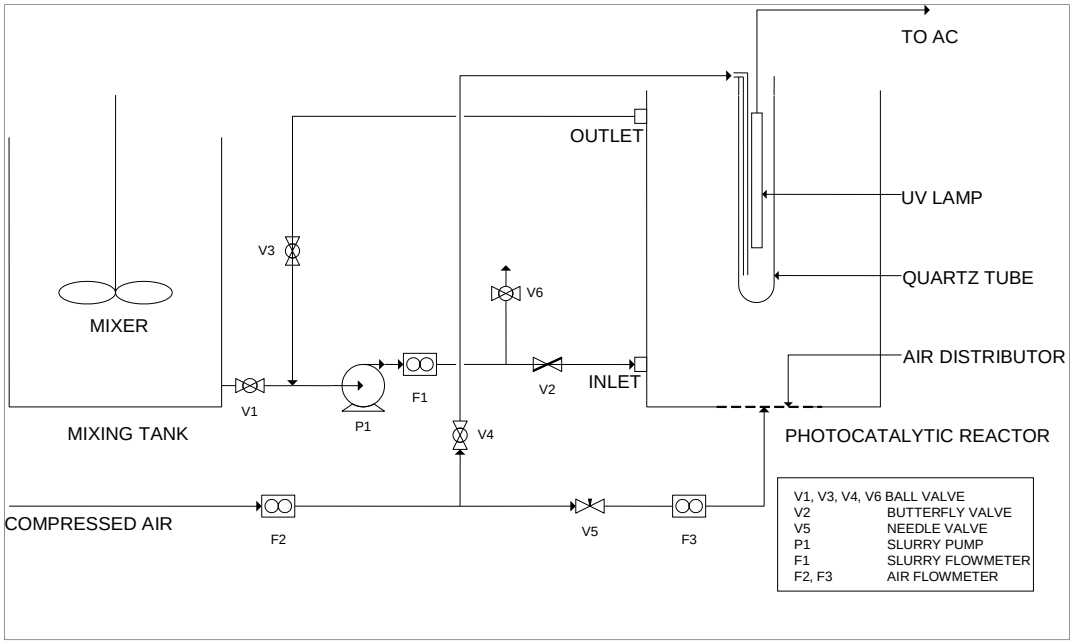

Figure 4. 1: Experimental set up for photocatalysis experiments. Shower water was mixed for 30 minutes with catalyst and acid in mixing tank initially before mixture was sent to the photocatalytic reactor via pump P1. Reactor was operated in recirculation mode.

Figure 4. 1 shows the reactor set up used in this study. The reactor volume was 31 L (30 cm diameter) and was operated in recirculation mode. Ambient air was supplied by a compressor via a 10 cm distributor centred at the bottom of the reactor. Part of the compressed air was also used as coolant for the UV lamp. The UV mercury lamp, purchased from Primarc Ltd. (PM 3426, 560 W, 20 cm length medium pressure mercury lamp) was fitted into a quartz tube and suspended in the middle of the reactor. A digital thermocouple provided the temperature within the reactor. The temperature was maintained between 26 and 28 ^{0}C by varying the rate of cooling water which ran through a coiled heat exchanger located around walls at the bottom of the reactor. An Iwaki magnetic pump was used for slurry circulation. Slurry flowrate was varied using valve V2 while air flow rate was varied via valve V5.

4.1.4 Procedure

Shower water was diluted with tap water (if required) and mixed with the titanium dioxide powder in a 60 L tank. The pH was adjusted and the slurry was allowed to mix for 30 minutes to allow for dark adsorption of pollutants onto the catalyst surface. Compressed air as well as cooling water was started and the slurry was transferred to the reactor via the Iwaki magnetic pump. Once the reactor was filled, valve V1 was closed and valve V3 was opened to allow the reactor to operate in recirculation mode and finally, the lamp was switched on. Samples were taken in 20 mL aliquots via sample valve V6 and were filtered with 0.45 microns syringe filters prior to analysis.

4.1.5 Mass balance

Due to the wastewater temperature during treatment (27˚ C), some evaporation will occur during the course of treatment, leading to the potential loss of TOC as volatile organic carbon (VOC). *A simple mass balance calculation is presented in Appendix A2 – Mass Balance on Reactor, showing that the maximum loss of VOC due to water evaporation is negligible compared to TOC degradation with respect to photocatalytic reactions.*

4.2 Results and Discussion

Since the shower water consisted of a myriad of organic components, a realistic way of reporting the pollutant concentration was by measuring the total organic carbon (TOC in mgL^{-1}) of the samples. The average reaction rate for TOC elimination was calculated using equation 4.1.

$$-R_{TOC} = \frac{TOC_{initial} - TOC_{final}}{\tau} \qquad (4.1)$$

where $-R_{TOC}$ is the average rate of degradation of TOC ($molL^{-1}min^{-1}$), $TOC_{initial}$ and TOC_{final} are the initial and final TOC concentration ($molL^{-1}$) and τ is the real contact time (minutes) in the reactor which is 360 minutes.

Please note that the detailed experimental results for all variables optimisation are presented in Appendix A3 – Detailed Experimental Results for Shower Water Photocatalysis.

4.2.1 Photocatalysis of shower water

The temporal course at optimum conditions for the photocatalysis of shower water in terms of TOC reduction is illustrated in Figure 4. 2. Part of the TOC was adsorbed onto the catalyst surface during the dark adsorption stage. Upon irradiation, the TOC concentration increased to a maximum within the first two hours of reaction that corresponded to the initial TOC concentration prior to dark adsorption. This phenomenon had been observed previously (Eng et al., 2010; Hidaka et al.; Zhang et al., 2004) for the photocatalytic oxidation of anionic surfactants at low initial concentrations. The initial increase in TOC can be attributed to the formation of intermediates on the catalyst surface followed by photo-desorption of the intermediates back into the liquid medium. Several types of intermediates are formed via the photo-oxidation of long chained hydrocarbons. Zhang *et al.* (2004) reported the formation of aldehyde and peroxide intermediates during the photo-oxidation of surfactants.

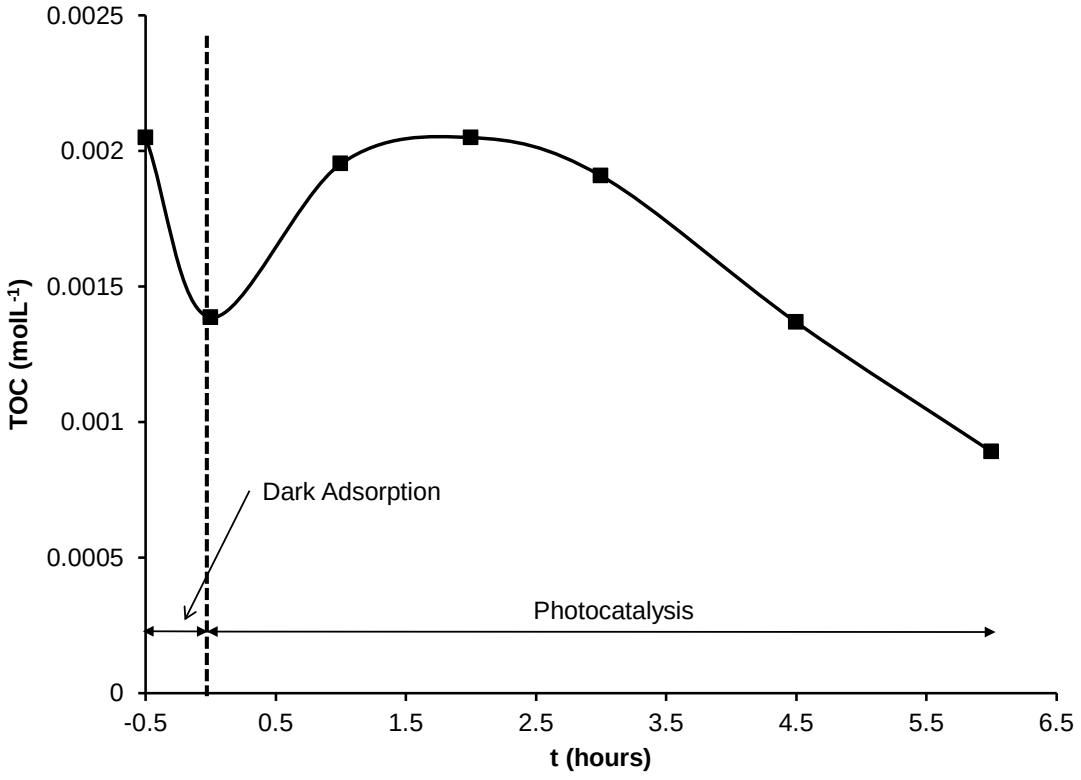

Figure 4. 2: Temporal course for shower water photocatalysis at optimum conditions (TOC initial concentration = 24.62 ±0.44 mgL^{-1}, Average reaction temperature = 27°C, Initial slurry pH = 3.00, 0.07 gL^{-1} catalyst loading, 1.8 $Lmin^{-1}$ air flow rate and 4.4 $Lmin^{-1}$ slurry flow rate).

A reduction in the TOC concentration was then observed after 2 hours due to the onset of oxidation of organic pollutants. This reduction was only moderate from t = 2

h to t = 3 h probably due to a large quantity of long chained organics/intermediates still remaining in the solution. However, as the photoreaction proceeded, the long chained organics/intermediates cleaved into smaller chained intermediates for which mineralisation to carbon dioxide, water and mineral acids took place at a faster rate, as observed after t = 3 h. A maximum of 57% TOC degradation was obtained within 6 hours of treatment at optimum conditions.

4.2.2 Effect of slurry initial pH

The initial pH of the slurry is an important parameter that needs to be considered as it influences the surface charge properties of the catalyst particles (Gaya and Abdullah, 2008), hence the adsorption of charged pollutants. Figure 4. 3 shows the effect of the slurry initial pH on the average rate of TOC degradation. There was a gradual increase in the average reaction rate as the pH was decreased from 7.4 (natural pH) to 5.0. The increase in reaction rate became steeper as the pH was further lowered and reached a maximum at pH = 3.0. Further lowering of the pH to 2.2 led to a sharp decrease in the reaction rate.

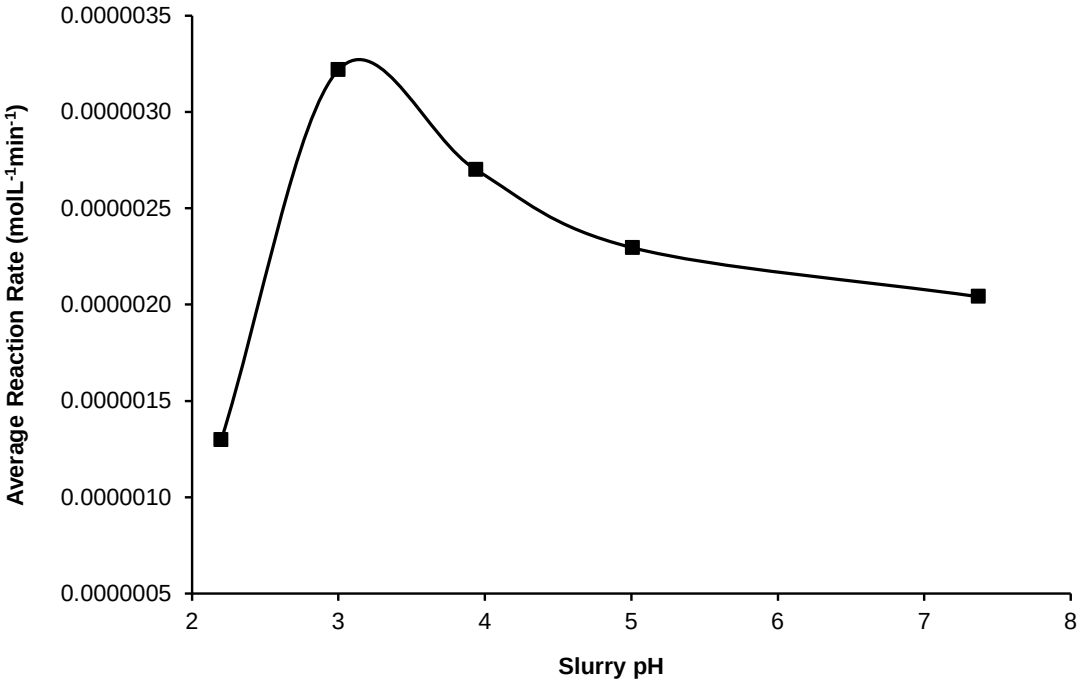

Figure 4. 3: Effect of slurry initial pH on average reaction rate (TOC initial concentration = 24.62 ±0.44 mgL^{-1}, Average reaction temperature = 27°C, 0.07 gL^{-1} catalyst loading, 1.8 $Lmin^{-1}$ air flow rate and 4.4 $Lmin^{-1}$ slurry flow rate).

Titanium dioxide is amphoteric by nature which means that past a certain pH, it can be either positively or negatively charged. That pH, which is called the point of zero

charge (ZPC), occurs at a value of 6.5 for Aeroxide® P25 titanium dioxide (Regalbuto, 2007). Hence when pH < ZPC the TiO_2 is positively charged while at pH > ZPC, it is negatively charged as shown in equations 4.2 and 4.3.

When pH $<$ ZPC: $TiOH + H^+ \leftrightarrow TiOH_2^+$ (4.2)

When pH $>$ ZPC: $TiOH + OH^- \leftrightarrow TiO^- + H_2O$ (4.3)

This implies that at lower pH, the positively charged TiO_2 surface can easily attract the negatively charged species from the solution hence facilitating their photo-oxidation. The main components of the shower water used were anionic surfactants as presented in Table 4. 1. As the pH of the slurry was decreased, the positive surface charge of the TiO_2 increased, attracting more and more anionic groups to its surface. This is further evident with the change in the dark adsorption with slurry pH in Figure 4. 4, which shows that pollutant species during the dark adsorption remained constant between pH of 7.4 and 5.0 but then increased sharply to reach a maximum of 32.4% adsorption at pH 3.0. Other research involving anionic surfactants have also shown preferential photo-oxidation at low pH (Oyama et al., 2004; Sanchez et al., 2010a).

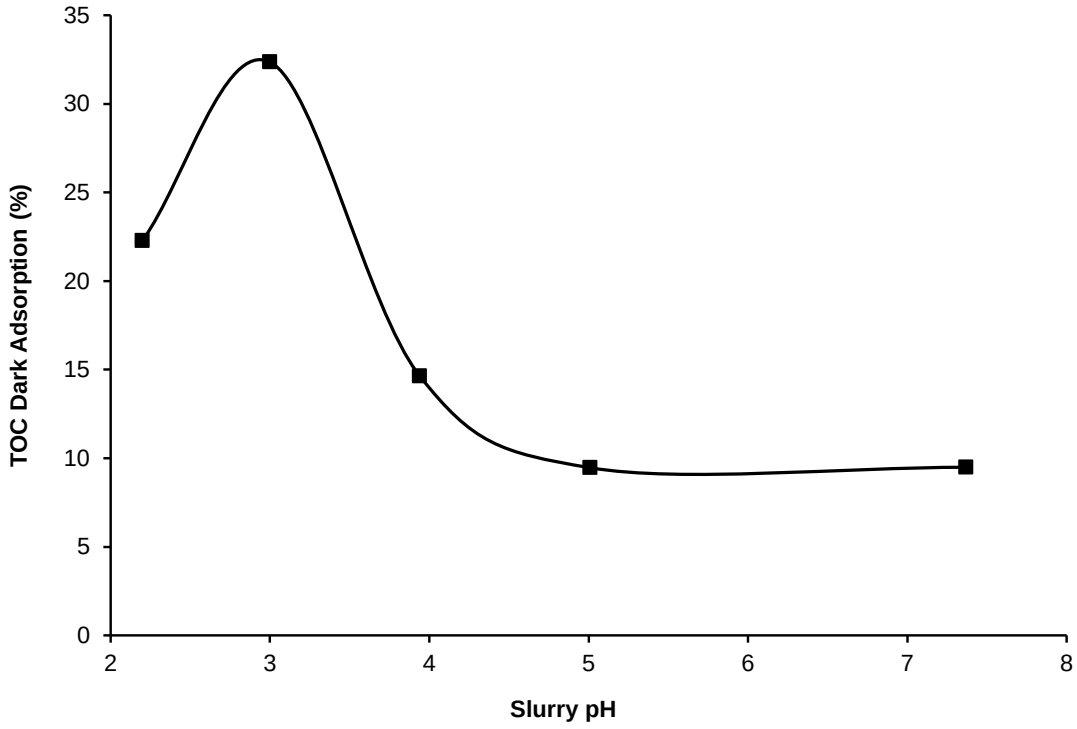

Figure 4. 4: Effect of slurry initial pH on amount of TOC adsorbed in the dark.

Being radical scavengers, carbonate anions present in the wastewater can inhibit photo-oxidation (Andreozzi et al., 1999). However an acidic medium can remove these unwanted anions as per equations 4.4 and 4.5.

$$HCO_3^- + H^+ \rightarrow H_2O + CO_2 \quad (4.4)$$

$$CO_3^{2-} + 2H^+ \rightarrow H_2O + CO_2 \quad (4.5)$$

Nonetheless, Figure 4. 3 shows that a further reduction of pH to 2.2 was in fact detrimental to the degradation of TOC. This was attributed to high levels of Cl^- ions in the solution. Cl^- ions are scavengers of hydroxyl radicals as well as holes (Chong et al., 2010) and can therefore greatly reduce the photo-oxidation process. As the pH was decreased from 3.0 to 2.2, the concentration of Cl^- increased exponentially from 1×10^{-3} M to 6.3×10^{-3} M, hence explaining the rapid decrease in the TOC removal rate. The optimum pH of 3.0 was maintained throughout subsequent experiments.

4.2.3 Effect of catalyst dosage

Most wastewater photocatalytic treatment studies report an optimum catalyst concentration. Beyond that optimum, the rate of reaction either remains unchanged or decreases. Figure 4. 5 shows the effect of catalyst loading on the average reaction rate with the range of catalyst loading investigated between 0.03 and 0.15 gL^{-1}. It is clear that the optimum catalyst concentration was about 0.07 gL^{-1}.

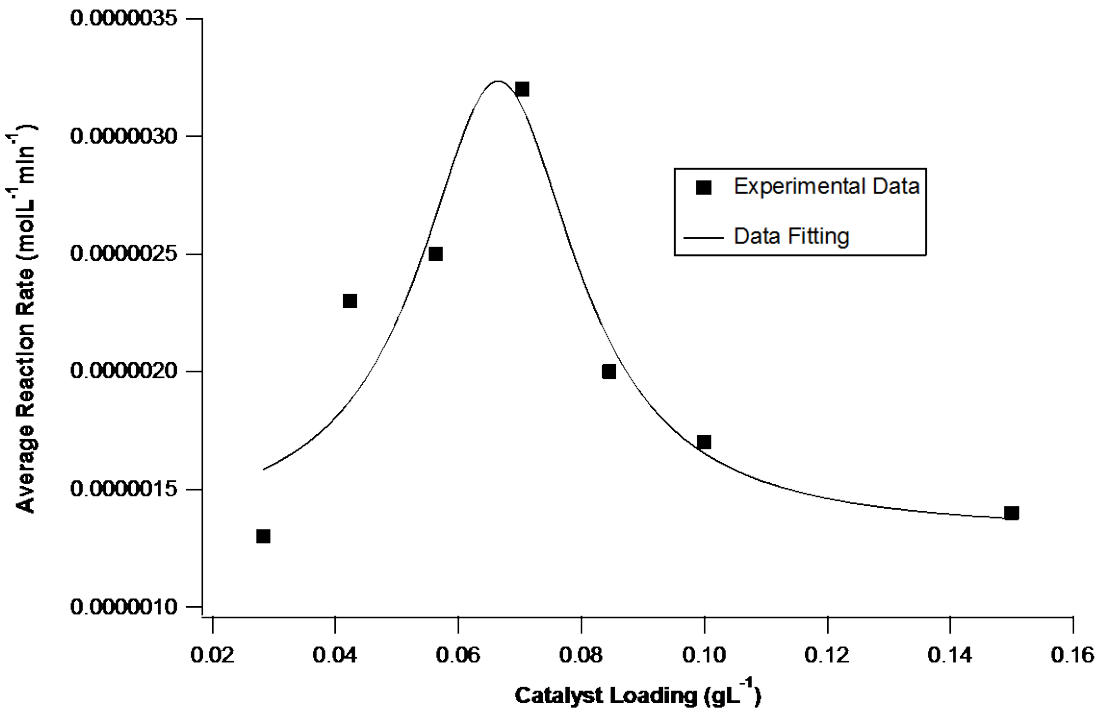

Figure 4. 5: Effect of catalyst loading on average reaction rate (TOC initial concentration = 24.62 ±0.44 mgL^{-1}, Average reaction temperature = 27°C, Initial slurry pH = 3.00, 1.8 $Lmin^{-1}$ air flow rate and 4.4 $Lmin^{-1}$ slurry flow rate).

Reported optimum catalyst loadings for wastewater treatment are usually within a range of 0.1 – 1 gL^{-1} (Belgiorno et al., 2007; Lea and Adesina, 1998; Pera-Titus et al., 2004), although some studies have also reported lower optimum loadings (0.05 gL^{-1}) (Machado et al., 2003). However, in all cases , the optimum value strongly depends on the reactor design, catalyst type, pollutant type and concentration (Gogate and Pandit, 2004).

In the current study, a relatively low value of optimum catalyst loading could be attributed to low concentrations of shower water as well as the large reactor diameter. Lower catalyst loadings provided sufficient sites for photo-reaction and allowed a maximum possible illumination of the reaction space. Beyond those loadings, the decrease in average reaction rate was probably due to the back scattering of light by the catalyst particles, entailing a shielding effect on the remaining reaction space. Simulation studies have been carried out to verify these hypotheses and are presented in Chapter 7 – .

The effect of catalyst concentration, W_{cat} ($g_{cat}L^{-1}$), on the average reaction rate, $-R_{TOC}$ ($molL^{-1}min^{-1}$), could be described as:

$$-R_{TOC} = A + \frac{B}{(W_{cat}-C)^2+D} \quad (4.6)$$

where the values for A, B, C and D are 1.31×10^{-6} $molL^{-1}min^{-1}$, 4.66×10^{-10} $g_{cat}^{2}molL^{-3}min^{-1}$, 6.64×10^{-2} $g_{cat}L^{-1}$ and 2.42×10^{-4} $g_{cat}^{2}L^{-2}$ respectively.

4.2.4 Effect of air flow rate

Upon irradiation, the catalyst particles generate positive holes and electrons. The photo-oxidation process requires an oxidising agent to remove electrons from the catalyst surface and prevent them from recombining with positive holes which are responsible for the creation of hydroxyl radicals. In this study, the oxidant was oxygen from the compressed air.

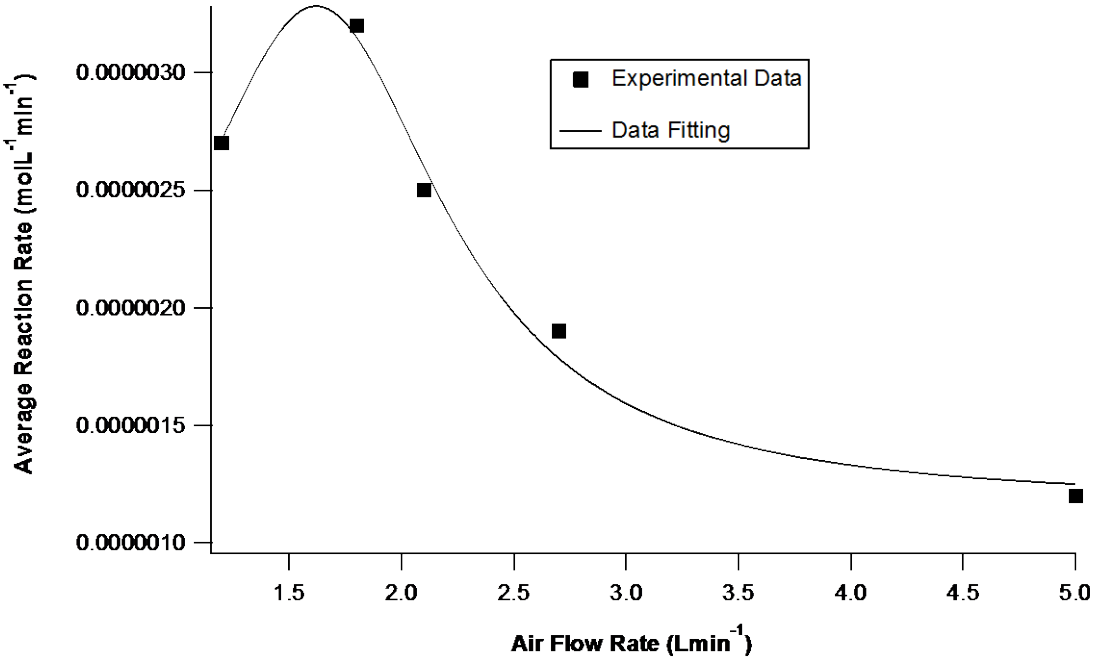

Figure 4. 6: Effect of air flow rate on average reaction rate (TOC initial concentration = 24.62 ±0.44 mgL^{-1}, Average reaction temperature = 27°C, Initial slurry pH = 3.00, 0.07 gL^{-1} catalyst loading and 4.4 $Lmin^{-1}$ slurry flow rate).

The range of air flow rate investigated was between 1.5 and 5.0 $Lmin^{-1}$ as depicted in Figure 4. 6. The average TOC degradation rate was found to increase until an optimum was reached at 1.8 $Lmin^{-1}$ air flow rate after which a steep decrease in the reaction rate was observed. Visual observations showed that fine bubbles were formed at the lower air flow rates. However, beyond the optimum air flow rate, larger bubbles of widespread sizes were observed. Larger bubbles meant reduced surface area for mass transfer of oxygen from the gas to liquid phase, hence the reduction in the average reaction rate. Agustina *et al.* (2008) made a similar

observation in their study of winery wastewater treatment with the same reactor. On the other hand, at low air flow rates in the vicinity of 1.5 $Lmin^{-1}$, air bubbles had a tendency to penetrate the slurry outlet, leading to irregular liquid pumping, hence a reduced average reaction rate.

The effect of air flow rate, Q_{Air} ($Lmin^{-1}$), on the average reaction rate, $-R_{TOC}$ ($molL^{-1}\,min^{-1}$), could be described as:

$$-R_{TOC} = A + \frac{B}{(Q_{air}-C)^2+D} \qquad (4.7)$$

where the values for A, B, C and D are 7.06×10^{-5} $molL^{-1}min^{-1}$, 5.93×10^{-5} $molLmin^{-3}$,1.62 $Lmin^{-1}$ and 0.47 L^2min^{-2} respectively.

4.2.5 Effect of slurry recirculation rate

The recirculation rate of the slurry was varied to study the effect of the residence time. The circulation rate was varied between 1.5 and 5.7 $Lmin^{-1}$ and its effect on the average reaction rate is presented in Figure 4. 7. Maximum degradation was obtained at a recirculation rate of 4.4 $Lmin^{-1}$. At higher recirculation rate, the slurry inlet momentum was high enough that air bubbles had the tendency to be pushed towards the slurry outlet. Introducing air bubbles into the pipelines made pumping irregular and therefore reduced the average reaction rate. Pareek *et al.* (2001) found maximum degradation at a recirculation rate of 0.2 $Lmin^{-1}$ in an 18 L volume reactor for the photodegradation of Bayer liquor. However in their study, catalyst suspension was assisted by fine air bubbles homogeneously distributed within the reactor. In this study, air bubbles were supplied from a 10 cm distributor centred at the bottom of the reactor. These bubbles were not dispersed throughout the reactor space and as a result, a relatively high volumetric flow rate was necessary to suspend the catalyst particles.

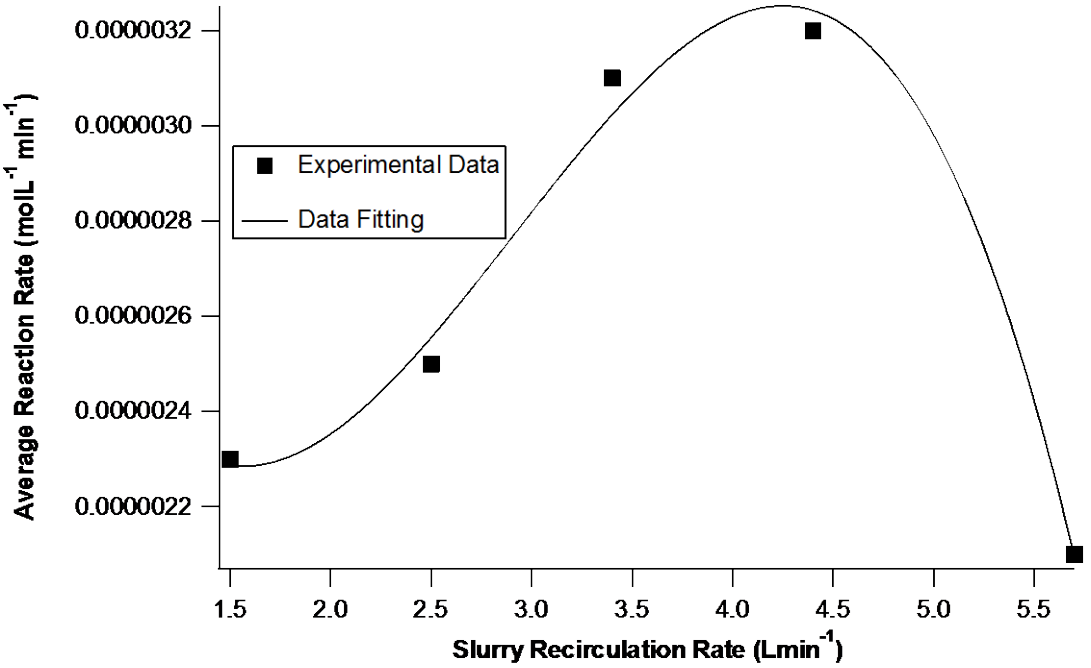

Figure 4. 7: Effect of slurry recirculation rate on average reaction rate (TOC initial concentration = 24.62 ±0.44 mgL^{-1}, Average reaction temperature = 27°C, Initial slurry pH = 3.00, 0.07 gL^{-1} catalyst loading and 1.8 $Lmin^{-1}$ air flow rate).

The effect of slurry recirculation rate, Q_{Slurry} ($Lmin^{-1}$), on the average reaction rate, $-R_{TOC}$ ($molL^{-1}min^{-1}$), could be described as:

$$-R_{TOC} = k_0 + k_1 Q_{Slurry} + k_2 {Q_{Slurry}}^2 + k_3 {Q_{Slurry}}^3 \quad (4.8)$$

The values of k_0, k_1, k_2 and k_3 are 3.66×10^{-6} $molL^{-1}min^{-1}$, -2.00×10^{-6} $molL^{-2}$, 8.75×10^{-7} $molminL^{-3}$ and -1.00×10^{-7} $molmin^2L^{-4}$ respectively.

4.2.6 Electricity cost analysis

Based on the current electricity cost in Perth, Australia (0.35 US$$kWh^{-1}$), a cost analysis was performed as detailed in Table 4. 2.

Table 4. 2: Break down of electrical cost for 1 run of photocatalytic shower water treatment at optimum conditions.

Equipment	Power Rating (kW)	Power Usage (%)	Usage (h)	Energy Usage (kWh)	Cost @ 0.35 US$kWh^{-1} (US$m^{-3})
Pump	0.135	70	6	0.57	6.5
UV Lamp	0.56	80	6	2.69	30.3
Total				**3.26**	**36.8**

Therefore for a 31 L throughput, the treatment cost for shower water amounted to 36.8 US$m^{-3}. This value was high and comparable to the price range obtained by Pareek *et al.* (2001) (60 – 270 US$m^{-3}) for the photocatalytic treatment of industrial Bayer liquor but is much larger than the reported 3.75 Eurosm^{-3} for the photocatalytic treatment of herbicides (Li Puma et al., 2007) most probably due to the size (bench scale) of the latter research. However, it is possible to operate the reactor with solar light, it is envisaged that operational cost of a large-scale photoreactor for shower water purification will be much less.

4.3 Conclusions

A pilot scale study for the photocatalytic degradation of real shower water showed that photocatalysis can be an efficient treatment process. At optimum conditions (3.0 slurry initial pH, 0.07 gL^{-1} catalyst concentration, 4.4 Lmin^{-1} slurry recirculation rate and 1.8 Lmin^{-1} air supply), a 57% of TOC degradation was obtained after 6 hours treatment time, although higher TOC degradation is expected if the treatment time is increased. This study showed that photocatalysis could be successfully transposed from bench scale to pilot scale. Furthermore, the ease of operation of the process makes photocatalysis an attractive prospect in terms of grey water treatment.

Chapter 5 - Determination of Catalyst Optical Parameters and Multiple Lamp Modelling

Strict pollution control legislations in several developed and developing countries has resulted in intensive research activities for developing new and efficient water treatment technologies (Bauer et al., 1999). Advanced Oxidation Processes (AOPs) for the degradation of non-biodegradable organic contaminants in waste water have emerged as efficient alternatives to established techniques such as flocculation, precipitation, adsorption on activated carbon, air stripping, reverse osmosis and biological methods.

Heterogeneous photocatalysis is one of the promising AOPs for the removal of organic pollutants from wastewater. The basis of the process is the use of low energy UV-A photons to excite a semiconductor catalyst (most usually TiO_2) leading to formation of electron-hole pairs. The electrons and holes then lead to production of the very reactive hydroxyl radicals in the aqueous phase having the ability to destroy many toxic organic pollutants considered to be unamenable to traditional methods. The overall process can be described by the following reaction equation (Chen and Ray, 1998):

$$\text{Organic Pollutants} + O_2 \xrightarrow{\text{Semiconductor+UVA Light}} CO_2 + H_2O + \text{Mineral Acid}$$

Most of current photocatalytic reactor designs only consist of a single lamp placed in the middle of the reaction mixture. However, to overcome excessive heating that may occur due to the use of one powerful lamp (such as medium pressure mercury lamps), achieve efficient cooling of a lamp assembly and optimize the radiation intensity, multiple lamp reactors should be used (Pareek, 2005).

Designing a photocatalytic reactor is significantly more challenging than conventional reactors due to the dependence of chemical reaction on the radiation. Consequently, rigorous mathematical models have been developed to describe the light irradiation within photochemical reactors. These models have been thoroughly reviewed by Alfano *et al.* (1986a, b) and Pareek *et al.* (2008). With increased

computational speeds, these models are now becoming available with standard CFD simulation packages. Yu *et al.* (2008) for instance, used the P-1 model successfully to simulate UV light distribution within an ozone-filled photoreactor.

Shon *et al.* (2005) studied the effect of the number of lamps (1, 2 and 3 lamps) on the bench scale photocatalysis of a wastewater. They found that the higher the number of lamps, the greater the pollutant degradation. The increase in degradation was attributed to the increase in surface area that was exposed to the reaction medium when using more lamps. However they did not study the effect of lamp separation (relative distance between lamps) on pollutant removal.

The effect of lamp placement and number of lamps for optimal surface illumination was studied for monolith photocatalytic reactors (in dimensionless form) (Singh et al., 2007) and a flat plate photocatalytic reactor (Salvadó-Estivill et al., 2007a; Salvadó-Estivill et al., 2007b). Pareek (2005) found that an optimum lamp separation existed when using two lamps in a slurry reactor. An optimum separation between two lamps was determined by conducting 2-dimensional computational fluid dynamics simulations.

In this chapter, experiments were carried out on a pilot scale photocatalytic reactor to measure the light intensity radially from the middle section (axially) of the lamp assembly, at two different catalyst concentrations. Computational fluid dynamics models were then used to replicate the experimental results and then investigate the effect of multiple lamps arrangement on light intensity distribution in 2- and 4-lamp photocatalytic reactor. The reactor configuration simulated in this paper was previously used for the treatment of shower water as described in Chapter 4 - Photocatalytic Treatment of Shower Water Using a Pilot Scale Reactor.

5.1 Model Development

The 2-dimensional model development of the photocatalytic reactor presented in this section results from the general radiation transport equation model presented in section 3.3.1.1.

5.1.1 Radiation transport equation (RTE)

The general radiation balance within an elemental volume of the reaction medium can be derived as (Cassano and Alfano, 2000; Romero et al., 1997, 2003; Siegel and Howell, 2002):

$$\frac{dI_\upsilon(s,\Omega)}{ds} = -\kappa_\upsilon(s)I_\upsilon(s,\Omega) + \frac{1}{4\pi}\sigma_\upsilon(s)\int_0^{4\pi} p(\Omega' \rightarrow \Omega)\, I_\upsilon(s,\Omega)d\Omega - \sigma_\upsilon(s)I_\upsilon(s,\Omega) \quad (5.1)$$

where, $\mathrm{I}_{\boldsymbol{\upsilon}}(\mathrm{s},\Omega)$ is a beam of monochromatic radiation intensity travelling in this medium in the direction Ω along the path s, $\kappa_{\boldsymbol{\upsilon}}$ and σ_υ are the absorption and scattering coefficients of the medium respectively, $\mathrm{p}(\Omega' \rightarrow \Omega)$ is a phase function representing the probability of incident radiation due to in-scattering onto the element from all other directions. In equation 5.1, the losses of photonic energy are due to the absorption and scattering terms while the gain in the energy is accounted by the in-scattering of radiation.

The following equations are related to 2-D RTE simulations on the cross sectional plane normal to the middle section of the lamp, or z = 0. The incident intensity (Wm^{-2}) at any point from all the directions is given by

$$G_\upsilon(r) = \int_{\Omega=0}^{\Omega=2\pi} I_\upsilon(r,\Omega)d\Omega \quad (5.2)$$

and the local volumetric rate of energy absorption (LVREA, Wm^{-3}) for a specific wavelength of light at any point is given by

$$LVREA_\upsilon(r) = \kappa_\upsilon(r)G_\upsilon(r) \quad (5.3)$$

For a wavelength spectrum such as UV, equation 5.1 will have to be computed for each wavelength/wavelength band and summed to obtain the LVREA.

A useful parameter is the area weighted average of incident light intensity ($\bar{G}_\upsilon$, Wm^{-2}) which gives the average radiation intensity within the medium at the middle section of the lamp, z = 0, for a particular wavelength. This is given by:

$$\bar{G}_\upsilon = \frac{\int_0^r G_\upsilon(r)rdr}{\int_0^r rdr} \quad (5.4)$$

so that the average LVREA (local volumetric rate of energy absorption, Wm^{-3}) within the medium, assuming a constant coefficient of absorption, is:

$$LVREA = \kappa_\upsilon \bar{G}_\upsilon \quad (5.5)$$

The optical parameters of the medium (absorption and scattering coefficients), as imparted by the titanium dioxide particles, have a known dependence with wavelength (Romero et al., 2003). To avoid the rigorous mathematics involved with calculating the RTE's for each individual wavelength, Romero *et al.* (1997) suggest using a wavelength averaged approximation. This procedure gives reasonable results and greatly reduces computational requirements (Romero et al., 1997). Pareek *et al.* (2003b) used this method successfully in modelling a photocatalytic reactor for the treatment of Bayer liquor. The wavelength averaged values of the scattering and absorption coefficients are related to the catalyst loading (W_{cat}, gm^{-3}) and are represented by the following relationships for Degussa P25 TiO_2 (Romero et al., 1997):

$$\sigma_\upsilon = \langle \sigma_\upsilon^* \rangle W_{cat} \quad (5.6)$$

$$\kappa_\upsilon = \langle \kappa_\upsilon^* \rangle W_{cat} \quad (5.7)$$

where $\langle \sigma_\upsilon^* \rangle$ and $\langle \kappa_\upsilon^* \rangle$ are the wavelength averaged specific scattering and absorption coefficients (in m^2g^{-1}) respectively and are calculated as (Li Puma et al., 2010):

$$\langle \sigma_\upsilon^* \rangle = \frac{\int_{\upsilon_{min}}^{\upsilon_{max}} \sigma_\upsilon^* I_\upsilon \, d\upsilon}{\int_{\upsilon_{min}}^{\upsilon_{max}} I_\upsilon \, d\upsilon} \quad (5.8)$$

$$\langle \kappa_\upsilon^* \rangle = \frac{\int_{\upsilon_{min}}^{\upsilon_{max}} \kappa_\upsilon^* I_\upsilon \, d\upsilon}{\int_{\upsilon_{min}}^{\upsilon_{max}} I_\upsilon \, d\upsilon} \quad (5.9)$$

Moreover, reflection on the surface of air bubbles can also induce some degree of light scattering. Trujillo *et al* (2007) used the following relationships for scattering by gas bubbles:

$$\sigma_{\upsilon,B} = \rho_\upsilon \pi R_B^2 N_B \quad (5.10)$$

where ρ_υ is the hemispherical spectral reflectivity, R_B is the bubble radius and N_B is the number of bubbles per unit volume which can be calculated by:

$$N_B = \frac{\alpha_G}{V_B} \quad (5.11)$$

where α_G is the gas hold-up and $V_B$is the volume of a single bubble. For estimates to find the bubble diameter and gas hold-up in bubble columns, the reader should refer to correlations by Akita and Yoshida (1974) and Yamashita and Inoue (1975) respectively.

The work by Cabrera *et al.* (1996) showed that, while the scattering coefficient for Degussa P25 TiO_2 remains relatively constant in the range $270 < v\ (nm) < 400$, the catalyst's absorption coefficient decreases considerably with increasing radiation wavelength. The specific absorption and scattering coefficients for sonicated suspensions of Degussa P25 TiO_2 at different wavelengths are shown in Table 5. 1.

Table 5. 1: Values of specific absorption and scattering coefficients for Degussa P25 TiO_2 at different wavelengths, adapted from (Cabrera et al., 1996), (*) - extrapolated values.

Wavelength (nm)	κ_v^* (m^2g^{-1})	σ_v^* (m^2g^{-1})
< 280	1.3*	5.2*
280	1.3	5.2
290	1.3	5.3
300	1.27	5.4
310	1.25	5.5
320	1.1	5.9
330	0.87	6
340	0.62	5.95
350	0.33	5.9
360	0.15	5.8
370	0.06	5.25
380	≈0	5
390	0	4.7
400	0	4.5

Although the values in Table 5. 1 were obtained from *sonicated* suspensions of Degussa P25 TiO_2, the experimental conditions used in this research (pH of 3, pump recirculation and air bubbling) did not compromise those values. This deduction was made as per the work of Martin *et al* (1993) who showed that the optical properties of Degussa P25 TiO_2 subjected to pump recirculation or air bubbling, were similar to that of sonicated suspensions as long as the pH was far from the isoelectric pH of

6.5. The low pH of 3 used in this research prevented the flocculation of TiO_2 particles which would have affected the optical properties of the catalyst. As a result, using equations 5.8 and 5.9, the values of $\langle \sigma_v^* \rangle$ and $\langle \kappa_v^* \rangle$ were calculated from the information in Table 5. 1 and the UV lamp spectrum in Figure 5. 2, giving $\langle \sigma_v^* \rangle$ = 5.448 m^2g^{-1} and $\langle \kappa_v^* \rangle$ = 0.9565 m^2g^{-1} for the range investigated ($226 < v\ (nm) < 400$).The other parameter required to close equation 5.1 is the phase function. The phase function can be approximated as wavelength independent (Romero et al., 2003) and its value is unity for isotropic scattering . For other cases, Fiveland (1984) suggests the following model:

$$p(\Omega' \rightarrow \Omega) = 1 + A cos\theta \qquad (5.12)$$

where θ is the scattering angle (radians) and *A* is a parameter that can take any value between -1 and +1. Then, if *A* = 0, scattering is isotropic; if *A* = -1 scattering is 100% backward and if *A* = +1, scattering is 100% forward.

5.1.2 Computational domain

A simple 2D computational domain was developed for the photocatalytic reactor. This is shown in Figure 5. 1 for single, 2 and 4 lamps (separated by the distance X_{lamp}) configurations respectively. The domain was constructed on GAMBIT (a mesh development software) using the real dimensions of the reactor (reactor diameter of 300 mm and lamp diameter of 57 mm). The domain, once constructed, was meshed and exported into FLUENT (a CFD software). The vicinity of the lamp was meshed finely since most radiation is absorbed there. Mesh independent results with one lamp were obtained with 16647 structured cells as shown in Figure 5. 1. The computational domains for 2 and 4 lamps were meshed with the same mesh density distribution as with the one lamp domain so as to obtain reliable results. Optimal angular discretizations of 8 control angles with a pixelation of 1×1 were determined and used in all simulations.

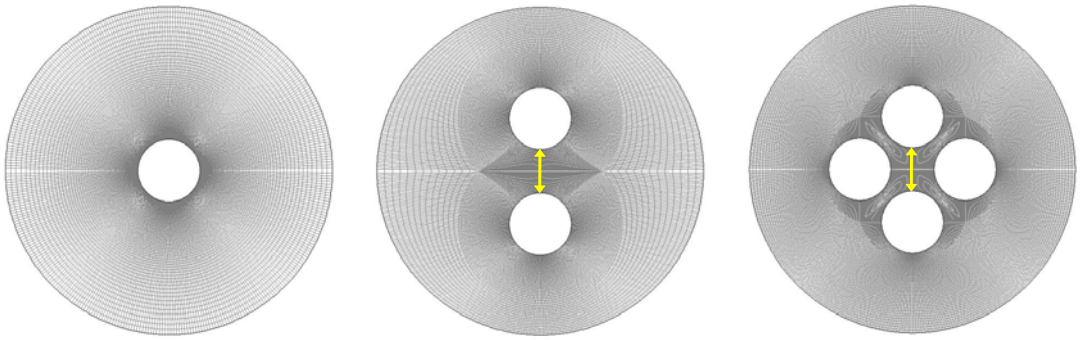

Figure 5. 1: Computational domain for a) 1 lamp, b) 2 lamps and c) 4 lamps; X_{lamp} is shown as the distance between the double headed arrow.

5.1.3 Numerical technique for solving the RTE

The RTE is in the integro-differential form. Only for very simplified and unrealistic situations will it be possible to obtain analytical solutions such that special numerical techniques need to be used to properly solve them (Romero et al., 1997). Some of the methods use a statistical approach to describe photons' trajectories until they are absorbed by the system (Monte Carlo method), while other routines divide the computational domain into discrete volumes whereby the integro-differential form of the RTE yields linear algebraic equations which can be solved iteratively (discrete ordinate, DO model and the finite volume, FV model). FLUENT uses the finite volume (FV) method to solve the RTE within the meshed domain.

5.1.4 Boundary conditions

Boundary conditions (BC) are required as a starting point to solve these equations. The BCs used in this study are as follows:

5.1.4.1 Lamp wall

The characteristics of the UV lamp used in this study are presented in Table 5. 2. Since the lamp was enclosed within a quartz tube, the outer surface of the tube was taken as being the lamp wall emitting a constant radiation. The emission spectrum of the UV lamp is shown in Figure 5. 2 and was derived from the information provided by the UV lamp manufacturer (*see Appendix A4* – Emission Spectrum for UV Lamp)

Table 5. 2: UV lamp specifications.

Type	Parameter	Value
Medium pressure mercury lamp (Primarc PM2326)	Diameter	22 mm
	Length	200 mm
	UV emission range	$226 < \upsilon\ (nm) < 435$
	Power Specification	560 W
	Radiation Intensity ($226 < \upsilon\ (nm) < 400$)	1435 Wm^{-2}

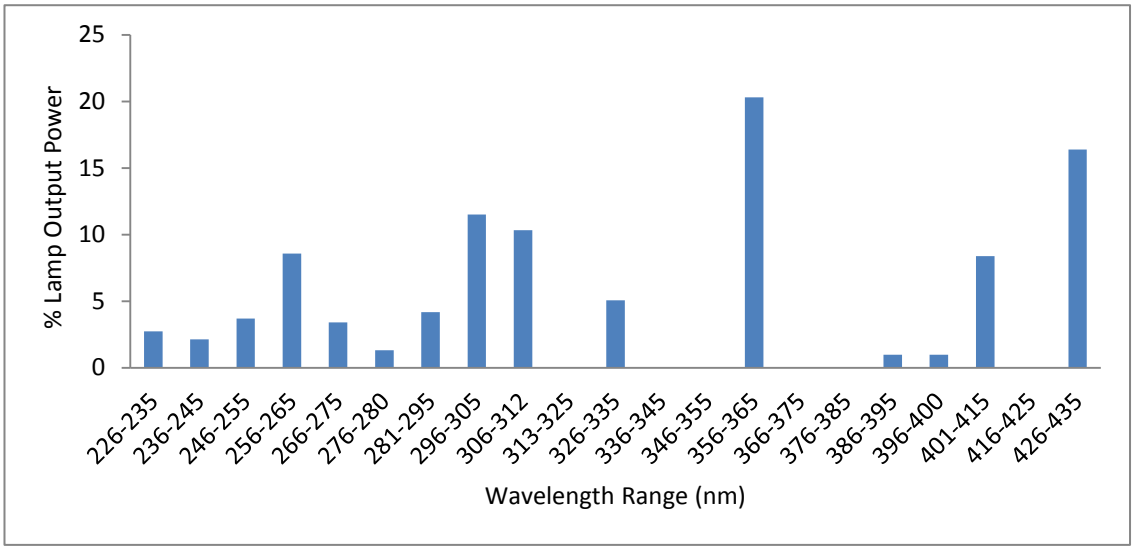

Figure 5. 2: UV lamp emission spectrum from manufacturer's data, *see Appendix A4* – Emission Spectrum for UV Lamp.

Titania particles have a specific threshold energy at which they can be activated. This energy can be supplied by photons of wavelength $\upsilon \leq 387.5$ nm (Cassano and Alfano, 2000; Romero et al., 1997). For simulation purposes, a non grey radiation model comprising of four wavelength bands in the range $220 < \upsilon\ (nm) < 400$ was adapted according to Figure 5. 2 and presented in Table 5. 3. The lamp radiation emitted from the lamp surface was considered to be completely diffuse.

Table 5. 3: UV radiation at different bands.

Wavelength range (nm)	Lamp emissive power (Wm^{-2})
Band 1: $(226 < \upsilon < 280)$	410 (Measured with probe 1)
Band 2: $(281 < \upsilon < 315)$	488.6 (Calculated from Figure 5. 2)
Band 3: $(316 < \upsilon < 385)$	506.2 (Measured with probe 2)
Band 4: $(386 < \upsilon < 400)$	29.8 (Measured with probe 2)
P_{lamp}	1435

5.1.4.2 Reactor wall

The reactor wall (stainless steel built) was considered as opaque. For an opaque wall the incident radiation will not be transmitted but will be partly reflected back into the medium and partly absorbed and emitted as heat energy such that:

$$e_w + r_w = 1 \qquad (5.13)$$

where e_w is the emissivity of the wall and r_w is the wall reflectivity. The total emissivity of stainless steel sheets ranges between 0.52 and 0.60 (Perry and Green, 2007) and is 0.17 for polished stainless steel (Incropera, 2009). The reflected portion of radiation was considered to be completely diffuse.

5.1.4.3 Reaction medium

The reaction medium was considered well mixed and isothermal at 300 K since cooling water was used to maintain the reaction mixture constant. Most of the physical properties of the slurry were assumed the same as liquid water.

Regarding the optical properties, the calculated wavelength averaged specific scattering coefficient ($\langle\sigma_{\upsilon}^{*}\rangle$ = 5.448 m^2g^{-1}) was used to find the wavelength averaged scattering coefficient from equation 5.6. On the other hand a value for the wavelength dependent specific absorption coefficient, $\langle\kappa_{\upsilon}^{*}\rangle$, was determined for each of the bands in Table 5. 3 by a trial and error method, starting with the calculated value $\langle\kappa_{\upsilon}^{*}\rangle$ = 0.9565 m^2g^{-1}, until the simulations results matched the experimental data

The scattering phase function was approximated from equation 5.12. The value of *A* was assumed as zero, implying isotropic scattering. Not only does this assumption make the model less computationally intensive but Cassano and Alfano (2000) had previously found that the isotropic scattering phase function provided the best

results. Moreover, Yu *et al.* (2008) found that the light intensity distribution in a photocatalytic reactor was not much influenced by the phase function parameter.

5.2 Experimental

The UV lamp was fitted into a 57 mm diameter quartz tube and set up at the centre of the photocatalytic reactor (31 L volume). A dedicated compressor was used for all air supplies. Part of the air was used to cool the UV lamp while the remaining (1.8 $Lmin^{-1}$) passed through the reactor via a 100 mm diameter air distributor centred at the bottom of the reactor. Aeroxide® P25 TiO_2 (>99.5% purity), supplied by Sigma Aldrich, was mixed with tap water at two different concentrations (W_{cat} = 0.05 and 0.10 gL^{-1}) in a 60 L mixing tank. The slurry pH was brought down to 3 and was then transferred to the reactor via an Iwaki magnetic pump. Once the reactor was full, it was operated in a slurry recirculation mode. Optimum values of slurry recirculation and air flow rates that kept the catalyst in suspension had been determined previously and were maintained during the experiments. Two Delta OHM UV light probes (probe 1 range: $220 < \upsilon\ (\mathrm{nm}) < 280$, probe 2 range: $315 < \upsilon\ (\mathrm{nm}) < 400$) were fitted into a quartz tube which was moved radially (49.5 < r (mm) < 66.5) to measure the light intensity within the slurry. Once lit, the UV lamp was allowed to stabilise for 2-3 minutes prior to each measurement. The experimental set up is shown in Figure 5. 3.

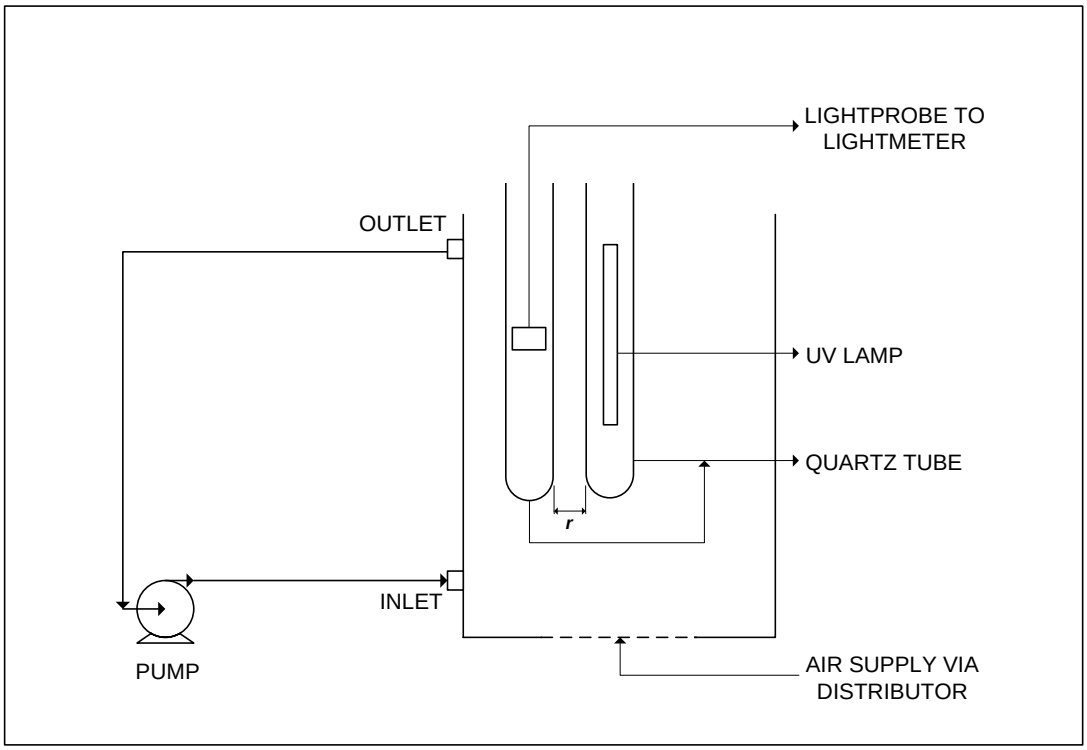

Figure 5. 3: Experimental setup of photocatalytic reactor.

5.3 Results and Discussion

This section describes and discusses the findings from the simulation results obtained.

5.3.1 Simulation of experimental data

The wavelength averaged scattering coefficient (equation 5.6) was maintained for all bands, with $\langle \sigma_{\upsilon}^{*} \rangle$ = 5.448 m^2g^{-1}. A value of 1 was used for the wall emissivity. Iterations were performed until the normalized residuals were less than 10^{-6}. The optimum fit closely matched the experimental data for the range experimented and occurred at values of $\langle \kappa_{\upsilon}^{*} \rangle$= 0.66 m^2g^{-1} and 0.70 m^2g^{-1} for bands 1 and 3 respectively. This is shown by the solid and dashed lines for both W_{cat} = 0.05 and 0.1 gL^{-1} on Figure 5. 4, which represents the variation of the circumferential averaged radial incident radiation (CARIR, Wm^{-2}) with radial distance (radial distance from the centre of the reactor, mm) at the mid-section of the lamp, or when z = 0. It can be seen that the actual value of $\langle \kappa_{\upsilon}^{*} \rangle$ for band 1 as obtained from the simulations was less than reported values from Table 5. 1 within that band range ($226 < \upsilon\ (nm) < 280$). Conversely, $\langle \kappa_{\upsilon}^{*} \rangle$ for band 3, (having a peak in the range $356 < \upsilon\ (\mathrm{nm}) < 365$), was higher than the reported values within that range . This is probably due to

the fact that the values reported by Cabrera *et al.* (1996) were applicable to Degussa P25 TiO_2 while in this exercise, a novel brand of TiO_2 (Aeroxide® P25) was used. This new brand is highly dispersed and has been developed to improve photocatalytic reactions (2011; Chaillou et al., 2011; Hernández Leal et al., 2011), hence explaining the relatively higher and more constant values of $\langle \kappa_v^* \rangle$ obtained within the UV-A radiation region. The average bubble diameter was calculated as 7.8 mm. Consequently, assuming a maximum value of 0.5 for the hemispherical spectral reflectivity (since most light will get transmitted through the bubbles), the maximum scattering coefficient imparted by the bubbles was only 2.8 m^{-1} which was negligible even when compared to the lowest catalyst concentration investigated (W_{cat} = 0.0075 gL^{-1}, corresponding to a scattering coefficient of 41 m^{-1}).

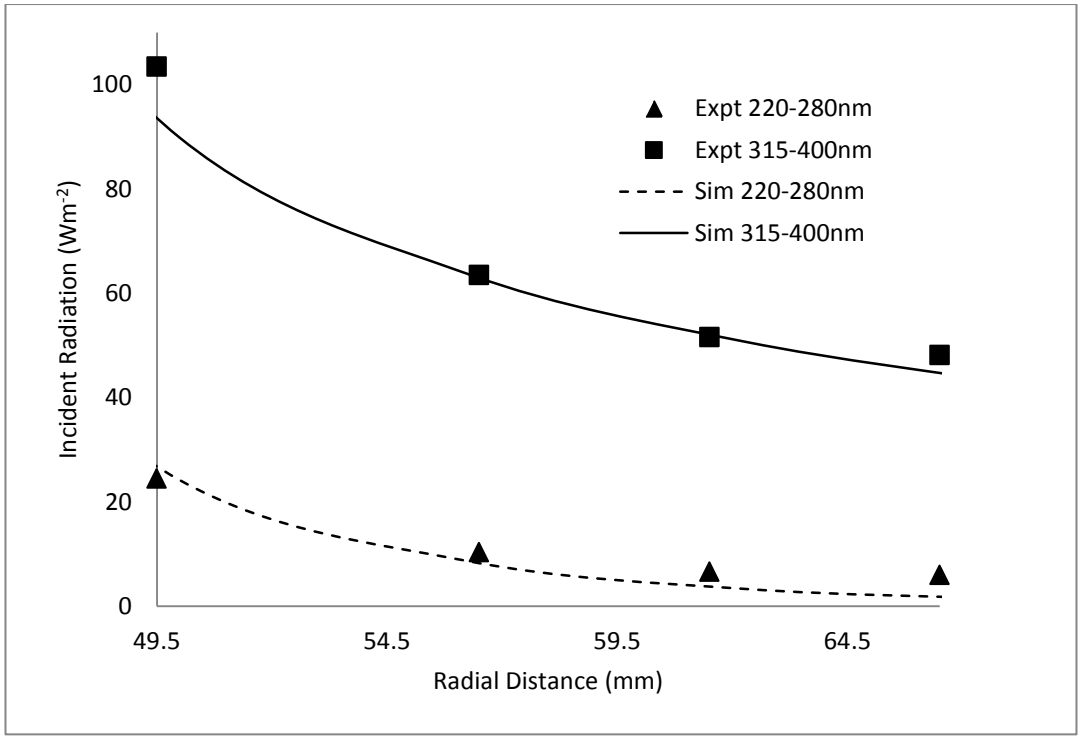

(a)

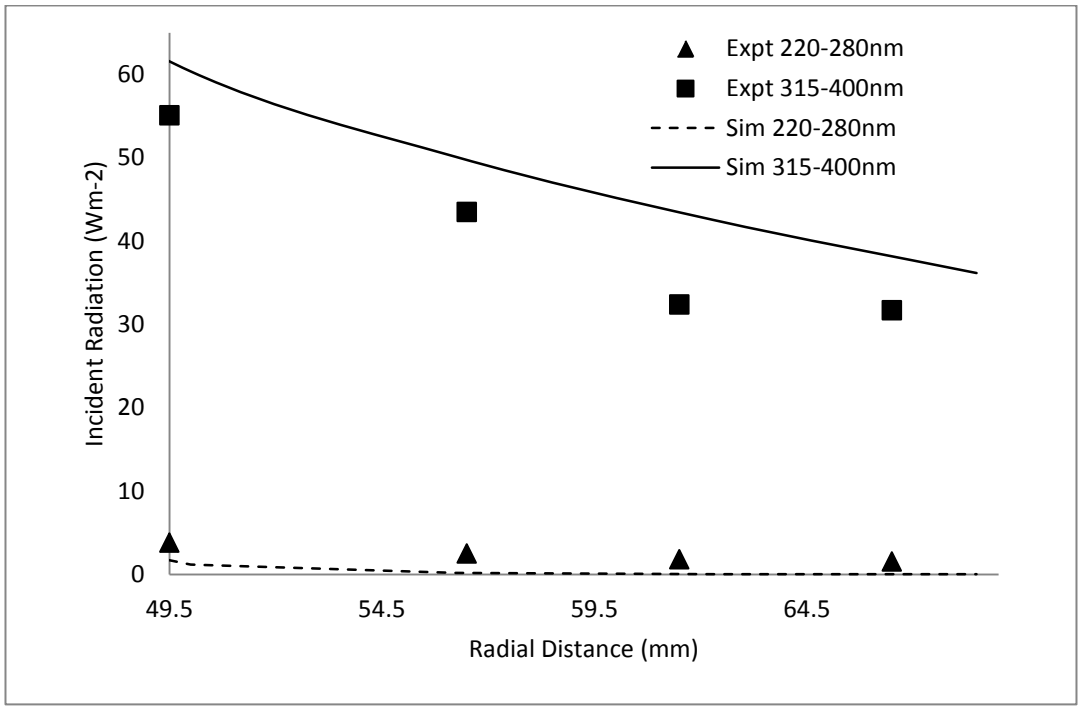

(b)

Figure 5. 4: Experimental validation of simulations, P_{Total} = 1435 Wm^{-2}, e_w = 1 and z = 0 (lamp middle). (a) W_{cat} = 0.05 gL^{-1}, (b) W_{cat} = 0.1 gL^{-1}.

5.3.2 Effect of wall emissivity

The reactor wall emissivity is an important parameter in designing photocatalytic reactors. If sufficient amount of incident radiation reaches the wall, part of it will be reflected back, affecting the incident radiation in the reactor space. To investigate the effect of wall emissivity on the incident radiation within the reactor, two limits of e_w were used, i.e. zero reflectivity or $e_w = 1$ and the maximum reflectivity for polished stainless steel, or $e_w = 0.17$. Figure 5. 5 shows the results for the final third of the reactor radius at 3 catalyst loadings (W_{cat} = 0.0075, 0.01 and 0.015 gL^{-1}).

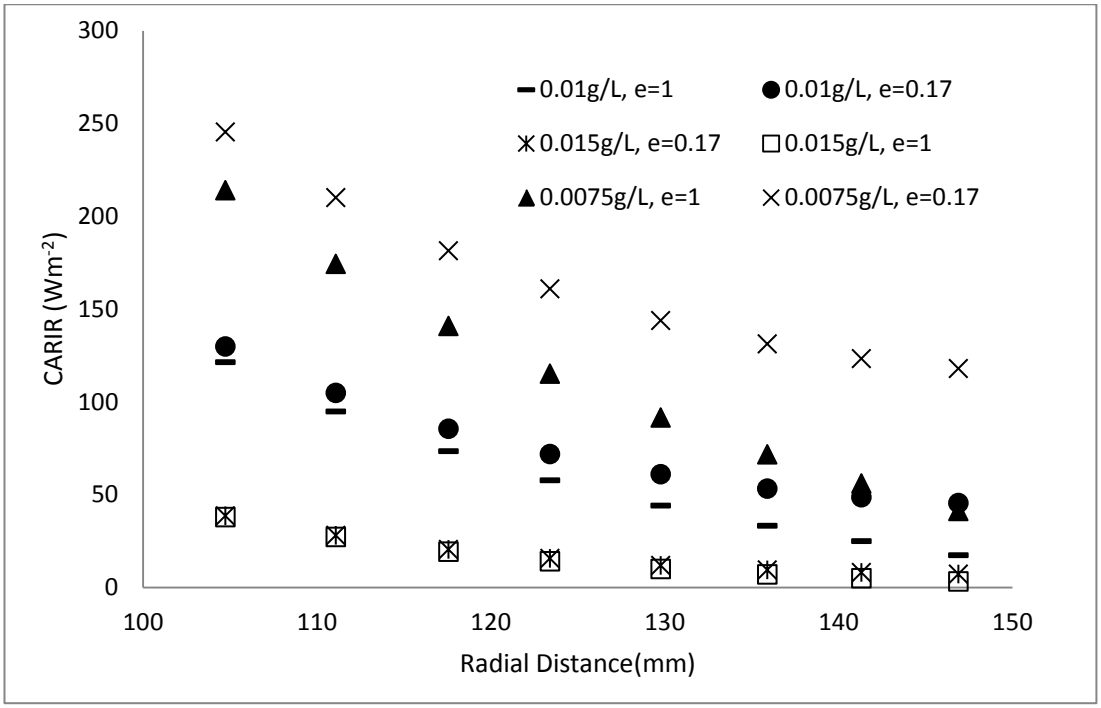

Figure 5. 5: Effect of reactor wall emissivity on CARIR (Wm^{-2}), P_{Total} = 1435 Wm^{-2} and z = 0 (lamp middle).

Figure 5. 5 shows that below W_{cat} = 0.015 gL^{-1}, a significant portion of incident radiation reaches the reactor wall. Consequently, there was a significant difference between the incident radiations for two simulated wall emissivities. However, for $W_{cat} \geq 0.015$ gL^{-1} the wall emissivity had little effect on the incident intensity. Hence a value of $e_w = 1$ was maintained for the rest of this study.

5.3.3 Simulations of multi-lamp systems

Simulations on multi-lamp configurations were performed by using $\langle \kappa_v^* \rangle$ values as calculated in section 4.1 (i.e., $\langle \kappa_v^* \rangle$ =0.66 m^2g^{-1} and 0.70 m^2g^{-1} for bands 1 and 3 respectively while an in-between value of 0.68 was deemed realistic for band 2).

Band 4 was omitted from the simulations since no absorption occurred. The value of 1 was retained for e_w and the total emission power (P_{Total}) of the lamp surfaces was 1435 Wm^{-2} unless stated otherwise.

5.3.3.1 2-lamp configuration

A 2-lamp configuration was simulated to analyse the effect of separation between the lamps (X_{lamp} = 2, 4, 6, 8 and 10 cm) at three different catalyst loadings (W_{cat} = 0.05, 0.10 and 0.20) on the LVREA. The results are shown in Figure 5. 6.

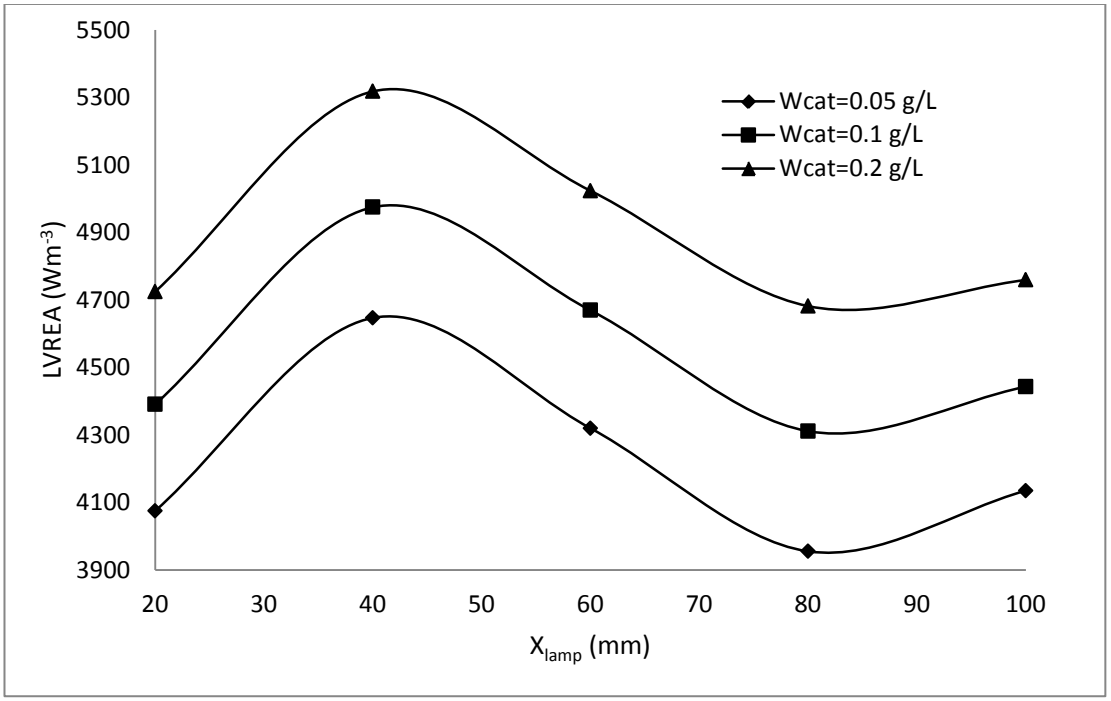

Figure 5. 6: Relationship between LVREA (Wm^{-3}) and X_{lamp} (mm) at different W_{cat} for 2 lamps configuration, P_{Total} = 1435 Wm^{-2}, e_w = 1 and z = 0 (lamp middle).

It is clear in Figure 5. 6 that an optimum LVREA occurred at X_{lamp} = 40 mm for the range of catalyst loadings investigated. The LVREA then reached a minimum at X_{lamp}= 80 mm but increased slightly again at X_{lamp}= 100 mm.

Figure 5. 7 shows the contours of the radiation intensity distribution for the 2-lamp system at W_{cat} = 0.05 gL^{-1} when X_{lamp} is varied between 20 and 80 mm.

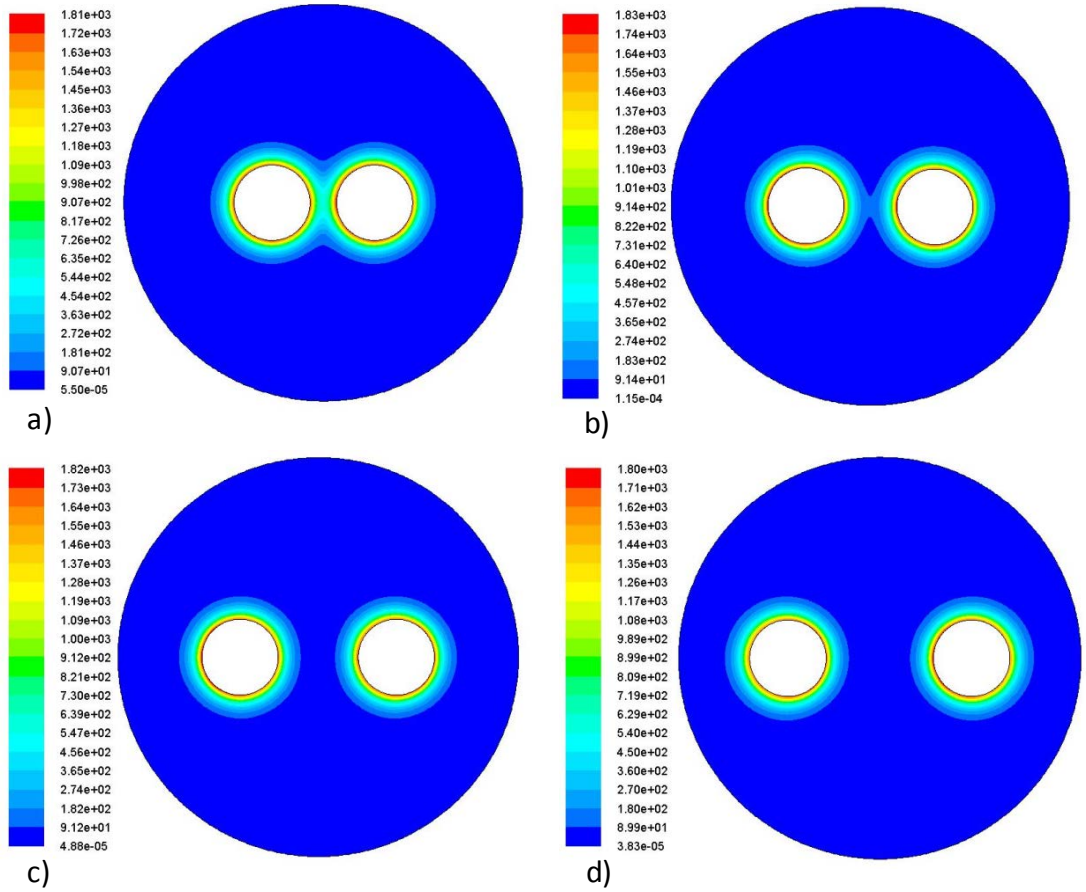

Figure 5. 7: Radiation intensity distribution contours (Scale on the left in Wm^{-2}) at W_{cat} = 0.05 gL^{-1}, P_{Total} = 1435 Wm^{-2},e_w = 1 and z = 0 (lamp middle) for 2 lamps configuration when: a) X_{lamp} = 20 mm, b) X_{lamp} = 40 mm, c) X_{lamp} = 60 mm, d) X_{lamp} = 80 mm.

It is evident in Figure 5. 7 that at X_{lamp} = 60 mm and above, the individual incident radiation intensity contours from respective lamps were virtually unaffected by each other and hence they operated as individual lamps. As the lamps got closer to each other, contours of similar radiation intensity gradually merged together which means that the spaces in between and around the lamps becomes more illuminated (X_{lamp}= 20 and 40 mm). This is clarified further in Figure 5. 8 which shows plots of CARIR along radial distance for W_{cat} = 0.05 gL^{-1} and X_{lamp}= 20, 40, 60 and 80 mm.

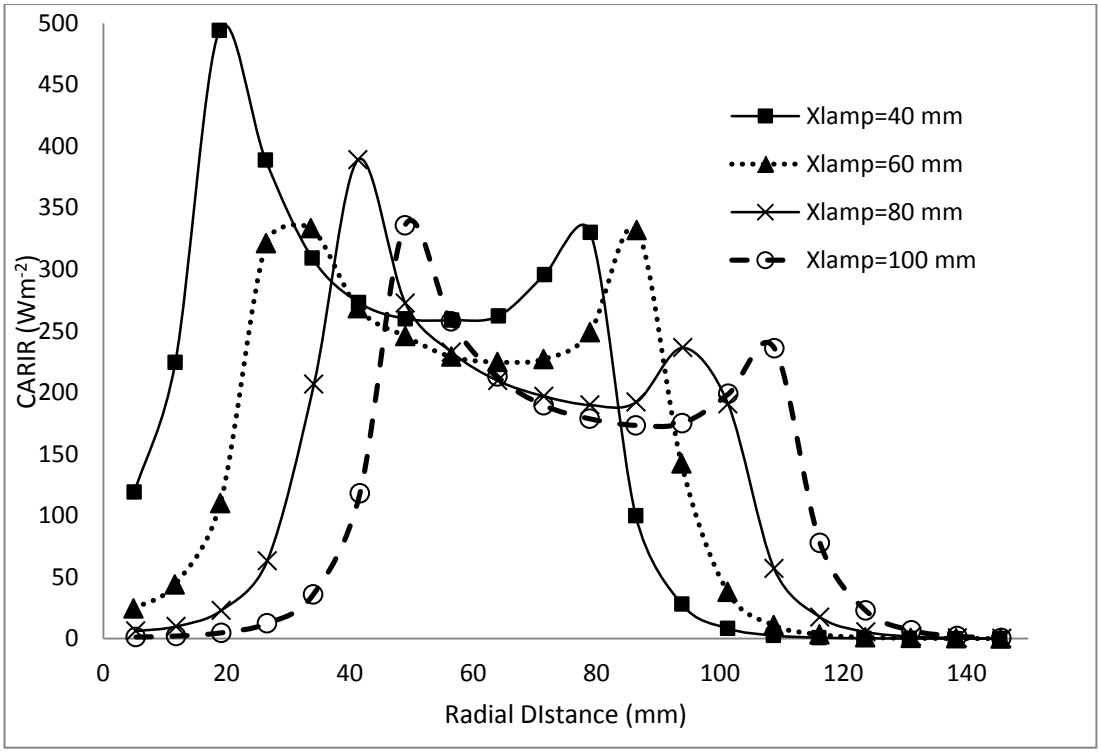

Figure 5. 8: Relationship between CARIR (Wm^{-2}) and radial distance (mm) at W_{cat} = 0.05 gL^{-1}, P_{Total} = 1435 Wm^{-2} e_w = 1 and z = 0 (lamp middle) for different lamp separations in a 2 lamps configuration.

The configuration X_{lamp} = 20 mm (not shown in Figure 5. 8) had the highest CARIR up to a radial distance of 70 mm after which the CARIR rapidly decreased to 50 Wm^{-2} at a radius of 80 mm. This means that with X_{lamp} = 20 mm, a large portion of the reactor was not illuminated. Figure 5. 8 also shows that X_{lamp} = 40 mm had a high CARIR up to a radial distance of 83 mm which covers a greater surface area hence making it the optimum arrangement. Beyond a radial distance of 84 mm, X_{lamp} = 60, 80 and 100 mm showed highest CARIR. However, those values did not affect a large area and decreased rapidly, while the middle region of the reactor remained poorly lit.

5.3.3.2 4-lamp configuration

The effect of lamp separation on the LVREA for the 4 lamp-configuration at different catalyst loadings is depicted in Figure 5. 9.

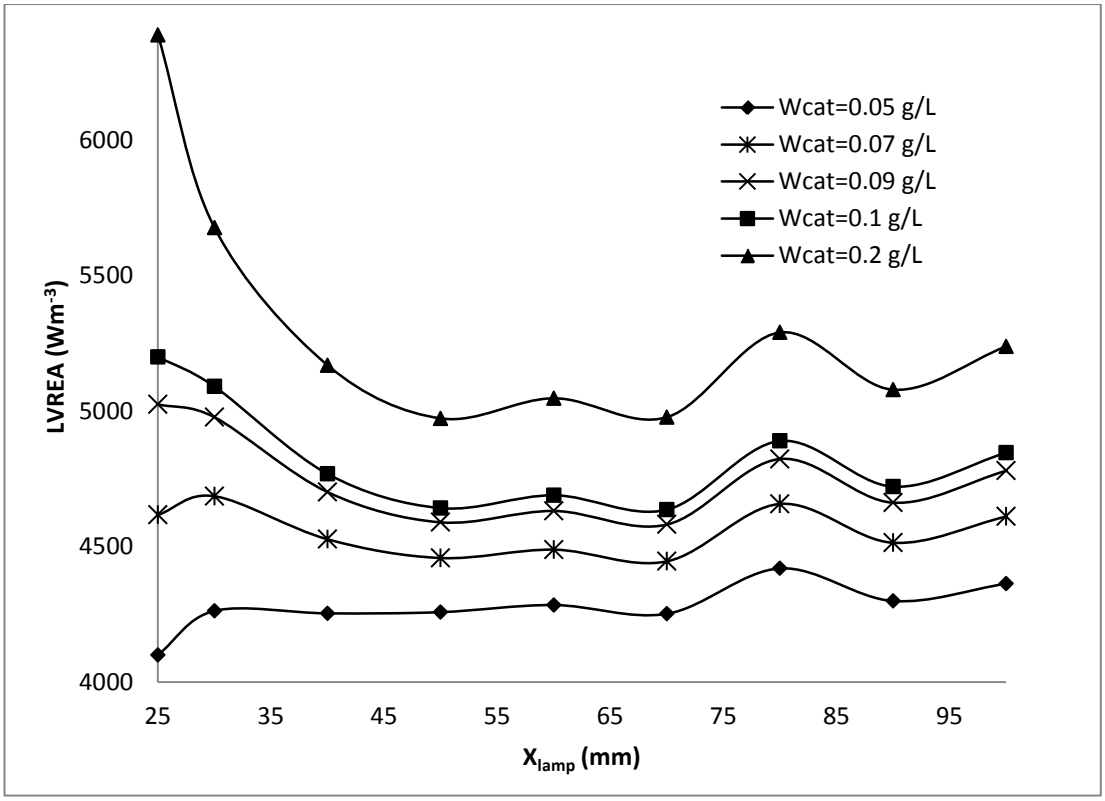

Figure 5. 9: Relationship between LVREA (Wm^{-3}) and X_{lamp} (mm) at different catalyst loadings for 4 lamps configuration, P_{Total} = 1435 Wm^{-2} e_w = 1 and z = 0 (lamp middle).

At low loads (up to W_{cat} = 0.06 gL^{-1}), the optimum X_{lamp} was 80 mm. However as the catalyst concentration increased beyond this value, the optimum lamp separation decreased considerably, from 30 mm at W_{cat} = 0.07 gL^{-1} to 25 mm at W_{cat} = 0.1 gL^{-1}.

The contours of radiation intensity for X_{lamp} = 25, 30, 40 and 50 mm and with W_{cat} = 0.1 gL^{-1} are shown in Figure 5. 10.

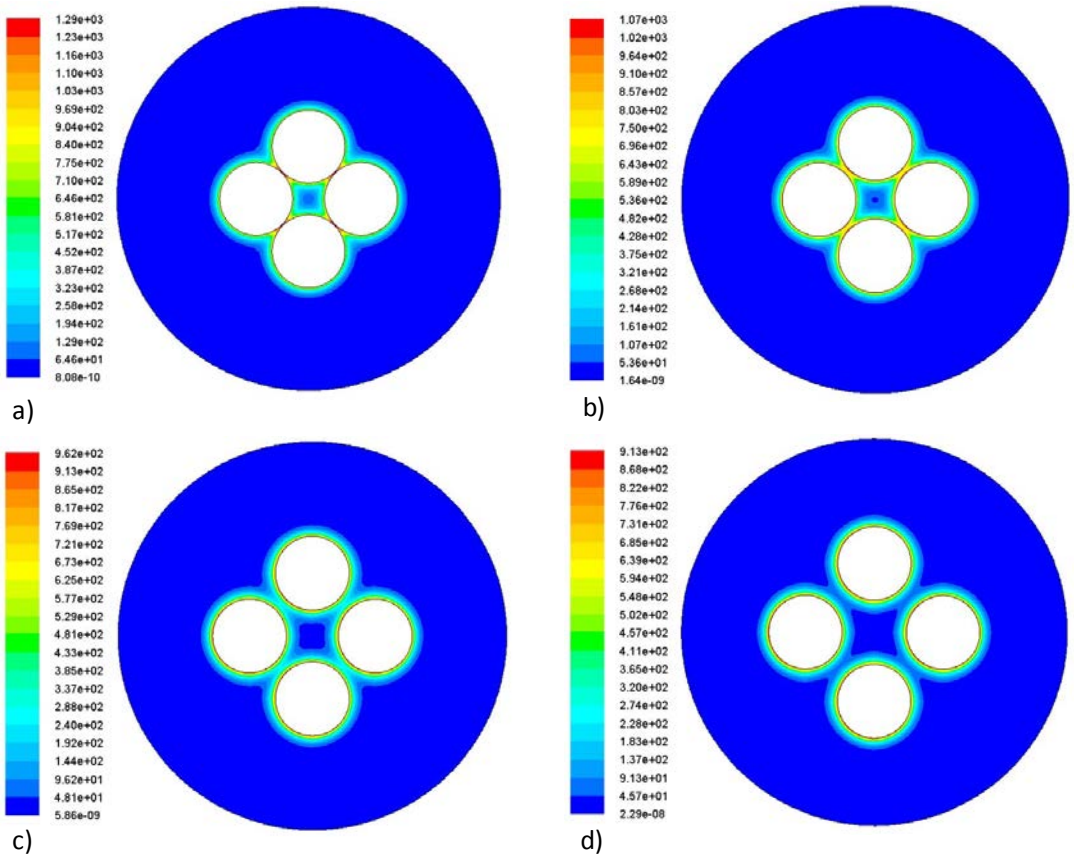

Figure 5. 10: Radiation intensity distribution contours (Scale on the left in Wm^{-2}) at W_{cat} = 0.1 gL^{-1}, P_{Total} = 1435 Wm^{-2} e_w = 1 and z = 0 (lamp middle) for 4 lamps configuration when: a) X_{lamp} = 25 mm, b) X_{lamp} = 30 mm, c) X_{lamp} = 40 mm and d) X_{lamp} = 50 mm.

The different values of radiation intensity in each figure differ due to the overlapping of radiation contours with similar intensity. The smaller the lamp separation, the higher will be the radiation intensity distribution between the lamp surfaces.

The occurrence of optimal intensity for higher W_{cat} is better understood with a plot of CARIR as a function of radial distance for W_{cat} = 0.05, 0.1 and 0.2 gL^{-1} in Figure 5. 11, which shows results for X_{lamp} = 25, 30, 40 and 50 mm.

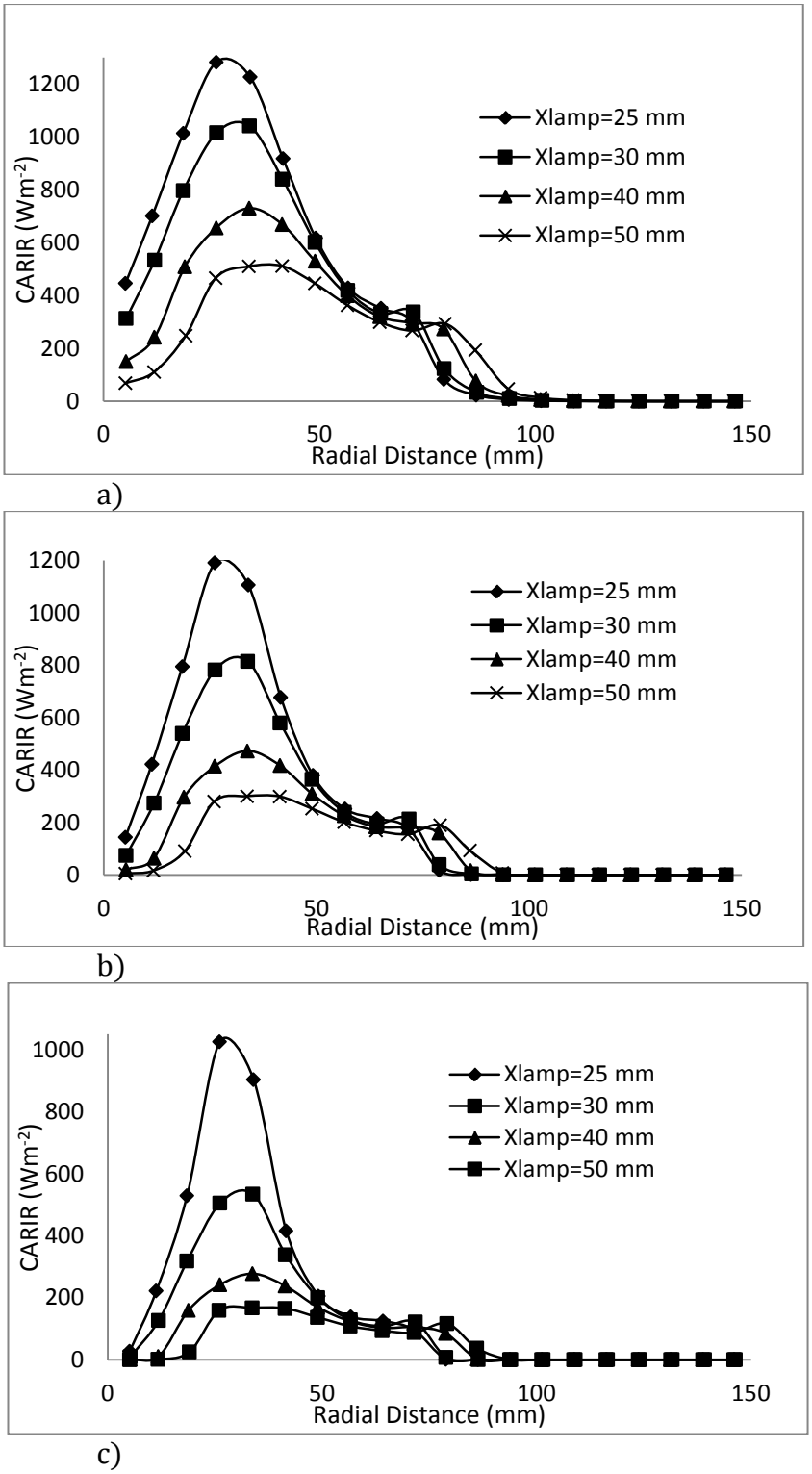

Figure 5. 11: Relationship between CARIR (Wm^{-2}) and radial distance (mm) at a) W_{cat} = 0.05, b) 0.1 and c) 0.2 (bottom) gL^{-1}. P_{Total} = 1435 Wm^{-2} e_w = 1 and z = 0 (lamp middle) at different lamp separations in a 4 lamps configuration.

It is clear from Figure 5. 11 that for W_{cat} = 0.05 gL^{-1}, the illuminated region between 20 and 40 mm was higher for both X_{lamp} = 25 and 30 mm. Nevertheless with an increase in W_{cat}, the difference in illumination in the region 20 – 40 mm (radial

distance) for X_{lamp} = 25 and 30 mm became more pronounced. This is due to the shorter adjacent distance between the lamps when X_{lamp} was 25 mm, implying small light attenuation despite the high catalysts loadings. As a result the CARIR remains very high. However, when X_{lamp} increased, the adjacent distance between the lamps also increased resulting in a higher attenuation of light at higher W_{cat}, hence the larger decrease in the peaks when X_{lamp} was 30 mm (at higher catalyst loads).

5.3.3.3 Effect of wall emissivity for multi-lamps

The effect of wall emissivity was investigated at catalyst loading W_{cat} = 0.05 gL^{-1} and with twice the initial lamp power (P_{Total} = 2870 Wm^{-2}) for both configurations (2 and 4 lamps). It was found that the wall emissivity had almost no effect on the LVREA even at such low catalyst loadings (W_{cat} = 0.05 gL^{-1}), at higher catalyst loadings it would be nearly zero. The results for only 2-lamp configuration are shown in Figure 5. 12, but they were similar for the 4-lamp configuration.

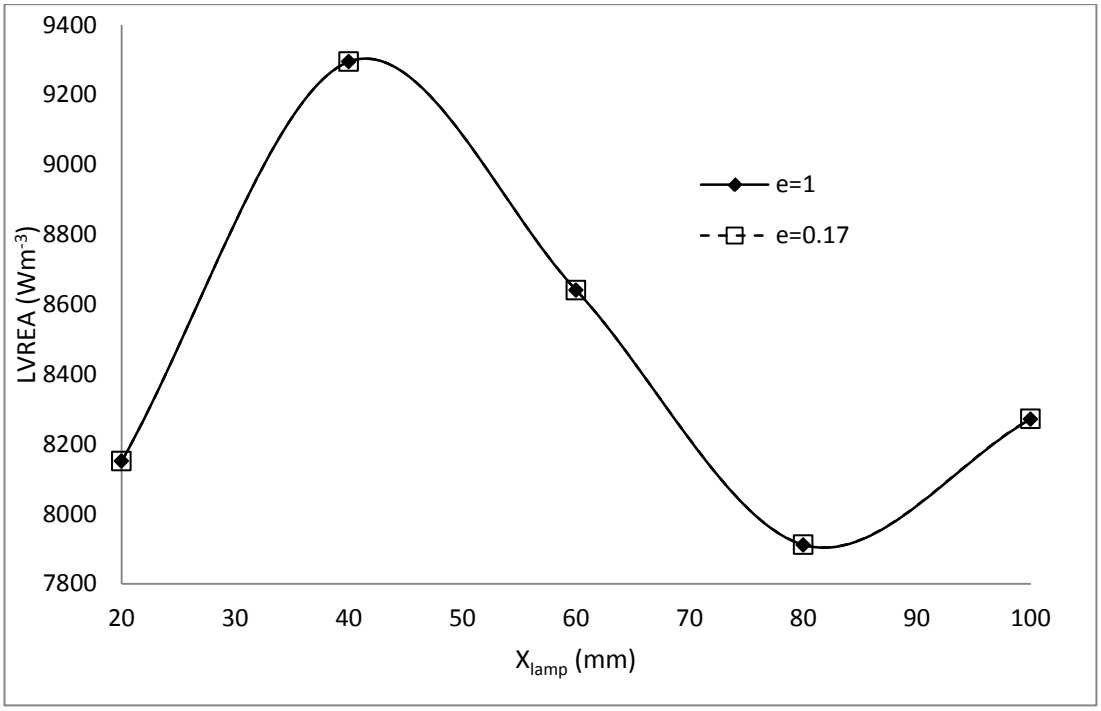

Figure 5. 12: Relationship between LVREA (Wm^{-3}) and X_{lamp} (mm) at different wall emissivities for W_{cat} = 0.05 gL^{-1} for 2 lamps configuration, P_{Total} = 2870 Wm^{-2} and z = 0 (lamp middle).

The wall effect is not evident even when the lamps are close to the wall. The maximum difference in LVREA was 0.02% only when X_{lamp} was 100 mm. The minimal effect of wall emissivity was due to the very high absorption capacity of the catalyst used.

5.3.3.4 Effect of lamp power (PTotal)

The effect of varying the lamp emission power from its initial value (P_{lamp} = 1435 Wm^{-2}) to half and twice of its initial value was investigated. It was found that for both 2 and 4 lamps, there was no change in optimum LVREA. Figure 5. 13 shows the results obtained in the case of 2 lamps when W_{cat} = 0.05 gL^{-1}.

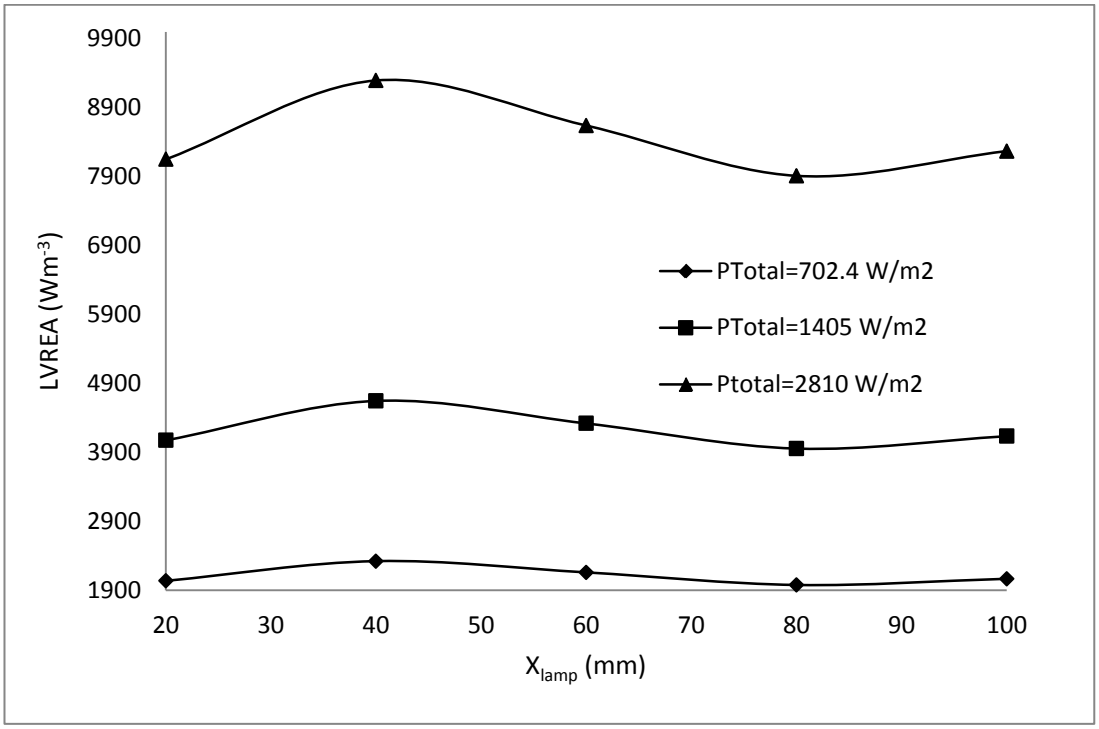

Figure 5. 13: Effect of P_{Total} on the LVREA (Wm^{-2}) for 2 lamps configuration; W_{cat} = 0.05 gL^{-1} and z = 0 (lamp middle)

5.4 Conclusion

In this study, rigorous simulations were performed to evaluate the light intensity distribution in photocatalytic reactors. Initially, simulations were conducted using a single lamp to calculate optical parameters of TiO_2 by comparing results with experimental observations. Since the UV light source had a wide emission spectrum, instead of using wavelength-averaged values, it was divided into 4 bands having different coefficients of absorption. Simulations on 2-lamp system showed that the optimum irradiation occurred at X_{lamp} = 40 mm and was independent of the catalyst loading. However, with the 4-lamp arrangement, the optimum lamp separation for maximum illumination was dependent on the catalyst loading. The wall emissivity had no effect on the LVREA for both multi-lamp configurations, even when the lamps were close to the wall, due to the high absorption capacity of the catalyst. The

optimum lamp separation was found to be independent of lamp emission power within the range investigated. This study will thus pave way for optimal design of multiple-lamp photoreactors.

Notation

E	local volumetric rate of energy absorption LVREA (Wm^{-3})
e_w	wall emissivity (dimensionless)
$\overline{G}$	area weighted average incident light intensity (Wm^{-2})
I	radiation intensity ($Wm^{-2}steradian^{-1}$)
N	number of (dimensionless)
$p(\Omega' \rightarrow \Omega)$	phase function for scattering in RTE (dimensionless)
P_{lamp}	lamp emissive power (Wm^{-2})
r	radial coordinate (m)
r_w	wall reflectivity (dimensionless)
R	radius (m)
s	direction vector (m)
V	volume (m^3)
W_{cat}	catalyst loading (gm^{-3})

Greek

α	volume fraction (dimensionless)
κ	absorption coefficient (m^{-1})
κ^*	specific absorption coefficient (m^2g^{-1})
Ω	solid angle (steradian)
σ	scattering coefficient (m^{-1})
σ^*	specific absorption coefficient (m^2g^{-1})
ρ	hemispherical spectral reflectivity (dimensionless)
θ	scattering angle (radian)

Subscript

B	bubble
G	gas

υ	frequency of radiation (s^{-1})

Other symbols

$\langle \quad \rangle$	denotes wavelength averaged values

Chapter 6 - Hydrodynamics and Kinetic Rate Modelling

Photocatalysis as a method of water treatment has been intensively investigated in the past three decades. However it is only recently that photocatalytic reactors for gas and liquid phase reactions have been modelled using computational fluid dynamics (CFD). The modelling of photocatalytic reactors requires solving the solution of the radiation transport equation (RTE). Mathematical models such as emission models have been developed for simple systems without absorption and scattering (Salvado-Estivill et al., 2007a). Other mathematical models have been developed for idealized flows (thin film slurry reactors) (Li Puma and Yue, 2003) or for specific designs, with varying levels of complexity that require numerical methods to be solved (Passalia et al., 2011b). Methods that involve statistical treatment such as the Monte Carlo method (Alexiadis, 2006) and approximations to the solution of the RTE such as the P1 model (Cuevas et al., 2007) and the DOM have also been devised and tested. Nonetheless, it is the discrete ordinate model (DOM) that has proven the most accurate and flexible along the years and it is now being used for several types of immobilised or slurry reactors (Chong et al., 2011; Denny et al., 2009; Denny et al., 2010a; Duran et al., 2011; Pareek, 2005; Pareek and Adesina, 2004; Pareek et al., 2003b; Qi et al., 2011; Trujillo et al., 2007, 2010). Since the proposal of the DOM to solve the RTE (Romero et al., 1997) in a medium and the development of powerful computers that use the DOM or related variants to solve the RTE, more research involving photocatalytic treatment have also involved a CFD treatment so as to validate experimental results. CFD treatment involves the simulation of fluid flows (single phase/multiphase) as well as solving the RTE within the treated medium. The hydrodynamics of multiphase flow in slurry reactors is solved by either the Euler-Euler (E-E) or Euler-Lagrange (E-L) formulations. Researchers in general have preferred the E-E method in solving multiphase flows compared to the E-L approach (Dhotre et al., 2008; Olmos et al., 2001; Pareek et al., 2003b; Sanyal et al., 1999; Tabib et al., 2008) due to its accuracy and relatively lower computational time requirement.

The rate of reaction in an immobilised system can be related to the incident radiation reaching the surface of the immobilised catalyst. This is slightly different for a slurry system. Here the concept of local volumetric rate of energy absorption (LVREA) needs introduction. The LVREA is the amount of energy absorbed in every elemental volume within a slurry reactor and is proportional to the local incident radiation. In slurry reactors, the incident light intensity decays exponentially with radial distance from the surface of the lamp (due to light absorption and shielding by the catalyst particles) and so does the LVREA.

The reaction order for a photocatalytic reaction can be half order, transitional order or first order with respect to the LVREA, depending on the incident light intensity reaching the surface of the catalyst particles. The higher the light intensity, the higher will be the rate of electron-hole recombination within the TiO_2 particles and therefore, the reaction order will be half order (or square root dependent) with respect to the LVREA. As the light intensity decreases, the reaction rate will tend towards first order dependency with respect to the LVREA. Herrmann (1999) mentioned that the rate of reaction was proportional to the radiant flux below a value of 250 Wm^{-2} and that above this value, the rate became proportional to the square root of the radiant flux. However immobilized systems can give a better indication of the influence of radiant flux on reaction rate since the radiant fluxes are measured at the catalyst surface. Consequently, for aqueous systems, linear regimes have been reported at $\leq 28.1 Wm^{-2}$ (Charles et al., 2011) and $\leq 110 Wm^{-2}$ (Romero et al., 2003) and a transitional regime was found in the range between 55 and $210 Wm^{-2}$ (Mehrotra et al., 2005).

In slurry reactors with large annulus (as in this study) or small catalyst loading, all reaction rate regimes are expected to occur. The aim of this study is to relate the average degradation rate of shower water (in terms of TOC – total organic carbon) with the reaction regimes (half and first order) prevailing within the reaction space and to validate the experimental results previously obtained with the devised model.

6.1 Experimental

The photodegradation of shower water was carried out in a 31 L pilot scale reactor operating in recirculation mode (i.e., slurry outlet was circulated back to the slurry inlet). The inlet concentration of shower water in terms of total organic carbon

(TOC) was $2.052 \times 10^{-3} \pm 3.67 \times 10^{-5}$ mol L^{-1}. A medium pressure Hg lamp (Primarc PM3426, 560 W) was used as the UV source. The lamp spectrum as obtained from the manufacturer was grouped into 3 bands in the absorbable UV range for P25 TiO_2 ($\upsilon \leq 387.5\, nm$). The radiation emission for each band is presented in Table 6. 1.

Table 6. 1: Lamp absorbable UV radiation for different bands.

Wavelength range (nm)	Lamp emissive power (Wm^{-2})
Band 1: ($226 < \upsilon < 280$)	410
Band 2: ($281 < \upsilon < 315$)	488.6
Band 3: ($316 < \upsilon < 387.5$)	506.2
Total absorbable power	1404.8

6.2 Theoretical Analysis

This section presents the E-E model for multiphase flow simulations followed by the solutions of the RTE to solve for the LVREA and species modelling due to TOC degradation within the reactor.

6.2.1 The Eulerian-Eulerian multiphase model

The Eulerian-Eulerian model allows for the modelling of multiple separate, yet interacting phases (Fluent, 2005). The phases are considered as interpenetrating continua for which equations representing the conservation of mass and momentum are solved. These are presented below (Fluent, 2005; Ranade, 2002).

The concept of volume fraction: for n phases in total is introduced here,

$$\sum_{k=1}^{n} \alpha_k = 1 \qquad (6.1)$$

where α_k is the volume fraction of phase k

The continuity equation can therefore be written as:

$$\frac{\partial(\alpha_k \rho_k)}{\partial t} + \nabla \cdot (\alpha_k \rho_k U_k) = \sum_{p=1, p\neq k}^{n} S_{pk} \qquad (6.2)$$

where the subscript k denotes phase k and S_{pk} is the rate of mass transfer from phase p to phase k. In this study, the rate of mass transfer of oxygen from the gas phase to liquid phase was so small that it can be safely neglected.

The momentum balance for phase k can be written as:

$$\frac{\partial(\alpha_k \rho_k U_k)}{\partial t} + \nabla \cdot (\alpha_k \rho_k U_k U_k) = -\alpha_k \nabla p - \nabla \cdot (\alpha_k \tau_k) + \alpha_k \rho_k g + F_k \qquad (6.3)$$

where F_k denotes the interphase momentum exchange terms between phase k and all other phases present in the system.

The main interfacial force acting between the phases is the drag force. From results obtained in previous works, other forces such as lift, virtual mass and turbulent dispersion were not deemed to be significant in this reactor (Buwa et al., 2006; Elena Diaz et al., 2009; Selma et al., 2010; Tabib et al., 2008). The Morsi and Alexander model (1972) was used for the calculation of the drag coefficient as it is the most complete model and can be adjusted frequently over a large range of Reynolds number.

6.2.2 Species balance

The concentration of reactants or final products in each control volume of the computational grid can be expressed in terms of mass fraction, Y_i. The species balance can be represented as:

$$\frac{\partial}{\partial t}(\rho_i Y_i) + \nabla \cdot (\rho_i U Y_i) = -\nabla \cdot J_i + r_i \qquad (6.4)$$

where J_i and r_i are the diffusion flux and net rate of production/destruction of species *i* respectively. The diffusion coefficient (*D*) of the organic species in water at 300K was taken as 1×10^{-9} m^2s^{-1} (Delgado, 2007).

6.2.3 The radiation transport equation (RTE)

The radiation balance for an incremental distance, *ds*, within the reactor can be represented by (Cassano and Alfano, 2000; Pareek et al., 2008):

$$\frac{dI_\upsilon(s,\Omega)}{ds} = -\kappa_\upsilon I_\upsilon(s,\Omega) - \sigma_\upsilon I_\upsilon(s,\Omega) + \frac{1}{4\pi}\sigma_\upsilon \int_0^{4\pi} p(\Omega' \longrightarrow \Omega) I_\upsilon(s,\Omega') d\Omega' \qquad (6.5)$$

where, $I_\upsilon(s,\Omega)$ is a beam of monochromatic radiation intensity travelling in this medium in the direction Ω along the path s, κ_υ and σ_υ are the absorption and scattering coefficients of the medium respectively and $p(\Omega' \rightarrow \Omega)$ is a phase function representing the probability of incident radiation due to in-scattering onto the element from all other directions. The absorption and scattering coefficients and

phase function are all optical parameters that are imparted by the TiO_2 particles in the wastewater medium. Expressions for these parameters are presented in section 6.2.3.1.

6.2.3.1 Optical properties

The values of the scattering and absorption coefficients can be related to the catalyst loading (W_{cat}, gm^{-3}) and the wavelength averaged specific scattering and absorption coefficients respectively ($\langle\sigma_v^*\rangle$ and $\langle\kappa_v^*\rangle$ in m^2g^{-1}). These are represented by the following relationships for Degussa P25 TiO_2 (Romero et al., 1997):

$$\sigma_v = \langle\sigma_v^*\rangle W_{cat} \tag{6.6}$$

$$\kappa_v = \langle\kappa_v^*\rangle W_{cat} \tag{6.7}$$

In this work, the relatively newly developed Aeroxide® P25 TiO_2 was used, which had enhanced photocatalytic activity (2011; Chaillou et al., 2011). Previous experimental studies using the same reactor demonstrated that the specific absorption coefficient was higher than the wavelength average value (in the UV-C region) and was wavelength dependent. The resulting absorption coefficient for each band was determined (equations 6.8 – 6.10) while using a wavelength average over the whole wavelength range was found to be satisfactory for the scattering coefficient (equation 6.11).

Band 1: $\kappa_1 = 0.66W_{cat}$ (6.8)

Band 2: $\kappa_2 = 0.68W_{cat}$ (6.9)

Band 3: $\kappa_3 = 0.70W_{cat}$ (6.10)

$\sigma_{1-3} = 5.448W_{cat}$ (6.14)

The linear anisotropic form of the phase function was used, as put forward by Fiveland (1984):

$$p(\Omega' \longrightarrow \Omega) = 1 + Acos\theta \tag{6.12}$$

where $A = -1, 0$ and 1 for backward, isotropic and forward scattering respectively.

The phase function parameter (constant A in equation 6.12) has a relatively low sensitivity on the light intensity distribution within a photocatalytic reactor (Pareek et

al., 2003a; Pareek et al., 2008; Yu et al., 2008). Pareek (2003a) investigated the effect of the phase function parameter on Aldrich TiO_2 in a slurry reactor. It was found that at low catalyst loading (0.03 gL^{-1}), backward scattering was favoured while at higher catalyst loading, isotropic scattering became dominant. Nonetheless, in most cases, isotropic scattering gave a mean absolute percentage error of less than 10% when compared to experimental values of radial incident intensity. Furthermore, when comparing the two extremes of scattering ($A = -1$ and 1), the maximum difference in volume averaged intensity for four different catalyst loadings was less than 2.5% for non-reflecting and 10% for reflecting walls. From these findings, isotropic scattering ($A = 0$) was used in this analysis.

User designed functions (UDFs) were required as an input to the catalyst particles' optical properties in the CFD package (in terms of a programming language). *Please refer to Appendix A5 – User Defined Functions (supplied in the attached CD) for the absorption and scattering coefficient UDFs.*

6.2.4 Rate of chemical reaction

In a slurry reactor with large diameter such as the one used in this research, it is expected that all reaction regimes (half order, transitional order and first order) take place. The rate of photocatalytic reaction for any regime is related to the LVREA as follows:

$$-r_p = k(f[P])(LVREA)^m \tag{6.13}$$

where k is a reaction rate constant, $f[P]$ is a function of the pollutant concentration and the values of m are 0.5, between 0.5 and 1 and 1 for half order, transitional and first order reaction regimes respectively.

The LVREA for a wavelength or wavelength band υ, at any point is expressed as:

$$LVREA_\upsilon(x,y,z) = \kappa_\upsilon \int_{\Omega=0}^{\Omega=4\pi} I_\upsilon(s,\Omega)\, d\Omega \tag{6.15}$$

such that the total LVREA at any point for the absorbable wavelength range is expressed as:

$$LVREA\,(x,y,z) = \sum_{\upsilon \le \upsilon_{max}} LVREA_\upsilon(x,y,z) \tag{6.16}$$

The reaction rate depends on the LVREA which in turn depends on the catalyst loading within the reaction medium. Since the pollutant concentration only changed very slightly with time for approximately the first 20 minutes of TOC degradation, the TOC concentration was assumed to vary linearly with time, i.e., the rate of TOC degradation was zero order for the first 20 minutes of TOC reduction *(the degradation of TOC with time is shown on a larger scale for more clarity in Figure A3- 5 - Figure A3- 11 from Appendix A3* – Detailed Experimental Results for Shower Water Photocatalysis*).* As a result, equation 6.13 can be simplified as:

$$-r_p = k'(LVREA)^m \qquad (6.16)$$

where k' encompasses the zero order reaction rate constant.

In this exercise, the transitional reaction regime will be ignored as it will be assumed that the main regimes existing within the reactor are of half and first order. Hence for a reaction domain that has been discretised into smaller volumes, the total average rate due to both regimes is:

$$-r_p = \frac{1}{V_W}\left[k_h' \int LVREA\,(V_W)^{0.5}\, dV_{W,I_h \le I < I_{max}} + k_f' \int LVREA\,(V_W)\, dV_{W,I<I_h}\right] \qquad (6.17)$$

where V_W is the volume occupied by the wastewater, k_h' and k_f' are the half and first order reaction rate constants (including the zero order reaction rate constant), I_{max} is the maximum incident light intensity, which occurs at the lamp surface and I_h is the minimum incident intensity at which half order reaction takes place.

Please refer to Appendix A5 – User Defined Functions (supplied in the attached CD) for the rate equation and other related UDFs.

6.3 Modelling

The Eulerian-Eulerian model was used to simulate the three phase flow (water-TiO_2 particles-air). The $\kappa - \varepsilon$ dispersed turbulence model was used (since the concentrations of the secondary phases were dilute (Fluent, 2005) and the model was preferentially used by various researchers, as per Table 3. 3), with standard wall functions. The momentum equations for the individual phases were solved using an extension of the SIMPLE algorithm (phase-coupled-SIMPLE). The overall

continuity was used as a pressure-velocity coupling (Ranade, 2002) criterion. The TiO_2 phase was simulated with the granular Eulerian model whereby the particulate phase was treated as liquid droplets. In the granular model, the solid phase momentum equation is modified by introducing several additional terms that account for the physical and rheological properties of the particles. In this model, particle coalescence was ignored and the diameter was constant at 2.1×10^{-8} m. The packing limit for TiO_2 particles was taken as 0.55 (Turian et al., 1997) and the restitution coefficient was zero, from the works of (Gondret et al., 2002; Marshall, 2011) that describe collisions of particles in a viscous fluid. The granular shear viscosity was determined using the approach of Gidaspow *et al.* (Fluent, 2005) while the granular bulk viscosity was expressed according to the model proposed by Lun *et al.* (Fluent, 2005). The main parameters used for the modelling of each phase are presented in Table 6. 2.

Radiation modelling was performed using the discrete ordinate method (DOM). The discrete ordinate model (DOM) transforms the integro-differential form of the RTE into a system of algebraic equations that can be solved by machine computation. In the DOM, the radiation field is divided into a number of discrete directions and the RTE is written and solved separately for each of the directions. Fluent uses a variant of the DOM called the finite volume (FV) method. The solution of the RTE was solved by discretising each control volume from Figure 6. 1 (right) into 72 directions (solid angles) and a pixelation of 1×1.

Table 6. 2: Phase parameters used in modelling

Phase	Modelling Parameters
Liquid (water)	Flow rate = 4.4 $Lmin^{-1}$ at 27°C
Gas (air)	Flow rate = 1.8 $Lmin^{-1}$ at 27°C Bubble diameter = 7.8 mm, from equation 3.34
Solid (TiO_2)	Loading range = 0.0282 – 0.15 gL^{-1} Diameter = 21 nm Density = 4260 kgm^{-3} Packing limit = 0.55 Coefficient of restitution = 0

6.3.1 Computational domain

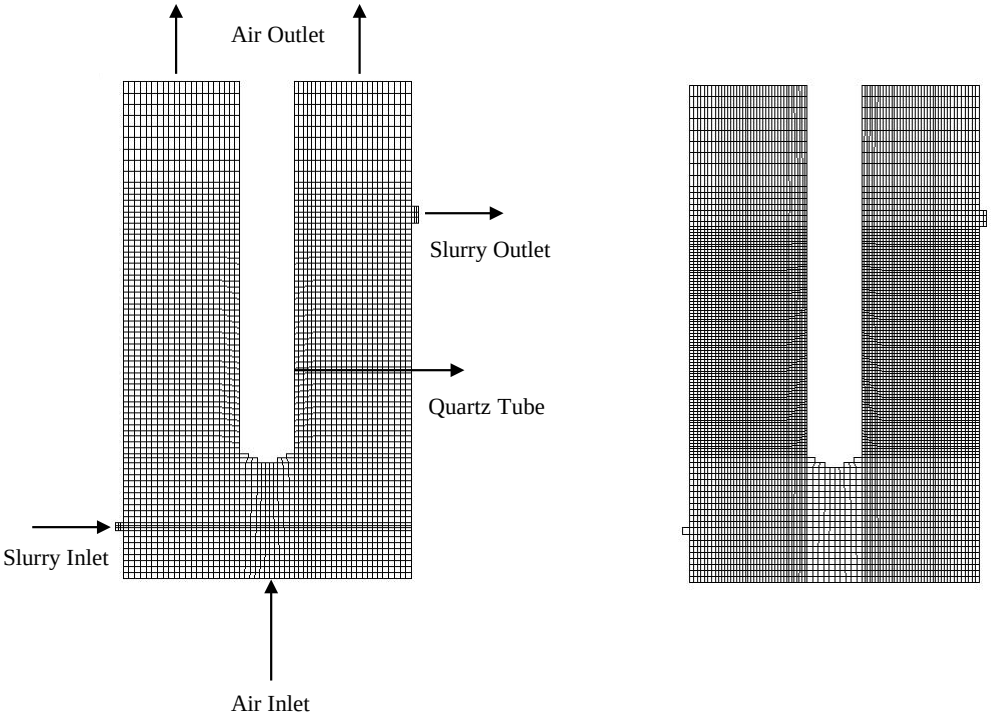

Figure 6. 1: Optimum meshing for multiphase modelling (Left) and radiation modelling (Right); symmetry planes of reactor shown.

A three dimensional computational domain of the photocatalytic reactor was constructed. For simplicity, only the symmetry planes are shown in Figure 6. 1. The reactor had the following dimensions: diameter = 30 cm, length = 52 cm, quartz tube diameter = 5.7 cm and lamp length = 20 cm. The UV lamp was enclosed within the quartz tube and as a result, the quartz surface was taken as the light emission surface with appropriate boundary conditions. Air was supplied via a 10 cm diameter perforated plate distributor and exited at the top open outlet. In this study, the exact geometry of the distributor was not considered. Instead, a uniform gas surface source was used, which made the modelling of individual holes unnecessary and therefore minimized computational requirements. This approximation has been used previously to successfully estimate the overall hydrodynamics in bubble columns (Buwa et al., 2006; Elena Diaz et al., 2009; Selma et al., 2010).

Multiphase flow was simulated using the grid in Figure 6. 1 (left). The grid was optimised by monitoring the velocity magnitude for water/TiO_2 at various locations within the computational space. The average cell size in the multiphase flow calculation grid was 6 mm. Following multiphase flow simulations, the values of mean TiO_2 concentration were stored and then interpolated onto the refined grid in

Figure 6. 1 (right) to solve for the RTE. The grid size was made thinner close to the lamp surface since most of the radiation was absorbed there. The optimum volume discretization for radiation modelling was performed by monitoring the volume averaged LVREA until no marked difference was observed.

6.3.2 Boundary conditions (BCs)

This section describes the boundary conditions used as starting points for multiphase flow modelling and radiation modelling.

6.3.2.1 Multiphase flow modelling BCs

The slurry inlet was assigned as a velocity inlet with given TiO_2 volume fractions. The slurry outlet was a velocity outlet for which the velocity assigned had to satisfy the mass flow rate at the inlet (mass in = mass out). Similarly, the air inlet was assigned a velocity inlet with air volume fraction = 1. A pressure outlet was used as the air outlet (open to the atmosphere). To ensure that no liquid and solid was entrained with the air out, an air backflow volume fraction of 1 had to be used.

6.3.2.2 Radiation modelling BCs

The central lamp assembly was considered as the emitting lamp surface. Since assuming a uniform distribution of radiant energy over the entire lamp surface does not represent its true characteristics, especially in the region close to the surface of the lamp, a suitable lamp emission model was required. In this exercise, the line source model with specular emission was chosen. The line source model (equations 6.18 and 6.19), which takes the lamp as an emitting line, was used due to its simplicity and proven reliability by numerous researchers (Pareek and Adesina, 2004; Qi et al., 2011; Salvado-Estivill et al., 2007b).

$$G_\upsilon = \frac{K_{l,\upsilon}}{4\pi r}\left(tan^{-1}\left(\frac{z+L}{r}\right) - tan^{-1}\left(\frac{z-L}{r}\right)\right) \quad (6.18)$$

where $K_{l,\upsilon}$ is the radiation power per unit length of the lamp (Wm^{-1}) for each wavelength or wavelength band.

$$K_{l,\upsilon} = \frac{P_\upsilon}{2L} \quad (6.19)$$

where L is the semilength of the lamp, z is the axial distance from the line centre, r is the radial distance from the line and P_υ is the useful power of the lamp for each wavelength or wavelength band.

Measurements previously made close to the lamp surface with a radiometer situated at the middle of the lamp (i.e., z = 0) gave values of $K_{l,\upsilon}$ = 56.8, 67.7 and 70.1 Wm^{-1} for bands 1, 2 and 3 respectively. Previous work had also shown that negligible radiation reached the reactor wall when $W_{cat} > 0.015\ gL^{-1}$. As a result, since the range of catalyst concentration investigated was between 0.0282 and 0.15 gL^{-1}, the exact value of the reactor wall reflectivity was redundant and therefore taken as zero. This meant that any radiation reaching the wall was converted into thermal energy but more importantly, it entailed a reduction in the computational time requirement.

Please refer to Appendix A5 – User Defined Functions (supplied in the attached CD) for the lamp profile (1 lamp) UDFs.

6.4 Results and Discussion

Since the light intensity at any point in the reactor vessel depends on the catalyst concentration, the RTE solution and multiphase calculations should be performed at the same time. Nevertheless, current capabilities of FLUENT do not allow simultaneous multiphase and RTE calculations. As a result, the multiphase simulation was performed first and the variables such as mean catalyst concentration for one apparent residence time interval (383 s) and liquid velocity vectors (at steady state) were stored in the memory. During radiation modelling, the catalyst mean concentration was accessed and used for the calculation of the optical properties of the medium followed by the LVREA. Next, the LVREA values were used with equation 6.17 to model the average reaction rate, which in turn was used with the mean liquid velocity vectors in equation 6.4 to model the species balance equation with reaction.

6.4.1 Multiphase modelling

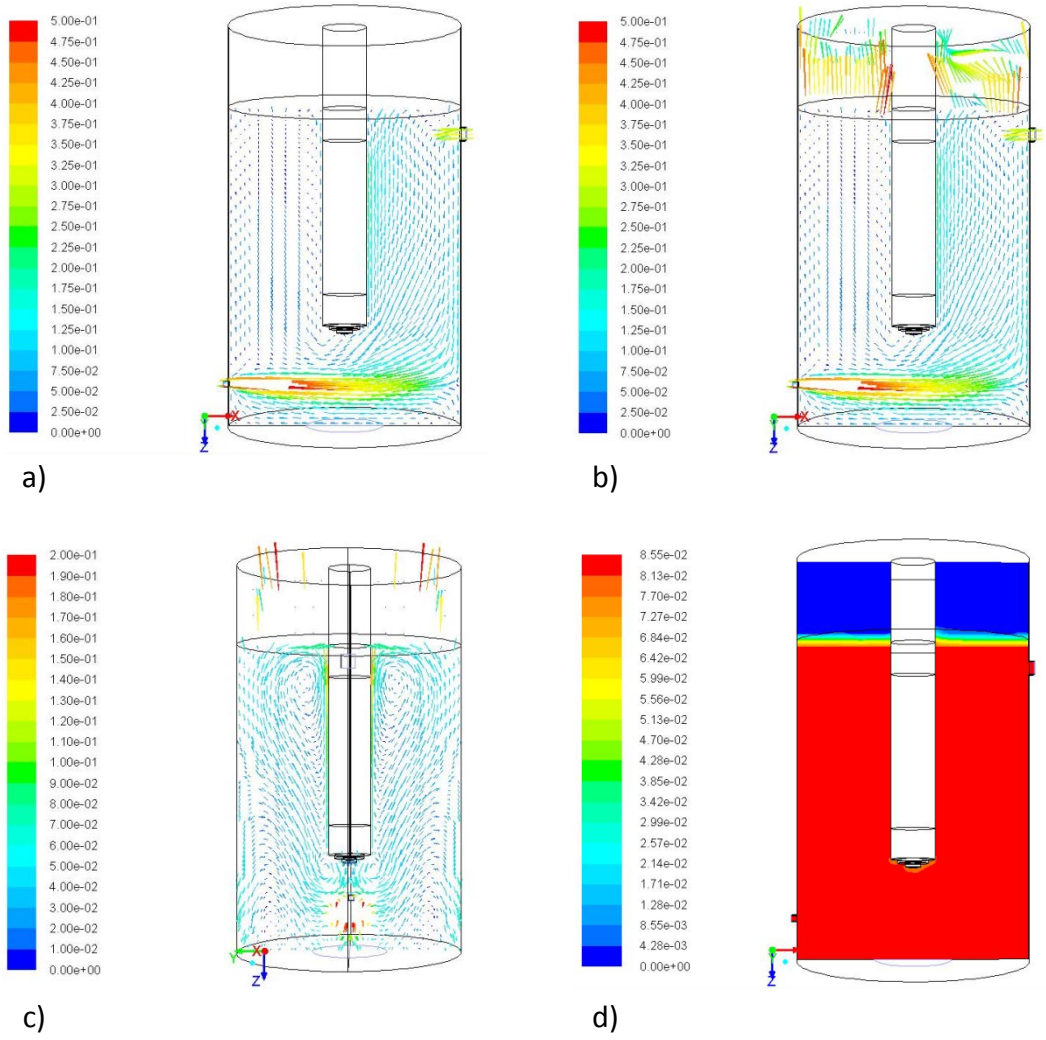

Figure 6. 2: Simulation results obtained with W_{cat} = 0.0845gL^{-1}, air flow rate = 1.8 Lmin^{-1} and liquid flow rate = 4.45 Lmin^{-1}; a) Velocity vectors (scale on left, ms^{-1}) of TiO_2 particles at steady state, b) Velocity vectors (scale on left, ms^{-1}) of water at steady state on x-z plane, c) Velocity vectors (scale on left, ms^{-1}) of water at steady state on y-z plane, d) Mean TiO_2 concentration (scale on left, gL^{-1}) contours for apparent residence time (383 s).

The E-E multiphase flow simulation was performed for a period corresponding to the apparent residence time of the fluid in the reactor, i.e., 383 seconds. For simplicity, velocity and TiO_2 concentration contours are shown on the symmetry plane of the reactor in Figure 6. 2 at a catalyst concentration of 0.0845 gL^{-1}. Figure 6. 2a and b show the velocity contours for TiO_2 and water respectively in the range 0-0.5 ms^{-1}. Higher velocity vectors (up to 1.6 ms^{-1}) are not shown here as they represent only a small fraction of the flow, close to the inlet. It can be seen that the TiO_2 and water have similar velocity contours. The small size of the TiO_2 particles means that they get dragged along with the water flow, which is consistent with observations made by Pareek *et al.* (2003b) who performed similar simulations. Due to the high inlet

flow rate, recirculation zones (shown in the plane normal to the symmetry plane, Figure 6. 2c) were formed on both sides of the lamp assembly, meaning that a large portion of the reaction medium remained within the reactor. However, this is not ideal for best results. It would be preferred to have a low velocity inlet and a uniform supply of air throughout the entire surface area of the reactor so as to reduce/eliminate the occurrence of recirculation zones as much as possible and induce plug flow regime within the reactor.

The backflow of water near the gas outlet in Figure 6. 2b represents the reverse flow of water particles, occurring due to the pressure outlet boundary condition specified in section 6.3.2.1 which stated that the exiting gas was free of solids and liquid. The TiO_2 mean concentration contours in Figure 6. 2d show a uniform catalyst concentration distribution within the reaction medium.

6.4.2 Radiation modelling

Radiation modelling was performed for catalyst concentrations in the range 0.0282 – 0.15 gL^{-1}. Figure 6. 3a and b shows 3-D contours of incident radiation when W_{cat} is 0.0845 and 0.0282 gL^{-1} respectively. It can be seen that the shielding effect caused by an increased amount of catalyst in Figure 6. 3a reduces the amount of useful incident radiation down to a narrow strip close to the lamp surface. As a result, as W_{cat} increased, most of the reaction space received very little radiation. Figure 6. 4a shows the corresponding contours of LVREA when W_{cat} = 0.0282 gL^{-1}. Since the catalyst distribution within the reaction space was essentially uniform (Figure 6. 2d), the contours of LVREA were qualitatively similar to the incident radiation contours in Figure 6. 3b.

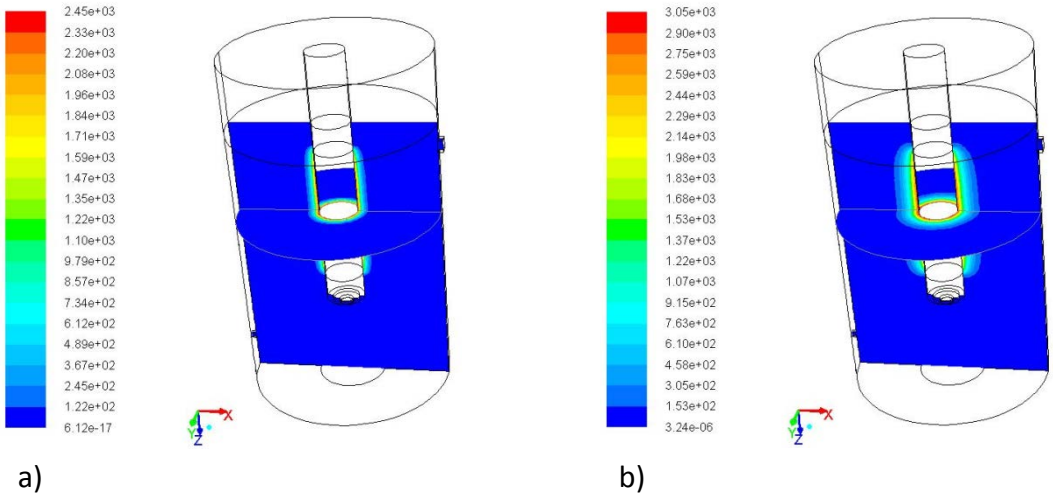

Figure 6. 3: a) Incident radiation contours when W_{cat} = 0.0845 gL^{-1} (scale on left, Wm^{-2}), b) Incident radiation contours when W_{cat} = 0.0282 gL^{-1} (scale on left, Wm^{-2}).

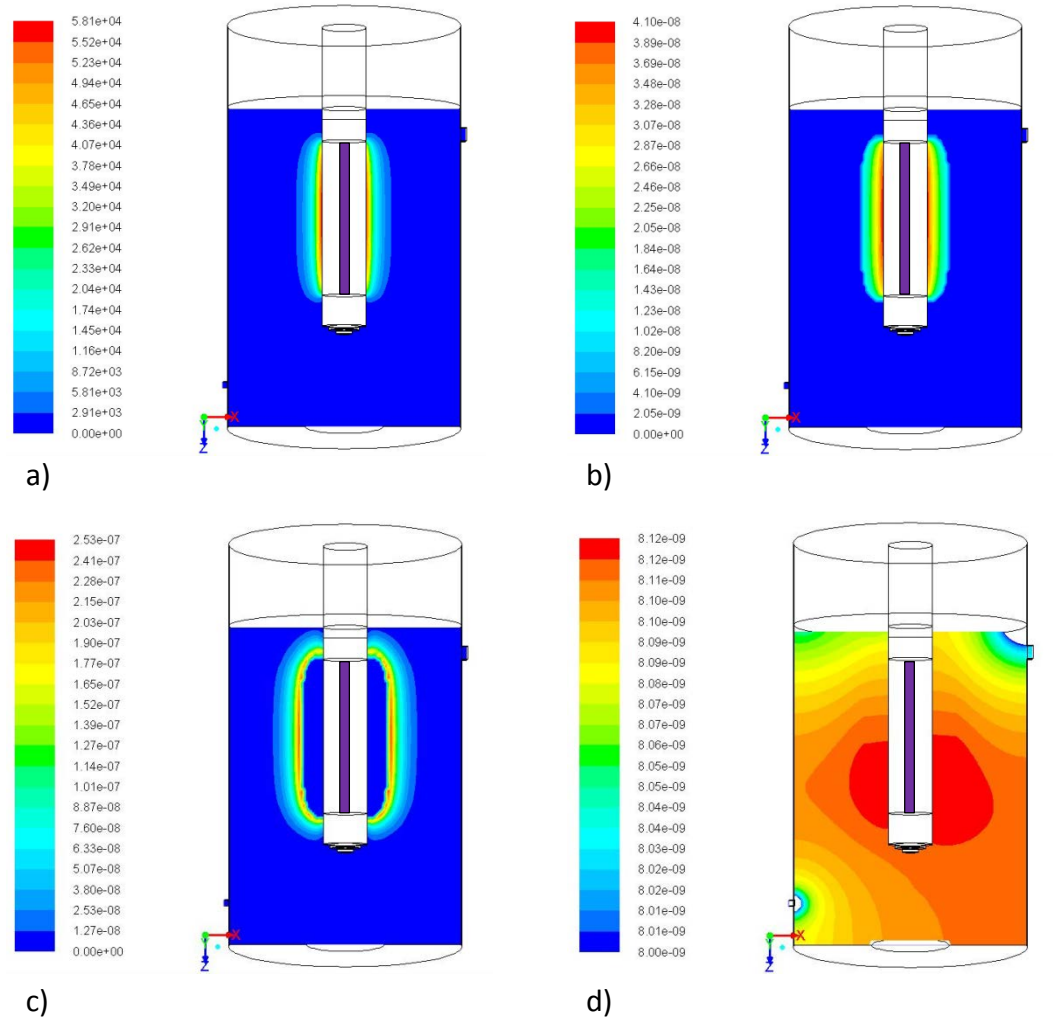

Figure 6. 4: a) LVREA contours when W_{cat} = 0.0282 gL^{-1} (scale on left, Wm^{-3}), b) Half order reaction rate contours when W_{cat} = 0.0282 gL^{-1} (scale on left, mol L^{-1} s^{-1}), c) First order reaction rate contours when W_{cat} = 0.0282 gL^{-1} (scale on left, $molL^{-1}s^{-1}$) and d) Oxidised carbon concentration contours when W_{cat} = 0.0282 gL^{-1} (scale on left, mass fraction); all contours shown on symmetry plane. UV lamp placed within quartz tube as shown.

The variation of the LVREA with W_{cat} is presented in Figure 6. 5. The LVREA increases steeply with increase in the catalyst loading up to a W_{cat} of around 0.03 gL^{-1}, after which the increase in LVREA becomes marginal. The very high absorption capacity of the TiO_2 catalyst means that a low catalyst concentration is required within the reactor and from Figure 6. 5, a W_{cat} of greater than 0.03 gL^{-1} appears to be unnecessary as the shielding effect occurring with increased catalyst concentration gives rise to a reduced illumination volume within the reactor. This can be visualised with Figure 6. 3a and b whereby at the higher W_{cat} of 0.0845 gL^{-1}, Figure 6. 3a, the LVREA is very high but within a very small volume of the reactor. From Figure 6. 5, it appears that the experiments have been carried out at catalyst concentrations whereby light shielding becomes apparent. It is expected that at W_{cat} < 0.0282 gL^{-1}, an optimum concentration should exist at which a larger volume of the reactor is illuminated, leading to a higher reaction rate.

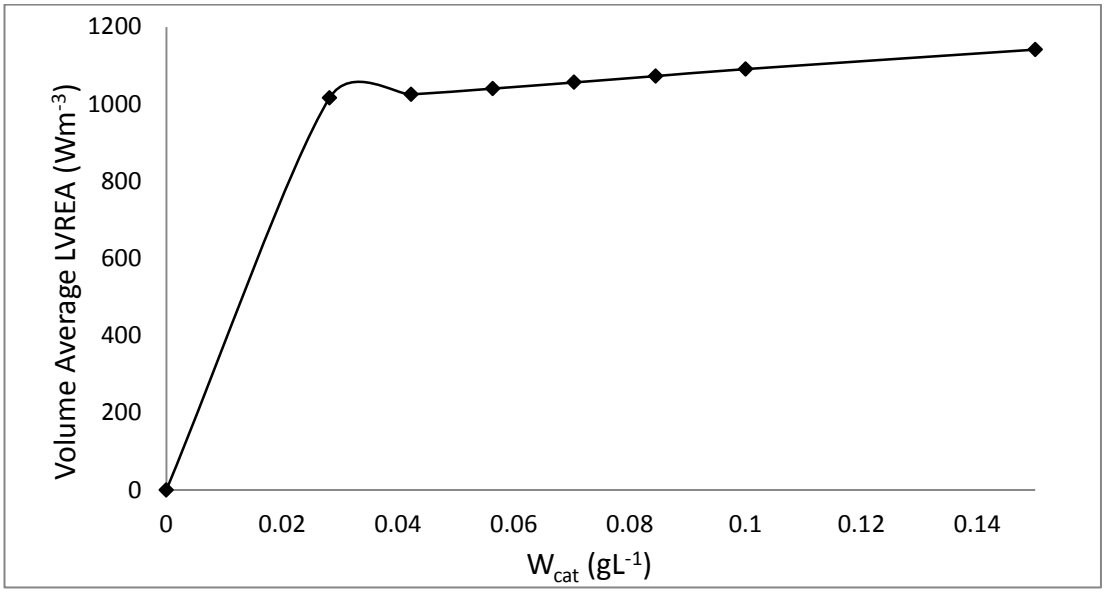

Figure 6. 5: Variation of the LVREA (Wm^{-3}) with W_{cat} (gL^{-1}).

A trial and error procedure was performed so as to determine the value of I_h followed by k_h' and k_f' from equation 6.17. Figure 6. 6 shows the experimental and model fitted values of the average volumetric reaction rate (mol L^{-1} s^{-1}) for the range of W_{cat} investigated. The best fit was obtained when $I_h = 225\, Wm^{-2}$, $k_h' = 1.7 \times 10^{-10}\ kmol\, W^{-0.5}\, m^{-1.5}\, s^{-1}$ and $k_f' = 6.8 \times 10^{-11}\ kmol\, W^{-1}\, s^{-1}$. For comparison, the best fit when $I_h = 250\, Wm^{-2}$ is also presented (dashed line).

Figure 6. 6 also presents the results obtained when using the model with a constant catalyst concentration within the reactor. This means that the assumption of a well distributed catalyst concentration is pertinent and could potentially save on simulation time. As a result, for such small sized, low catalyst loadings, a two phase Euler-Euler model (representing liquid and air phases) can be used with the liquid phase having average properties (i.e., catalyst concentration well distributed). From Figure 6. 6, the proposed model provided a satisfactory fit to the experimental data within the range investigated. The model also shows that a radiant flux of $I_h = 250\ Wm^{-2}$ as a minimum limit to half order reaction cannot be generalised to all types of photocatalytic reactions but will instead depend on the pollutant species, reactor design, type of catalyst and type of UV source used. A Pearson coefficient of 0.88 between experimental and predicted data in Figure 6. 6 indicated that the proposed model satisfactorily described the experimental observations.

Figure 6. 4b and c show the contours of half order and first order reaction rate respectively when W_{cat} = 0.0282 gL^{-1}. Despite the high value of radiation intensity and corresponding LVREA in the region of half order reaction, the square root dependency of the reaction rate in the region closest to the lamp surface means that the effective degradation rate of pollutants in that region is lower than in the first order reaction region. This is due to the high rate of electron-hole recombination in regions of high radiation intensity, which drastically reduces the oxidation potential of the catalyst particles.

Figure 6. 4d shows the contours of oxidised TOC concentration (in terms of mass fraction) at W_{cat} = 0.0282 gL^{-1}. The mass fraction range between 8×10^{-9} and 8.12×10^{-9} is presented here for clarity. It can be seen that more carbon was oxidised on the right hand side of the reactor as compared to the left hand side, due to the longer path taken by the water from the inlet to the outlet (Figure 6. 2b).

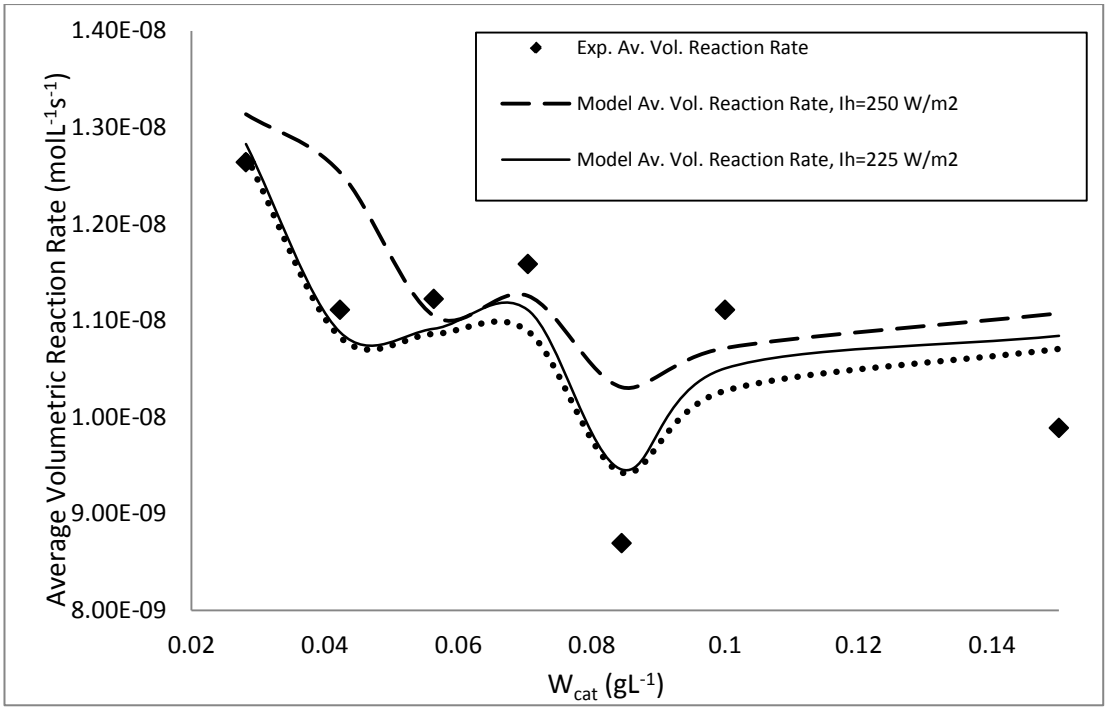

Figure 6. 6: Experimental and model predicted average volumetric reaction rate ($molL^{-1}s^{-1}$) as a function of W_{cat} (gL^{-1}).

Figure 6. 7 shows the reaction rate due to first order and half order reactions respectively. It can be seen that the overall reaction rate was largely dependent upon first order reactions. The magnitude of the first order volumetric reaction rate within the reactor was between 12 and 20 times that of half order reaction, despite the higher rate constant for half order reactions ($k_h'/k_f' = 2.5$). The related average volumetric reaction rate for half order reaction was lower due to the square root dependency with respect to the LVREA that occurs due to the high rate of electron-hole recombination in the regions of high light intensity, close to the lamp surface, i.e., when $I > 225\ Wm^{-2}$.

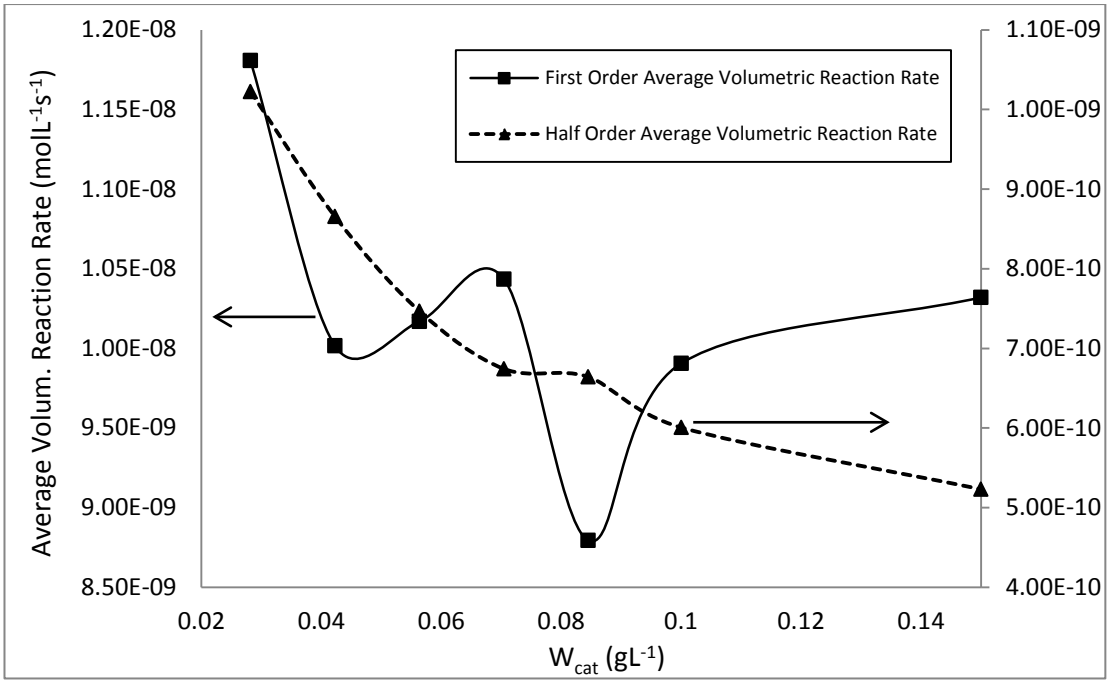

Figure 6. 7: Variation of average volumetric reaction rate (first order – scale on left, mol L^{-1} s^{-1}; half order – scale on right, $molL^{-1}s^{-1}$) with W_{cat} (gL^{-1}).

6.5 Conclusions

The granular Eulerian model was used to solve the 3 phase hydrodynamics occurring inside a pilot scale slurry photocatalytic reactor treating shower water while the DOM was used to simulate radiation. The existence of regions of varying orders (half and first order) within the reactor was acknowledged in the development of the rate equation to model pollutant degradation. Using a value of 225 Wm^{-2} as the minimum incident light intensity at which half order reactions take place, a Pearson correlation of 0.88 between simulated and experimental data indicated that the proposed model satisfactorily described the experimental observations. The average volumetric reaction rate within the reactor was largely dependent upon first order reactions. The magnitude of the first order volumetric reaction rate within the reactor was between 12 and 20 times that of half order reaction due to the square root dependency of reaction rate with respect to the LVREA in regions of high radiation light intensity.

Notation

D – diffusion coefficient of specie (m^2s^{-1})

F – interphase momentum exchange force ($kgm^{-2}s^{-2}$)

g – gravitational acceleration (ms^{-2})

I - intensity (Wm^{-2})

J – diffusion flux ($kgm^{-2}s^{-1}$)

k – reaction rate constant

K_l – line emission model radiation power per unit length constant (Wm^{-1})

L – lamp semi length (m)

LVREA – local volumetric rate of energy absorption (Wm^{-3})

p – pressure shared by all phases (Nm^{-2})

$p(\Omega' \longrightarrow \Omega)$ – phase function for in scattering of radiation

P – lamp power (W)

$[P]$ – pollutant concentration ($molL^{-1}$)

r – rate of production/destruction (species balance, $kgm^{-3}s^{-1}$) / radial distance (lamp emission modelling, m)

s, z – distance (m)

S – rate of mass transfer ($kgm^{-3}s^{-1}$)

U – velocity (ms^{-1})

V – volume (m^3)

W_{cat} – catalyst loading (gm^{-3})

Y – mass fraction

Greek letters

α – volume fraction

θ – angle between 2 directions of propagation

κ – absorption coefficient (radiation modelling, m^{-1})

υ –wavelength (nm)

ρ – density (kgm^{-3})

σ – scattering coefficient (m^{-1})

τ – viscous stress tensor (Nm^{-2})

Ω – solid angle (steradian)

Subscript

f – first order

h – half order

i – specie

k, *p* – fluid phase

W – wastewater

Chapter 7 – Multiple Lamp Photocatalytic Reactors

It has been established in Chapter 6 - Hydrodynamics and Kinetic Rate that the average reaction rate within a photocatalytic reactor was mainly governed by first order reactions, i.e., reactions occurring at incident intensities < 225 Wm^{-2} within the reactor, while half order (HO) reactions were responsible for a minor fraction of the rate of pollutant degradation. This chapter considers using multiple lamps instead of only one powerful lamp and investigates the effects that lamp arrangement has on the average reaction rate in the reactor. Using a system of multiple lamps within the reactor could potentially increase the rate of reaction compared to using only 1 lamp. It is expected that an optimum lamp arrangement (with the lamps separated by the distance X_{lamp}) can maximise the incident radiation contours at which first order (FO) reactions take place.

The aim of this work was to determine the effect of using 2 and 4 lamps on the average reaction rate within the reactor and compare with the results obtained with 1 lamp. The total emissive power of the lamps in the multi-lamps system was equal to the emissive power when using 1 lamp.

Since the average rate was only dependent on the LVREA within the reactor and was zero order with respect to the pollutant concentration, the momentum equations for the multiphase system were not solved. By assuming a constant catalyst distribution within the reactor, radiation modelling was performed and the results used to obtain estimates of the average reaction rate.

7.1 Modelling

Multiphase modelling was not performed since the rate was zero order with respect to pollutant concentration and the assumption of a uniform catalyst concentration within the reactor was applicable, as presented in section 6.4.2.

The optical parameters of the medium are given in section 6.3.2.2. The boundary conditions for radiation modelling were also as in section 6.3.2.2 with the only difference being the values of the constants $K_{l,v}$ in the case of N_{lamps} = 2 and 4 respectively. These values are listed in Table 7. 1. Furthermore, according to the

results obtained in section 5.3.2, since negligible amount of radiation reaches the reactor wall, the reflectivity of the reactor wall was taken as zero.

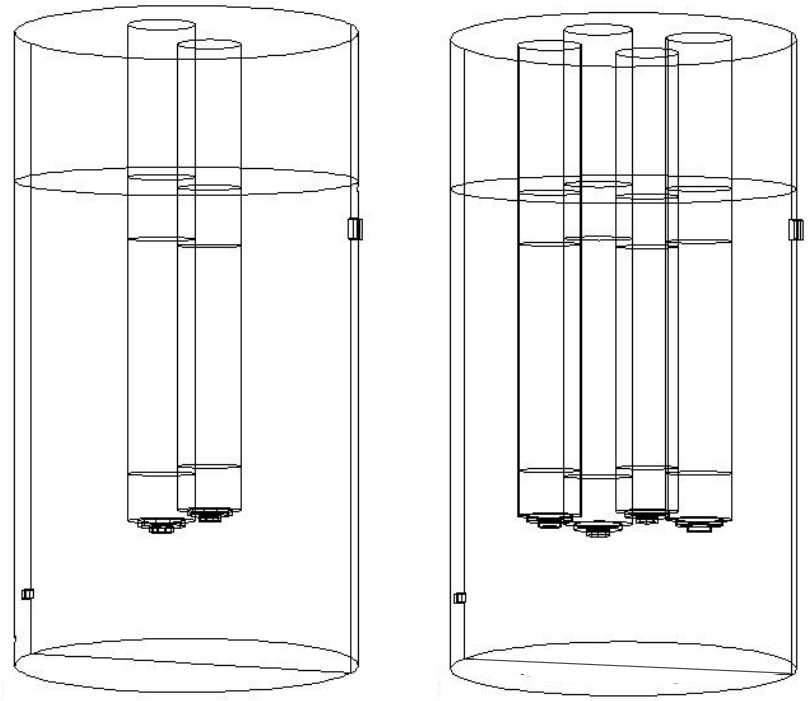

Figure 7. 1: 3-dimensional geometry of photocatalytic reactor using 2 (left) and 4 (right) lamps.

Figure 7. 1 shows the 3-dimentional constructed geometry for a reactor setup using 2 (left) and 4 (right) lamps respectively. The distance X_{lamp} that measures the lamp separation is shown in Figure 5. 1b and c. The geometry was meshed with grid size and distribution similar to the case where 1 lamp was used, as per Figure 6. 1 (right).

7.1.1 LSSE parameters

The lamp emission model used was according to the LSSE model, equations 6.18 and 6.19. The value of the constant $K_{l,\upsilon}$ was changed in the case where N_{lamps} = 2 and 4 so that the total emissive power from the lamp surfaces was the same in all cases. The values of the constant $K_{l,\upsilon}$ were obtained experimentally using 1 lamp. The corresponding values for N_{lamps} = 2 and 4 are given in Table 7. 1.

Table 7. 1: Values of LSSE parameter $K_{l,v}$ (Wm^{-1}) when N_{lamps} = 1, 2 and 4

	$K_{l,v}$ (Wm^{-1})		
Band number	Nlamps = 1	Nlamps = 2	Nlamps = 4
0	56.8	28.4	14.2
1	67.7	33.9	16.9
2	70.1	35.1	17.5

Please refer to Appendix A5 – User Defined Functions (supplied in the attached CD) for the lamp profile (2 and 4 lamps) UDFs.

7.2 Discussion

Figure 7. 2 shows the variation of the LVREA with X_{lamp} for the range of W_{cat} investigated. It shows that an optimum LVREA occurs at X_{lamp} = 4 cm, irrespective of the catalyst concentration within the reactor, confirming the predictions obtained with 2D simulations (Figure 5. 6). However the values of LVREA obtained with 3D simulations were lower to the 2D results since half of the reactor length was not illuminated (17 cm and 3 cm below and above the lamp assembly respectively) as displayed in Figure 6. 1. Furthermore, using the LSSE model for the lamp radiation profile along the lamp length gives overall lower radiation emission intensity at the lamp surface as compared to using a uniform emission surface.

The average reaction rate was calculated using equation 6.17 and is presented in Figure 7. 3. Interestingly, the maximum average reaction rate did not necessarily appear at X_{lamp} = 4 cm as per the occurrence of the optimum LVREA. At the lower W_{cat} of 0.028 gL^{-1} and 0.050 gL^{-1}, the maximum reaction rate occurred at X_{lamp} = 6 cm while at higher W_{cat} of 0.070 gL^{-1} and 0.084 gL^{-1}, the optimum lamp separation reduced to 4 cm.

Similar to the results obtained with 1 lamp, the average reaction rate was dominated by first order (FO) reactions, i.e., reactions occurring when the incident radiation intensity within the reactor was less than 225 Wm^{-2}. This is illustrated by Figure 7. 4 - Figure 7. 6 showing the variation with X_{lamp} of FO average reaction rate, HO average reaction rate and FO/HO reaction rate ratio respectively. As an example, the ratio of FO/HO reaction rates, Figure 7. 6, is 17 at the optimum X_{lamp} when W_{cat} = 0.028 gL^{-1}. This ratio increases as W_{cat} increases.

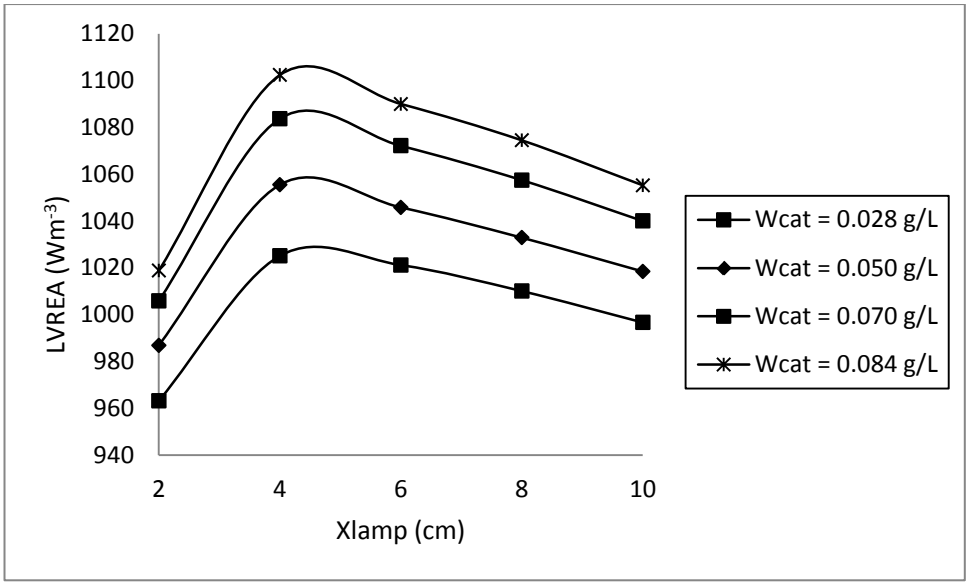

Figure 7. 2: Variation of LVREA (Wm^{-3}) with X_{lamp} (cm) at different catalyst loadings, N_{lamps} = 2.

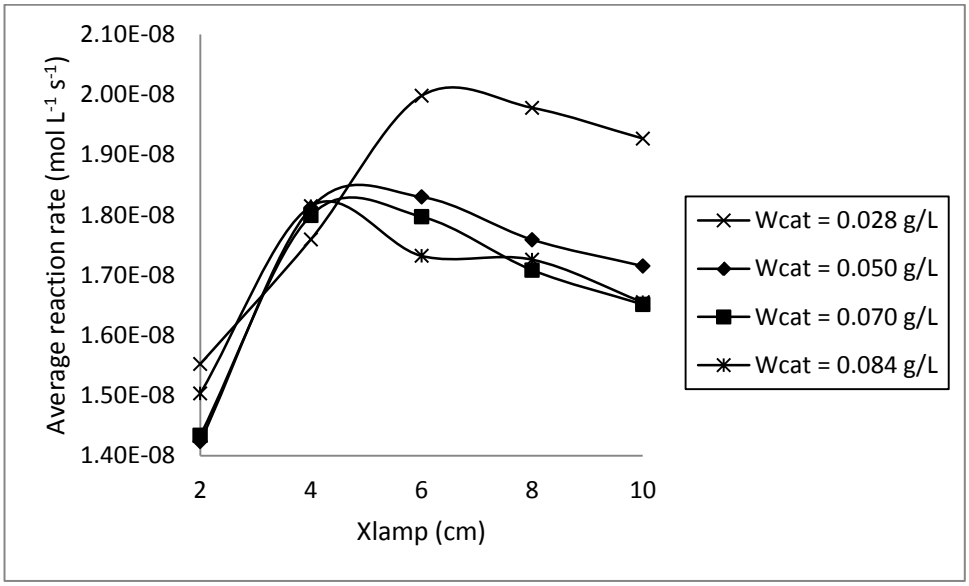

Figure 7. 3: Variation of average reaction rate ($molL^{-1}s^{-1}$) with X_{lamp} (cm) at different catalyst loadings, N_{lamps} = 2

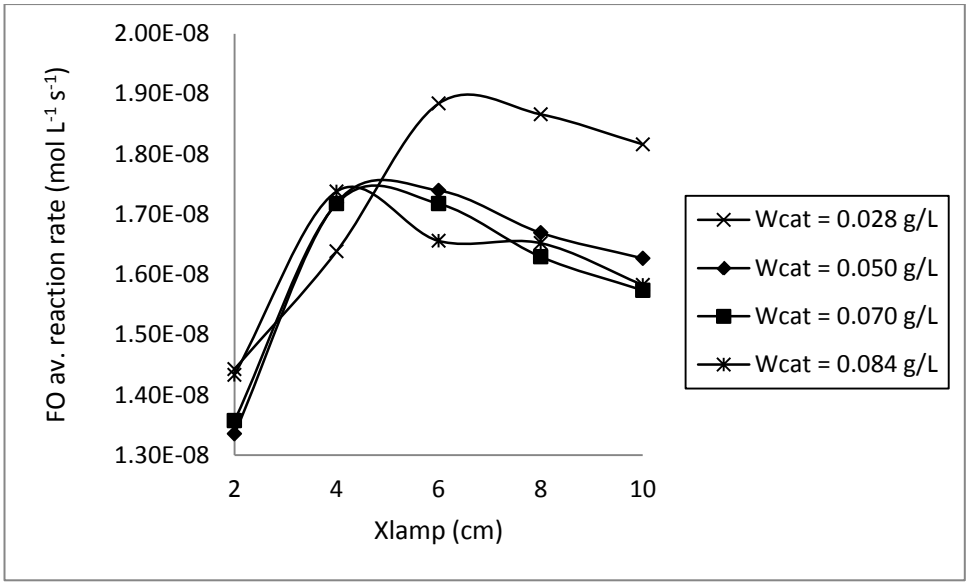

Figure 7. 4: Variation of FO average reaction rate ($molL^{-1}s^{-1}$) with X_{lamp} (cm) at different catalyst loadings, N_{lamps} = 2.

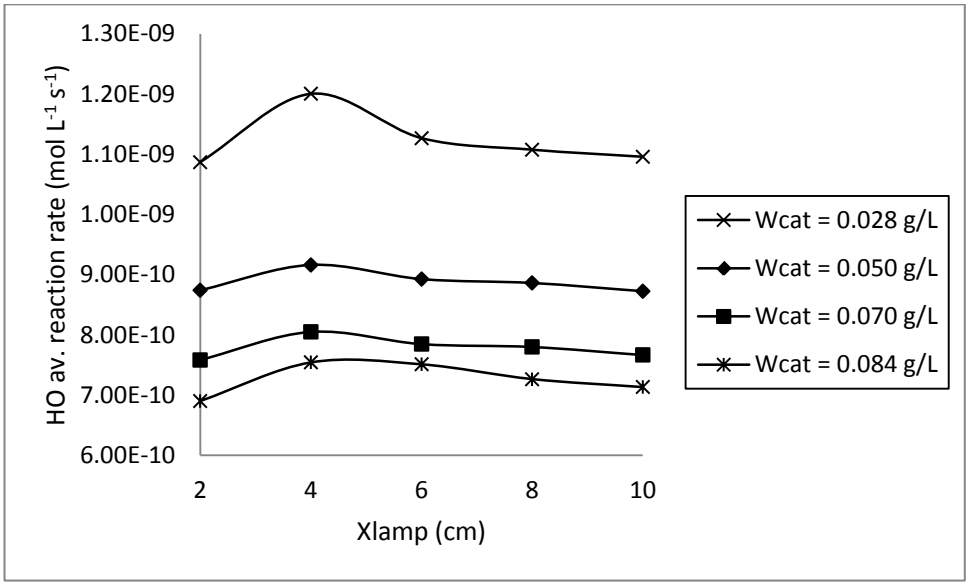

Figure 7. 5: Variation of HO average reaction rate ($molL^{-1}s^{-1}$) with X_{lamp} (cm) at different catalyst loadings, N_{lamps} = 2.

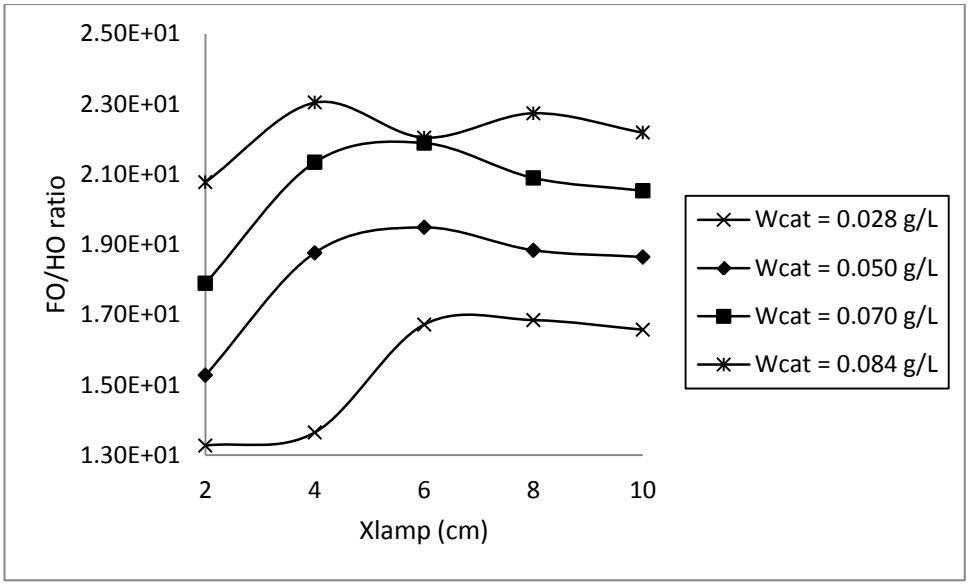

Figure 7. 6: Variation of FO/HO average reaction rate ratio with X_{lamp} (cm) at different catalyst loadings, N_{lamps} = 2.

Similar conclusions (regarding the maximisation of FO reaction regions) can be drawn from using 4 lamps within the reactor (Figure 7. 7 - Figure 7. 11). Within the range of X_{lamp} and W_{cat} investigated, maximum reaction rate occurred at X_{lamp} = 10 cm when W_{cat} = 0.028 gL^{-1}, X_{lamp} = 8 cm when W_{cat} = 0.050 and 0.070 gL^{-1} and X_{lamp} = 7 cm when Wcat = 0.084 gL^{-1}. The decrease in the average reaction rate past the optimum X_{lamp} was sharper in a system of 2 lamps compared with that of 4 lamps due to improved illumination of the reactor volume when using 4 lamps. This will be discussed shortly.

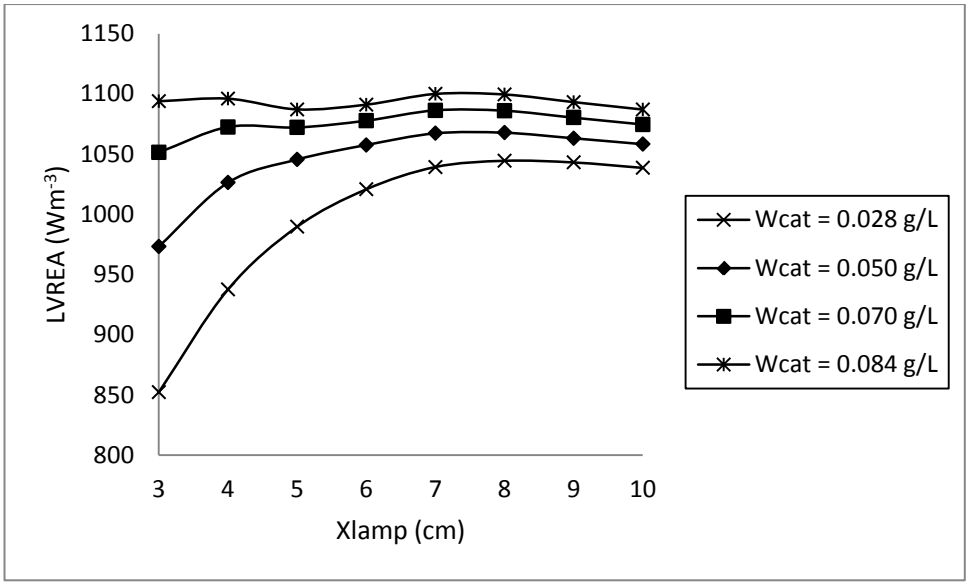

Figure 7. 7: Variation of LVREA (Wm^{-3}) with X_{lamp} (cm) at different catalyst loadings, N_{lamps} = 4.

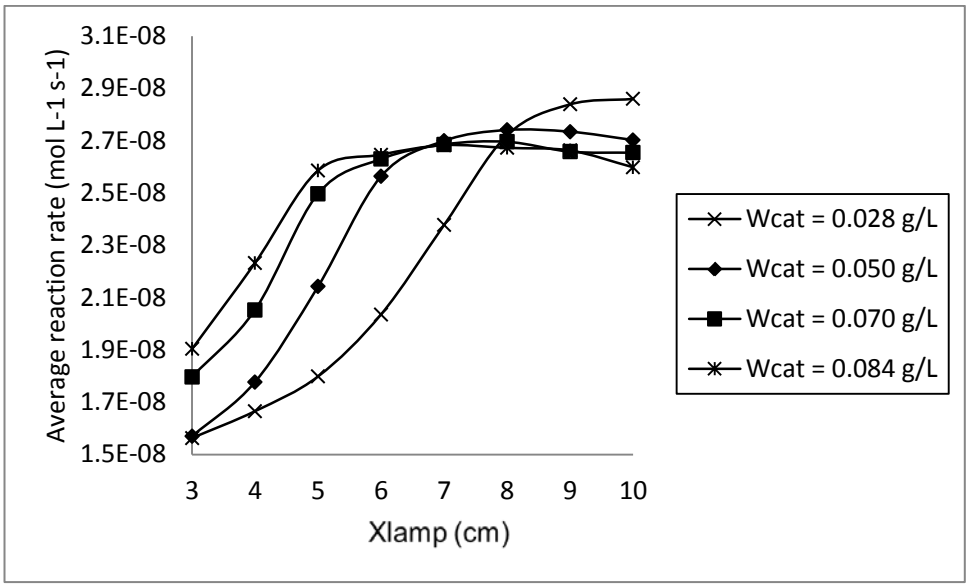

Figure 7. 8: Variation of average reaction rate ($molL^{-1}s^{-1}$) with X_{lamp} (cm) at different catalyst loadings, N_{lamps} = 4.

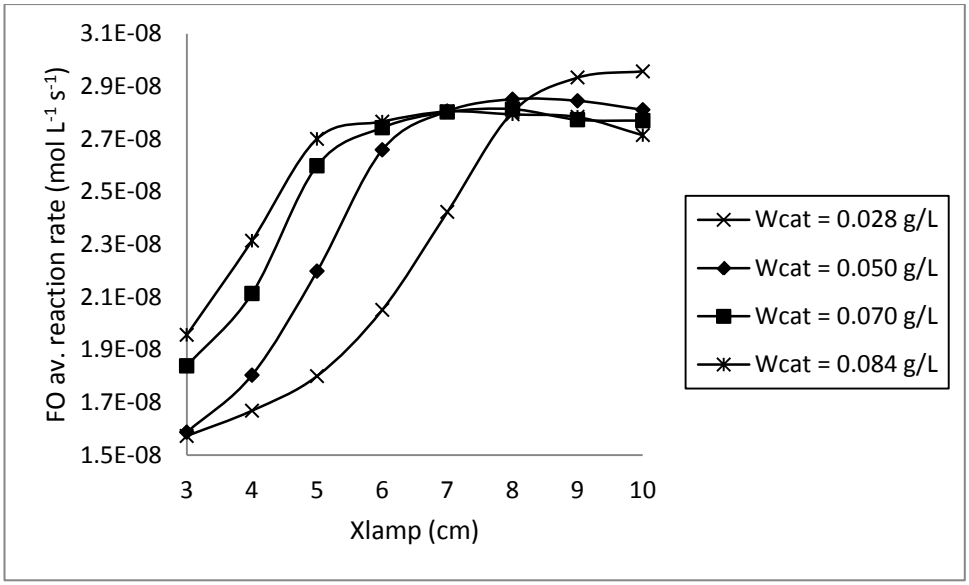

Figure 7. 9: Variation of FO average reaction rate ($molL^{-1}s^{-1}$) with X_{lamp} (cm) at different catalyst loadings, N_{lamps} = 4.

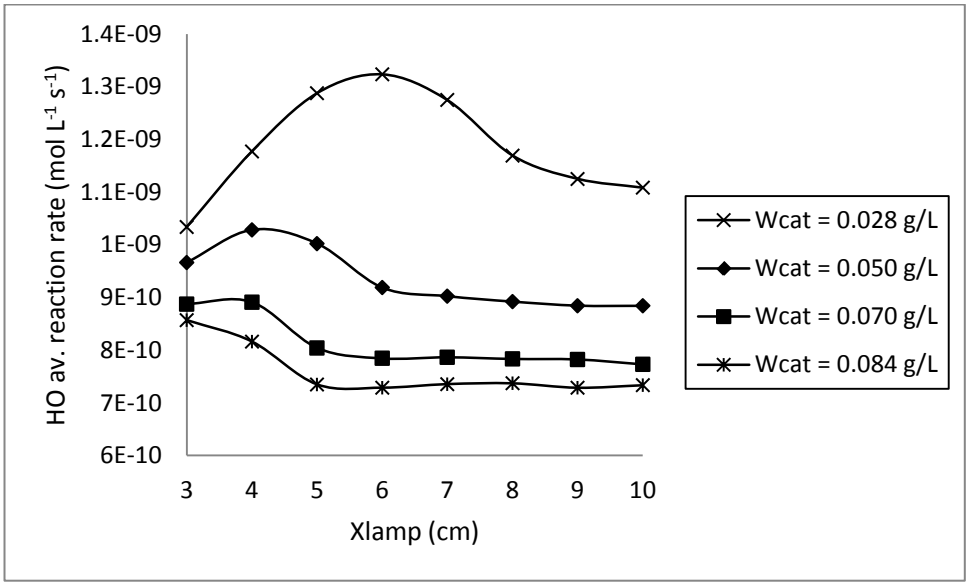

Figure 7. 10: Variation of HO average reaction rate ($molL^{-1}s^{-1}$) with X_{lamp} (cm) at different catalyst loadings, N_{lamps} = 4.

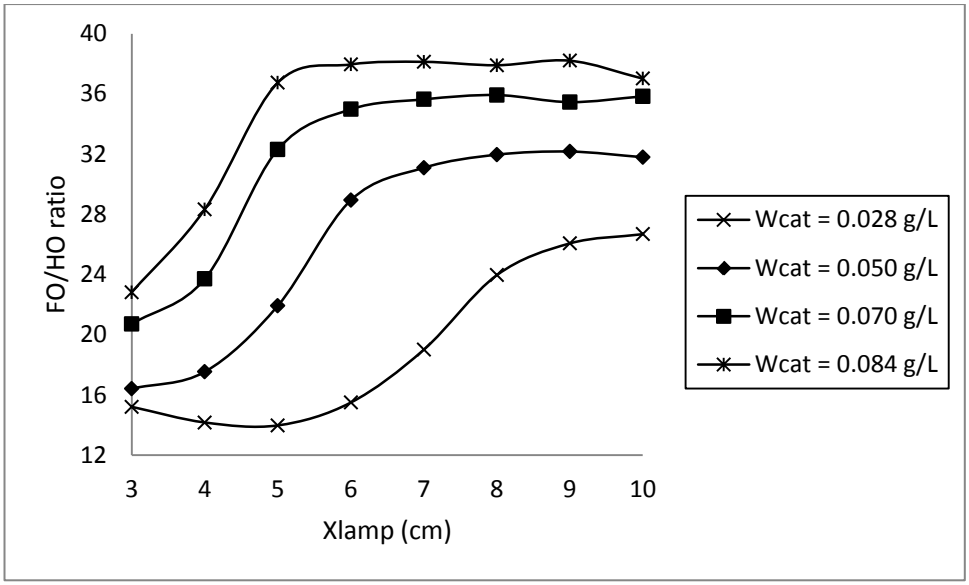

Figure 7. 11: Variation of FO/HO average reaction rate ratio with X_{lamp} (cm) at different catalyst loadings, N_{lamps} = 4.

For the same total emissive power of the lamps, it can be seen that increasing the number of lamps can significantly increase the average reaction rate in the reactor. Figure 7. 12 represents the variation of the maximum average reaction rate at optimum X_{lamp} (for both FO and HO reactions) with respect to N_{lamps} at W_{cat} = 0.028 gL^{-1} (the optimum catalyst concentration required for pollutant degradation). The average reaction rate with respect to HO reaction remained constant with increasing N_{lamps} while the rate due to FO reaction increased. The total average reaction rate was 1.28×10^{-8} $molL^{-1}s^{-1}$, 2×10^{-8} $molL^{-1}s^{-1}$ and 2.86×10^{-8} $molL^{-1}s^{-1}$ when N_{lamps} = 1, 2 and 4 respectively. Hence the potential increase in average reaction rate relative to 1 lamp was 56% and 123% when N_{lamps} = 2 and 4 respectively. This increase was due to the increase in FO reactions within the reactor (while HO reactions remained unchanged), ensuing because of the maximisation of contours of incident radiation intensities of less than 225 Wm^{-2}.

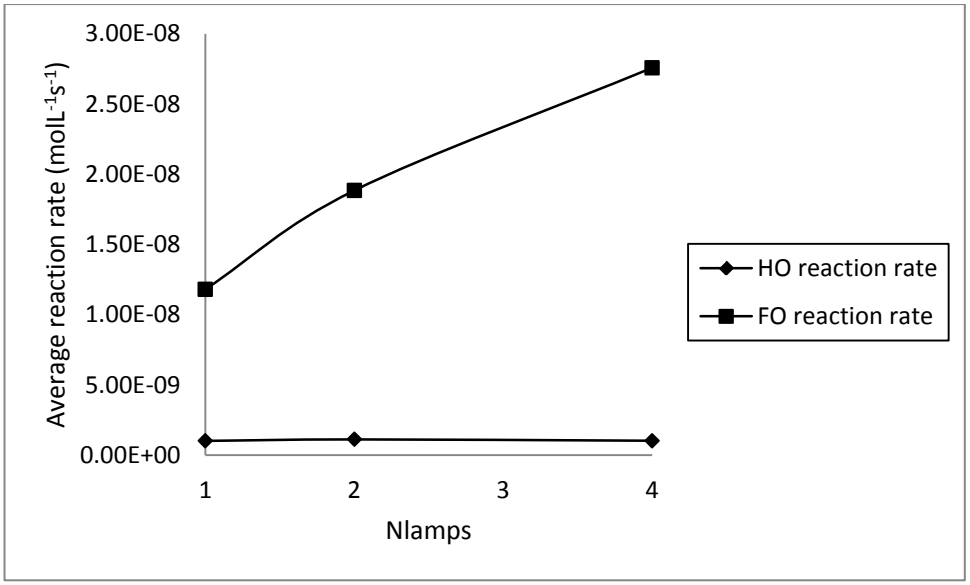

Figure 7. 12: Variation of FO and HO average reaction rate ($molL^{-1}s^{-1}$) with N_{lamps} at optimum X_{lamp}, W_{cat} = 0.028 gL^{-1}.

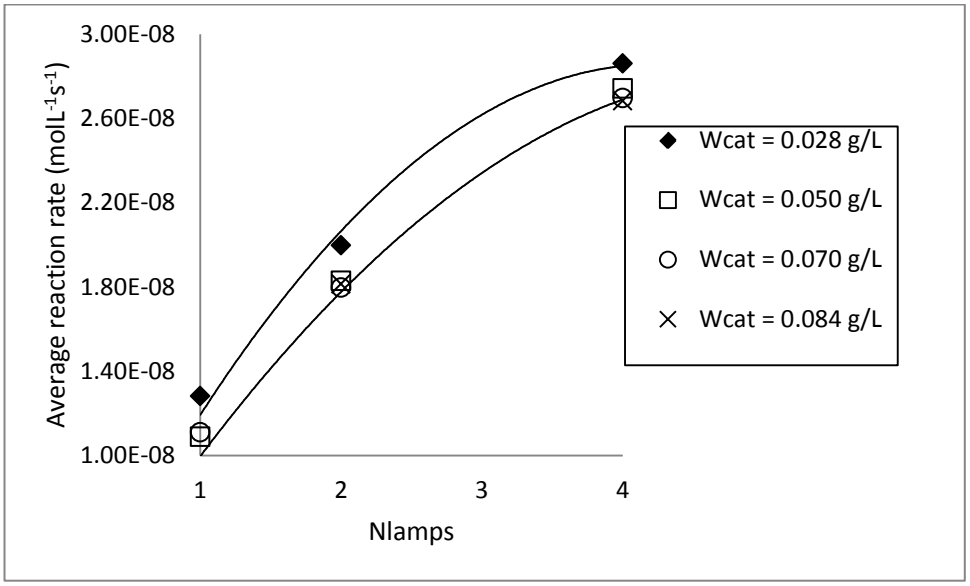

Figure 7. 13: Variation of average reaction rate ($molL^{-1}s^{-1}$) with N_{lamps} at optimum X_{lamp} and different catalyst loadings.

The change in average reaction rate with respect to N_{lamps} at all four W_{cat} investigated is shown in Figure 7. 13. The variation of the average reaction rate with N_{lamps} could be represented by the following relationship:

$$-r_p = AN_{lamps}^2 + BN_{lamps}$$

where

$A = -2 \times 10^{-9}$ mol L^{-1} s^{-1} and $B = 1 \times 10^{-8}$ mol L^{-1} s^{-1} when W_{cat} = 0.028 gL^{-1} and

$A = -1 \times 10^{-9}$ mol L^{-1} s^{-1} and $B = 1 \times 10^{-8}$ mol L^{-1} s^{-1} when W_{cat} = 0.050, 0.070 and 0.084 gL^{-1}.

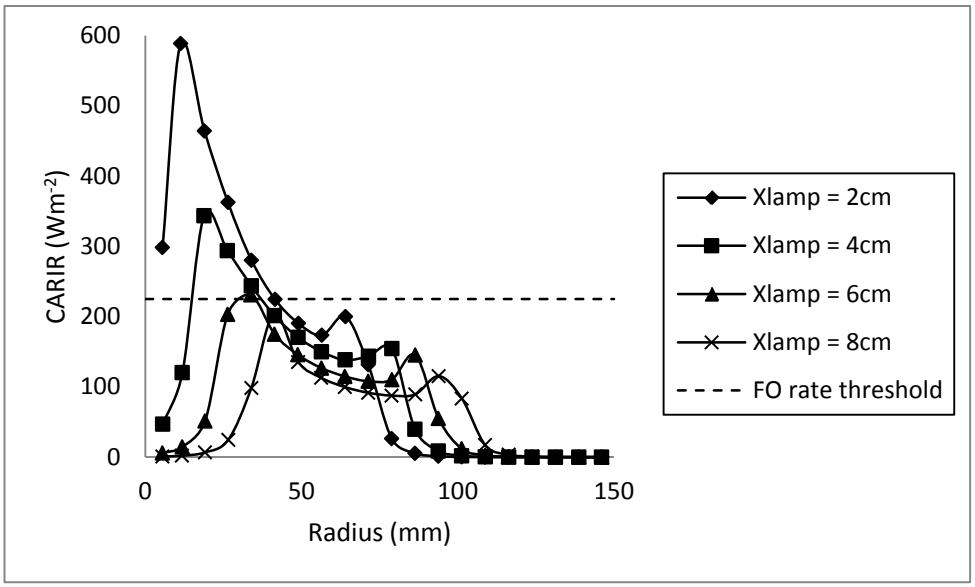

Figure 7. 14: Variation of CARIR (Wm^{-2}) with radius (mm) on mid-lamp cross sectional plane, N_{lamps} = 2 and W_{cat} = 0.084 gL^{-1}.

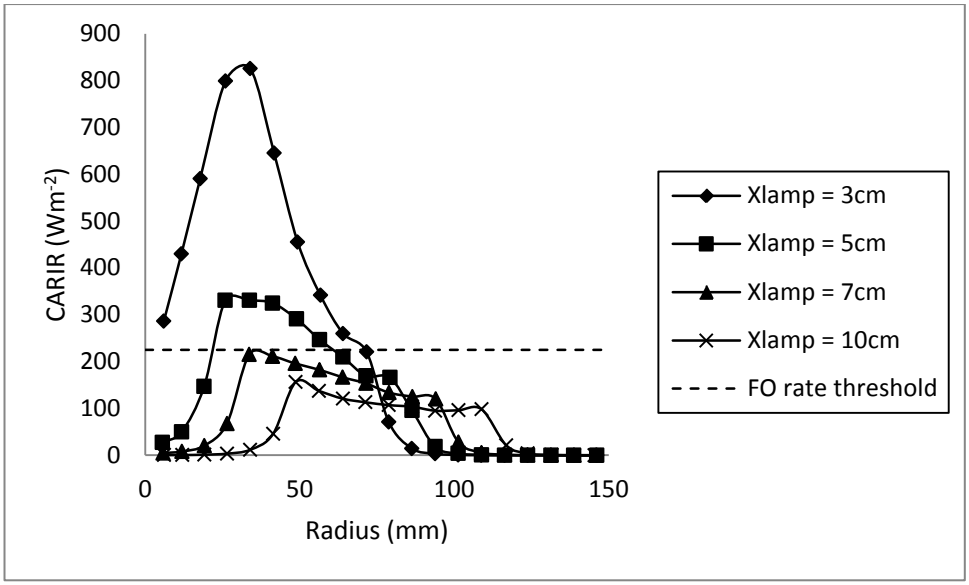

Figure 7. 15: Variation of CARIR (Wm^{-2}) with radius (mm) on mid-lamp cross sectional plane, N_{lamps} = 4 and W_{cat} = 0.084 gL^{-1}.

Figure 7. 14 presents the circumferential averaged radial incident radiation (CARIR, Wm^{-2}) along the radial axis at the cross sectional plane corresponding to the middle of the lamp in the case where N_{lamps} = 2 and W_{cat} = 0.084 gL^{-1}, for different lamp separations. The dashed horizontal line represents the threshold radiation limit at and below which FO reactions take place, i.e., 225 Wm^{-2}. The average reaction rate when X_{lamp} = 2 cm is low since the incident radiation is very high (> 225 Wm^{-2}) when the radius is less than 41 mm. This means that despite high activity (high LVREA), the high rate of electron-hole recombination entails HO reaction in the middle of the reactor. The optimum lamp separation occurs at X_{lamp} = 4 cm due to the higher rate of FO reactions (higher radiation intensity within the threshold limit of 225 Wm^{-2}) compared to X_{lamp} = 6, 8 and 10 cm (X_{lamp} = 10 cm not shown here), despite the fact that HO reactions occur within a small area of the reactor between a radius of 15 and 33 mm. At the optimum lamp separation, the merging of incident radiation contours increases the incident radiation within the threshold limit and allows for maximum FO reaction. These FO reaction contours are depicted in Figure 7. 16 showing the mid-lamp cross sectional plane for the range of W_{cat} investigated and Xlamp = 2 – 10 cm. The dark regions in the lamp vicinity represent the HO reaction regions (not quantitatively shown) due to high incident radiation (> 225 Wm^{-2}).

Figure 7. 15 presents the circumferential averaged radial incident radiation (CARIR, Wm^{-2}) along the radial axis at the cross sectional plane corresponding to the middle of the lamp in the case where N_{lamps} = 4 and W_{cat} = 0.084 gL^{-1}, for different lamp separations. Similar conclusions can be derived as with N_{lamps} = 2. Moreover, it can be seen that at the optimum X_{lamp} = 7 cm, the reaction rate is mainly FO (except at the lamps vicinity) and better distributed than when N_{lamps} = 2, explaining the higher reaction rate when N_{lamps} = 4 as compared to when N_{lamps} = 2. FO reaction contours for N_{lamps} = 4 are depicted in Figure 7. 17 showing the mid-lamp cross section for the range of W_{cat} investigated and X_{lamp} = 6 – 10 cm. The dark regions in the lamp vicinity represent the HO reaction regions (not quantitatively shown).

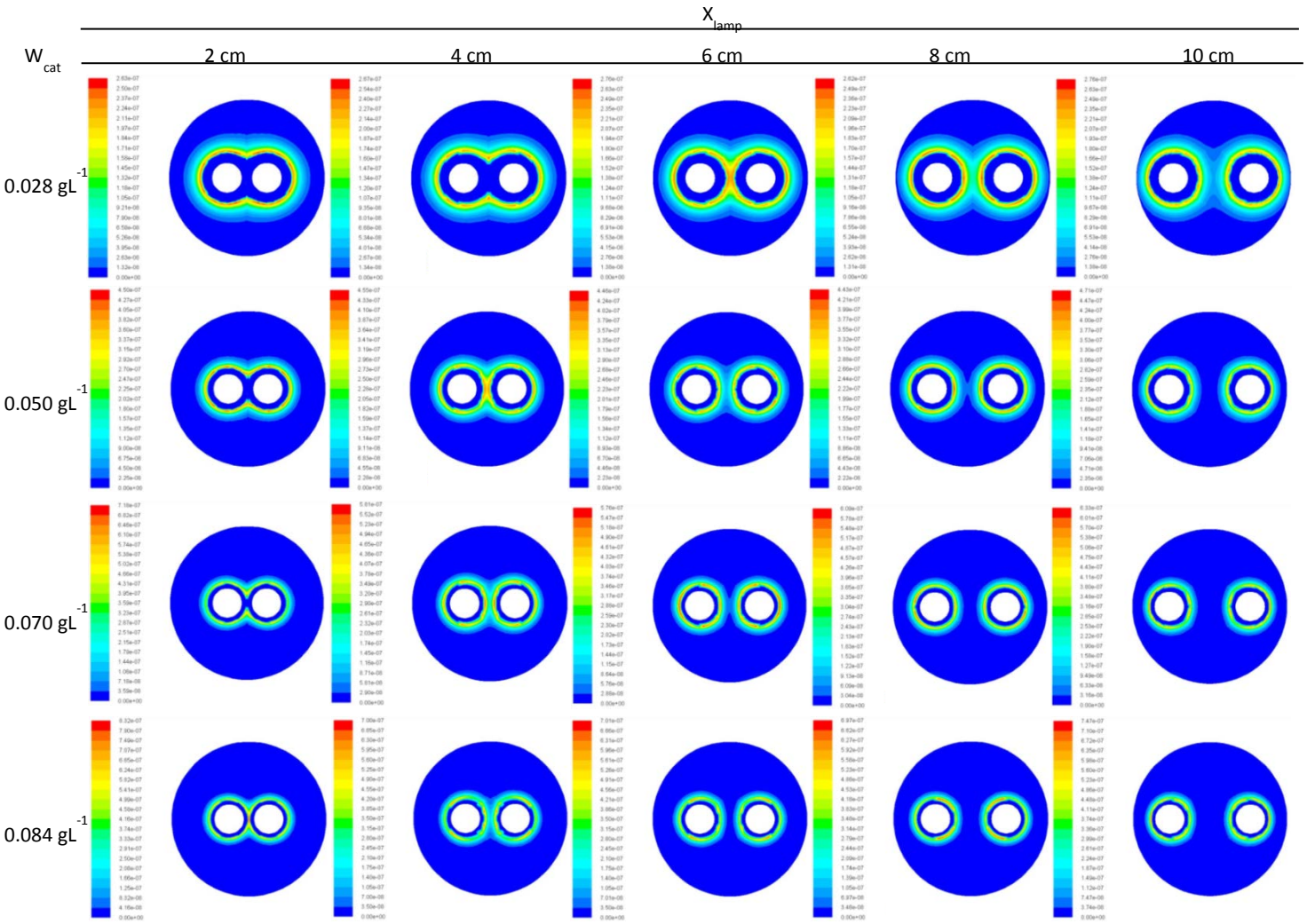

Figure 7. 16: FO reaction rate contours on mid-lamp cross sectional plane at different catalyst loadings, X_{lamp} = 2 – 10 cm and N_{lamps} = 2.

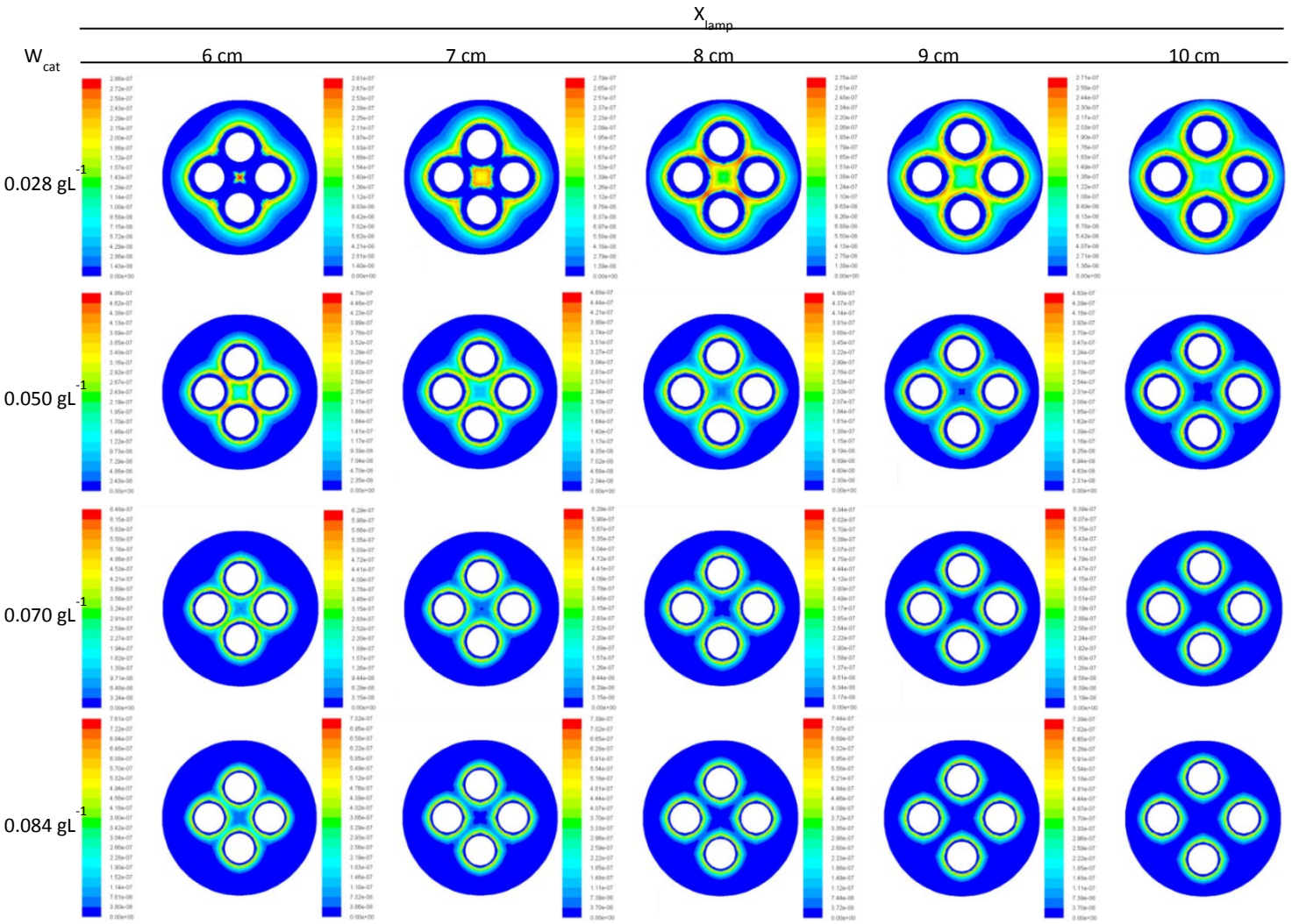

Figure 7. 17: FO reaction rate contours on mid-lamp cross sectional plane at different catalyst loadings, X_{lamp} = 6 – 10 cm and N_{lamps} = 4.

7.3 Conclusion

Using multiple lamps instead of only one powerful lamp in the middle of the reactor can significantly increase the rate of reaction within a photocatalytic reactor. Simulations showed that within the range of catalyst concentration investigated, the maximum potential increase in reaction rate was 56% and 123% when using 2 and 4 lamps respectively, as compared to using one lamp. The increase in reaction rate occurred due to the maximisation of incident radiation contours at which first order reactions take place. The optimum lamp separation was dependent on the catalyst concentration in the wastewater and decreased with increasing catalyst concentration.

Chapter 8 - Conclusions and Recommendations for Future Work

8.1 Conclusions

The treatment of greywater for reuse deserves consideration due to its large quantity produced and relatively low pollutant loading. An extensive review on the treatment of greywater in Chapter 1 presented the advantages and limitations of current treatment systems (biological, physical, chemical or natural) being employed. Hazardous xenobiotic organic compounds (XOCs) present in greywater have a recalcitrant nature towards degradation with the conventional treatment methods. On the other hand, new methods of advanced oxidation processes (AOPs) such as photocatalysis have shown promising results with respect to the complete mineralisation of recalcitrant organic compounds found in wastewater. Since photocatalysis works best at low pollutant concentration, it was deemed a viable candidate for the treatment of greywater. The type of greywater chosen in this study was real shower water that was collected from the researcher's home.

The photocatalytic treatment of real shower water was performed in a pilot scale slurry type annular reactor having a maximum capacity of 31 L and diameter of 30 cm. The temporal course of the photocatalytic degradation showed 2 stages which were: desorption of the pollutants from the catalyst surface followed by complete mineralisation to CO_2 and H_2O. A maximum of 57% TOC degradation was observed at optimum conditions (pH = 3.0, catalyst loading = 0.07 gL^{-1}, air flow rate = 1.8$Lmin^{-1}$ and slurry recirculation rate = 4.4 $Lmin^{-1}$) after 6 hours treatment time. The degradation process was slow initially due to the breaking of long-chained hydrocarbons (such as surfactants) but then became faster as smaller, simpler chains started to form.

Experiments were carried out to measure the incident radiation distribution within the reactor at typical catalyst concentrations (0.05 and 0.10 gL^{-1}). The data obtained was then modelled using CFD so as to obtain the optical parameters (absorption and scattering coefficients) of the catalyst used (Aeroxide® P25 TiO_2) throughout the experiments. It was found that a wavelength averaged scattering coefficient corresponding to that of traditional Degussa P25 TiO_2 could be used, but the

absorption coefficient was wavelength dependent. Since the UV lamps employed had a wide emission spectrum ($200 < \upsilon\ (nm) < 440$), the UV absorbable range ($\upsilon\ (nm) < 387.5$) was divided into 3 bands. The absorption coefficient for each band was determined and it was found to be higher than that of Degussa P25 TiO_2 in the UV-C range. This was expected as the Aeroxide® brand was developed to give enhanced photocatalytic activity. The high absorption capacity of the catalyst also showed that the wall emissivity had no effect on the radiation field distribution within the medium down to a catalyst loading of 0.015 gL^{-1}.

In a photocatalytic reactor with large diameter, as the one used in this research, all reaction regimes in terms of half order, transitional order and first order reactions were expected to occur (with respect to the LVREA) due to light attenuation with radial distance. With the high light intensity at the vicinity of the lamps, half order and transitional order reactions occur because of high electron rate recombination. However, further from the lamp, below a certain value of radiation intensity, the rate of reaction is first order. As a result, a general rate equation was devised to relate the rate or pollutant degradation in terms of the LVREA according to all the reaction regimes occurring within the reactor. A novel contribution of this work was to validate the devised rate equation with experimental data so as to determine to reaction regimes occurring within the reactor and explore their significance with respect to pollutant degradation.

Three dimensional hydrodynamics modelling of the slurry reactor showed the formation of recirculation zones in the reactor due to the high slurry inlet flow rate. The optical parameters formerly obtained were used to model the light distribution which in turn was used to calculate the LVREA within the reactor. The validity of the devised rate equation was tested (ignoring the transitional regime for simplicity) by modelling the average reaction rate at different catalyst loadings. It was found that using a value of 225 Wm^{-2} as the minimum incident light intensity at which half order reactions take place, a Pearson correlation of 0.88 between simulated and experimental data was obtained, indicating the model adequacy. The average volumetric reaction rate within the reactor was largely dependent upon first order reactions, having a magnitude up to 20 times that of half order reactions. This was due to the square root dependency of reaction rate with respect to LVREA in regions

of high incident radiation intensity despite the higher reaction rate constant with respect to half order reactions ($k'_h / k'_f = 2.5$).

In terms of modelling, since the Stokes number and concentration of the catalyst used were very small, the use of the kinetic theory of granular flow to model the solid phase is redundant. The assumption of a well-mixed liquid phase with average properties (i.e., uniformly distributed catalyst) becomes pertinent and thereby significantly reduces the computational time requirement for hydrodynamics simulations.

Following the validation of the rate model, predictive simulations were performed with a system of multiple lamps (2 and 4 lamps) so as to gauge the effect of using multiple lamps at different geometrical placements as opposed to one powerful lamp in the middle of the reactor. It was found that within the range of catalyst concentration investigated, the maximum potential increase in reaction rate was 56% and 123% when using 2 and 4 lamps respectively as compared to using one lamp. The increase in reaction rate occurred due to the maximisation of incident radiation contours at which first order reactions took place. Two and three dimensional simulations showed that the optimum lamp separation for maximum LVREA was 4 cm and independent of catalyst concentration in the case of 2 lamps but in the case of 4 lamps the optimum lamp separation for maximum LVREA was dependent on the catalyst concentration. However, the optimum lamp separation for maximum reaction rate did not necessarily occur at the maximum LVREA (for either 2 or 4 lamps) and was dependent on the catalyst concentration.

8.2 Recommendations

Following the findings from this research project, the following recommendations have been put forward:

8.2.1 Experiments with immobilised system

The cost for operation of the pilot scale slurry reactor was calculated to be 37 US$m^{-3} (mainly for UV lamp operation), which is too expensive to be a viable treatment method. Also need to be added the cost of catalyst separation which can be considerable given the nanometre size particles. However, it is possible to operate

the reactor with solar light and immobilised catalyst. This could drastically reduce the operational cost of a large-scale photoreactor for shower water purification. Since the weather in Perth, WA is appropriate, it is therefore recommended to perform experiments using an immobilised catalyst system such as the thin-film loop or inclined plate reactor. However, possible extra investment might be required for a motorised system that will direct the reactor towards maximum sunlight throughout the day.

8.2.2 Improvements to slurry reactor design

Regarding the reactor used in this research, the main improvement that can be brought is the design of the air distributor. In this research, air was supplied from a 10 cm distributor found in the middle of the reactor. As a result, air bubbles were not distributed uniformly and could not be used efficiently for catalyst suspension. Hence a high slurry recirculation rate was employed for this purpose. This high recirculation rate brought about the formation of recirculation zones in the reactor. If the air distributor is redesigned properly, the air bubbles could be used for catalyst suspension and a low recirculation rate can then be employed. This will induce plug flow in the reactor, a lower residence time and therefore possibly enhanced reaction rates.

Furthermore, approximately half of the reactor length was not illuminated (lamp length = 20 cm, water level = 43 cm), meaning no reaction took place in more than half of the reactor space. Future slurry reactor designs should take this into consideration and make the water level length coincide with the lamp length as much as possible.

8.2.3 Experiments with multiple lamps

Unfortunately, the lamps could not be operated at reduced powers so that experiments involving multiple lamps could not be executed. According to the lamp manufacturer, UV arc lamps operate at a certain value of around $30 Wcm^{-1}$ of the lamp. This meant that to operate 2 lamps at a total power of 560W (the initial power of one 20 cm lamp), 10 cm or 5 cm lamps had to be used in the case of 2 and 4 lamps respectively, which would defeat the purpose of comparison with results obtained with experiments using 1 lamp. This issue could not be resolved by using lamps of

slightly smaller diameter. However, the lamps could be customised to suit multiple lamps design.

8.2.4 Catalyst concentration

Due to the large absorption capacity of the catalyst used in this research, it is recommended to use low catalyst loadings (less than 0.10 gL^{-1} of Aeroxide® P25 TiO_2) for future work involving large diameter reactors.

8.2.5 Determination of reaction regimes for modelling

In the rate modelling part of this work, the transitional regime was ignored and only half and first order reactions were assumed to occur in the reactor. The threshold radiation intensity below which first order reaction took place was estimated to be 225 Wm^{-2}. Since this threshold depends on factors such as pollutant type, catalyst type and lamp power, preliminary work to determine the threshold value need to be carried out. This can be done with a bench scale thin film immobilised type reactor. By varying the irradiation intensity on the surface of the immobilised TiO_2 film (by moving the lamps towards or away from the catalyst surface) and measuring the pollutant degradation with time, the range of radiation intensities at which each reaction regime takes place can be determined.

References

1992. US EPA. Office of Wastewater Enforcement and Compliance, Washington DC.

2004. ACT Greywater Use: Guidelines for residential properties in Canberra. Available at www.actpla.act.gov.au.

2008. Information Sheet: Greywater Reuse and Recycling available at www.watercorporation.com.au/waterforever.

2011. Inorganic materials for catalyst innovation . AEROSIL, AEROXIDE and SIPERNAT metal oxides and silica based materials industry information 2242. Evonik Industries.

Abegglen, C., Ospelt, M., Siegrist, H., 2008. Biological nutrient removal in a small-scale MBR treating household wastewater. Water research 42, 338-346.

Abu Ghunmi, L., Zeeman, G., Fayyad, M., Lier, J.B., 2010. Grey water treatment in a series anaerobic-Aerobic system for irrigation. Bioresource technology 101, 41-50.

Agustina, T.E., Ang, H.M., Pareek, V.K., 2008. Treatment of winery wastewater using a photocatalytic/photolytic reactor. Chem. Eng. J. 135, 151-156.

Akita, K., Yoshida, F., 1974. Bubble Size, Interfacial Area, and Liquid-Phase Mass Transfer Coefficient in Bubble Columns. Industrial & Engineering Chemistry Process Design and Development 13, 84-91.

Al-Hamaiedeh, H., Bino, M., 2010. Effect of treated grey water reuse in irrigation on soil and plants. Desalination 256, 115-119.

Al-Jayyousi, O.R., 2003. Greywater reuse: towards sustainable water management. Desalination 156, 181-192.

Al-Sayyed, G., D'Oliveira, J.C., Pichat, P., 1991. Semiconductor-sensitized photodegradation of 4-chlorophenol in water. Journal of Photochemistry and Photobiology A: Chemistry 58, 99-114.

Alexiadis, A., 2006. 2-D radiation field in photocatalytic channels of square, rectangular, equilateral triangular and isosceles triangular sections. Chemical Engineering Science 61, 516-525.

Alexiadis, A., Baldi, G., Mazzarino, I., 2001. Modelling of a photocatalytic reactor with a fixed bed of supported catalyst. Catalysis Today 66, 467-474.

Alfano, O.M., Cabrera, M.I., Cassano, A.E., 1997. Photocatalytic reactions involving hydroxyl radical attack. Journal of Catalysis 172, 370-379.

Alfano, O.M., Negro, A.C., Cabrera, M.I., Cassano, A.E., 1995. Scattering effects produced by inert particles in photochemical reactors. 1. Model and

experimental verification. Industrial & engineering chemistry research 34, 488-499.

Alfano, O.M., Romero, R.L., Cassano, A.E., 1986a. Radiation field modelling in photoreactors--I. homogeneous media. Chem. Eng. Sci. 41, 421-444.

Alfano, O.M., Romero, R.L., Cassano, A.E., 1986b. Radiation field modelling in photoreactors--II. Heterogeneous media. Chem. Eng. Sci. 41, 1137-1153.

Andreadakis, A., Gavalaki, E., Mamais, D., Tzimas, A., 2001. Wastewater reuse criteria in Greece, pp. 3-6.

Andreozzi, R., Caprio, V., Insola, A., Marotta, R., 1999. Advanced oxidation processes (AOP) for water purification and recovery. Catal. Today 53, 51-59.

Aonghusa, C.N., Gray, N.F., 2002. Laundry detergents as a source of heavy metals in Irish domestic wastewater.

Asano, T., 2002. Water from(waste) water- the dependable water resource. Water Sci. Technol. 45, 24.

Asano, T., Maeda, M., Takaki, M., 1996. Wastewater reclamation and reuse in Japan: overview and implementation examples. Water Science and Technology 34, 219-226.

Atasoy, E., Murat, S., Baban, A., Tiris, M., 2007. Membrane bioreactor (MBR) treatment of segregated household wastewater for reuse. CLEAN–Soil, Air, Water 35, 465-472.

Balcioglu, I.A., Arslan, I., 1998. Application of photocatalytic oxidation treatment to pretreated and raw effluents from the Kraft bleaching process and textile industry. Environ. Pollut. 103, 261-268.

Bauer, R., Waldner, G., Fallmann, H., Hager, S., Klare, M., Krutzler, T., Malato, S., Maletzky, P., 1999. The photo-fenton reaction and the TiO2/UV process for waste water treatment- novel developments. Catal. Today 53, 131-144.

Belgiorno, V., Rizzo, L., Fatta, D., Della Rocca, C., Lofrano, G., Nikolaou, A., Naddeo, V., Meric, S., 2007. Review on endocrine disrupting-emerging compounds in urban wastewater: occurrence and removal by photocatalysis and ultrasonic irradiation for wastewater reuse. Desalination 215, 166-176.

Bingley, E.B., 1996. Greywater reuse proposal in relation to the palmyra project. Desalination 106, 371-375.

Brandi, R.J., Alfano, O.M., Cassano, A.E., 2000. Evaluation of radiation absorption in slurry photocatalytic reactors. 1. Assessment of methods in use and new proposal. Environmental science & technology 34, 2623-2630.

Buwa, V.V., Deo, D.S., Ranade, V.V., 2006. Eulerian-Lagrangian simulations of unsteady gas-liquid flows in bubble columns. International Journal of Multiphase Flow 32, 864-885.

Cabrera, M.I., Alfano, O.M., Cassano, A.E., 1996. Absorption and Scattering Coefficients of Titanium Dioxide Particulate Suspensions in Water. The Journal of Physical Chemistry 100, 20043-20050.

Cassano, A.E., Alfano, O.M., 2000. Reaction engineering of suspended solid heterogeneous photocatalytic reactors. Catalysis Today 58, 167-197.

Castrillon, S.R.V., de Lasa, H.I., 2007. Performance evaluation of photocatalytic reactors for air purification using computational fluid dynamics (CFD). Industrial & engineering chemistry research 46, 5867-5880.

Chaillou, K., Gérente, C., Andrès, Y., Wolbert, D., 2011. Bathroom Greywater Characterization and Potential Treatments for Reuse. Water, Air, & Soil Pollution 215, 31-42.

Chanan, A., Kandasamy, J., Vigneswaran, S., Sharma, D., 2009. A gradualist approach to address Australia's urban water challenge. Desalination 249, 1012-1016.

Charles, G., Roques-Carmes, T., Becheikh, N., Falk, L., Commenge, J.-M., Corbel, S., 2011. Determination of kinetic constants of a photocatalytic reaction in micro-channel reactors in the presence of mass-transfer limitation and axial dispersion. Journal of Photochemistry and Photobiology A: Chemistry 223, 202-211.

Chen, D., 2001. Removal of toxic metal ions from wastewater by semiconductor photocatalysis. Chemical Engineering Science 56, 1561-1570.

Chen, D., Ray, A.K., 1998. Photodegradation kinetics of 4-nitrophenol in TiO2 suspension. Water research 32, 3223-3234.

Chen, J., Deng, B., Kim, C.N., 2011. Computational fluid dynamics (CFD) modeling of UV disinfection in a closed-conduit reactor. Chemical Engineering Science 66, 4983-4990.

Chen, P., Sanyal, J., Dudukovic, M.P., 2004. CFD modeling of bubble columns flows: implementation of population balance. Chemical Engineering Science 59, 5201-5207.

Chen, P., Sanyal, J., Dudukovic, M.P., 2005. Numerical simulation of bubble columns flows: effect of different breakup and coalescence closures. Chemical Engineering Science 60, 1085-1101.

Chin, W.H., Roddick, F.A., Harris, J.L., 2009. Greywater treatment by UVC/H2O2. Water research 43, 3940-3947.

Chong, M.N., Jin, B., Chow, C.W.K., Saint, C., 2010. Recent developments in photocatalytic water treatment technology: A review. Water Res. 44, 2997-3027.

Chong, S., Wang, S., Tade, M., Ang, H.M., Pareek, V., 2011. Simulations of photodegradation of toluene and formaldehyde in a monolith reactor using computational fluid dynamics. AIChE journal 57, 724-734.

Christova-Boal, D., Eden, R.E., McFarlane, S., 1996. An investigation into greywater reuse for urban residential properties. Desalination 106, 391-397.

Ciabattia, I., Cesaro, F., Faralli, L., Fatarella, E., Tognotti, F., 2009. Demonstration of a treatment system for purification and reuse of laundry wastewater. Desalination 245, 451-459.

Cornelissen, J.T., Taghipour, F., Escudie, R., Ellis, N., Grace, J.R., 2007. CFD modelling of a liquid-solid fluidized bed. Chemical Engineering Science 62, 6334-6348.

Coroneo, M., Mazzei, L., Lettieri, P., Paglianti, A., Montante, G., 2011. CFD prediction of segregating fluidized bidisperse mixtures of particles differing in size and density in gas-solid fluidized beds. Chemical Engineering Science 66, 2317-2327.

Cosgrove, W.J., Rijsberman, F.R., 2000. Challenge for the 21st century: making water everybody's business. Sustainable Development International (2), 149-156.

Cuevas, S.A., Arancibia-Bulnes, C.A., Serrano, B., 2007. Radiation field in an annular photocatalytic reactor by the P1 approximation. International Journal of Chemical Reactor Engineering 5, 58.

D'Oliveira, J.C., Al-Sayyed, G., Pichat, P., 1990. Photodegradation of 2- and 3-chlorophenol in titanium dioxide aqueous suspensions. Environmental science & technology 24, 990-996.

Dalahmeh, S.S., Assayed, M., Suleiman, W.T., 2009. Themes of stakeholder participation in greywater management in rural communities in Jordan. Desalination 243, 159-169.

Dallas, S., Scheffe, B., Ho, G., 2004. Reedbeds for greywater treatment--case study in Santa Elena-Monteverde, Costa Rica, Central America. Ecological Engineering 23, 55-61.

Danion, A., Disdier, J., Guillard, C., Abdelmalek, F., Jaffrezic-Renault, N., 2004. Characterization and study of a single-TiO2-coated optical fiber reactor. Applied Catalysis B: Environmental 52, 213-223.

De Fraiture, C., Wichelns, D., 2010. Satisfying future water demands for agriculture. Agricultural Water Management 97, 502-511.

Deckwer, W.D., Field, R.W., 1992. Bubble column reactors. Wiley.

Deen, N.G., Solberg, T., Hjertager, B.H., 2001. Large eddy simulation of the Gas-Liquid flow in a square cross-sectioned bubble column. Chemical Engineering Science 56, 6341-6349.

Delgado, J.M.P.Q., 2007. Molecular Diffusion Coefficients of Organic Compounds in Water at Different Temperatures. Journal of Phase Equilibria and Diffusion 28, 427-432.

Denny, F., Scott, J., Pareek, V., Ding Peng, G., Amal, R., 2009. CFD modelling for a TiO2-coated glass-bead photoreactor irradiated by optical fibres: Photocatalytic degradation of oxalic acid. Chemical Engineering Science 64, 1695-1706.

Denny, F., Scott, J., Pareek, V., Peng, G.-D., Amal, R., 2010a. Computational fluid dynamics modelling and optimal configuring of a channelled optical fibre photoreactor. Chemical Engineering Science 65, 5029-5040.

Denny, F., Scott, J., Peng, G.D., Amal, R., 2010b. Channelled optical fibre photoreactor for improved air quality control. Chemical Engineering Science 65, 882-889.

Dhotre, M.T., Niceno, B., Smith, B.L., 2008. Large eddy simulation of a bubble column using dynamic sub-grid scale model. Chemical Engineering Journal 136, 337-348.

Dijkstra, M.F.J., Koerts, E.C.B., Beenackers, A., Wesselingh, J.A., 2003. Performance of immobilized photocatalytic reactors in continuous mode. AIChE journal 49, 734-744.

Dixon, A., Butler, D., Fewkes, A., Robinson, M., 2000. Measurement and modelling of quality changes in stored untreated grey water. Urban Water 1, 293-306.

Domenech, L., Saurí, D., 2010. Socio-technical transitions in water scarcity contexts: Public acceptance of greywater reuse technologies in the Metropolitan Area of Barcelona. Resources, Conservation and Recycling.

Donner, E., Eriksson, E., Scholes, L., Revitt, M., 2008. Priority pollutant behaviour in treatment and reuse systems for household wastewater. ScorePP.

Du, W., Bao, X., Xu, J., Wei, W., 2006. Computational fluid dynamics (CFD) modeling of spouted bed: Assessment of drag coefficient correlations. Chemical Engineering Science 61, 1401-1420.

Duran, J.E., Mohseni, M., Taghipour, F., 2010a. Modeling of annular reactors with surface reaction using computational fluid dynamics (CFD). Chemical Engineering Science 65, 1201-1211.

Duran, J.E., Mohseni, M., Taghipour, F., 2011. Computational fluid dynamics modeling of immobilized photocatalytic reactors for water treatment. AIChE journal.

Duran, J.E., Taghipour, F., Mohseni, M., 2010b. Irradiance modeling in annular photoreactors using the finite-volume method. Journal of Photochemistry and Photobiology A: Chemistry 215, 81-89.

Dutta, P.K., Ray, A.K., 2004. Experimental investigation of Taylor vortex photocatalytic reactor for water purification. Chemical Engineering Science 59, 5249-5259.

Ekambara, K., Dhotre, M.T., Joshi, J.B., 2005. CFD simulations of bubble column reactors: 1D, 2D and 3D approach. Chemical Engineering Science 60, 6733-6746.

El Hajjouji, H., Barje, F., Pinelli, E., Bailly, J.R., Richard, C., Winterton, P., Revel, J.C., Hafidi, M., 2008. Photochemical UV/TiO2 treatment of olive mill wastewater (OMW). Bioresour. Technol. 99, 7264-7269.

Elena Diaz, M., Montes, F.J., Galan, M.A., 2009. Influence of the lift force closures on the numerical simulation of bubble plumes in a rectangular bubble column. Chemical Engineering Science 64, 930-944.

Elmitwalli, T.A., Otterpohl, R., 2007. Anaerobic biodegradability and treatment of grey water in upflow anaerobic sludge blanket (UASB) reactor. Water research 41, 1379-1387.

Elyasi, S., Taghipour, F., 2010a. General method of simulating radiation fields using measured boundary values. Chemical Engineering Science 65, 5573-5581.

Elyasi, S., Taghipour, F., 2010b. Simulation of UV Photoreactor for Degradation of Chemical Contaminants: Model Development and Evaluation. Environmental science & technology 44, 2056-2063.

Eng, Y.Y., Sharma, V.K., Ray, A.K., 2010. Photocatalytic degradation of nonionic surfactant, Brij 35 in aqueous TiO2 suspensions. Chemosphere 79, 205-209.

Eriksson, E., Andersen, H.R., Madsen, T.S., Ledin, A., 2009. Greywater pollution variability and loadings. Ecological Engineering 35, 661-669.

Eriksson, E., Auffarth, K., Henze, M., Ledin, A., 2002. Characteristics of grey wastewater. Urban Water 4, 85-104.

Esmaili, E., Mahinpey, N., 2011. Adjustment of drag coefficient correlations in three dimensional CFD simulation of gas-solid bubbling fluidized bed. Advances in Engineering Software 42, 375-386.

Esteban Duran, J., Taghipour, F., Mohseni, M., 2009. CFD modeling of mass transfer in annular reactors. International Journal of Heat and Mass Transfer 52, 5390-5401.

Esterkin, C.R., Negro, A.C., Alfano, O.M., Cassano, A.E., 2002. Radiation field inside a reactor of glass-fiber meshes coated with TiO2. AIChE journal 48, 832-845.

Esterkin, C.R., Negro, A.C., Alfano, O.M., Cassano, A.E., 2005. Air pollution remediation in a fixed bed photocatalytic reactor coated with TiO2. AIChE journal 51, 2298-2310.

Farrelly, M.a.D., C., 2009. Demonstration Projects: Case Studies from Melbourne, Australia. Available at www.urbanwatergovernance.com.

Farzpourmachiani, A., Shams, M., Shadaram, A., Azidehak, F., 2011. Eulerian-Lagrangian 3-D simulations of unsteady two-phase gas-liquid flow in a rectangular column by considering bubble interactions. International Journal of Non-Linear Mechanics 46, 1049-1056.

Fatta-Kassinos, D., Kalavrouziotis, I.K., Koukoulakis, P.H., Vasquez, M.I., 2010. The risks associated with wastewater reuse and xenobiotics in the agroecological environment. Science of the Total Environment.

Fiveland, W.A., 1984. Discrete-ordinates solutions of the radiative transport equation for rectangular enclosures. Journal of Heat Transfer 106, 699.

Fluent, M., 2005. Version 6.2. 16, Fluent. Inc.

Foerster, S.F., Louge, M.Y., Chang, H., Allia, K., 1994. Measurements of the collision properties of small spheres. Physics of Fluids 6, 1108.

Fotiadis, C., Xekoukoulotakis, N.P., Mantzavinos, D., 2007. Photocatalytic treatment of wastewater from cottonseed processing: Effect of operating conditions, aerobic biodegradability and ecotoxicity. Catal. Today 124, 247-253.

Friedler, E., Gilboa, Y., 2010. Performance of UV disinfection and the microbial quality of greywater effluent along a reuse system for toilet flushing. Science of the Total Environment 408, 2109-2117.

Friedler, E., Hadari, M., 2006. Economic feasibility of on-site greywater reuse in multi-storey buildings. Desalination 190, 221-234.

Friedler, E., Katz, I., Dosoretz, C.G., 2008. Chlorination and coagulation as pretreatments for greywater desalination. Desalination 222, 38-49.

Friedler, E., Kovalio, R., Galil, N.I., Mathew, K., Ho, G., 2005. On-site greywater treatment and reuse in multi-storey buildings. IWA Publishing, Alliance House 12 Caxton Street London SW 1 H 0 QS UK, pp. 187-194.

Friedler, E., Lahav, O., Jizhaki, H., Lahav, T., 2006. Study of urban population attitudes towards various wastewater reuse options: Israel as a case study. Journal of environmental management 81, 360-370.

Fujishima, A., Zhang, X., 2006. Titanium dioxide photocatalysis: present situation and future approaches. C.R. Chim. 9, 750-760.

Gamwo, I.K., Halow, J.S., Gidaspow, D., Mostofi, R., 2003. CFD models for methanol synthesis three-phase reactors: reactor optimization. Chemical Engineering Journal 93, 103-112.

Garland, J.L., Levine, L.H., Yorio, N.C., Hummerick, M.E., 2004. Response of graywater recycling systems based on hydroponic plant growth to three classes of surfactants. Water research 38, 1952-1962.

Gaya, U.I., Abdullah, A.H., 2008. Heterogeneous photocatalytic degradation of organic contaminants over titanium dioxide: a review of fundamentals, progress and problems. Journal of Photochemistry and Photobiology C: Photochemistry Reviews 9, 1-12.

Gidaspow, D., Bezburuah, R., Ding, J., 1991. Hydrodynamics of circulating fluidized beds: Kinetic theory approach.

Gilboa, Y., Friedler, E., 2008. UV disinfection of RBC-treated light greywater effluent: Kinetics, survival and regrowth of selected microorganisms. Water research 42, 1043-1050.

Goddard, M., 2006. Urban greywater reuse at the D'LUX development. Desalination 188, 135-140.

Godfrey, S., Labhasetwar, P., Wate, S., 2009. Greywater reuse in residential schools in Madhya Pradesh, India--A case study of cost-benefit analysis. Resources, Conservation and Recycling 53, 287-293.

Gogate, P.R., Pandit, A.B., 2004. A review of imperative technologies for wastewater treatment I: oxidation technologies at ambient conditions. Adv. Environ. Res. 8, 501-551.

Goldschmidt, M.J.V., Kuipers, J.A.M., Van Swaaij, W.P.M., 2001. Hydrodynamic modelling of dense gas-fluidised beds using the kinetic theory of granular flow: effect of coefficient of restitution on bed dynamics. Chemical Engineering Science 56, 571-578.

Gondret, P., Lance, M., Petit, L., 2002. Bouncing motion of spherical particles in fluids. Physics of Fluids 14, 643-652.

Gross, A., Azulai, N., Oron, G., Ronen, Z., Arnold, M., Nejidat, A., 2005. Environmental impact and health risks associated with greywater irrigation: a case study. IWA Publishing, Alliance House 12 Caxton Street London SW 1 H 0 QS UK, pp. 16-169.

Gross, A., Kaplan, D., Baker, K., 2007a. Removal of chemical and microbiological contaminants from domestic greywater using a recycled vertical flow bioreactor (RVFB). Ecological Engineering 31, 107-114.

Gross, A., Shmueli, O., Ronen, Z., Raveh, E., 2007b. Recycled vertical flow constructed wetland (RVFCW)--a novel method of recycling greywater for irrigation in small communities and households. Chemosphere 66, 916-923.

Gross, A., Wiel-Shafran, A., Bondarenko, N., Ronen, Z., 2008. Reliability of small scale greywater treatment systems and the impact of its effluent on soil properties. International Journal of Environmental Studies 65, 41-50.

Gual, M., Moi, A., March, J.G., 2008. Monitoring of an indoor pilot plant for osmosis rejection and greywater reuse to flush toilets in a hotel. Desalination 219, 81-88.

Gulyas, H., 2007. Greywater Reuse: Concepts, Benefits, Risks and Treatment Technologies.

Gulyas, H., Choromanski, P., Furmanska, M., Muelling, N., Otterpohl, R., 2007a. Photocatalytic oxidation of biologically treated greywater in the presence of powdered activated carbon.

Gulyas, H., Reich, M., Otterpohl, R., 2007b. Qualitative non-target screening of trace organics in greywater treated in vertical-flow constructed wetlands.

Halalsheh, M., Dalahmeh, S., Sayed, M., Suleiman, W., Shareef, M., Mansour, M., Safi, M., 2008. Grey water characteristics and treatment options for rural areas in Jordan. Bioresource technology 99, 6635-6641.

Hanjra, M.A., Qureshi, M.E., 2010. Global water crisis and future food security in an era of climate change. Food Policy 35, 365-377.

Hernández Leal, L., Soeter, A.M., Kools, S.A.E., Kraak, M.H.S., Parsons, J.R., Temmink, H., Zeeman, G., Buisman, C.J.N., 2012. Ecotoxicological assessment of grey water treatment systems with Daphnia magna and Chironomus riparius. Water research 46, 1038-1044.

Hernández Leal, L., Temmink, H., Zeeman, G., Buisman, C.J.N., 2010a. Bioflocculation of grey water for improved energy recovery within decentralized sanitation concepts. Bioresource technology.

Hernández Leal, L., Temmink, H., Zeeman, G., Buisman, C.J.N., 2010b. Comparison of Three Systems for Biological Greywater Treatment. Water 2, 155-169.

Hernández Leal, L., Temmink, H., Zeeman, G., Buisman, C.J.N., 2011. Characterization and anaerobic biodegradability of grey water. Desalination.

Herrmann, J.M., 1999. Heterogeneous photocatalysis: fundamentals and applications to the removal of various types of aqueous pollutants. Catalysis Today 53, 115-129.

Hidaka, H., Graatzel, M., Pelizzetti, E., Serpone, N., 1986. Photodegradation of surfactants II: Degradation of sodium dodecylbenzene sulphonate catalysed by titanium dioxide particles. J. Photochem. 35, 219-230.

Hidaka, H., Ihara, K., Fujita, Y., Yamada, S., Pelizzetti, E., Serpone, N., 1988. Photodegradation of surfactants IV: Photodegradation of non-ionic surfactants

in aqueous titanium dioxide suspensions. J. Photochem. Photobiol., A 42, 375-381.

Hidaka, H., Oyama, T., Horiuchi, T., Koike, T., Serpone, N., Photo-induced oxidative degradation of mixed anionic/cationic surfactant systems in aqueous dispersions A detailed study of the DBS/HTAB system. Appl. Catal., B.

Hidaka, H., Zhao, J., 1992. Photodegradation of surfactants catalyzed by a TiO2 semiconductor. Colloids Surf., A 67, 165-182.

Hills, S., Birks, R., McKenzie, B., 2002. The Millennium Dome" Watercycle" experiment: to evaluate water efficiency and customer perception at a recycling scheme for 6 million visitors. Water Science & Technology 46, 233-240.

Himmelblau, D.M., Riggs, J.B., 2004. Basic Principles and Calculations in Chemical Engineering. Prentice Hall PTR.

Hossain, M.M., Raupp, G.B., Hay, S.O., Obee, T.N., 1999. Three dimensional developing flow model for photocatalytic monolith reactors. AIChE journal 45, 1309-1321.

Howell, J.R., 1998. The Monte Carlo method in radiative heat transfer. TRANSACTIONS-AMERICAN SOCIETY OF MECHANICAL ENGINEERS JOURNAL OF HEAT TRANSFER 120, 547-560.

Huang, Q., Liu, T., Yang, J., Yao, L., Gao, L., 2011. Evaluation of radiative transfer using the finite volume method in cylindrical photoreactors. Chemical Engineering Science 66, 3930-3940.

Huelgas, A., Funamizu, N., 2010. Flat-plate submerged membrane bioreactor for the treatment of higher-load graywater. Desalination 250, 162-166.

Hulme, I., Clavelle, E., van der Lee, L., Kantzas, A., 2005. CFD modeling and validation of bubble properties for a bubbling fluidized bed. Industrial & engineering chemistry research 44, 4254-4266.

Hussainova, I., Kubarsepp, J., Shcheglov, I., 1999. Investigation of impact of solid particles against hardmetal and cermet targets. Tribology international 32, 337-344.

Imoberdorf, G.E., Cassano, A.E., Irazoqui, H.A., Alfano, O.M., 2007. Simulation of a multi-annular photocatalytic reactor for degradation of perchloroethylene in air: Parametric analysis of radiative energy efficiencies. Chemical Engineering Science 62, 1138-1154.

Imoberdorf, G.E., Taghipour, F., Keshmiri, M., Mohseni, M., 2008. Predictive radiation field modeling for fluidized bed photocatalytic reactors. Chemical Engineering Science 63, 4228-4238.

Imoberdorf, G.E., Vella, G., Sclafani, A., Rizzuti, L., Alfano, O.M., Cassano, A.E., 2010. Radiation model of a TiO2 coated, quartz wool, packed bed photocatalytic reactor. AIChE journal 56, 1030-1044.

Imre, B., Rabsamen, S., Springman, S.M., 2008. A coefficient of restitution of rock materials. Computers & Geosciences 34, 339-350.

Incropera, F.P., 2009. Fundamentals Of Heat And Mass Transfer, 5Th Ed. Wiley India Pvt. Ltd.

Itayama, T., Kiji, M., Suetsugu, A., Tanaka, N., Saito, T., Iwami, N., Mizuochi, M., Inamori, Y., 2006. On site experiments of the slanted soil treatment systems for domestic gray water. Water science and technology: a journal of the International Association on Water Pollution Research 53, 193.

Jacobs, H.E., Van Staden, S., 2008. DIRECT ON-SITE GREY WATER REUSE–AN ILLICIT OR ILLUSTRIOUS OPTION?

Jakobsen, H.A., Lindborg, H., Dorao, C.A., 2005. Modeling of bubble column reactors: progress and limitations. Industrial & engineering chemistry research 44, 5107-5151.

Jarandehei, A., De Visscher, A., 2009. Three dimensional CFD model for a flat plate photocatalytic reactor: Degradation of TCE in a serpentine flow field. AIChE journal 55, 312-320.

Jefferson, B., Burgess, J.E., Pichon, A., Harkness, J., Judd, S.J., 2001. Nutrient addition to enhance biological treatment of greywater. Water research 35, 2702-2710.

Jefferson, B., Laine, A., Parsons, S., Stephenson, T., Judd, S., 2000. Technologies for domestic wastewater recycling. Urban Water 1, 285-292.

Jenkins, D., 1998. The effect of reformulation of household powder laundry detergents on their contribution to heavy metals levels in wastewater. Water environment research, 980-983.

Jin, S., Linden, K.G., Ducoste, J., Liu, D., 2005. Impact of lamp shadowing and reflection on the fluence rate distribution in a multiple low-pressure UV lamp array. Water research 39, 2711-2721.

Joseph, G.G., Zenit, R., Hunt, M.L., Rosenwinkel, A.M., 2001. Particle-wall collisions in a viscous fluid. Journal of fluid mechanics 433, 329-346.

Kim, J., Song, I., Oh, H., Jong, J., Park, J., Choung, Y., 2009. A laboratory-scale graywater treatment system based on a membrane filtration and oxidation process--characteristics of graywater from a residential complex. Desalination 238, 347-357.

Kim, R.H., Lee, S., Jeong, J., Lee, J.H., Kim, Y.K., 2007. Reuse of greywater and rainwater using fiber filter media and metal membrane. Desalination 202, 326-332.

Kivaisi, A.K., 2001. The potential for constructed wetlands for wastewater treatment and reuse in developing countries: a review. Ecological Engineering 16, 545-560.

Kraume, M., Scheumann, R., Baban, A., El Hamouri, B., 2010. Performance of a compact submerged membrane sequencing batch reactor (SM-SBR) for greywater treatment. Desalination 250, 1011-1013.

Krishna, R., Van Baten, J.M., Urseanu, M.I., 2000. Three-phase Eulerian simulations of bubble column reactors operating in the churn-turbulent regime: a scale up strategy. Chemical Engineering Science 55, 3275-3286.

Krozer, Y., Hophmayer-Tokich, S., Van Meerendonk, H., Tijsma, S., Vos, E., 2010. Innovations in the water chain-experiences in The Netherlands. Journal of Cleaner Production 18, 439-446.

Kubba, S., 2009. LEED Practices, Certification, and Accreditation Handbook. Butterworth-Heinemann/Elsevier.

Lai, K.Y., 2005. Liquid detergents. Taylor & Francis.

Lazarova, V., Hills, S., Birks, R., 2003. Using recycled water for non-potable, urban uses: a review with particular reference to toilet flushing. Water Science & Technology: Water Supply 3, 69-77.

Lazarova, V., Levine, B., Sack, J., Cirelli, G., Jeffrey, P., Muntau, H., Salgot, M., Brissaud, F., 2001. Role of water reuse for enhancing integrated water management in Europe and Mediterranean countries. Water Science & Technology 43, 25-33.

Le-Minh, N., Khan, S.J., Drewes, J.E., Stuetz, R.M., 2010. Fate of antibiotics during municipal water recycling treatment processes. Water research 44, 4295-4323.

Lea, J., Adesina, A.A., 1998. The photo-oxidative degradation of sodium dodecyl sulphate in aerated aqueous TiO2 suspension. J. Photochem. Photobiol., A 118, 111-122.

Leal, L.H., Temmink, H., Zeeman, G., Buisman, C.J., 2011. Removal of micropollutants from aerobically treated grey water via ozone and activated carbon. Water research.

Leal, L.H., Zeeman, G., Temmink, H., Buisman, C., 2007. Characterisation and biological treatment of greywater. Water Science and Technology 56, 193-200.

Li, F., Wichmann, K., Otterpohl, R., 2009a. Review of the technological approaches for grey water treatment and reuses. Sci. Total Environ. 407, 3439-3449.

Li, F., Wichmann, K., Otterpohl, R., 2009b. Review of the technological approaches for grey water treatment and reuses. Science of the Total Environment 407, 3439-3449.

Li Puma, G., 2005. Dimensionless analysis of photocatalytic reactors using suspended solid photocatalysts. Chemical Engineering Research and Design 83, 820-826.

Li Puma, G., Puddu, V., Tsang, H.K., Gora, A., Toepfer, B., 2010. Photocatalytic oxidation of multicomponent mixtures of estrogens (estrone (E1), 17β-estradiol (E2), 17α-ethynylestradiol (EE2) and estriol (E3)) under UVA and UVC radiation: Photon absorption, quantum yields and rate constants independent of photon absorption. Applied Catalysis B: Environmental 99, 388-397.

Li Puma, G., Toepfer, B., Gora, A., 2007. Photocatalytic oxidation of multicomponent systems of herbicides: Scale-up of laboratory kinetics rate data to plant scale. Catalysis Today 124, 124-132.

Li Puma, G., Yue, P.L., 2003. Modelling and design of thin-film slurry photocatalytic reactors for water purification. Chemical Engineering Science 58, 2269-2281.

Li, Z., Boyle, F., Reynolds, A., 2010. Rainwater harvesting and greywater treatment systems for domestic application in Ireland. Desalination 260, 1-8.

Li, Z., Gulyas, H., Jahn, M., Gajurel, D.R., Otterpohl, R., 2003. Greywater treatment by constructed wetlands in combination with TiO2-based photocatalytic oxidation for suburban and rural areas without sewer system. Water science and technology: a journal of the International Association on Water Pollution Research 48, 101.

Lin, C.J., Lo, S.L., Kuo, C.Y., Wu, C.H., 2005. Pilot-scale electrocoagulation with bipolar aluminum electrodes for on-site domestic greywater reuse. Journal of environmental engineering 131, 491.

Lodge, B., Judd, S.J., Smith, A.J., 2004. Characterisation of dead-end ultrafiltration of biotreated domestic wastewater. Journal of membrane science 231, 91-98.

Lorenz, A., Tuozzolo, C., Louge, M.Y., 1997. Measurements of impact properties of small, nearly spherical particles. Experimental Mechanics 37, 292-298.

Lun, C., Savage, S., 1986. The effects of an impact velocity dependent coefficient of restitution on stresses developed by sheared granular materials. Acta Mechanica 63, 15-44.

Lun, C.K.K., Savage, S.B., Jeffrey, D.J., Chepurniy, N., 1984. Kinetic theories for granular flow: inelastic particles in Couette flow and slightly inelastic particles in a general flowfield. J. Fluid. Mech. 140, 223-256.

Machado, A.E.H., de Miranda, J.A., de Freitas, R.F., Duarte, E.T.F.M., Ferreira, L.F., Albuquerque, Y.D.T., Ruggiero, R., Sattler, C., de Oliveira, L., 2003. Destruction of

the organic matter present in effluent from a cellulose and paper industry using photocatalysis. J. Photochem. Photobiol., A 155, 231-241.

Madany, I.M., Al-Shiryan, A., Lori, I., Al-Khalifa, H., 1992. Public awareness and attitudes toward various uses of renovated water. Environment international 18, 489-495.

Mandal, D., Labhasetwar, P., Dhone, S., Dubey, A.S., Shinde, G., Wate, S., 2011. Water conservation due to greywater treatment and reuse in urban setting with specific context to developing countries. Resources, Conservation and Recycling 55, 356-361.

Mankad, A., Tapsuwan, S., 2011. Review of socio-economic drivers of community acceptance and adoption of decentralised water systems. Journal of environmental management.

March, J.G., Gual, M., Orozco, F., 2004. Experiences on greywater re-use for toilet flushing in a hotel (Mallorca Island, Spain). Desalination 164, 241-247.

Marshall, J.S., 2011. Viscous damping force during head-on collision of two spherical particles. Physics of Fluids 23, 013305.

Martín, C.A., Baltanás, M.A., Cassano, A.E., 1993. Photocatalytic reactors I. Optical behavior of titanium oxide particulate suspensions. Journal of Photochemistry and Photobiology A: Chemistry 76, 199-208.

Masi, F., El Hamouri, B., Shafi, H.A., Baban, A., Ghrabi, A., Regelsberger, M., 2010. Treatment of segregated black/grey domestic wastewater using constructed wetlands in the Mediterranean basin: the zer0-m experience. Water Sci. Technol 61, 97-105.

McAdam, E., Judd, S.J., Gildemeister, R., Drews, A., Kraume, M., 2005. Critical analysis of submerged membrane sequencing batch reactor operating conditions. Water research 39, 4011-4019.

Mehrotra, K., Yablonsky, G.S., Ray, A.K., 2005. Macro kinetic studies for photocatalytic degradation of benzoic acid in immobilized systems. Chemosphere 60, 1427-1436.

Memon, F.A., Zheng, Z., Butler, D., Shirley-Smith, C., Lui, S., Makropoulos, C., Avery, L., 2007. Life Cycle Impact Assessment of Greywater Recycling Technologies for New Developments. Environmental monitoring and assessment 129, 27-35.

Merz, C., Scheumann, R., El Hamouri, B., Kraume, M., 2007. Membrane bioreactor technology for the treatment of greywater from a sports and leisure club. Desalination 215, 37-43.

Misra, R.K., Patel, J.H., Baxi, V.R., 2010. Reuse potential of laundry greywater for irrigation based on growth, water and nutrient use of tomato. Journal of Hydrology 386, 95-102.

Misra, R.K., Sivongxay, A., 2009. Reuse of laundry greywater as affected by its interaction with saturated soil. Journal of Hydrology 366, 55-61.

Mohseni, M., Taghipour, F., 2004. Experimental and CFD analysis of photocatalytic gas phase vinyl chloride (VC) oxidation. Chemical Engineering Science 59, 1601-1609.

Molden, D., Oweis, T., Steduto, P., Bindraban, P., Hanjra, M.A., Kijne, J., 2010. Improving agricultural water productivity: Between optimism and caution. Agricultural Water Management 97, 528-535.

Morel, A., Diener, S., 2006. Greywater management in low and middle-income countries, review of different treatment systems for households or neighbourhoods. Swiss Federal Institute of Aquatic Science and Technology (Eawag). Dübendorf, Switzerland http://www2. gtz. de/Dokumente/oe44/ecosan/en-greywatermanagement-2006. pdf.

Morsi, S.A., Alexander, A.J., 1972. An investigation of particle trajectories in two-phase flow systems. J. Fluid Mech 55, 193-208.

Nolde, E., 2000. Greywater reuse systems for toilet flushing in multi-storey buildings-over ten years experience in Berlin. Urban Water 1, 275-284.

Nolde, E., 2005. Greywater recycling systems in Germany--results, experiences and guidelines. Water science and technology: a journal of the International Association on Water Pollution Research 51, 203.

Obee, T.N., Brown, R.T., 1995. TiO2 photocatalysis for indoor air applications: effects of humidity and trace contaminant levels on the oxidation rates of formaldehyde, toluene, and 1, 3-butadiene. Environmental science & technology 29, 1223-1231.

Ogawa, S., Umemura, A., Oshima, N., 1980. On the equations of fully fluidized granular materials. Zeitschrift für Angewandte Mathematik und Physik (ZAMP) 31, 483-493.

Okamoto, K., Yamamoto, Y., Tanaka, H., Itaya, A., 1985. Kinetics of heterogeneous photocatalytic decomposition of phenol over anatase TiO2 powder. Bulletin of the Chemical Society of Japan 58, 2023-2028.

Olmos, E., Gentric, C., Vial, C., Wild, G., Midoux, N., 2001. Numerical simulation of multiphase flow in bubble column reactors. Influence of bubble coalescence and break-up. Chemical Engineering Science 56, 6359-6365.

Oschmann, N., Nghiem, L.D., Schafer, A.I., 2005. Fouling mechanisms of submerged ultrafiltration membranes in greywater recycling. Desalination 179, 215-223.

Ottosson, J., 2003. Hygiene aspects of greywater and greywater reuse. Royal Institute of Technology/SMI, TRITALWR LIC.

Oyama, T., Aoshima, A., Horikoshi, S., Hidaka, H., Zhao, J., Serpone, N., 2004. Solar photocatalysis, photodegradation of a commercial detergent in aqueous TiO2 dispersions under sunlight irradiation. Sol. Energy 77, 525-532.

Palmquist, H., Hanæus, J., 2005. Hazardous substances in separately collected grey-and blackwater from ordinary Swedish households. Science of the Total Environment 348, 151-163.

Panneerselvam, R., Savithri, S., Surender, G.D., 2009. CFD simulation of hydrodynamics of gas-liquid-solid fluidised bed reactor. Chemical Engineering Science 64, 1119-1135.

Pareek, V., 2005. Light intensity distribution in a dual-lamp photoreactor. International Journal of Chemical Reactor Engineering 3, 56.

Pareek, V., Brungs, M.P., Adesina, A.A., 2003a. A new simplified model for light scattering in photocatalytic reactors. Industrial & engineering chemistry research 42, 26-36.

Pareek, V., Chong, S., Tadé, M., Adesina, A.A., 2008. Light intensity distribution in heterogenous photocatalytic reactors. Asia Pac. J. Chem. Eng. 3, 171-201.

Pareek, V.K., Adesina, A.A., 2004. Light intensity distribution in a photocatalytic reactor using finite volume. AIChE journal 50, 1273-1288.

Pareek, V.K., Brungs, M.P., Adesina, A.A., 2001. Continuous process for photodegradation of industrial Bayer liquor. Industrial & engineering chemistry research 40, 5120-5125.

Pareek, V.K., Cox, S.J., Brungs, M.P., Young, B., Adesina, A.A., 2003b. Computational fluid dynamic (CFD) simulation of a pilot-scale annular bubble column photocatalytic reactor. Chemical Engineering Science 58, 859-865.

Paris, S., Schlapp, C., 2010. Greywater recycling in Vietnam--Application of the HUBER MBR process. Desalination 250, 1027-1030.

Passalia, C., Alfano, O.M., Brandi, R.J., 2011a. A Methodology for Modeling Photocatalytic Reactors for Indoor Pollution Control using Previously Estimated Kinetic Parameters. Journal of Hazardous Materials.

Passalia, C., Alfano, O.M., Brandi, R.J., 2011b. Modeling and Experimental Verification of a Corrugated Plate Photocatalytic Reactor Using Computational Fluid Dynamics. Industrial & engineering chemistry research 50, 9077-9086.

Paulo, P.L., Begosso, L., Pansonato, N., Shrestha, R.R., Boncz, M.A., 2009. Design and configuration criteria for wetland systems treating greywater. Water Science and Technology 60, 2001-2007.

Pekakis, P.A., Xekoukoulotakis, N.P., Mantzavinos, D., 2006. Treatment of textile dyehouse wastewater by TiO2 photocatalysis. Water Res. 40, 1276-1286.

Pera-Titus, M., Garcia-Molina, V., Banos, M.A., Gimenez, J., Esplugas, S., 2004. Degradation of chlorophenols by means of advanced oxidation processes: a general review. Applied Catalysis B: Environmental 47, 219-256.

Peral, J., Ollis, D.F., 1992. Heterogeneous photocatalytic oxidation of gas-phase organics for air purification: acetone, 1-butanol, butyraldehyde, formaldehyde, and m-xylene oxidation. Journal of Catalysis 136, 554-565.

Perry, R.H., Green, D.W., 2007. Perry's chemical engineers' handbook. McGraw-Hill Professional.

Pettersson, A., Adamsson, M., Dave, G., 2000. Toxicity and detoxification of Swedish detergents and softener products. Chemosphere 41, 1611-1620.

Pham, T.T.N., Ngo, H.H., Guo, W., Dang, H.P.D., Mainali, B., Johnston, A., Listowski, A., 2011. Responses of community to the possible use of recycled water for washing machines: A case study in Sydney, Australia. Resources, Conservation and Recycling.

Pidou, M., Avery, L., Stephenson, T., Jeffrey, P., Parsons, S.A., Liu, S., Memon, F.A., Jefferson, B., 2008. Chemical solutions for greywater recycling. Chemosphere 71, 147-155.

Pidou, M., Memon, F.A., Stephenson, T., Jefferson, B., Jeffrey, P., 2007. Greywater recycling: treatment options and applications. Landscape 2, 1000.

Pidou, M., Parsons, S.A., Raymond, G., Jeffrey, P., Stephenson, T., Jefferson, B., 2009. Fouling control of a membrane coupled photocatalytic process treating greywater. Water research 43, 3932-3939.

Pinto, U., Maheshwari, B.L., 2010. Reuse of greywater for irrigation around homes in Australia: Understanding community views, issues and practices.

Pinto, U., Maheshwari, B.L., Grewal, H.S., 2010. Effects of greywater irrigation on plant growth, water use and soil properties. Resources, Conservation and Recycling 54, 429-435.

Po, M., Nancarrow, B.E., Kaercher, J.D., 2003. Literature review of factors influencing public perceptions of water reuse. CSIRO Land and Water.

Pozzo, R.L., Baltanas, M.A., Cassano, A.E., 1999. Towards a precise assessment of the performance of supported photocatalysts for water detoxification processes. Catalysis Today 54, 143-157.

Prathapar, S.A., Jamrah, A., Ahmed, M., Al Adawi, S., Al Sidairi, S., Al Harassi, A., 2005. Overcoming constraints in treated greywater reuse in Oman. Desalination 186, 177-186.

Puma, G.L., 2003. Modeling of thin-film slurry photocatalytic reactors affected by radiation scattering. Environmental science & technology 37, 5783-5791.

Puma, G.L., Khor, J.N., Brucato, A., 2004. Modeling of an annular photocatalytic reactor for water purification: oxidation of pesticides. Environmental science & technology 38, 3737-3745.

Qi, N., Zhang, H., Jin, B., Zhang, K., 2011. CFD modelling of hydrodynamics and degradation kinetics in an annular slurry photocatalytic reactor for wastewater treatment. Chemical Engineering Journal.

Quan, Y., Pehkonen, S.O., Madhumita, B., 2004. Evaluation of three different lamp emission models using novel application of potassium ferrioxalate actinometry. Industrial & engineering chemistry research 43, 948-955.

Queffeulou, A.l., Geron, L., Schaer, E., 2010. Prediction of photocatalytic air purifier apparatus performances with a CFD approach using experimentally determined kinetic parameters. Chemical Engineering Science 65, 5067-5074.

Ramona, G., Green, M., Semiat, R., Dosoretz, C., 2004. Low strength graywater characterization and treatment by direct membrane filtration. Desalination 170, 241-250.

Ranade, V.V., 2002. Computational flow modeling for chemical reactor engineering. Academic Press.

Regalbuto, J.R., 2007. Catalyst preparation: science and engineering. CRC Press/Taylor & Francis.

Revitt, D.M., Eriksson, E., Donner, E., 2011. The implications of household greywater treatment and reuse for municipal wastewater flows and micropollutant loads. Water research.

Rivero, M.J., Parsons, S.A., Jeffrey, P., Pldou, M., Jefferson, B., 2006. Membrane chemical reactor (MCR) combining photocatalysis and microfiltration for grey water treatment. Water Science and Technology 53, 173-180.

Rodda, N., Salukazana, L., Jackson, S.A.F., Smith, M.T., 2011. Use of domestic greywater for small-scale irrigation of food crops: Effects on plants and soil. Physics and Chemistry of the Earth, Parts A/B/C 36, 1051-1062.

Rodrigues, A.C., Boroski, M., Shimada, N.S., Garcia, J.C., Nozaki, J., Hioka, N., 2008. Treatment of paper pulp and paper mill wastewater by coagulation-flocculation followed by heterogeneous photocatalysis. J. Photochem. Photobiol., A 194, 1-10.

Romero-Vargas Castrillon, S., Ibrahim, H., De Lasa, H., 2006. Flow field investigation in a photocatalytic reactor for air treatment (Photo-CREC-air). Chemical Engineering Science 61, 3343-3361.

Romero, R.L., Alfano, O.M., Cassano, A.E., 1997. Cylindrical photocatalytic reactors. Radiation absorption and scattering effects produced by suspended fine particles in an annular space. Industrial & engineering chemistry research 36, 3094-3109.

Romero, R.L., Alfano, O.M., Cassano, A.E., 2003. Radiation field in an annular, slurry photocatalytic reactor. 2. Model and experiments. Industrial & engineering chemistry research 42, 2479-2488.

Romero, R.L., Alfano, O.M., Cassano, A.E., 2009. Photocatalytic reactor employing titanium dioxide: from a theoretical model to realistic experimental results. Industrial & engineering chemistry research 48, 10456-10466.

Ronen, Z., Guerrero, A., Gross, A., 2010. Greywater disinfection with the environmentally friendly Hydrogen Peroxide Plus (HPP). Chemosphere 78, 61-65.

Rose, J.B., Sun, G.S., Gerba, C.P., Sinclair, N.A., 1991. Microbial quality and persistence of enteric pathogens in graywater from various household sources. Water research 25, 37-42.

Ryan, A.M., Spash, C.L., Measham, T.G., 2009. Socio-economic and psychological predictors of domestic greywater and rainwater collection: Evidence from Australia. Journal of Hydrology 379, 164-171.

Salvadó-Estivill, I., Brucato, A., Li Puma, G., 2007a. Two-Dimensional Modeling of a Flat-Plate Photocatalytic Reactor for Oxidation of Indoor Air Pollutants. Industrial & engineering chemistry research 46, 7489-7496.

Salvado-Estivill, I., Brucato, A., Puma, G.L., 2007a. Two-dimensional modeling of a flat-plate photocatalytic reactor for oxidation of indoor air pollutants. Industrial & engineering chemistry research 46, 7489-7496.

Salvadó-Estivill, I., Hargreaves, D.M., Li Puma, G., 2007b. Evaluation of the Intrinsic Photocatalytic Oxidation Kinetics of Indoor Air Pollutants. Environmental science & technology 41, 2028-2035.

Salvado-Estivill, I., Hargreaves, D.M., Puma, G.L., 2007b. Evaluation of the intrinsic photocatalytic oxidation kinetics of indoor air pollutants. Environmental science & technology 41, 2028-2035.

Sanchez, M., Rivero, M.J., Ortiz, I., 2010a. Kinetics of dodecylbenzenesulphonate mineralisation by TiO2 photocatalysis. Appl. Catal., B.

Sanchez, M., Rivero, M.J., Ortiz, I., 2010b. Photocatalytic oxidation of grey water over titanium dioxide suspensions. Desalination.

Sanyal, J., Roy, S., Dudukovic, M.P., 1999. Numerical simulation of gas-liquid dynamics in cylindrical bubble column reactors. Chemical Engineering Science 54, 5071-5083.

Schafer, A.I., Nghiem, L.D., Oschmann, N., 2006. Bisphenol A retention in the direct ultrafiltration of greywater. Journal of membrane science 283, 233-243.

Scheumann, R., Merz, C., Atasoy, E., Murat, S., Baban, A., ElHamouri, B., Kraume, M., 2007. Greywater Treatment with Membrane Bioreactors: Comparison of

Three Different Reactors Operated with Synthetic and Real Greywater. Aachener Tagung Wasser und Membranen (30.-31.10. 2007), Aachen.

Schiller, L., Naumann, Z., 1935. A drag coefficient correlation. Z. Ver. Deutsch. Ing. 77, 318-320.

Seckler, D.W., 1998. World water demand and supply, 1990 to 2025: Scenarios and issues. Iwmi.

Selma, B., Bannari, R., Proulx, P., 2010. A full integration of a dispersion and interface closures in the standard k-[epsilon] model of turbulence. Chemical Engineering Science 65, 5417-5428.

Shin, H.S., Lee, S.M., 1998. Pilot-scale SBR and MF operation for the removal of organic and nitrogen compounds from greywater. Water Science and Technology 38, 79-88.

Shon, H.K., Vigneswaran, S., Ngo, H.H., Kim, J.H., 2005. Chemical coupling of photocatalysis with flocculation and adsorption in the removal of organic matter. Water Res. 39, 2549-2558.

Siegel, R., Howell, J.R., 2002. Thermal radiation heat transfer. Hemisphere Pub.

Simonnet, M., Gentric, C., Olmos, E., Midoux, N., 2008. CFD simulation of the flow field in a bubble column reactor: Importance of the drag force formulation to describe regime transitions. Chemical Engineering and Processing: Process Intensification 47, 1726-1737.

Singh, M., Salvado-Estivill, I., Li Puma, G., 2007. Radiation field optimization in photocatalytic monolith reactors for air treatment. AIChE journal 53, 678-686.

Smith, A., Khow, J., Hills, S., Donn, A., 2000. Water reuse at the UK's Millennium Dome. Membrane Technology 2000, 5-8.

Sostar-Turk, S., Petrinic, I., Simonic, M., 2005. Laundry wastewater treatment using coagulation and membrane filtration. Resources, Conservation and Recycling 44, 185-196.

Sozzi, D.A., Taghipour, F., 2006. Computational and experimental study of annular photo-reactor hydrodynamics. International journal of heat and fluid flow 27, 1043-1053.

Srinivasa, T., Jayanti, S., 2007. An eulerian/lagrangian study of solid suspension in stirred tanks. AIChE journal 53, 2461-2469.

Stephan, B., Ludovic, L., Dominique, W., 2011. Modelling of a falling thin film deposited photocatalytic step reactor for water purification: Pesticide treatment. Chemical Engineering Journal 169, 216-225.

Stikker, A., 1998. WATER TODAY AND TOMORROW:: Prospects for overcoming scarcity. Futures 30, 43-62.

Sudduth, R.D., 1993. A new method to predict the maximum packing fraction and the viscosity of solutions with a size distribution of suspended particles. II. Journal of applied polymer science 48, 37-55.

Syamlal, M., Rogers, W., O`Brien, T.J., 1993. MFIX documentation theory guide, Other Information: PBD: Dec 1993, p. Medium: ED; Size: 49 p.

Tabib, M.V., Roy, S.A., Joshi, J.B., 2008. CFD simulation of bubble column--An analysis of interphase forces and turbulence models. Chemical Engineering Journal 139, 589-614.

Tandlich, R., Zuma, B.M., Whittington-Jones, K.J., Burgess, J.E., 2009. Mulch tower treatment system for greywater reuse Part II: destructive testing and effluent treatment. Desalination 242, 57-69.

Toepfer, B., Gora, A., Li Puma, G., 2006. Photocatalytic oxidation of multicomponent solutions of herbicides: Reaction kinetics analysis with explicit photon absorption effects. Applied Catalysis B: Environmental 68, 171-180.

Travis, M.J., Weisbrod, N., Gross, A., 2008. Accumulation of oil and grease in soils irrigated with greywater and their potential role in soil water repellency. Science of the Total Environment 394, 68-74.

Trujillo, F.J., Safinski, T., Adesina, A.A., 2007. CFD analysis of the radiation distribution in a new immobilized catalyst bubble column externally illuminated photoreactor. Journal of Solar Energy Engineering 129, 27.

Trujillo, F.J., Safinski, T., Adesina, A.A., 2010. Oxidative Photomineralization of Dichloroacetic Acid in an Externally-Irradiated Rectangular Bubble Tank Reactor: Computational Fluid Dynamics Modeling and Experimental Verification Studies. Industrial & engineering chemistry research 49, 6722-6734.

Turchi, C.S., Ollis, D.F., 1990. Photocatalytic degradation of organic water contaminants: mechanisms involving hydroxyl radical attack. Journal of Catalysis 122, 178-192.

Turian, R.M., Ma, T.W., Hsu, F.L.G., Sung, D.J., 1997. Characterization, settling, and rheology of concentrated fine particulate mineral slurries. Powder technology 93, 219-233.

Van Grieken, R., Marugán, J., Sordo, C., Pablos, C., 2009. Comparison of the photocatalytic disinfection of E. coli suspensions in slurry, wall and fixed-bed reactors. Catalysis Today 144, 48-54.

Vella, G., Imoberdorf, G.E., Sclafani, A., Cassano, A.E., Alfano, O.M., Rizzuti, L., 2010. Modeling of a TiO2-coated quartz wool packed bed photocatalytic reactor. Applied Catalysis B: Environmental 96, 399-407.

Victoria. Environment Protection, A., 2003. Use of reclaimed water. EPA Victoria.

Wang, T., Wang, J., Jin, Y., 2007. Slurry reactors for gas-to-liquid processes: A review. Industrial & engineering chemistry research 46, 5824-5847.

Widiastuti, N., Wu, H., Ang, H.M., Zhang, D., 2011. Removal of ammonium from greywater using natural zeolite. Desalination.

Widiastuti, N., Wu, H., Ang, M., Zhang, D., 2008. The potential application of natural zeolite for greywater treatment. Desalination 218, 271-280.

Wiel-Shafran, A., Ronen, Z., Weisbrod, N., Adar, E., Gross, A., 2006. Potential changes in soil properties following irrigation with surfactant-rich greywater. Ecological Engineering 26, 348-354.

Winward, G.P., Avery, L.M., Frazer-Williams, R., Pidou, M., Jeffrey, P., Stephenson, T., Jefferson, B., 2008a. A study of the microbial quality of grey water and an evaluation of treatment technologies for reuse. Ecological Engineering 32, 187-197.

Winward, G.P., Avery, L.M., Stephenson, T., Jefferson, B., 2008b. Chlorine disinfection of grey water for reuse: Effect of organics and particles. Water research 42, 483-491.

Winward, G.P., Avery, L.M., Stephenson, T., Jefferson, B., 2008c. Essential oils for the disinfection of grey water. Water research 42, 2260-2268.

World Health, O., 2006. Guidelines for the Safe Use of Wastewater, Excreta and Greywater: Vol. 4. Excreta and greywater use in agriculture. World Health Organization.

Xiaoyan, H., 2011. CFD modeling of liquid-solid fluidization: Effect of drag correlation and added mass force. Particuology 9, 441-445.

Yamashita, F., Inoue, H., 1975. GAS HOLDUP IN BUBBLE COLUMNS. Journal of Chemical Engineering of Japan 8, 334-336.

Yang, F.L., Hunt, M.L., 2006. Dynamics of particle-particle collisions in a viscous liquid. Physics of Fluids 18, 121506.

Yang, Q., Ling Ang, P., Ray, M.B., Pehkonen, S.O., 2005a. Light distribution field in catalyst suspensions within an annular photoreactor. Chemical Engineering Science 60, 5255-5268.

Yang, Q., Pehkonen, S.O., Ray, M.B., 2005b. Light Distribution Model for an Annular Reactor with a Cylindrical Reflector. Industrial & engineering chemistry research 44, 3471-3479.

Yu, B., Deng, B., Kim, C.N., 2008. Performance evaluation of P-1 model in a photocatalytic reactor. Chemical Engineering Science 63, 5552-5558.

Zaizen, M., Urakawa, T., Matsumoto, Y., Takai, H., 2000. The collection of rainwater from dome stadiums in Japan. Urban Water 1, 355-359.

Zhang, L., Anderson, W.A., 2010. A finite model for the prediction of the UV radiation field around a linear lamp. Chemical Engineering Science 65, 1513-1521.

Zhang, R., Gao, L., Zhang, Q., 2004. Photodegradation of surfactants on the nanosized TiO2 prepared by hydrolysis of the alkoxide titanium. Chemosphere 54, 405-411.

Zhao, J., Oota, H., Hidaka Ezio, H., 1992. Photodegradation of surfactants X. Comparison of the photo-oxidation of the aromatic moieties in sodium dodecylbenzene sulphonate and in sodium phenyldodecyl sulphonate at TiO2---H2O interfaces. J. Photochem. Photobiol., A 69, 251-256.

Zhong, L., Haghighat, F., 2011. Modeling and validation of a photocatalytic oxidation reactor for indoor environment applications. Chemical Engineering Science 66, 5945-5954.

Zhu, X., Nanny, M.A., Butler, E.C., 2008. Photocatalytic oxidation of aqueous ammonia in model gray waters. Water research 42, 2736-2744.

Zuma, B.M., Tandlich, R., Whittington-Jones, K.J., Burgess, J.E., 2009. Mulch tower treatment system Part I: Overall performance in greywater treatment. Desalination 242, 38-56.

Appendices

Appendix A1 – Shower water detailed composition

Table A1- 1: Greywater chemical composition

Soap/shampoo brand	Ingredients	Chemical type	Main function(s)
Neutrogena Deep Clean-Facial Cleaner	Water	Not Applicable	Carrier
	Sodium Laureth Sulphate	Primary Surfactant- Anionic	Cleaning, Foaming
	Glycerin	Alcohol	Skin Conditioning Agent
	Lauryl Glucoside	Primary Surfactant- Nonionic	Cleaning, Foaming
	Cocamidopropyl Betaine	Primary Surfactant- Amphoteric	Cleaning, Foaming
	PEG-120 Methyl Glucose Dialeate	Polymer/Surfactant	Lather and Viscosity Enhancer
	Salicylic acid	Organic Acid	Anti-acne agent
	Sodium Cocoamphoacetate	Secondary Surfactant- Amphoteric	Non Irritating Foaming
	Polysorbate 20	Secondary Surfactant- Nonionic	Non Irritating Foaming
	Sodium Citrate	Salt	Product Aesthetics
	Citric Acid	Acid	pH Adjuster
	Fragrance	Not Specified	Product Aesthetics
	Methylparaben	Paraben	Antimicrobial
	Disodium EDTA	Amino Acid Salt	Product Aesthetics/Chelating Agent
	Yellow 5	Dye	Product Aesthetics
	Red 33	Dye	Product Aesthetics
Head and Shoulders for Men-Hair Retain (Shampoo)	Sodium Laureth Sulphate	Primary Surfactant- Anionic	Cleaning, Foaming
	Sodium Lauryl Sulphate	Primary Surfactant- Anionic	Cleaning, Foaming
	Cocamide MEA	Secondary Surfactant- Nonionic	Lather and Viscosity Enhancer
	Zinc Carbonate	Salt	Opacifying Agent
	Glycol Distearate	Secondary Surfactant- Nonionic	Opacifying Agent
	Zinc Pyrithione	Particulate	Antidandruff Agent
	Sodium Chloride	Salt	Viscosity Modifier
	Dimethicone	Silicone	Hair Aesthetics
	Fragrance	Not Specified	Product Aesthetics
	Cetyl Alcohol	Alcohol	Hair Conditioning Agent
	Guar Hydroxypropyltrimonium Chloride	Cationic Polymer	Skin Conditioning Agent
	Sodium Xylenesulphonate	Aromatic Sulphonates	Product Stability/Solubiliser
	Magnesium Sulphate	Salt	Viscosity Modifier
	Sodium Benzoate	Organic Sodium Salt	Antimicrobial
	Ammonium Laureth Sulphate	Primary Surfactant- Anionic	Cleaning, Foaming
	Magnesium Carbonate Hydroxide	Insoluble Salt	Hair Conditioning Agent
	Benzyl Alcohol	Alcohol	Product Aesthetics/Fragrance
	Tocopheryl Acetate	Acetate Ester	Skin Conditioning Agent
	Methylchloroisothiazolinone/Methylisothiazolinone	Heterocyclic Organic Compound	Antimicrobial
	CI 19140	Dye	Product Aesthetics
	CI 42090	Dye	Product Aesthetics
Palmolive Active-Shower Gel	Aqua (Water)	Not Applicable	Carrier
	Sodium Laureth Sulphate	Primary Surfactant- Anionic	Cleaning, Foaming

Cocamidopropyl Betaine	Primary Surfactant-Amphoteric	Cleaning, Foaming
Fragrance	Not Specified	Product Aesthetics
Sodium Chloride	Salt	Viscosity Modifier
Sodium Benzoate	Organic Sodium Salt	Antimicrobial
Cocamide MEA	Secondary Surfactant-Nonionic	Lather and Viscosity Enhancer
Sodium Salicylate	Organic Sodium Salt	Antimicrobial
Tetrasodium EDTA	Amino Acid Salt	Antimicrobial/Chelating Agent
Polyquartenium 7	Cationic Polymer	Skin Conditioning Agent
Benzophenone 4	Organic Compound	UV absorber
Citric Acid	Acid	pH Adjuster
Sea Salt	Particulate	Exfoliating Agent
CI 42090	Dye	Product Aesthetics
CI 45100	Dye	Product Aesthetics

Note: The highlighted chemicals are organic compounds that are prone to photocatalytic degradation

Appendix A2 – Mass Balance on Reactor

This is to calculate the maximum amount of volatile TOC that can potentially evaporate with water

Assumptions

Inlet air is dry (no water vapour)

Air at reactor outlet is saturated with water at 300 K (reaction temperature)

Inlet conditions

Maximum air pressure, P = 600 kPa

Average ambient air temperature, T = 300 K

Average air volumetric flow rate = 1.8 $Lmin^{-1}$

Air flow for reaction time (6 hours), $V = 1.8\ \frac{L}{min} \times 6\ h \times 60 \frac{min}{h} = 648\ L = 0.648\ m^3$

Calculation of air molar flow at inlet

$PV = ZnRT$

The compressibility factor (Z) is taken into account here since the inlet pressure is fairly high

Determination of Z

For air (Himmelblau and Riggs, 2004):

$T_c = 132.5$ K, hence $T_r = {}^{T}/_{T_c} = 2.26$

$P_c = 37.2$ atm, hence $P_r = {}^{P}/_{P_c} = 0.16$

From the generalised compressibility chart for lower pressures, figure 14.4a (Himmelblau and Riggs, 2004), the compressibility factor is very close to 1, hence Z = 1

$$n_{air,in} = \frac{PV}{RT} = \frac{600\ kPa\ \times 0.648\ m^3}{8.314\ \frac{kPa.\ m^3}{Kmol.\ K} \times 300\ K} = 0.156\ kmol$$

Calculation of water and TOC content in outlet

At 300 K, $P^*_{H2O} = 3.63$ kPa

$$\frac{n_{H2O}}{n_{Total}} = \frac{n_{H2O}}{n_{H2O} + n_{air,in}} = \frac{P^*_{H2O}}{P_{Total}}$$

$$\frac{n_{H2O}}{n_{H2O} + 0.156} = \frac{3.63}{101.3}$$

$n_{H2O} = 5.8 \times 10^{-3}$ kmol

Maximum volume of water evaporating = $18 \frac{kg}{kmol} \times 5.8 \times 10^{-3}$ kmol $\times \frac{1}{996.2} \frac{m^3}{kg} \times 1000 \frac{L}{m^3} = 0.105$ L

Maximum TOC content in greywater = 25.06 mgL^{-1}

Maximum TOC potentially evaporating with water as VOC (Volatile Organic Carbon) = $25.06 \times 0.105 = 2.6313$ mg

Total TOC content in reactor volume (31 L) = $25.06 \times 31 = 776.9$ mg

Maximum % of VOC lost = $\frac{2.6313}{776.9}\% = 0.34\%$

The MAXIMUM amount of TOC lost with evaporated water is 0.34% of the total TOC. This is very small compared to the amount of TOC oxidised via photocatalysis and hence can be safely neglected.

Appendix A3 – Detailed Experimental Results for Shower Water Photocatalysis

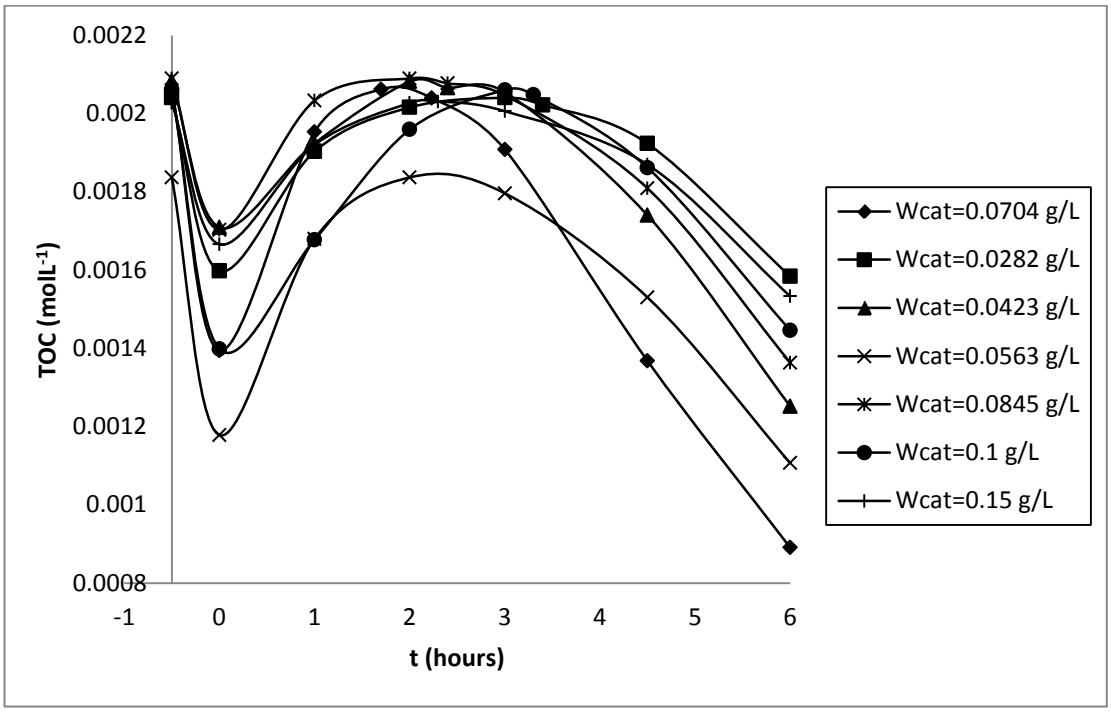

Figure A3- 1: Effect of catalyst loading (W_{cat}, g L^{-1}) with TOC degradation (Average reaction temperature = 27° C, pH = 3, air flow rate = 1.8 $Lmin^{-1}$ and slurry recirculation rate = 4.4 $Lmin^{-1}$)

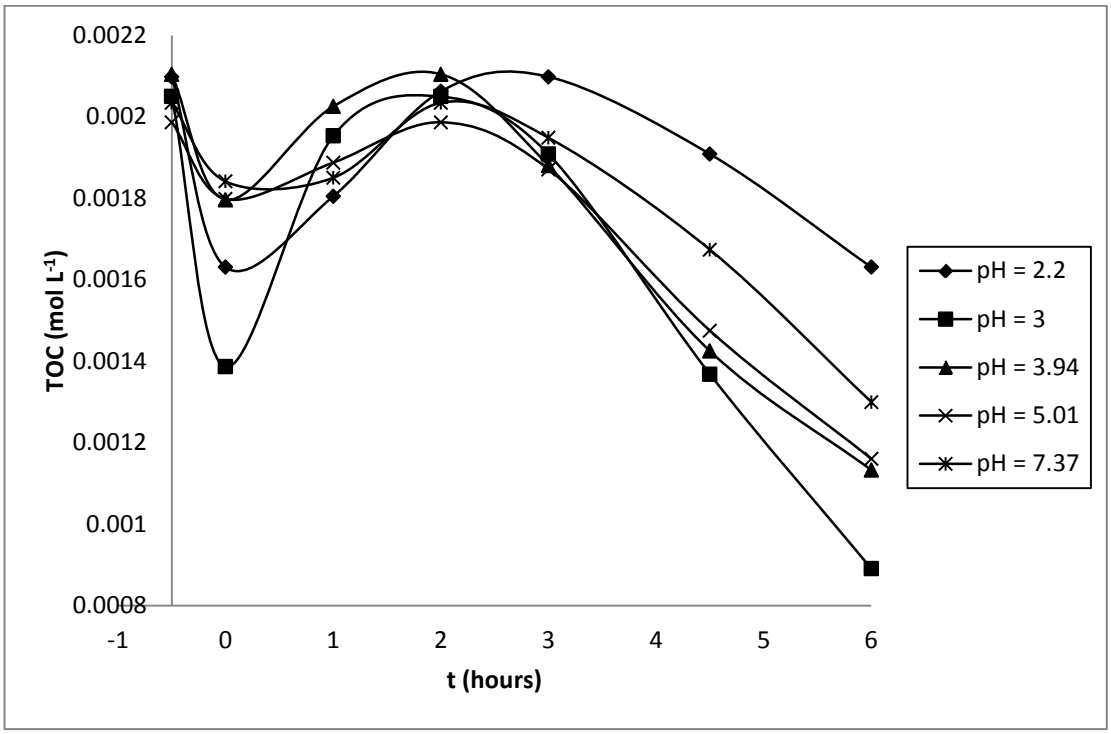

Figure A3- 2: Effect of slurry pH with TOC degradation (Average reaction temperature = 27° C, W_{cat} = 0.0704 gL^{-1}, air flow rate = 1.8 $Lmin^{-1}$ and slurry recirculation rate = 4.4 $Lmin^{-1}$)

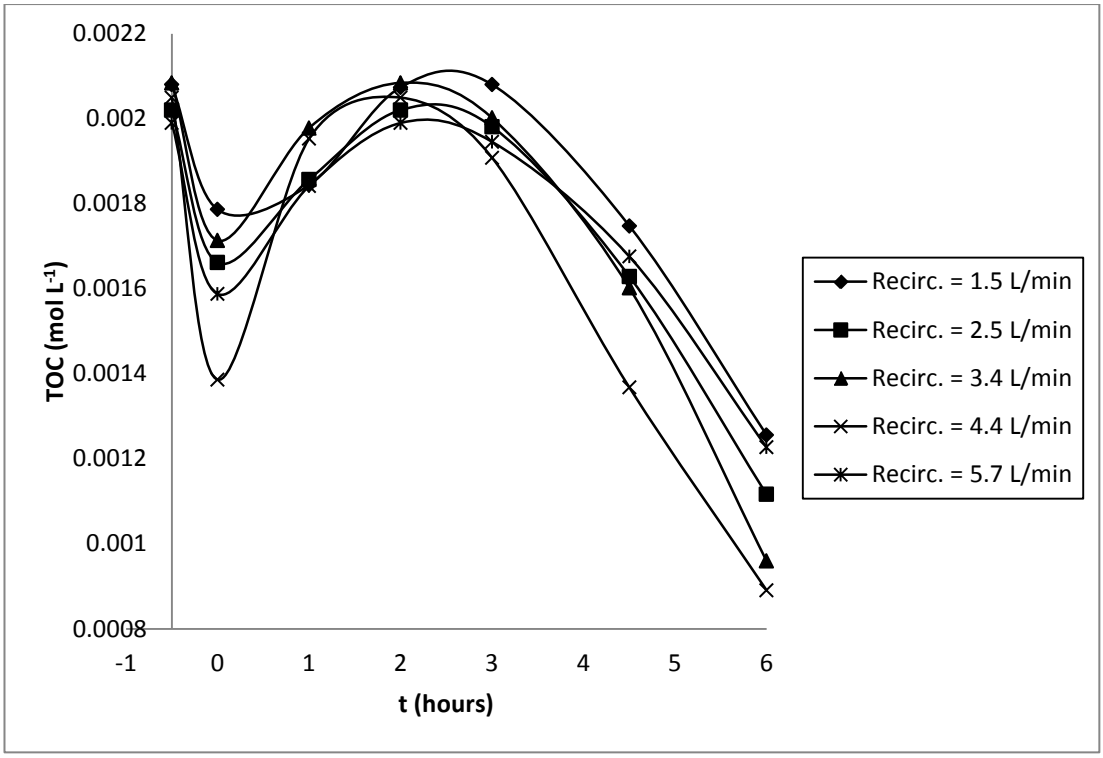

Figure A3- 3: Effect of slurry recirculation rate with TOC degradation (Average reaction temperature = 27° C, W_{cat} = 0.0704 gL^{-1}, air flow rate = 1.8 $Lmin^{-1}$ and pH = 3)

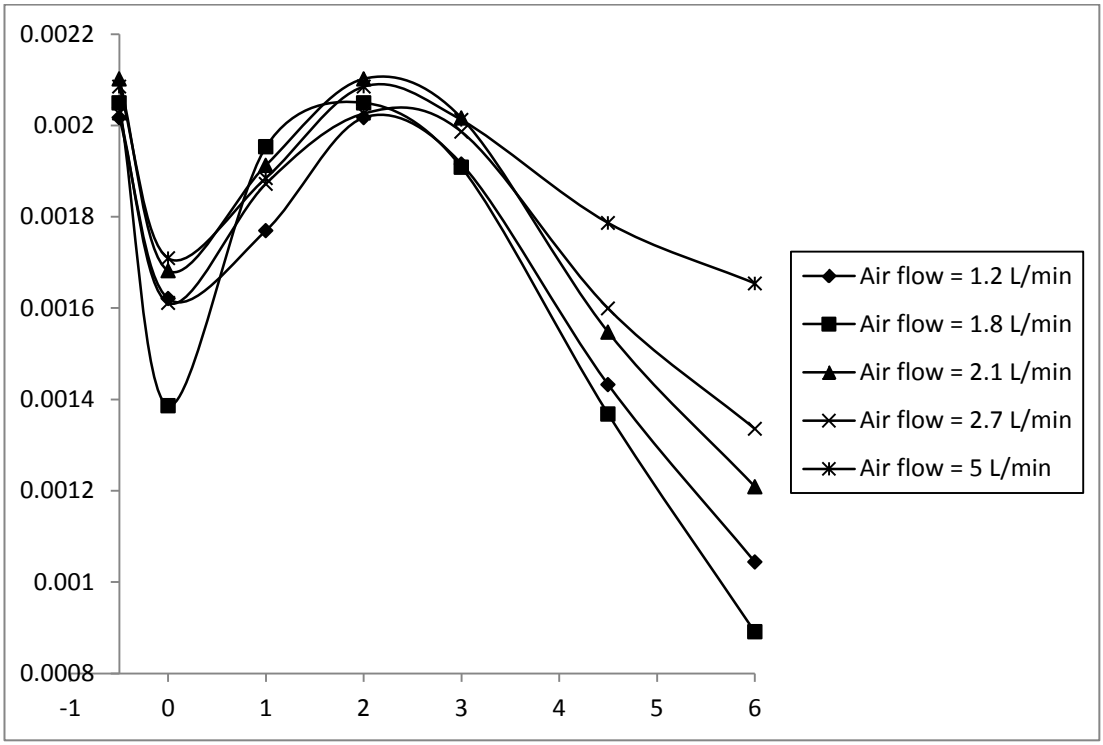

Figure A3- 4: Effect of air flow rate with TOC degradation (Average reaction temperature = 27° C, W_{cat} = 0.0704 gL^{-1}, slurry recirculation rate = 4.4 $Lmin^{-1}$ and pH = 3)

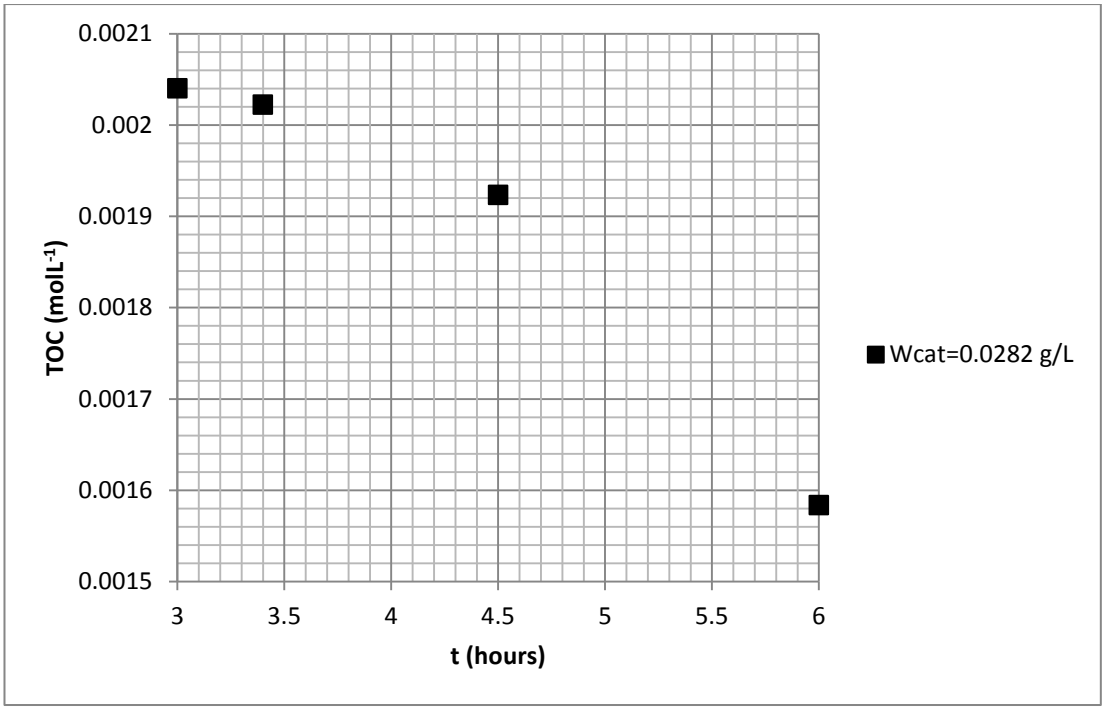

Figure A3- 5: Degradation stage of TOC (shown on larger scale) when W_{cat} = 0.0282 gL^{-1}

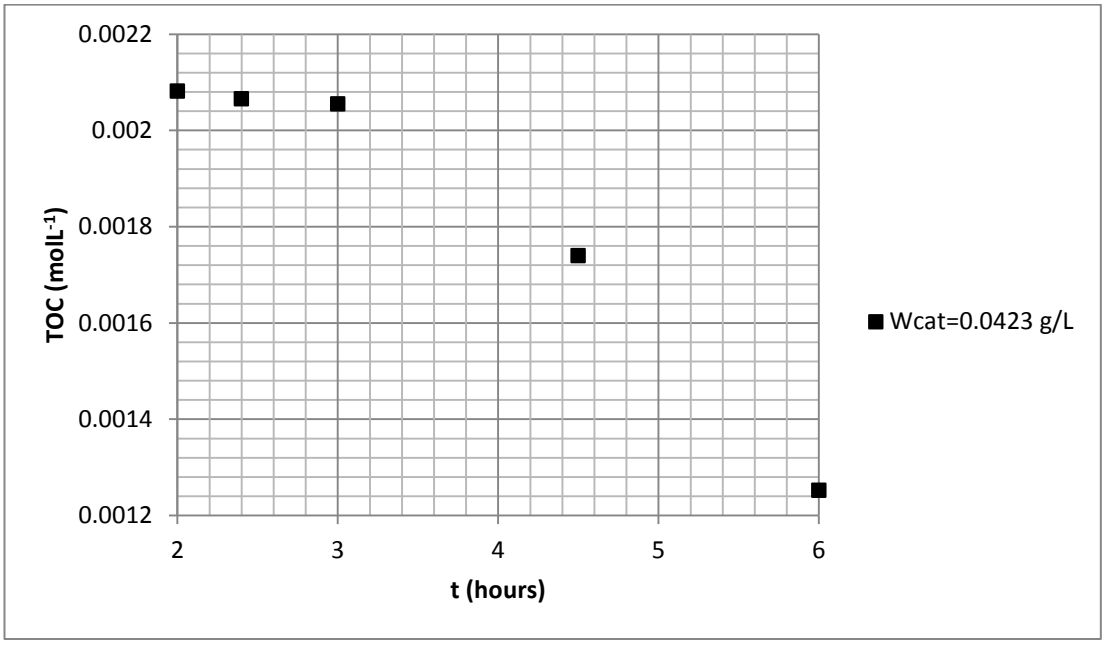

Figure A3- 6: Degradation stage of TOC (shown on larger scale) when W_{cat} = 0.0423 gL^{-1}

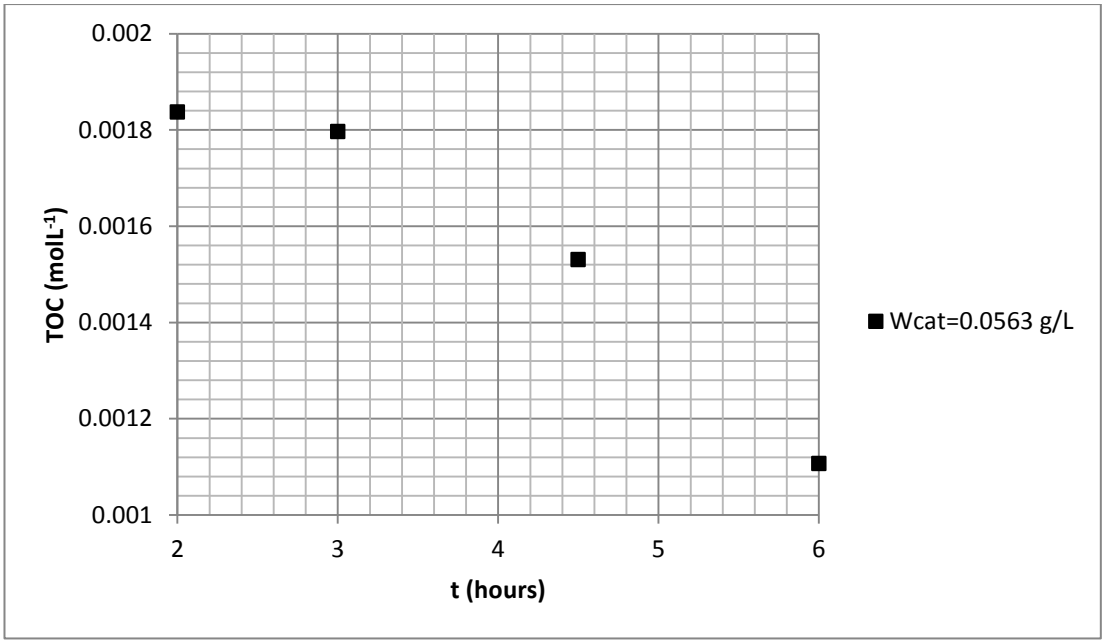

Figure A3- 7: Degradation stage of TOC (shown on larger scale) when W_{cat} = 0.0563 gL^{-1}

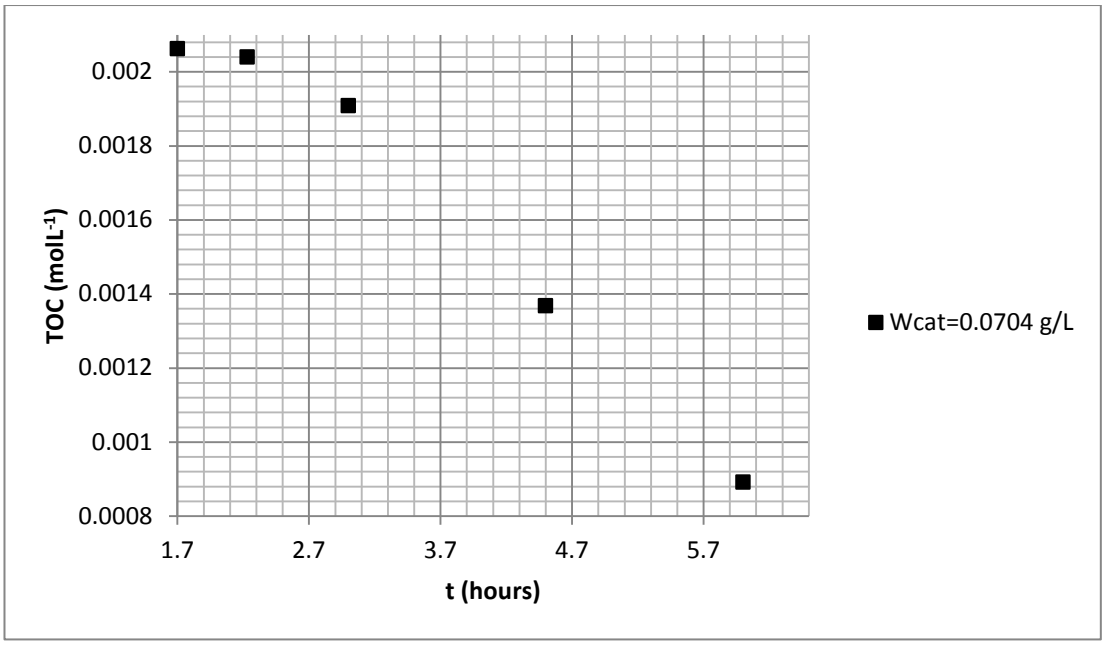

Figure A3- 8: Degradation stage of TOC (shown on larger scale) when W_{cat} = 0.0704 gL^{-1}

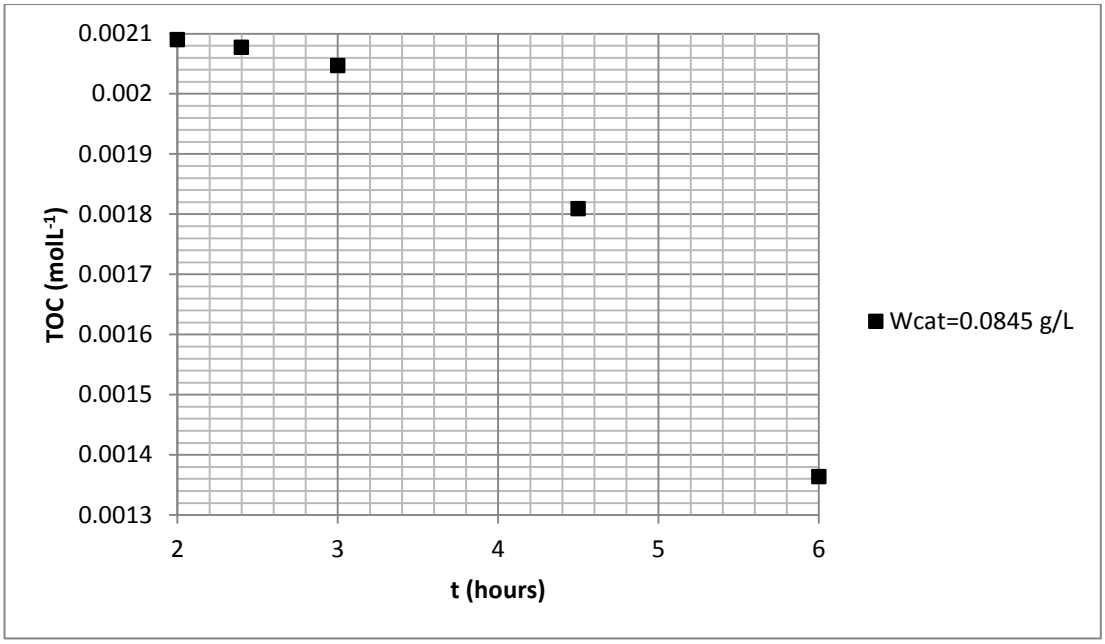

Figure A3- 9: Degradation stage of TOC (shown on larger scale) when W_{cat} = 0.0845 gL^{-1}

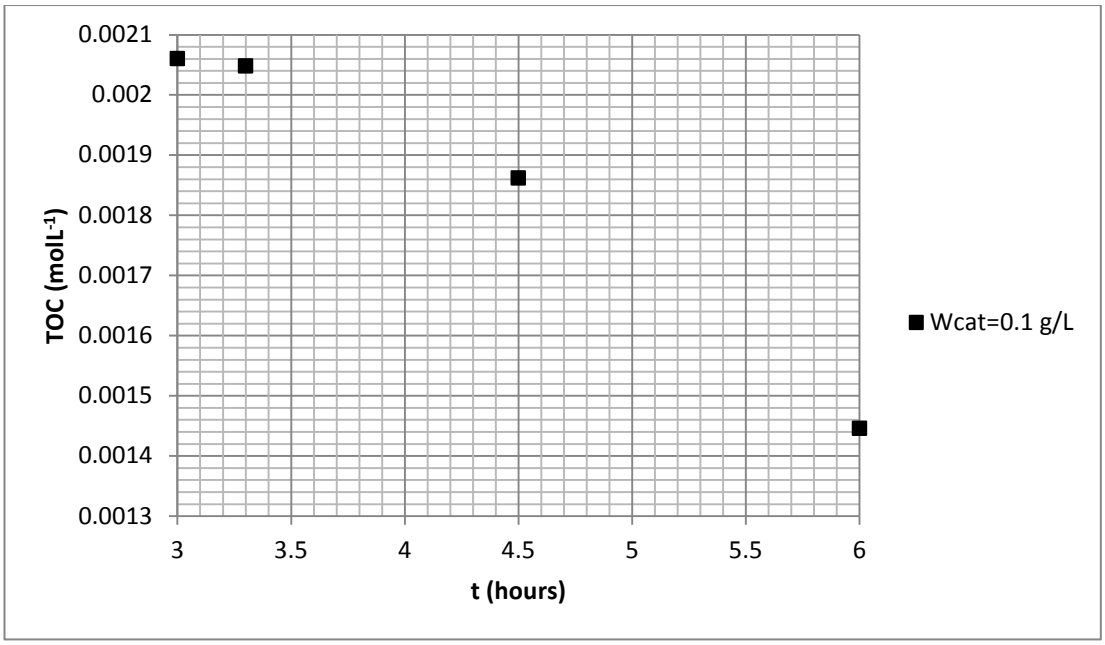

Figure A3- 10: Degradation stage of TOC (shown on larger scale) when W_{cat} = 0.1 gL^{-1}

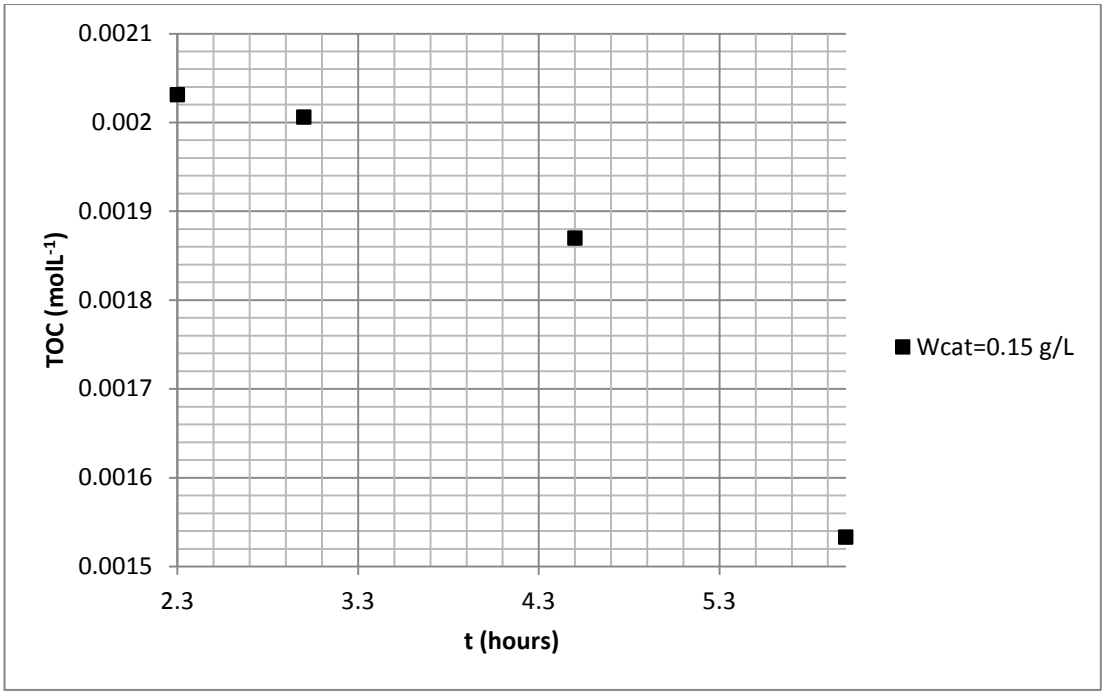

Figure A3- 11: Degradation stage of TOC (shown on larger scale) when W_{cat} = 0.15 gL^{-1}

Appendix A4 – Emission Spectrum for UV Lamp